Evaluation of Various CO_2 Injection Strategies Including Carbonated Water Injection for Coupled Enhanced Oil Recovery and Storage

By

Nor Idah Kechut

Submitted for the degree of **Doctor of Philosophy** in

Petroleum Engineering

Heriot-Watt University

Institute of Petroleum Engineering

August 2012

Abstract

In view of current interest in geological CO_2 sequestration and EOR, this study investigated water-based and gas-based CO_2 injection strategies for coupled EOR and storage purposes.

For water-based CO_2 injection strategy, carbonated water injection (CWI) was investigated as an alternative injection mode that could improve sweep efficiency and provide safe storage of CO_2. Despite its potential, CWI has not been very much studied. This thesis presents the details on the performance of CWI of moderately viscous oil (>100 cP), which has not been reported before. The effects of oil viscosity, rock wettability and brine salinity on oil recovery from CWI were also studied and significant findings were observed. To the author's knowledge, no attempt has been made to experimentally quantify the CO_2 storage by CWI process and to model the non-equilibrium effects in the CWI at the core scale using the commercial reservoir simulators. These are amongst the main innovative aspects of this thesis.

The experimental results reveal that CWI under both secondary and tertiary recovery modes increase oil recovery and CO_2 storage with higher potential when using light oil, low salinity carbonated brine and mixed-wet core. In this study, the compositional simulator over-predicts the oil recovery. The instantaneous equilibrium and complete mixing assumptions appear to be inappropriate, where local equilibrium was not in fact achieved during the CW process at this scale. The author evaluated the use of the transport coefficient (the α-factor) to account for the dispersive mixing effects, and found that the approach gives a more accurate prediction of the CWI process.

For the gas-based CO_2 injection strategies, a practical yet comprehensive approach using reservoir simulation, Design of Experiment (DOE) and the Response Surface Model (RSM) to screen for and co-optimize the most technically and economically promising injection strategy for coupled EOR and CO_2 storage is presented. For the reservoir model used in this study, miscible WAG was found to be most economically promising, while miscible continuous CO_2 injection was ranked as the most technically viable. The duration of the preceding waterflood, relative permeability (wettability) and injected gas composition are the three most significant factors to the profitability of oil recovery and CO_2 storage through tertiary WAG injection.

Dedication

I wish to dedicate my thesis:

To my beloved husband, Nor Azman Januri, my daughter Nor Iman Izzaty and my son Nor Iman Hakim whose patience, understanding and encouragement were essential to the completion of this thesis.

To my parents, Haji Kechut Haji Anuar and Hajjah Ramlah Selamat for all their support, encouragement and especially for their unconditional loves and prayers.

To all my teachers and friends from whom I have learned.

Acknowledgements

Glory and praise be to Allah, the Most Beneficent, the Most Merciful.

First and foremost, I want to express my deep gratitude to my supervisors, Prof. Mehran Sohrabi and Dr. Mahmoud Jamiolahmady, for their guidance, encouragement, support and patience throughout my thesis work. This thesis could never be completed without their constructive criticism and help.

Special thanks to Mr. Shaun Ireland and Mr. Graeme Robertson for their help with the experiments. I appreciate the valuable inputs and feedback from all the steering committee members of Carbonated Water Injection JIP. I appreciate both my examiners; Dr Karl Stephen and Dr Reza Fassihi, for their useful suggestions and valuable feedback.

I would also like to thank my colleagues: Dr. Masoud Riazi, Hamidreza Shahverdi, Jamal M. Ibrahim and many others who have been sharing their knowledge, had numerous valuable discussions with me and lend their support during these few years. I would like also to acknowledge the excellent cooperation from the staff of the Computer Support and the John Archer Library of IPE.

I also owe a debt of gratitude to my husband, Nor Azman Januri, who has endured so much sacrifice throughout my study, for his love, understanding and continuous encouragement.

Finally, the financial support provided by PETRONAS and support from PETRONAS Research and PETRONAS Talent Sourcing & Mobility Department throughout my study is gratefully acknowledged.

Table of Contents

List of Figures

List of Tables

List of Publications

1. **Kechut, N.I.**, Riazi, M., Sohrabi, M. and Jamiolahmady, M.: Experimental and Numerical Evaluation of Carbonated Water Injection (CWI) for Improved Oil Recovery and CO_2 Storage, SPE 143005, SPE EUROPEC/EAGE Annual Conference and Exhibition, Vienna, Austria, 23–26 May 2011.

2. **Kechut N.I.**, Jamiolahmady M., Sohrabi M.: Numerical Simulation of Experimental Carbonated Water injection (CWI) for Improved Oil Recovery and CO_2 Storage, Journal of Petroleum Science and Engineering, 77 (1), 111-120, April 2011.

3. **Kechut, N.I.**, Riazi, M., Sohrabi, M. and Jamiolahmady, M.: Tertiary Oil Recovery and CO_2 Sequestration by Carbonated Water Injection (CWI), SPE 139667, SPE International Conference on CO_2 Capture, Storage, and Utilization held in New Orleans, Louisiana, USA, 10–12 November 2010.

4. Sohrabi M., **Kechut N.**, Jamiolahmady M. Ireland S. and Robertson G.: Coreflooding Studies to Investigate the Potential of Carbonated Water Injection as an Injection Strategy for Improved Oil Recovery and CO_2 storage, Journal of Transport in Porous Media, DOI 10.1007/s11242-011-9783-0, 2011.

5. Sohrabi, M., **Kechut N.**, Riazi M., Jamiolahmady M., Ireland, S and Robertson, G.: Safe storage of CO_2 Together with Improved Oil Recovery by CO_2-enriched Water Injection, accepted to be included in a special issue on Carbon Capture and Storage, Chemical Engineering Research and Design, DOI 10.1016/ j.cherd.2011.01.027.

6. Sohrabi, M., Riazi M., Jamiolahmady M., **Kechut N.**, Ireland, S and Robertson, G. and Brown, C.: Carbonated Water Injection (CWI) – A Productive Way of Using CO_2 for Oil Recovery and CO_2 Storage, International Conference on Greenhouse Gas Technologies (GHGT), RAI Amsterdam, The Netherlands, 19-23 September 2010.

Chapter 1

Introduction

1.1. Background

The theme of this thesis is CO_2 EOR and storage. Currently around 86% of the world primary energy use is supplied by oil, gas and coal and the demand is anticipated to increase with the increasing global energy consumption between now and 2030 (IEA, 2009). The increasing fossil fuel consumption irrefutably brings the damaging increase in the concentration of the anthropogenic greenhouse gases (GHG), particularly carbon dioxide (CO_2), which is believed to have contributed to the problem of global warming. As of December 2010, CO_2 concentration in the atmosphere has increased to 389 ppm (NOAA Research, 2011) from 380 ppm in 1994 (IPCC, 2007).

CO_2 from the burning of the fossil fuel represents the majority of the anthropogenic GHG emissions in the atmosphere, Figure 1.1. In 2006, slightly more than 29 million metric tons of CO_2 was released worldwide from the consumption and flaring of fossil fuels (IEA, 2006). The energy related CO_2 emissions was predicted to escalate from 27 Gt (gigatonnes) in 2005 to 42 Gt by 2030. Without proper mitigation measures the continuing increase in CO_2 concentration in the atmosphere could lead to a rise in global temperature with disastrous consequences for the climate (IEA, 2009).

Massive decarbonisation of the energy system by reducing our dependence on fossil fuels and increasing energy production from renewable resources is required if significant CO_2 emission reduction is to be achieved. However, the relevant measures such as energy conservation, energy efficiency improvement, and use of renewable resources (IEA, 2009), are either insufficient on their own at present, or take some time to be developed and applied at large-scale.

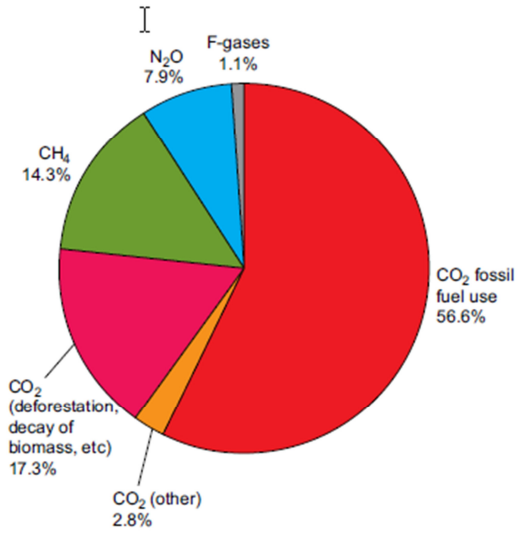

Figure 1.1: Global anthropogenic greenhouse gas emissions in 2004 (IPCC, 2007).

Continuing oil production is therefore necessary to provide time for other energy sources to be established to meet the increasing energy demand. However, conventional oil production generally is in the decline. The global output from the existing oil fields is predicted to drop by almost two-third by 2030 (World Energy Outlook, 2009). Most of the new discoveries are just small accumulations and exploration for new discoveries is becoming increasingly more difficult and costly.

Many reservoirs today are produced efficiently with water injection and have been for some time. However, after water flooding, quite a large volume of oil is still left in the reservoir. There is thus scope for processes that can unlock some of the remaining oil to maximise oil recovery from the existing reservoirs. Increasing the ultimate oil recovery from the available resources through enhanced oil recovery (EOR) methods is thus becoming more significant. EOR here is defined as the method of producing oil by the introduction of external fluids or the use of external energy into the reservoir fluid system to increase the oil production above the amounts that could be recovered during primary or secondary recovery.

CO_2 injection solely for EOR has been in practice for more than 40 years, and mostly in onshore oil reservoirs. The motivation for EOR is mainly to produce 65-75 % of the original oil in place (OOIP) remained in the reservoir after the conventional gas or water drives (van

Poolen, 1980). The remaining oil can either be bypassed due to poor sweep efficiency or trapped by capillary force as the consequence of the interfacial tension (IFT) between the oil and displacing fluid that prevents complete displacement. While the bypassed oil can be recovered by many improved oil recovery (IOR) methods such as production enhancement techniques, recompletion, workover or infill drilling and better reservoir management, the trapped oil however can only be mobilized and produced through EOR. The associated economic benefits of the trapped oil could be lost if EOR is not implemented.

In EOR, the target is to reduce the residual oil saturation to its lowest possible value, which gives the highest oil recovery. As shown in Figure 1.2, very low residual oil saturation can be reached if the capillary number becomes infinite, which in turn can be achieved when the IFT between the oil and the displacing fluid becomes zero i.e., when the two phases become miscible with each other. Miscible CO_2 flooding is one of the effective EOR techniques for achieving low IFT.

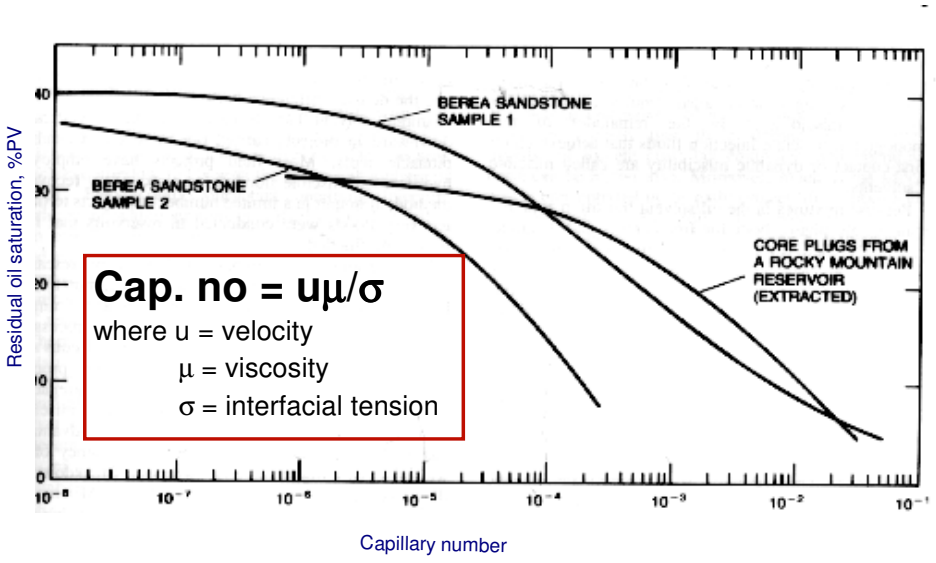

Figure 1.2: Dependence of residual oil saturation on capillary number (Stalkup, 1984).

The capture of man-made CO_2 and its subsequent storage in geological formations, such as deep saline aquifers, depleted oil and gas reservoirs and un-mineable coal beds, is one of the important, immediately available and technologically feasible strategies for achieving

substantial reductions in anthropogenic CO_2 emissions levels while enabling continued use of existing energy supply (IPCC, 2007).

Storing CO_2 through EOR is more likely to be implemented first even though saline aquifers represent a much larger storage capacity compared to hydrocarbon reservoirs. The revenue from the incremental oil, which may partly offset the CO_2 storage cost, the existence of an infrastructure, the wealth of data on the geological structure and physical properties of the reservoirs, the presence of proven structural traps to hold the injected CO_2 (Stevens et al., 2000, Bachu, 2008, Kuuskra and Ferguson, 2008), a more or less established legal and regulatory framework (Marston and More, 2008) as well as widespread expertise and experience in the industry, are amongst the main advantages of exploiting CO_2 EOR for CO_2 storage. Moreover, CO_2 injection can be continued after the end of the EOR phase, converting the oil reservoir into underground storage. IEA (2006) estimated that at the cost of \$20/t of CO_2 stored, approximately 130 Gt of CO_2 could be stored in depleted and depleting oilfields through CO_2 EOR worldwide.

1.2. Problem statement and research objectives

In view of the renewed global interest in CO_2 EOR for CO_2 storage, many other reservoir settings in addition to the conventional light oil reservoirs and injection strategies are being considered for CO_2 injection, especially those fit for offshore reservoirs or in cases where the supply of CO_2 can be variable or limited. This study looked into a water-based CO_2 EOR that could address this scenario as well as evaluated, through numerical simulation, the potential of various gas-based CO_2 injection methods for coupled EOR and CO_2 storage purpose.

1.2.1. Carbonated water injection

Gas-based CO_2 EOR is a more commonly studied and applied form of CO_2 injection in the field. One of the characteristics of these gas-based injection strategies, such as the CO_2

flooding, is that they require relatively large quantities of CO_2 and thus making them ideal as CO_2 storage measures. The most probable source of the anthropogenic CO_2 is from the coal-fired plants, which contribute approximately 40% of the total CO_2 emission (Key World Energy Statistics, 2009). However, the high cost associated with the capture, pressurization and transport of CO_2 from these plants (Bachu, 2008) and their location that is normally far from the oil fields, is unlikely to make the conventional CO_2 flooding using this CO_2 source economical. There are, however, smaller sources of anthropogenic CO_2 located closer to the candidate fields, such as CO_2 separated from natural or associated gas, or from refineries and petrochemicals plants, that might be available at much lower price.

CO_2 gas-based injections are also well-known to experience poor sweep efficiency due to the high mobility of the CO_2 gas as compared to the displaced oil bank. The adverse mobility ratio leads to undesirable gravity override, channelling and viscous fingering (Perkins et al., 1965; Juanes et al., 2007; Berenblyum et al., 2008), which in turn result in premature CO_2 breakthrough causing serious curtailment of oil production and requiring significant CO_2 separation and re-injection.

In this study, carbonated water injection (CWI) was investigated as an alternative injection mode with potential of exploiting smaller sources of CO_2 that could improve sweep efficiency and provide safe storage of CO_2. Despite its potential, this injection mode has not been very much studied, especially the experimental work related to CO_2 storage aspect. Most of the information was dated way back in the 1950s and 60s. Reported field implementation of CWI was mainly as the secondary recovery method. In spite of the extensive modelling studies reported on CO_2 EOR, very limited attempts of modelling CWI have been published.

The important contribution of this study would be therefore, to further understand the oil recovery mechanisms of CWI and to quantify the increase in the oil recovery and the amount of CO_2 stored by both secondary and tertiary CWI particularly for moderately viscous oil (81 and 145 cP). Through a series of high temperature and high pressure coreflood experiments using outcrop and reservoir cores at temperature and pressures typical of reservoir conditions, this research further adds to the knowledge about the effects of the oil viscosity, rock wettability and brine salinity on the performance of CWI. The results of CWI on

medium viscous oil are relatively novel in the industry as the limited information available in the literature thus far is only on light oils. Significant findings were recorded on the mixed wet case. Another contribution of this study is the quantification of CO_2 storage through CWI. The CO_2 front propagation was monitored to understand the behaviour of the dissolved CO_2 at the displacement front. This provides the evidence of diffusion/dispersion as one of the recovery mechanisms in CWI at the core scale and good delivery of CO_2 from CW to oil.

This research also assessed three compositional reservoir simulators namely E300, GEM and STARS for their suitability in modelling the CWI process, as no similar simulation study of the process, to the best of the author's knowledge, has ever been reported. The results of the study demonstrate that the inherent simultaneous equilibrium and complete mixing assumptions in the compositional reservoir simulators cannot adequately model the physics of CWI at the core scale. The use of the transient coefficient (α-factor) and several simulation approaches to model CWI process at the core scale were also examined.

1.2.2. Co-optimization of CO_2 EOR and storage

Most of CO_2 EOR projects to date are driven to improve oil production from the field only, without much regard to CO_2 storage. Consequently, despite the long successful history of CO_2 EOR implementation in the industry, requirements for integrating CO_2 EOR projects with CO_2 storage have not yet clearly established. Storing CO_2 through EOR in an oilfield not only aims to increase the oil recovery but also to maximize the amount of CO_2 left behind at the end of the recovery. These objectives are significantly different from maximizing the oil recovery alone and require optimization. Co-optimization in the flood design is therefore necessary for the integrated processes to be technically and economically viable.

In this thesis, a practical yet comprehensive approach was developed to screen for the most promising (technically and economically) CO_2 injection strategy for CO_2 EOR and storage. Using Design of Experiment (DOE) and the associated technique of Response Surface Model (RSM) to make effective use of reservoir simulation, this study examined the

requirements for an optimized CO_2 EOR coupled with storage by evaluating several gas-based CO_2 EOR injection schemes. Whilst almost all of the published studies were focusing on CO2I and conventional WAG injections only, this study also evaluated the potential of newly conceptualized intermittent WAG (INTWAG) injection and three other WAG injection schemes namely hybrid WAG (HYWAG), tapered WAG (TAPWAG) and selective simultaneous WAG (SSWAG) injection for EOR and CO_2 storage. The oil recovery and storage from these injection strategies were evaluated and ranked, based solely on technical viability as well as with the economic factors incorporated.

As optimization requires understanding of how all the pertinent operational factors interact to change the project response, a parametric simulation study was then carried out on the most favourable injection scheme to identify the influential factors on the oil recovery and CO_2 stored. The most influential flood design parameters were then optimized for maximum profit of the oil recovery and CO_2 storage.

1.3. Review of chapters

This thesis is divided into two main parts, with a total of seven chapters including this chapter. As there are remarkable amount of field and laboratory studies on CO_2 EOR and more recently on the combination of EOR and storage, the research was kicked-off with a literature review aimed at better understanding the major contributing factors affecting CO_2 injection into the depleting oil fields for both CO_2 EOR and storage. Chapter 2 presents some theories and the screening criteria of the processes. The available approaches, issues and challenges to implement the integrated project are reviewed. Background information on modelling the CWI process is also presented.

The two main parts are not explicitly related. Each of the chapters discussed slightly different aspects of CO_2 EOR and storage. The first main part of the thesis consists of Chapter 3 and Chapter 4, which deal with the experimental studies and numerical simulation studies of CWI as a water-based CO_2 injection technique, respectively. A thorough discussion from the literature on CWI from both EOR and CO_2 storage perspectives is first given in Chapter 3, followed by details on the CWI coreflood experimental facilities,

procedures and results. This chapter ends with a discussion on the potential of CWI application in the North Sea reservoirs. In Chapter 4, the simulation study of the CWI process is presented. This involves the evaluation of three commonly used compositional reservoir simulators and the alternative approaches in modelling CWI process. A simulation approach to appropriately model the CWI at the core scale is also presented.

Chapters 5 and 6 represent the second part of the thesis, concentrating on the evaluation of several gas-based CO_2 injection strategies for EOR and storage and examine the co-optimization of enhancing oil recovery and storing CO_2 from technical and economic point of view. In Chapter 5, advantages and drawbacks of several commonly used CO_2 injection strategies are reviewed. Details are also given of the compositional reservoir simulations of various CO_2 injection strategies in finding the one with the highest potential for co-optimizing the profitability of the oil recovery and CO_2 storage. The author also discusses on the potential of a newly conceptualised injection scheme, the intermittent WAG (INTWAG) injection, as an EOR and CO_2 storage injection strategy in this chapter.

Chapter 6 deals with the investigation of the factors affecting the performance of CO_2 EOR and storage of the selected injection scheme identified in Chapter 5 in both homogeneous and heterogeneous reservoirs. One of the main outcomes from this investigation is the identification of the most influential factors of the coupled process using the selected injection scheme to the oil recovery and CO_2 stored. Based on the identified influential operational factors, the co-optimization of the integrated CO_2 EOR and storage process using a real reservoir model is then detailed.

The thesis is concluded with Chapter 7 with a summary and conclusions drawn from the current research work. Recommendations for future research work are also given.

1.4. References

[1.1] Bachu, S.: CO_2 Storage in Geological Media: Role, Means, Status and Barriers to Deployment, Progress in Energy and Combustion Science, 34, 254-273, 2008.

[1.2] Berenblyum, R., Calderon, G., Kollbotn, L., and Surguchev, L.M.: Modelling CO_2 Injection: IOR Potential after Waterflooding, SPE 113436, SPE/DOE Symposium on Improved Oil Recovery, Tulsa, Oklahoma, 2008.

[1.3] Bryant, S.: Geologic CO_2 Storage - Can the Oil and Gas Industry Help Save the Planet?, J. Petroleum Technology, Vol. 59, 9, 98-105, 2007.

[1.4] Burton, M. and Bryant, S.L.: Eliminating Buoyant Migration of Sequestered CO_2 through Surface Dissolution: Implementation Costs and Technical Challenges, SPE 110650, SPE Annual Technical Conference and Exhibition, Anaheim, California, U.S.A, 11-14 November 2007.

[1.5] Christensen, J.R., Stenby, E.H. and Skauge, A.: Review of WAG Field Experience, SPE 110650, International Petroleum Conference and Exhibition of Mexico, Villahermosa, Mexico, 3-5 March 1998.

[1.6] Forooghi, A., Hamouda, A.A and Eilertsen, T.: Co-optimization of CO_2 EOR and Sequestration in a North Sea Chalk Reservoir, SPE 125550, SPE/EAGE Reservoir Characterization and Simulation Conference, 19-21 October 2009.

[1.7] Ghomian, Y., Pope, G.A. and Sepehmoori, K.: Hysteresis and Field-Scale Optimization of WAG Injection for Coupled CO_2-EOR and Sequestration, SPE 110639, SPE/DOE Improved Oil Recovery Symposium, Tulsa, Oklahoma, 2008.

[1.8] Hebach A., Oberhof, A. and Dahmen, N.: Density of Water + Carbon Dioxide at Elevated Pressures: Measurements and Correlation, J. Chem. Eng. Data, 49, 950-953, 2004.

[1.9] Hickok C.W. and Ramsay H.J.: Case Histories of Carbonated Waterfloods in Dewey-Bartlesville Field, SPE 333, SPE Secondary Recovery Symposium, Wichita Falls, Texas, 7-8 May 1962.

[1.10] Hickok C.W., Christensen, R.J. and Ramsay H.J.: Progress Review of the K&S Carbonated Waterflood Project, J. Petroleum Technology, Vol. 12, 20-24, 1960.

[1.11] Holm, L.W.: CO_2 Requirements in CO_2 Slug and Carbonated Water Oil Recovery Process, Producers Monthly, September 1963.

[1.12] International Energy Annual 2006 available at http://www.eia.doe.gov/iea/overview.html, accessed on 19th February 2009.

[1.13] International Energy Agency, Key World Energy Statistics, © OECD/IEA, 2008.

[1.14] International Energy Annual 2006, http://www.eia.doe.gov/iea/overview.html, accessed on 19th February 2009.

[1.15] IEA/CSLF Report to the Muskoka 2010 G8 Summit, Carbon Capture and Storage Progress and Next Steps, 2010.

[1.16] IPCC Fourth Assessment Report Working Group III, Climate Change 2007: Mitigation of Climate Change in Metz, B., et al. (Eds), Cambridge University Press, Cambridge, United Kingdom, 2007.

[1.17] IPCC Working Group III: Special Report on Carbon Dioxide Capture and Storage: Metz, B. et al. (Eds), Cambridge University Press, 2005.

[1.18] Juanes, R. and Blunt, M. J.: Impact of Viscous Fingering on the Prediction of Optimum WAG Ratio, SPE Journal, Vol. 12, No. 4, 486-495, 2007.

[1.19] Kovscek, A. R. and Cakici, M. D.: Geological Storage of Carbon Dioxide and Enhanced Oil Recovery II: Cooptimization of Storage and Recovery, Energy Conversion & Management, 46, 13, 2005.

[1.20] Kuuskraa, V. A. and Ferguson, R.: Storing CO_2 with Enhanced Oil Recovery, DOE/NETL-402/1312/02-07-08, 2008.

[1.21] Marston, P. M. and Moore, P. A.: From EOR to CCS: The Evolving Legal and Regulatory Framework for Carbon Capture and Storage, Energy Law Journal, Vol. 29, 421-489, 2008.

[1.22] NOAA Research: Trends in Atmospheric Carbon Dioxide, available at http://www.esrl.noaa.gov/gmd/ccgg/trends/, accessed on 21 January 2010.

[1.23] Perkins, T.K., Johnston, O.C. and Hoffman, R.: Mechanics of Viscous Fingering in Miscible Systems, SPE Journal, 5, 17, 1965.

[1.24] Preston, C., Monea, M., Jazrawi, W., Brown, K., Whittaker, S., White, D., Law, D., Chalaturnyk, R. and Rostron, B.: IEA GHG Weyburn CO_2 Monitoring and Storage Project, Fuel Processing Technology 86, 1547-1568, 2005.

[1.25] Qi, R., La Force, T. C. and Blunt, M. J.: Design of Carbon Dioxide Storage in Oilfields, SPE 115663, SPE Annual Technical Conference and Exhibition, Denver, Colorado, USA, 2008.

[1.26] Ramsay, H.J.J. and Small, F.R.: Use of Carbon Dioxide for Water Injectivity Improvement, Journal of Petroleum Technology, 25, 1964.

[1.27] Sohrabi, M., Riazi, M., Jamiolahmady, M., Ireland, S. and Brown, C.: Mechanisms of Oil Recovery by Carbonated Water Injection, SCA2009-26, International Symposium of the Society of Core Analysts, Noordwijk, the Netherlands, 27-30 September, 2009.

[1.28] Stevens, S.H., Kuuskra, V.A. and Taber, J.J.: Sequestration of CO_2 in Depleted Oil and Gas Fields: Barriers to Overcome in Implementation of CO_2 Capture and Storage (1) – Storage in Disused Oil and Gas Fields, Report PH3/22/IEA/CON/98/31, 2000.

[1.29] World Energy Outlook 2009 fact sheet, International Energy Agency, http://www.worldenergyoutlook.org/docs/weo2009/fact_sheets_WEO_2009.pdf, 2009.

[1.30] Worldwide EOR Survey, Oil & Gas Journal, April 2008, Vol. 106, 15, 2008.

Chapter 2

Literature Review

2.1. Introduction

This chapter presents an overview of CO_2 EOR and CO_2 storage processes in near-depleted oil reservoirs. Basic properties of CO_2 are given first, followed by a review of the screening criteria and the main mechanisms involved in CO_2 EOR and storage processes. Next is a brief review of CO_2 sources, CO_2 capture technology, reservoir selection, implementation approaches as well as issues and challenges in implementing the coupled CO_2 EOR and storage process. Finally, a review of models of CWI process is also given.

2.2. CO_2 properties

When CO_2 contacts the fluids in the reservoir, mass transfer will occur bringing about the changes in the fluid properties, which in turn mainly depends on the reservoir pressure, temperature and the composition of the reservoir fluids. Understanding the phase behaviour of CO_2 and the reservoir fluids is therefore essential in order to accurately model the CO_2 EOR and storage processes, especially since the reservoir pressure will change throughout the life of the project.

At room pressure and temperature, CO_2 exists as a thermodynamically stable gas phase with density of 1.872 kg/m^3; heavier than that of air (Vesovic et al., 1990). CO_2 reaches supercritical conditions at 1030 psig (7.377 MPa) and 87.8 ^{o}F (31 ^{o}C), at which it behaves like a gas but has a liquid-like density. It is a good solvent for oils at typical reservoir pressures and temperatures. Increasing pressure and decreasing temperature increase CO_2

solubility in oil (Simon, 1964). CO_2 EOR and storage processes would normally involve injecting CO_2 at its supercritical state. In this thesis, the term CO_2 gas is used to refer to the gas in the form of a "supercritical fluid" unless otherwise stated. Figure 2.1 shows the phase plot of CO_2 calculated by the Peng Robinson Equation-of-State (PREOS) (PVTi, 2007.1) while Figure 2.2 shows the CO_2 density and viscosity as a function of pressure and temperature.

Figure 2.3 shows pressure, temperature and salinity effect on solubility of CO_2 in water, (Baviere, 1991). CO_2 solubility in water increases with pressure but inversely related to temperature and brine salinity. The increase in CO_2 solubility is more pronounced at lower pressure. CO_2 has the highest solubility in water as compared with hydrocarbon gases found in the oil and gas fields (e.g., Bando et al., 2003). It is this property that leads to CO_2 sequestration in the saline aquifer being extensively pursued as one of the Carbon Capture and geological Storage (CCS) strategies. CCS is "*the removal of CO_2 directly from anthropogenic sources (capture) prior to potential release and its disposal in geological media, either permanently (sequestration) or for significant time periods (storage)*" (Bachu, 2008). It involves separation and capture of the CO_2 from large stationary sources such as power plants and refineries, transportation to a storage site and isolation from the atmosphere for long periods of time, in the order of centuries to millions of years.

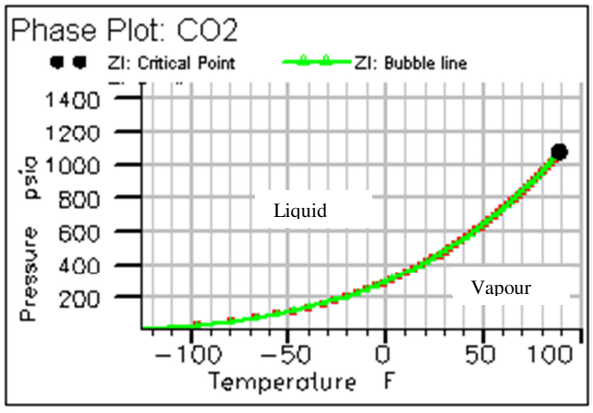

Figure 2.1: Phase plot of CO_2 showing the critical point.

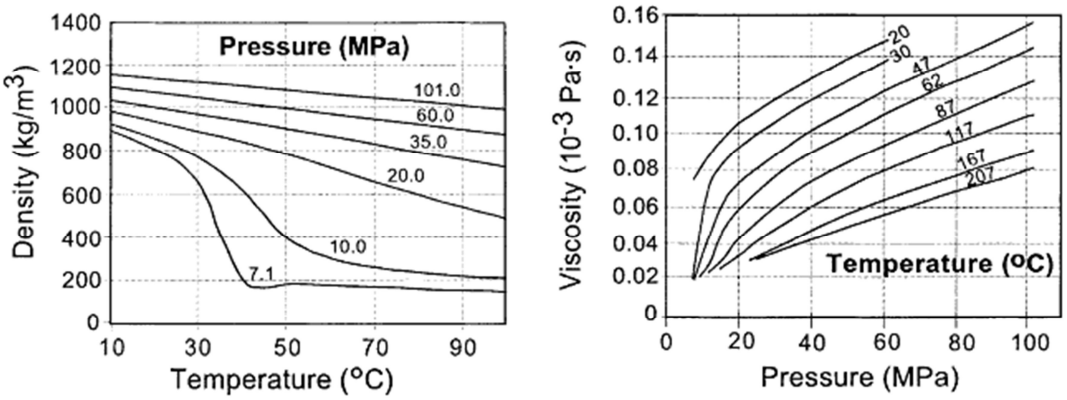

Figure 2.2: CO_2 density and viscosity as a function of temperature and pressure (Bachu, 2002).

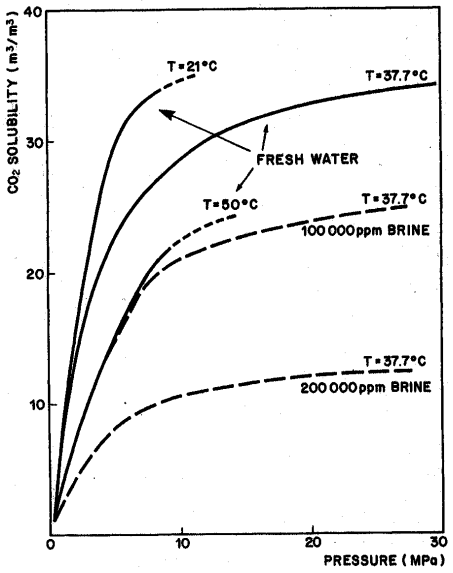

Figure 2.3: The effect of pressure, temperature and salinity on CO_2 solubility in water (Baviere, 1991).

2.3. CO_2 Enhanced Oil Recovery and Storage

2.3.1. The target resources

The application of CO_2 EOR is influenced by the availability of suitable resources. The most suitable EOR process for a reservoir depends largely on the depositional environment

of the reservoir, fluid properties, and reservoir pressure, temperature and heterogeneity (Taber et al., 1983, 1997). CO_2 EOR is suitable for reservoirs having oil gravity greater than 22 ^{o}API (oil density < 920 kg/m^3), viscosity less than 10 cP and depth of 600 m (2500 feet) or more, which relates to the pressure at which CO_2 is in supercritical condition (Taber et al., 1983; Rivas and Bolivar, 1994).

Field experiences indicate that the remaining oil saturation should be at least 25% or $S_o\phi$ where ϕ is the porosity, between 0.05-0.07 (Kovscek, 2002) for economic success. A large gas cap is not favourable for CO_2 EOR due to the large amount of gas which needs to be injected to reach the minimum miscibility pressure (MMP). MMP, more details are given later, is the minimum pressure at which the injected gas becomes miscible with the reservoir oil. The oil achieves dynamic miscibility with CO_2 at relatively lower pressure than with natural gas, flue gas or nitrogen (Stalkup, 1984). The vertical heterogeneity (reflected in the vertical to horizontal permeability ratio, k_v/k_h) is also very important, as it controls the rate at which CO_2 segregates. Since fractures provide conduit from the injection to the production well resulting in early gas breakthrough and hence poor sweep efficiency, highly fractured reservoirs are not preferred. Thin reservoirs might have an advantage of lesser gravity override but thick reservoirs are advantageous in terms of oil volume (Jarrel et al., 2002).

Despite the wide variety of factors which can affect the suitability of reservoirs for CO_2 EOR, it is one of the most commonly used gas injection EOR techniques in the world particularly in the onshore United States (US) oilfields, where abundant natural resources of CO_2 are available. The process, nevertheless, has not been used at field scale offshore, so far. In 2008, there were 72 active CO_2-floods worldwide producing around 206,000 bpd of incremental oil (Oil & Gas Journal, 2008). The US Department of Energy (US DOE, 2006) predicted that as much as 43 billion barrels of "stranded" oil in six basins and areas in the US could become technically recoverable by this EOR method.

The literature review indicates that the field application of CO_2 EOR will be successful if the candidate reservoir meets the technical criteria for miscible flooding and favourable economic factors, such as having reliable sources of CO_2 at affordable costs, appropriate oil price and availability of capital and technical expertise. More often applied as tertiary oil recovery method, successful CO_2 injections can yield 7-23% of OOIP in additional oil recovery (Martin, 1992; Christensen et al., 1998; Rogers and Grigg, 2000).

Most of the CO_2 EOR projects to date are designed and implemented to increase the oil production and to extend the productive life of the assets with additional reserves. But much of this injected CO_2 remains trapped in the reservoir and this presents an opportunity to employ EOR as CO_2 storage strategy. Holt and Lindeberg (1993) estimated that the world technical CO_2 storage potential in petroleum reservoirs corresponds to two thirds of the CO_2 produced by combustion of the reserves. A study by Kuuskraa et al. (2008) identifies 39 to 48 billion barrels of incremental oil could economically be produced and 5 to 6 Mcf of CO_2 per barrel of oil is used by timely application of CO_2 EOR technology in the US, while Bergen et al. (2004) identify 420 possible CO_2 EOR opportunities for CO_2 capture and storage/sequestration worldwide.

Unlike the CO_2 EOR process, for which the screening criteria are based on the history of successful projects worldwide, no similar data is yet available for coupled CO_2 EOR and storage projects. Since the oil production in the miscible displacement is highest, and thus can offset the cost of storage more, it is expected that miscible CO_2 EOR is aimed for in the coupled process. The screening criteria, particularly the fluid properties, favourable for miscible CO_2 EOR should be preferred for the coupled process as well (Kovscek, 2002; Holtz, 2009). However, the immiscible CO_2 injection may also be economically viable if the sequestration capacity of the reservoir is large. The candidate reservoir must also have the capacity to store the intended volume of CO_2 over the life of the project and the necessary injectivity to take in the CO_2 at the rate that it is supplied from the source. The integrity of the reservoirs' containment also needs to be ascertained.

Kovscek (2002) has proposed screening criteria for coupled EOR and CO_2 storage encompassing the geophysical, reservoir engineering and surface facilities aspects of the process (Table 2.1). Specific sequestration capacity as described by Equation 2.1 was used to compare various reservoirs with respect to depth, porosity and moveable fluid saturation.

$$C = \rho(1 - S_{or} - S_{wir})\emptyset + S_{wir}\emptyset C_s \tag{2.1}$$

where C is the sequestration capacity of the rock expressed as the mass of CO_2 per volume of rock (kg-CO_2/m^3-rock), ρ is the density of CO_2 (kg/m^3) as a function of pressure and temperature, S_{or} is the residual oil saturation (in fraction), S_{wir} is the irreducible water saturation (in fraction), ϕ is the porosity (in fraction) and C_s is the mass of CO_2 dissolved per

unit volume of water (kg-CO_2/m^3). From this equation, high CO_2 density, reservoir porosity and fraction of moveable fluids are favourable for CO_2 storage.

Table 2.1: Screening criteria for anthropogenic CO_2 EOR and CO_2 sequestration (Kovscek, 2002).

Reservoir properties	Positive indicators	Cautionary indicators
$S_o\phi$	≥ 0.05	< 0.05 - Consider filling reservoir voidage if capacity is large.
kh (m^3)	$\geq 10^{-14} - 10^{-13}$	$<10^{-14}$ if kh is less, consider whether injectivity will be sufficient.
Capacity (kg/m^3)	>10	< 10
Pre pressure gradient (kPa/m)	≤ 17.4	> 17.4
Location	Divergent basin	Convergent basin
Seals	Adequate characterization of caprock; minimal formation damage.	Areas prone to fault slippage.
Oil properties		
ρ (°API)	> 22	< 22 - Consider immiscible CO_2 EOR, fill reservoir voidage if C is large.
μ (mPas)	< 5	> 5 - Consider immiscible CO_2 EOR.
Composition	High concentration of C_5-C_{12}, relatively few aromatics.	
Surface facilities		
Corrosion	CO_2 can be separated to 90% purity economically.	H_2O and H_2S concentration above 500 ppm each.
Pipelines	Anthropogenic CO_2 source is within 500 km of a CO_2 pipeline or oilfield.	Source to sink distance is more than 500 km.
Synergy	Pre-existing oil production and surface facilities expertise.	Little or no expertise in CO_2 EOR within a geographic region.

Injectivity is directly proportional to permeability and affected by the reservoir thickness, therefore, the product of permeability and thickness, kh, is also used as a screening parameter, which value should preferably be greater than 10^{-14} m^3. It is also crucial that the

overlying caprock of the reservoir still provides an effective seal: it is favourable if the reservoir is located in a divergent basin and adequate characterization of the caprock has been carried out. Other criteria are shown in Table 2.1. Rock compressibility and water salinity have also been found to influence the storage processes (Codreanu and Gallo, 2003; Jessen et al., 2005).

Shaw and Bachu (2002) developed an analytical method and a ranking procedure to rapidly estimate oil recovery and CO_2 storage for a large number of reservoirs prior to engineering and economic evaluation. They screened 8,637 oil reservoirs, based on technical criteria for application of CO_2 EOR published by various authors, which include the oil gravity and viscosity, reservoir depth, temperature and pressure, MMP and remaining oil saturation, to determine their suitability for CO_2 flooding. Then the incremental oil recovery at breakthrough and the reservoir capacity for CO_2 sequestration were estimated. Weights were assigned to technical and reservoir performance parameters and the reservoirs were ranked according to the final score. They found that the top ranked reservoirs are characterized by light oil, high initial reservoir pressure, low-range reservoir temperature, and low heterogeneity.

Damen et al. (2005) used a more or less similar approach of multi-criteria analysis of weighted summation to select and rank the oilfields for CO_2 sequestration. They extended the criteria used to include the techno-economic aspect such as emission source and socio-economic criteria like the population density and the quality of government. For each weight factor a higher total score indicates the more promising opportunity.

2.3.2. Mechanisms of oil recovery and CO_2 storage

Depending on the pressure and temperature of the reservoir during injection, CO_2 flooding can be a miscible, near miscible or immiscible process. Figure 2.4 shows the pressure-temperature region of applicability of CO_2 injection and the corresponding simulation technique (in brackets) appropriate for the region whether by black oil or compositional model (Klins, 1984).

For optimal displacement efficiency, CO_2 flooding should be conducted at pressures greater

than the MMP. At or above the MMP, CO_2 dynamically develops miscibility as it mixes with the oil in the porous media, where a mixing zone between oil and CO_2 is developed at the displacement front. The supercritical CO_2 vaporizes the lighter oil fractions of the oil into the CO_2 phase, creating a CO_2-rich phase and an oil-rich phase. As the mass transfer between the CO_2 and the oil continues, the CO_2-rich phase becomes heavier and is a better solvent than the originally injected CO_2, extracting heavier portions of the oil. Eventually, the fluid properties of the two mixtures become identical. Gardner and Ypma (1984) reported that the capillary forces, which initially hold the oil immobile, diminish as miscibility is reached. The resulting single phase fluid has improved mobility to flow to the producing well.

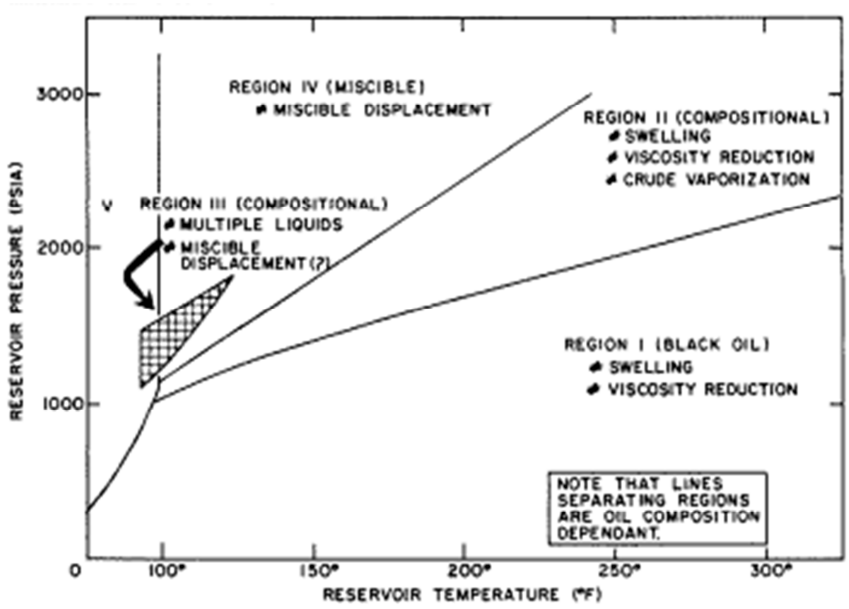

Figure 2.4: The effect of reservoir temperature and pressure on CO_2 injection displacement mechanisms and the applicable simulation technique (Klins, 1984).

The overall recovery efficiency, E_R, of the CO_2 flood, described by Equation 2.2, is governed by microscopic and macroscopic displacement efficiency (Klins, 1984) *viz*:

$$E_R = E_A.E_V.E_D.E_M \tag{2.2}$$

where E refers to efficiency, while subscripts A, V, D and M refer to areal sweep, vertical sweep, displacement and mobilization, respectively. The displacement efficiency, which is the fraction of mobile oil being swept, is defined by Equation 2.3:

$$E_D(V_{pi}) = \frac{S_{oi} - \bar{S}_o}{S_{oi} - S_{orp}} \tag{2.3}$$

where S_{oi} is the initial oil saturation, S_{orp} is the ultimate residual oil, $\bar{S}_o$ is the average oil saturation in the swept zone and V_{pi} is the pore volume injected.

The microscopic displacement efficiency (E_D) is greatly influenced by the solubility of CO_2 in the oil, which in turn is strongly influenced by pressure, temperature, the oil composition, purity of the injected CO_2 stream, reservoir heterogeneity and gravity segregation (Klins, 1984). We can see from Equation 2.3 that the displacement efficiency is high when the residual oil saturation is low, as in the miscible displacement.

The macroscopic sweep efficiency is affected by the areal and vertical sweep efficiencies. The areal sweep efficiency (E_A) is "*the fraction of the total reservoir area that is invaded by the injected fluid*" (Klins, 1984) and is affected by permeability variations in the reservoir rocks, the mobility ratio, the injection-production well patterns and the injection scheme used (Araktingi et al., 1990). Mobility ratio, M, measures the mobility of the displacing phase relative to that of the displaced fluid:

$$M = \frac{(k_r/\mu)_{ing}}{(k_r/\mu)_{ed}} \tag{2.4}$$

where k_r is the relative permeability and μ is the viscosity. At M greater than 1, the injected fluid has higher mobility than the displaced fluid, leading to viscous instability or preferential flow of the injected phase through the oil. Caudle and Witte (1959) showed that the areal sweep efficiency for a five-spot pattern decrease as the mobility ratio increases and for any given M, areal sweep efficiency increases with continued injection after breakthrough.

Vertical sweep efficiency, E_V, is the fraction of the vertical section of a reservoir that has been contacted by the injected fluid. It is affected by the viscous/gravity ratio, Equation 2.5, dip angle, and vertical heterogeneity (Gardner and Ypma, 1984).

$$R_{v/g} = \left(\frac{u\mu_o}{kg\Delta\rho}\right)\left(\frac{L}{h}\right) \tag{2.5}$$

where u the Darcy velocity, μ_o the oil viscosity, L the distance between wells, k the permeability, g the gravity force, $\Delta\rho$ the density difference between the fluids and h the height of the displacement zone.

Figure 2.5 shows the breakthrough sweep-out efficiency as a function of viscous/gravity ratio and mobility ratio for miscible displacement at irreducible water saturation. For a given mobility ratio, increasing the viscous/gravity ratio increases the sweep efficiency whilst the efficiency reduces with increasing mobility ratio. In Region I, the flow is characterized by a single gravity tongue overriding the oil. In Region II, the single gravity tongue persists but the vertical sweep out becomes independent of viscous/gravity ratio until a critical value is reached. Secondary fingers start to form beneath the gravity tongue in Region III where increasing the viscous/gravity ratio increases the vertical sweep out efficiency markedly. At very high viscous/gravity ratio in Region IV, displacement is dominated by multiple fingering across the cross section (Stalkup, 1983).

Gravity override (or tonguing) develops when the fluid velocity, u, is higher than the critical rate, u_c, given by Equation 2.6. Vertical sweep is dominated by viscous fingering at rates exceeding the critical rate, which is given by:

$$u_c = \frac{(\rho_o - \rho_g)}{\left(\frac{\mu_o}{k_o} - \frac{\mu_g}{k_g}\right)}(g.sin\theta) \tag{2.6}$$

where ρ is the density, μ is the viscosity, k is the endpoint relative permeability and θ is the dip angle (Klins, 1984).

Inefficient sweep and filling the reservoir voidage causes part of the injected CO_2 left in the reservoir. Four trapping mechanisms i.e., stratigraphical/structural, residual, solubility and mineral trapping maybe involved (Bachu et al., 1994). CO_2 is less dense than the oil and formation water even at supercritical state, thus, it rises upwards but is prevented from moving further upward by the structural trap, such as the top of an anticline, or a tilted fault block along the flow pathway (structural trapping). However, CO_2 is still in the mobile

phase and leakage from the formation can occur if the sealing is compromised.

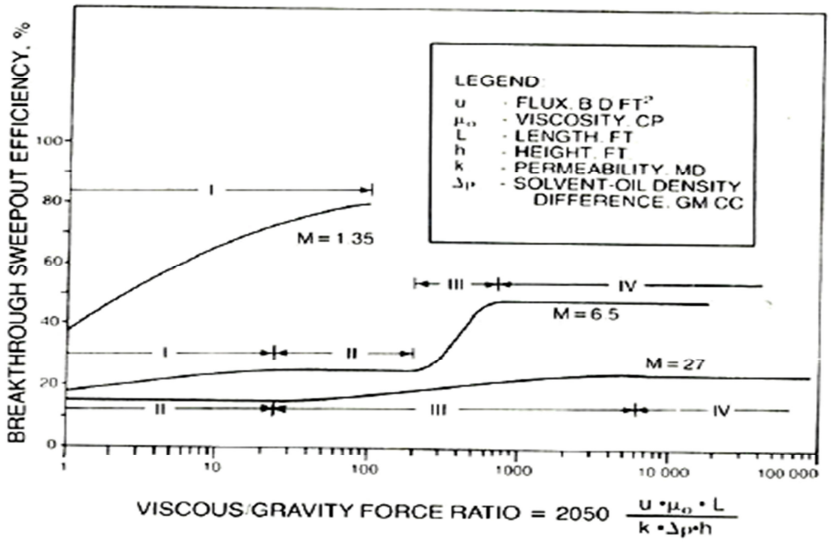

Figure 2.5: Schematic of the flow regimes in a 2D, uniform linear system (Stalkup, 1983).

CO_2 can also be hold in place by solubility trapping through its dissolution in oil and formation water. When dissolved in water, CO_2 reacts with water to form carbonic acid ($CO_2 + H_2O \rightleftharpoons H_2CO_3$) with a pH between 3 and 4. The carbonic acid reacts with the minerals of the rock, causing dissolution of mineral components as well as precipitation of carbonate minerals such as calcite, dolomite and siderite (Bachu et al., 1994; Linderberg et al., 2002; Nghiem et al., 2009). CO_2 trapped in the form of carbonate (mineral trapping) is considered the safest form of storage as the immobile gas can be kept away from the caprock but this is a very slow process that may take thousands of years.

Part of the injected CO_2 is also stored in empty pores in the rock that were once filled with oil. Maximizing the oil production would ideally maximize the volume available for storage. Some of the CO_2 bubbles are snapped-off and trapped in pore spaces between the rock due to capillary force from the water particularly in low permeability reservoirs (residual trapping or capillary trapping). Injecting water alternating with or after the CO_2 injection is found to accelerate this trapping (Juanes et al., 2006; Qi et al., 2008).

2.3.3. CO_2 sources and capture technology

Adequate and continuous source of the CO_2 gas is crucial to the implementation of CO_2 EOR in the field. Most of the major CO_2 EOR projects in the US, such as the Permian Basins in West Texas, benefit from natural CO_2 supply from Colorado and New Mexico (US DOE, 2011). However, new capture technologies enable CO_2 from industrial applications such as natural gas processing, power generation, and petrochemical plants to be used for EOR in locations where naturally occurring reservoirs are not available. In 2008, 17% of the CO_2 used for EOR in the US came from the anthropogenic sources (Moritis, 2010).

The coal-fired plants, cement manufacturing and petroleum refinery are the three biggest contributors to CO_2 emission followed by the steel and petrochemicals industry (World Energy Outlook, 2009). However, not all of these sources are applicable to EOR. Apart from impurities in the gas stream that imposes significant increase in capture and separation costs, the long distance from the candidate oil reservoirs further prohibits some man-made CO_2 from being used in the EOR application.

Another source of CO_2 is the CO_2 produced offshore as a by-product of oil extraction or high-CO_2 gas fields production. However, smaller volumes and inaccessibility makes this source of CO_2 more unlikely to be captured for conventional CO_2 EOR than that generated onshore. Furthermore, offshore platforms are space-constrained to accommodate the necessary infrastructure for capturing and separating the CO_2, hence necessitates extensive investment in platform extension. But, this source of CO_2 can be exploited for the non-conventional CO_2 injection such as the CO_2-enriched water injection, which the author will discuss in more detail in the next chapter.

The number of field scale CO_2 EOR using anthropogenic CO_2 is presently still limited, but is increasing. Examples include the Weyburn-Midale project where 1 Mt of CO_2 from a coal gasification plant was injected per year (Preston et al., 2005), the Rangely Weber Sand project, which is supplied by the La Barge gas processing plant in Southwest Wyoming, and the Salt Creek project (Anadarko, 2010). There are plans for similar project in the Daqing and Liaohe fields in China (NETL, 2010), the Hobbs carbonate oil field in New Mexico and the Northwest McGregor Oil Field (Carbon Capture Journal, 2011). In the North Sea, the CENS project plans to bring man-made CO_2 from factories and power stations around the

North Sea Basin to depleted oilfields for EOR.

Most of the anthropogenic CO_2 sources emit CO_2 streams diluted with contaminants such as hydrogen sulphide, hydrogen cyanide, ammonia, particulates and alkali (CCSTRM, 2006). The CO_2 partial pressure would be low and this increases the cost of compression and transportation of the gas. Moreover, the contaminants would also increase the MMP that adversely affect the oil recovery. Thus, the CO_2 needs to be separated from the other components before it can be used for EOR or stored. For economy of scale, the capture process is applicable only to major CO_2 source points such as energy generation and industrial plants. In the U.K, capturing and storing from 85% of the largest 25 industrial sources would contribute to a 17% reduction in total U.K emission (POST, 2005).

CO_2 capture technologies available can be classified as post-, pre- and oxy-combustion capture, which could involve either chemical or physical absorption or adsorption, membranes or cryogenic fractionation (Feron, 2005; Ravagnani, 2007; Figueroa et al., 2008). The pre-combustion process involves the extraction of carbon from the fuel before the fuel is combusted for energy generation (Aasen et al., 2004). The separation is carried out by integrated coal-fired combined cycle systems or natural gas-fired combined cycle systems that convert the fossil fuel to a hydrogen rich stream and a carbon rich stream. In the post-combustion processes, CO_2 is recovered from flue gases through chemical cleansing using an absorbent such as monoethanolamine (MEA) solution. The oxy-fuel combustion uses oxygen in the separation process that could results in almost all the CO_2 being removed.

Hendriks et al. (2004) and Damen et al. (2005) estimated the typical costs of CO_2 capture for power plants and industrial sources are more or less within the same range of \$37-\$62/tCO_2 and \$40-\$60/tCO_2 avoided, respectively. The costs mainly depend on the capture system used, which in turn depends on many factors such as the partial pressure of CO_2 in the gas stream, the recovery and purity of the CO_2 required. If we look from capture system point of view, the cost ranges approximately from \$50-\$70/tCO_2 captured for post-combustion systems, to \$20-\$50/tCO_2 captured for pre-combustion and to \$13-\$80/tCO_2 captured for oxy-fuel combustion (Thambimuthu, 2004 as quoted in CCSTRM, 2006). The oxy-fuel combustion seems much cheaper since the input gas has high CO_2 concentration. Most of the approaches available are nevertheless still under investigation or at the stage of development not economically feasible on a large-scale CO_2 capture due to high use of

energy.

The high cost associated with the capture of CO_2 from these plants, its pressurization and transport dominates the CCS cost and is one of the key barriers to the introduction of CO_2 sequestration technology (Bergen et al., 2004; Bachu, 2008). This is where the revenue from the additional oil recovery is advantageous to offset some of these costs. Many research and development projects in reducing the CO_2 capture costs are directed towards the use of membrane, cryogenic and amine process (Steven and Gale, 2000). A recent development includes a post-combustion VeloxoTherm™ technology that uses a proprietary structured adsorbent that is able to capture CO_2 from industrial flue gas streams for US$15 per tonne of CO_2 (http://www.inventysinc.com/technology/). Other related initiatives are the Basic Immobilized Amine Sorbent (BIAS) process that uses low-cost, regenerable, solid CO_2 sorbents (NETL, 2011) and European CO_2 Test Centre at Mongstad, Norway, built to test improved CO_2 capture technology (Kaarstad, 2008).

2.3.4. Implementation approach

In traditional CO_2 EOR, the flood is designed to minimize the CO_2 retention and the decommissioning of the project usually involves reservoir depressurisation (blowdown) to maximize oil recovery (Irwin and Batycky, 1997). This is not beneficial for the CO_2 storage since only a minimum amount of CO_2 remains stored in the immobile phases in the reservoir. Storing CO_2 through EOR implementation requires different injection/production designs and strategies as compared with those for CO_2 EOR or CO_2 storage alone. For coupled EOR and storage, it is envisaged that early in the CO_2 injection phase, the aim is to optimize the oil recovery, which is later switched to maximising the amount of CO_2 stored towards the end of the project. This will looked at in more detail in Chapter 5 and 6.

The author is of the opinion that with some additions of appropriate parameters, the parameters for the injection design and their interaction for CO_2 sequestration in a deep saline aquifer suggested by Davis et al. (2001) and by Bachu (2002), shown in Figure 2.6 and 2.7, respectively, are relevant to and can be adopted for integrated CO_2 EOR and storage projects. These additional design parameters may include the technical screening criteria for

the miscible displacement as discussed earlier, the estimates of the oil recovery and the amount of CO_2 stored, the number of wells required to inject the CO_2 and the best injection strategy (location and intervals, injection pressure, injection rate and, injection pump requirement, economics) that results in co-optimized oil recovery and CO_2 storage.

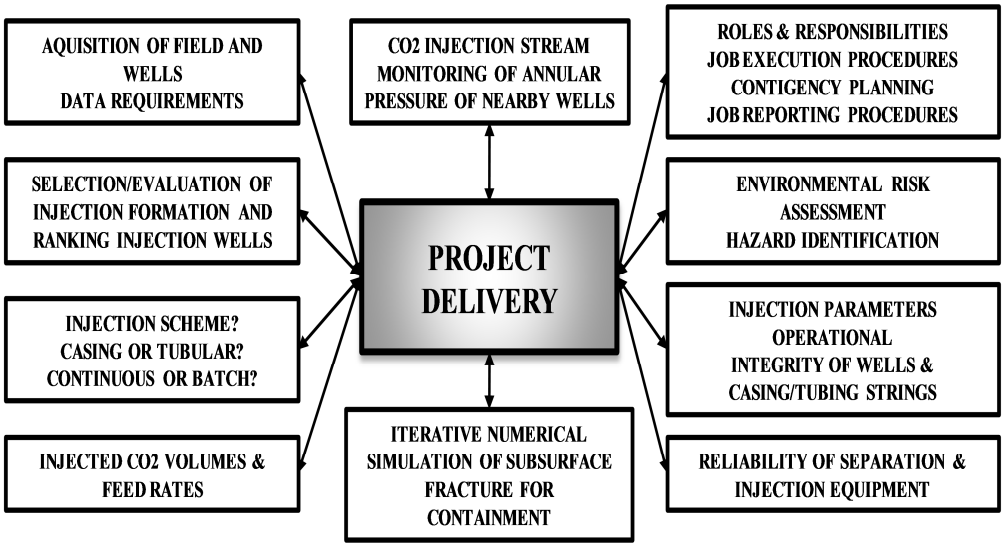

Figure 2.6: Parameters for the injection design and their interaction to provide assurance for the CO_2 sequestration in deep saline aquifer (Davis et al., 2001).

2.3.5. Issues and challenges

Despite years of CO_2 EOR experience of the industry that can be drawn upon, there are nonetheless several technical, economic and social issues and challenges in materializing the coupled CO_2 EOR and storage projects.

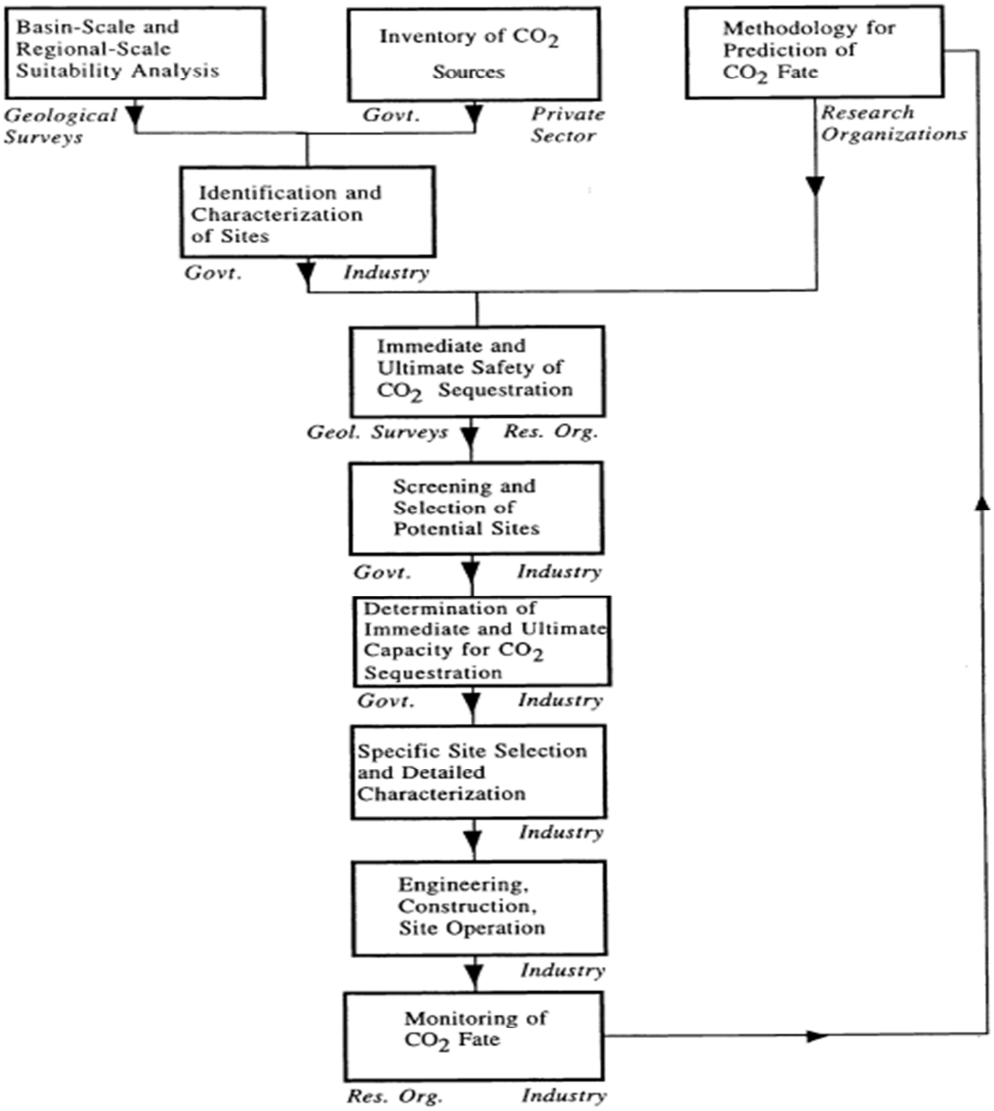

Figure 2.7: Recommended steps toward the geosciences-based assessment of site selection for CO_2 geological sequestration, and the main drivers of respective activity (Bachu, 2002).

Technical/economic issues and challenges

Storage integrity: One of the major risks associated with sequestration in a geological formation is the potential leakage of CO_2 through caprock, overburden and aging wells leading to the escape of CO_2 into shallow potable aquifers or into the atmosphere. Mapping and characterizing the geological features of the reservoir such as the spill points, caprock, faults and fractures thoroughly is therefore essential so that seal integrity over time can be ensured and the injected CO_2 remains safely trapped over the required timescale (Stevens et

al, 2002; Espie, 2005; Nghiem et al., 2009). CO_2 can cause Portland cement, typically used for well completion, to lose its strength over time. The seal and well integrity requires on-going risk assessment and monitoring.

Costs: The higher cost of anthropogenic CO_2, mainly due to the cost of CO_2 capture from its industrial sources, transportation to the candidate oilfields and the energy required for further compression of CO_2 prior to injection, is a key barrier to the implementation of the integrated process at commercial scale (Stevens et al., 2000). Significant reductions in the cost, particularly that of the capture of CO_2 from combustion processes, are required to overcome this barrier. Incorporation of CCS with new advanced coal-fuelled power plant was found not to be economically realistic due to the increase in energy required that reduces plant's efficiency. The revenues from selling captured CO_2 emissions into the CO_2 EOR market can, however change the competitive outlook (CCSTRM, 2006).

The price of an emissions permit, as well as incentives for CO_2 EOR application, is also affecting the viability of the coupled CO_2 EOR and storage projects. For example, Norway's carbon emission tax of about €40/tCO_2 ($57/t$CO_2$) encourages CO_2 storage in the Sleipner field (Kongsjorden et al., 1997; Torp and Gale, 2004).

Stability of CO_2 supply: CO_2 EOR creates an early opportunity for CO_2 storage. However, this early storage is temporary in nature, since most of the CO_2 will be produced and recycled during the flooding until the reservoirs become available for permanent CO_2 sequestration, which time in the future depends on the economics.

At the beginning of the injection phase, the CO_2 volume required is large. Over time, the volume of CO_2 being recycled will increase especially after the gas breakthrough and this may upset the planned injection and storage, to the extent that there might be excess of CO_2 that requires separate handling. On the other hand, there is also the possibility of CO_2 source plant shutdown that might affect the continuity of CO_2 supply to the reservoir. Therefore, in the integrated process, the candidate oilfield and project design must be able to receive the amount of CO_2 produced from the anthropogenic source as well as accommodating to the fluctuation in the CO_2 supply and demand.

Performance prediction: Despite the fast-paced development of reservoir modelling,

uncertainties in the reservoir performance and recovery efficiency predictions remains one of the challenges in the planning of the project. This is particularly true for complex or highly heterogeneous reservoirs with high uncertainty in the geological characterization. As highlighted by Stevens et al. (2000), besides the complex nature of CO_2 compositional phase behaviour effects and fluid flow in the porous media, the use of un-scaled laboratory data for field scale simulation may also affect the prediction reliability.

Operational challenges: Conflicts between oil recovery and CO_2 storage may arise, as field operations can differ significantly for CO_2 EOR and storage. In the coupled CO_2 EOR and storage projects, the main objective is no longer just maximizing the oil recovery but also maximizing the amount of CO_2 stored in the reservoir at the end of the process. Co-optimization is necessary yet finding the optimal flood design to result in co-optimized oil recovery and CO_2 storage is rather challenging.

CO_2 has the potential to increase corrosion rates in wells, flow lines and facilities. Nevertheless, corrosion has been reported to be a common problem in many CO_2 EOR projects, particularly in the wet CO_2 portion of the injection system, such as in meter runs, wellheads and tubing. With the extensive experience in CO_2 EOR worldwide, material for combating corrosion, such as the corrosion-inhibitor, corrosion-resistant alloys, stainless steel and anticorrosive equipment (Jarrel et al., 2002) has already been established with reasonable cost (Mcintyre, 1986).

Hydrate formation and asphaltene precipitation in the wellbore and production facilities may also pose operational challenges in the process (Christensen et al., 1998; Rogers and Grigg, 2000). Dissolution of reservoir minerals into the acidic displacing fluids will often result in an increase in wellbore scaling after gas breakthrough.

Challenges in operation are also foreseeable for offshore CO_2 EOR and storage application as the existing experience and technology are predominantly for onshore application. Apart from being much more expensive than the onshore venture, the offshore challenges include the weight, space and power limitations of retrofitting existing offshore facilities; and fewer more widely spaced wells contributing to displacement, sweep and lag time.

Social issues and challenges

One of the social challenges of geological storage is the acceptance of the public as to whether sequestering CO_2 underground is a safe alternative to emitting CO_2 to the atmosphere (Bryant, 2007; Bachu, 2008). A survey of public perceptions conducted in the U.K (Gough et al., 2004) shows that majority of people, in the absence of information as to its purpose; either does not have an opinion at all or are somewhat sceptical of the technology. As CCS is still considered in its infancy, lack of case studies and experience makes the convincing the public a challenging task. But the public support is getting better with time as a result of more support from the government and relevant authorities especially when CCS was put clearly into the context of climate change and the need for large long-term reductions in CO_2 emissions into the atmosphere, together with portfolio including renewable energy technologies, energy efficiency and lifestyle changes.

Another significant barrier is the lack of policy, legislation and a proper regulatory framework, such as a taxation or credit system (Stevens et al., 2002; Espie, 2005; Bachu, 2008). This includes legislation on the ownership of the pore space and the competition between storage rights and other mineral rights as well as long-term financial and operational liability, credits and third party transfer. Without these being established, the economics and financial risk of the process cannot be finalized and will cause delay in the commercial deployment of CCS.

2.4. A review of models of CWI process

Mathematical models and numerical simulation tools play an important role in evaluating the feasibility of any process in the oil reservoirs. This section is aimed at reviewing the modelling of CWI process in porous media.

Injection of CWI in a reservoir may involve a number of physical and chemical phenomena such as dissolution of CO_2 with the aqueous phase to make up the injected carbonated water. Key issues arising in the simulation of the process also include the diffusion and dispersion of CO_2 from the carbonated water into the in-situ oil and water, the PVT properties of mixtures of carbonated water (CO_2) with oil and natural gas, single and multi-phase flow, and the coupled hydro-chemical and hydro-mechanical effects due to interactions between

carbonated water, reservoir fluids, and minerals of the rock.

De Nevers (1964) was the first to present a calculation method for a secondary CWI based on Buckley-Leveret type linear flow for predicting the oil recovery. Instantaneous equilibrium was assumed and no capillary pressure or gravity effects were considered. Molecular and convective diffusion of CO_2 in the flow direction were also assumed to be zero. The rate of advance was assumed to be dependent on the CO_2 concentration in water. The effect of a change in injection fluid composition is propagated only as fast as changed saturations and compositions move from the injection well. In this model, the injected carbonated water gave up all its CO_2 to the oil it contacted and then, as plain water, moved faster than the CO_2.

Ramesh et al. (1972) later reported an improved three-phase black-oil model capable of handling heterogeneous reservoir properties, compressible fluids, gravity and capillary forces but not free hydrocarbon gas in the reservoir. Simultaneous saturation of CO_2 in the oil and water phases was assumed, where CO_2 solubility was proportional to the relative capabilities of these phases to dissolve CO_2 at the prevailing block pressure.

Most of the early published compositional models (e.g. Kazemi, 1978; Fussel, 1979; Coats, 1980 and Young, 1983) were unable to model CO_2 dissolution into the aqueous phase. However, as Klins (1984) pointed out, the solubility of CO_2 in water is relatively higher than that of hydrocarbon components, especially in the process where CO_2 is injected with water, that it cannot be neglected in simulation. Mansoori (1982) was among the earliest to report the use of Henry's Law to account for CO_2 solubility in water in a compositional model.

Enick and Klara (1992) reviewed several models for CO_2 solubility in water and concluded that Krichevsky-Ilinskaya equations, which require accurate calculation of the partial molar volume of CO_2 in brine and the fugacity of CO_2 from the EOS, are the most reliable. Chang et al. (1998) developed correlations for estimating CO_2 solubility in water and NaCl brine as a function of pressure and temperature, which were later incorporated in E300 compositional simulator. The current commercial reservoir simulators basically apply the same concept of two phase behaviour models combined through the constraints of thermodynamic equilibrium by equilibration of component fugacities in different phases in each gridblock.

To the best of the author knowledge, there has been no simulation study reported in the literature specifically on CWI process using the commercially available compositional reservoir simulators. In order to establish the credibility of numerical simulator as a practical engineering tool, it is necessary to demonstrate that it can model accurately and reliably the important physical processes that are taking place in the system of interest.

2.4.1. Modelling the non-equilibrium effects

The basic governing equations in conventional reservoir simulator are conservation equations, Darcy's equations, capillary pressure equations, and phase equilibrium. The relevant formulations of the numerical model are given in Appendix A2.

These formulations are generally based on the assumption that the fluid mixture contained in each grid block is in a state of equilibrium and complete mixing takes place everywhere; an assumption that may not be true for different fluid phases coexisting in a grid block, for various reasons, not having sufficient contact time with each other. For the CWI process, this unstable displacement may occur as a result of the adverse mobility ratio between the displaced oil and displacing carbonated water as well as the diffusion and dispersion of CO_2 from the injected carbonated water into the oil. With the displacement rate higher than the diffusion rate, there would be insufficient time for the system to reach equilibrium and thus a state of complete mixing will not be a valid assumption.

Several attempts to model these unstable, incomplete mixing or non-equilibrium phenomena have been published in the literature. Koval (1963) predicted the viscous fingering using heterogeneity factor that alters the fractional flow of the solvent. He based his approach on the assumptions that the fractional flow of the displacing fluid in an immiscible displacement is a function of the saturation of the displacing fluid, the heterogeneity factor of the system and the difference between the viscosity of the displaced and displacing fluids. Dougherty (1963) later extended Koval's approach to also include a three-parameter rate equation to account for the dispersive-type mixing. Later, Todd and Longstaff (1972) developed a mixing parameter, which work conceptually similar to the heterogeneity factor, to represent the degree of mixing due to viscous fingering for a first contact miscible system in a black oil

simulator. Barker and Fayers (1994) have proposed the use of transport coefficients that modify the component flow terms, and a density coefficient that modifies the accumulation terms to account for the incomplete mixing effect. These approaches rely on the empirical parameter, which in turn varies with the characteristics of the reservoir and fluid system.

More recently, Nghiem et al. (1997) develop an EOS compositional simulator where the oil and gas approach thermodynamic equilibrium through a rate process. They assumed that there are two distinct zones of fluids in each grid block and thermodynamic equilibrium prevails only at the interface between the oil and gas phases and mixing mechanisms such as diffusion, transverse dispersion, viscous crossflow and density driven crossflow, drives the two phases towards equilibrium. The key to the proposed techniques is the transfer term between these two zones. They reported that the non-equilibrium results lie in between the equilibrium and the no-mixing results. Details of the flow equations used in this approach are presented in Appendix A2.

From the literature review thus far, the author is in the opinion that the model by Nghiem et al. (1997), if also extended to include the water phase, is possibly the best representation of the non-equilibrium system. However, this feature is not available in the three compositional reservoir simulators evaluated in this study. Consequently, the use of the transport coefficient and mixing parameter, which are available in the simulator and work by modifying the component flow terms, and a density coefficient to account for the incomplete mixing effect, was further examined. Further results and discussion are given in Chapter 4.

2.5. Summary

Carbon capture and geological storage of CO_2 is undoubtedly one of the viable options to reduce man-made CO_2 emission into the atmosphere. Near-depleted and depleted oil reservoirs, particularly those apt for CO_2 EOR, provide a near term geological storage of CO_2 that is highly likely to be economic due to the revenue from the additional oil production.

Despite the extensive experience of CO_2 EOR in the industry, there are still many challenges

and issues to be looked at before more commercial-scale coupled CO_2 EOR and sequestration projects can be put into operation. A successful CO_2 EOR and storage project requires collaboration by industry, governments, the private sectors and research organizations to address the technology gap and risk sharing mechanisms.

This thesis investigates further two technical challenges in CO_2 injection for EOR and storage. The first challenge relates to the fact that the high mobility of CO_2 as compared to oil and water, if without proper control, could result in early breakthrough of the gas and thus poor sweep efficiency and lower oil recovery. Increased gas recycling will increase the operating costs and lower the net amount of CO_2 stored. The adverse effect of the high mobility ratio may be less in a water-based CO_2 EOR method, where CO_2 is dissolved in water prior to injection. The CO_2-enriched water injection was investigated further as it has the potential of increasing the oil recovery and at the same time offers secure storage of CO_2 yet has not been studied much since its introduction back in the 1960s. Three commercial compositional reservoir simulators, with and without the transport coefficient, were also evaluated for their suitability and adequacy to model CWI process at the core scale. Alternative modelling approaches not using the compositional simulator were also presented.

Another challenge investigated is the co-optimization of the oil recovery and CO_2 storage. Routine CO_2 EOR projects only focus on maximizing the oil recovery at the minimum amount of CO_2 used. In the integrated CO_2 EOR and storage project, both oil recovery and CO_2 stored need to be maximized, which requires optimization.

2.6. References

[2.1] Aasen, K., Vigeland, B., Norby, T., Larring, Y. and Mejdell, T.: Development of a Hydrogen Membrane-based Reformer Based CO_2 Emission Free Gas Fired Power Plant, Proceedings of the 7th International Conference on Greenhouse Gas Control Technologies, Vancouver, Canada, 2004.

[2.2] Anadarko, Enhanced Oil Recovery, Anadarko website, accessed in August 2010.

[2.3] Araktingi, U.G., Orr Jr., F.M.: Viscous Fingering, Gravity Segregation, and

Reservoir Heterogeneity in Miscible Displacements in Vertical Cross Sections, SPE 20176, SPE/DOE Enhanced Oil Recovery Symposium, Tulsa, Oklahoma, 22-25 April 1990.

[2.4] Bachu, S., Gunter, W.D and Perkins, E.H.: Aquifer Disposal of CO_2: Hydrodynamic and Mineral Trapping, Energy Conversion and Management, 35, 269-79, 1994.

[2.5] Bachu, S.: Sequestration of CO_2 in Geological Media in Response to Climate Change- Road Map for Site Selection using the Transform of the Geological Space into the CO_2 Phase Space, Energy Conversion and Management, 43, 87-102, 2002.

[2.6] Bachu, S.: CO_2 Storage in Geological Media: Role, Means, Status and Barriers to Deployment, Progress in Energy and Combustion Science, 34, 254-273, 2008.

[2.7] Baviere, M.: Basic Concepts in Enhanced Oil Recovery Processes, Elsevier Applied Science, 1991.

[2.8] Bergen, F., Gale, J., Damen, K.J. and Wildenborg, A.F.B.: Worldwide Selection of Early opportunities for CO_2-enhanced Oil Recovery and CO_2-enhanced Coal Bed Methane Production, Energy 29, 1611-1621, 2004.

[2.9] Bryant, S.: Geologic CO_2 Storage - Can the Oil and Gas Industry Help Save the Planet? Journal of Petroleum Technology, Vol. 59, 9, 98-105, 2007.

[2.10] Carbon Capture Journal, http://www.carboncapturejournal.com/displaynews.php?NewsID=736&PHPSESSID=duin4hbugqo0kj0n6b18vbq7n1, Feb 14, 2011, accessed on 4th March 2011.

[2.11] Caudle, B.H. and Dyes, A.B.: Improving Miscible Displacement by Gas-Water Injection, Petroleum Transactions, AIME, Vol. 213, 281-283, 1958.

[2.12] Caudle, B.H. and Witte, M.D.: Production Potential Changes during Sweep-out in a Five-spot System, SPE 1334, Journal of Petroleum Technology, Vol. 12, 63-65, 1959.

[2.13] CCSTRM (Canada's CO_2 Capture & Storage Technology Roadmap), available at www.co2trm.gc.ca, 2006.

[2.14] Chang, Y. B., Coats, B.K. and Nolen, J.S.: A Compositional Model for CO_2 Floods Including CO_2 Solubility in Water, SPE 33164, SPE Reservoir Evaluation & Engineering, Vol. 1, No. 2, 133-160, 1998.

[2.15] Christensen, J. R., Stenby, E. H. and Skauge, A.: Review of the WAG Field Experience, SPE 71203, SPE International Petroleum Conference and Exhibition of Mexico, Villhermosa, March 3-5, 1998.

[2.16] Coats, K.H.: An Equation of State Compositional Model, SPE 8284, SPE Journal, Vol. 20, No. 5, 363-376, 1980.

[2.17] Codreanu, B.D. and Le Gallo, Y.: A Simulation Method for the Rapid Screening of Potential Depleted Oil Reservoirs for CO_2 Sequestration, Energy, 29, 12, 2004.

[2.18] Damen, K., Faaij, A., van Bergen, F., Gale, J. and Lysen, E.: Identification of Early Opportunities for CO_2 Sequestration - Worldwide Screening for CO_2 EOR and CO_2-ECBM Projects, Energy 30, 1931-1952, 2005.

[2.19] Davis, L. A.: Maximizing Storage Rate and Capacity and Insuring the Environmental Integrity of Carbon Dioxide Sequestration in Geological Reservoirs, http://www.netl.doe.gov/publications/proceedings/01/carbon_seq/p35.pdf; accessed on 15th February 2010.

[2.20] De Nevers, N.: A Calculation Method for Carbonated Water Flooding, SPE 569, SPE Journal, 9-20, March 1964.

[2.21] Dougherty, E.L.: Mathematical Model of an Unstable Miscible Displacement, SPE Journal, p155-163, June 1963.

[2.22] Enick, R.M. and Klara, S.M.: Effects of CO_2 Solubility in Brine on the Compositional Simulation of CO_2 Floods, SPE Reservoir Engineering, Vol. 7, No. 2, 253-258, 1992.

[2.23] Espie, A.A.: CO_2 Capture and Storage: Contributing to Sustainable World Growth, International Petroleum Technology Conference, Doha, Qatar, 21-23 November 2005.

[2.24] Feron, P.H.M.: Challenges in Capture Processes: The Way Forward, Oil & Gas

Science and Technology, Rev. IFP, Vol. 60, No. 3, 509-510, 2005.

[2.25] Figueroa, J.D., Fout, T., Plasynski, S., McIlvried, H. and Srivastava, R.D.: Advances in CO_2 Capture Technology - The U.S. Department of Energy's Carbon Sequestration Program, International Journal of Greenhouse Gas Control 2, 9-20, 2008.

[2.26] Gardner, J.W. and Ypma, J.G.J.: An Investigation of Phase Behavior-Macroscopic Bypassing Interaction in CO_2 Flooding, SPE 10686, SPE Journal, Vol. 24, 5, 508-520, 1984.

[2.27] Gough, C., McLachlan, C. and Shackley, S.: The Public Perceptions of Carbon Capture and Storage In Tyndall Centre Working Paper 44, 2004. Available at: http://www.tyndall.ac.uk/biblio/working-papers.

[2.28] Hendriks, C., Graus, W. and van Bergen, F.: Global Carbon Dioxide Storage Potential and Costs, Report EEP-02001, Rijksinstituut voor Volksgezondheid en Milieu, 2004.

[2.29] Holt, T. and Lindeberg, E.: CO_2 from Industrial Sources as Injection Gas in Oil Reservoirs, Energy Conversion and Management, Vol. 34, Issues 9-11, 1993.

[2.30] Holtz, M.H.: Geologic CO_2 Storage in Oil Fields: Considerations for Successful Sites, SPE 126198, SPE International Conference on CO_2 Capture, Storage, and Utilization, San Diego, California, USA, 2-4 November 2009.

[2.31] International Energy Agency: CO_2 Storage in Depleted Oilfields: Global Applications Criteria for Carbon Dioxide Enhanced Oil Recovery, Technical Report No 2009-12, IEA Greenhouse Gas R&D Programme, 2009.

[2.32] IPCC (Intergovernmental Panel on Climate Change) Fourth Assessment Report Working Group III, Climate Change 2007: Mitigation of Climate Change in Metz, B. et al. (Eds), Cambridge University Press, Cambridge, United Kingdom, 2007.

[2.33] Irwin, D.D. and Batycky, J.P.: The Successive Displacement Process: Oil Recovery during Blowdown, SPE 36719, SPE Reservoir Engineering, Vol. 12, 4, 240-245, 1997.

[2.34] Jarrell, P.M., Fox. C., Stein, M. and Webb, S.: Practical Aspects of CO_2 Flooding, SPE Monograph Series Vol. 22, Society of Petroleum Engineers, 2002.

[2.35] Jessen, K., Kovscek, A. R. and Orr, F. M.: Increasing CO_2 Storage in Oil Recovery, Energy Conversion and Management, 46, 18, 2005.

[2.36] Juanes, R., Spiteri, E.J., Orr, F.M. and Blunt, M.J.: Impact of Relative Permeability Hysteresis on Geological CO_2 Storage, Water Resources Research, 42, W12418, doi:10.1029/2005WR004806, 2006.

[2.37] Kaarstad, O.: Experience From Real CCS Projects - And the Way Forward, Paper 19-2875, 19th World Petroleum Congress, Madrid, Spain, 2008.

[2.38] Kazemi, H., Vestal, C.R., and Deane G.: An Efficient Multicomponent Numerical Simulator, SPE 6890, SPE Journal, Vol. 18, No. 5, 355-368, 1978.

[2.39] Klins, M.A.: Carbon Dioxide Flooding Basic Mechanisms and Project Design, International Human Resources Development Corp., Boston, 1984.

[2.40] Kongsjorden, E., Karstad, O. and Torp. T. A.: Saline Aquifer Storage of Carbon Dioxide in the Sleipner Project, Waste Management, Vol. 17, No. 5/6, 303-308, 1997.

[2.41] Koval, E.J.: A method for predicting the performance of unstable miscible displacement in heterogeneous porous media, SPE Journal, p153-154, June 1963.

[2.42] Kovscek, A. R.: Screening Criteria for CO_2 Storage in Oil Reservoirs, Journal of Petroleum Science and Technology, Vol. 29, 841-866, 2002.

[2.43] Kuuskraa, V. A. and Ferguson, R.: Storing CO_2 with Enhanced Oil Recovery, DOE/NETL-402/1312/02-07-08, February 7, 2008.

[2.44] Linderberg, E., Bergamo, P. and Moen, A.: The Long-term Fate of CO_2 Injected into an Aquifer, 6^{th} International Conference on Greenhouse Gas Control Technology (GHGT-6), Kyoto, Japan, 2002.

[2.45] Mansoori, J.: Compositional Modelling of CO_2 Flooding and the Effect of CO_2 Water Solubility, SPE 11438, Unsolicited.

[2.46] Martin, F. D.: Enhanced Oil Recovery for Independent Producers, SPE/DOE Eighth Symposium on Enhanced Oil Recovery, Tulsa, Oklahoma, 1992.

[2.47] Mcintyre, K.J.: Design Considerations for Carbon Dioxide Injection Facilities, Journal of Canadian Petroleum Technology, Vol. 25, 2, 90-95, 1986.

[2.48] National Energy Technology Laboratory, U.S. Dept. of Energy, http://www.netl.doe.gov/technologies/carbon_seq/database/index.html, accessed in August 2010.

[2.49] National Energy Technology Laboratory, U.S. Dept. of Energy, Article 'NETL-Developed Process for Capturing CO_2 Emissions Wins National Award for Excellence in Technology Transfer', http://www.netl.doe.gov/technologies/carbon_seq/database/index.html, Release Date: February 3, 2011; accessed in March 2011.

[2.50] Nghiem, L., Shrivastava, V., Tran, D., Kohse, B., Hassam, M and Yang, C.: Simulation of CO_2 Storage in Saline Aquifers, SPE 125848, SPE/EAGE Reservoir Characterization and Simulation Conference, 19-21 October 2009.

[2.51] Nghiem, L.X., Li, Y.K. and Agarwal, R.K.: A Method for Modelling Incomplete Mixing Phenomenon in Compositional Simulations of Unstable Displacements, SPE 18439, SPE Symposium on Reservoir Simulation, Houston, Texas, 6-8 February 1989.

[2.52] Parliamentary Office of Science and Technology (POST), Carbon Capture and Storage, Postnote 238, March 2005 at www.parliament.uk/post/home.htm.

[2.53] Preston, C., Monea, M., Jazrawi, W., Brown, K., Whittaker, S., White, D., Law, D., Chalaturnyk, R. and Rostron, B.: IEA GHG Weyburn CO_2 Monitoring and Storage Project, Fuel Processing Technology 86, 1547-1568, 2005.

[2.54] Qi, R., LaForce, T. C. and Blunt, M. J.: Design of Carbon Dioxide Storage in Oilfields, SPE 115663, Proceedings of the SPE Annual Technical Conference and Exhibition, Denver, Colorado, 21-24 September, 2008.

[2.55] Ramesh, A.B. and Dixon, T.N.: Numerical Simulation of CW flooding in a

Heterogeneous Reservoir, SPE 4075, Fall Meeting of the Society of Petroleum Engineers of AIME, San Antonio, Texas, 8-11 October 1972.

[2.56] Ravagnani, G., Ligero, E.L. and Suslick, S.B.: CO_2 Sequestration through Enhanced Oil Recovery in a Mature Oil Field, Journal of Petroleum Science and Engineering 65, 129-138. 2009.

[2.57] Rivas, O., Embid, S. and Bolivar, F.: Ranking Reservoirs for Carbon Dioxide Flooding Processes, SPE Advanced Technology Series, 2, 95-103, 1994.

[2.58] Rogers, J. D. and Grigg, R. B.: A Literature Analysis of the WAG Injectivity Abnormalities in the CO_2 Process, SPE 59329, SPE/DOE Improved Oil Recovery Symposium, Tulsa, April 3-5, 2000.

[2.59] Shaw, J. and Bachu, S.: Screening, Evaluation, and Ranking of Oil Reservoirs Suitable for CO_2-Flood EOR and Carbon Dioxide Sequestration, Journal of Canadian Petroleum Technology, Vol. 41, 9, 2002.

[2.60] Stalkup, F.I.: Displacement of Oil by Solvent at High Water Saturation, SPE Journal, Vol. 10, 4, 337-348, 1970.

[2.61] Stephenson, D.J., Graham, A.G. and Luhning, R.W.: Mobility Control Experience in the Joffre Viking Miscble CO_2 Flood, SPERE, 183-188, 1993.

[2.62] Stevens, S.H, Kuuskra, V.A. and Taber, J.J.: Sequestration of CO_2 in Depleted Oil and Gas Fields: Barriers to Overcome in Implementation of CO_2 Capture and Storage, Report PH3/22/IEA/CON/98/31, 2000.

[2.63] Stevens, S.H. and Gale, J.: Geologic CO_2 Sequestration may Benefit Upstream Industry, Oil and Gas Journal, 40-44, 2000.

[2.64] Taber, J. J.: Technical Screening Guides for the Enhanced Recovery of Oil, SPE Annual Technical Conference and Exhibition, San Francisco, California, 1983.

[2.65] Taber, J. J.: EOR Screening Criteria Revisited-Part 2: Applications and Impact of Oil Prices, SPE Reservoir Engineering, 12, 199-206, 1997.

[2.66] Torp, T. A. and Gale, J.: Demonstrating Storage of CO_2 in Geological Reservoirs:

The Sleipner and SACS Projects, Energy, 29, 1361-1369, 2004.

[2.67] US DOE Report: Undeveloped Domestic Oil Resources: The Foundation for Increasing Oil Production and a Viable Domestic Oil Industry, U.S. Department of Energy, 2006.

[2.68] US DOE, Enhanced Oil Recovery/CO_2 Injection http://www.fossil.energy.gov/programs/oilgas/eor/index.html, accessed on 3rd March 2011.

[2.69] Van Lingen P.P., Barzanji, O.H.M. and van Kruijsdijk, C.P.J.W.: WAG Injection to Reduce Capillary Entrapment in Small Scale Heterogeneities, SPE 36662, SPE Annual Meeting, Colorado, 1996.

[2.70] Van Poolen, H.: Fundamentals of Enhanced Oil Recovery, Published by Pennwell Corp., June 1980.

[2.71] Vesovic, V., Wakeham, W.A., Olchowy, G.A., Sengers, J.V., Watson, J.T.R. and Millat, J.: The Transport Properties of Carbon Dioxide, J. Phys. Chem. Ref. Data, Vol. 19, No.3, 1990.

[2.72] World Energy Outlook 2009 fact sheet, International Energy Agency, http://www.worldenergyoutlook.org/docs/weo2009/ fact_sheets_WEO_2009.pdf

[2.73] Worldwide EOR Survey, Oil & Gas Journal, April 2008, Vol. 106, Issue 15, 2008.

[2.74] Young, L.C. and Stephenson, R.E.: A Generalized Compositional Approach for Reservoir Simulation, SPE 10516, SPE Journal Vol. 23, No. 5, 727-742, 1983.

Chapter 3

Carbonated Water Injection (CWI): Experimental Studies

3.1. Introduction

Carbonated water is plain water into which CO_2 gas under pressure has been dissolved. In CWI, carbonated water is injected at a predefined pressure and rate into the reservoir. Under typical reservoir conditions at salinity of 3%, the CO_2 solubility is between 47 and 51 kg/m^3, corresponding to a volume of free CO_2 of 6.7 to 7.3% of the pore volume (Linderberg et al., 2002), which is much higher than that of hydrocarbon gases.

CO_2 solubility in crude oils is typically five to six times higher than in water and hence, during CWI, as the injected carbonated water comes in contact with the oil, its CO_2 content partitions between the oil and water. At 2000 psig and 100.4 ^oF for example, the liquid-liquid (LL) K-value of CO_2 i.e., the ratio of mole fraction of the CO_2 in the aqueous phase to the oil phase mole fraction of CO_2, calculated using the PVT package Winprop, is around 0.0472. The transfer of CO_2 from carbonated water to oil reduces the oil viscosity causing the oil to be swept more easily by the flood water.

In CWI, CO_2 is dissolved in the injected water/brine prior to injection and then transported through the reservoir by the flood water i.e., carbonated water acts as both the CO_2 source and the means of transporting CO_2 throughout the oil-bearing formation. As a single phase flow, the mobility contrast of carbonated water with oil is more favourable than in the CO_2 gas-oil system. For example, at 2000 psig and 100.4 ^oF, the endpoint mobility ratio of decane and CO_2 gas is about 10 whereas that of decane and carbonated water is favourably

lower at 1.2. The problems of mobility contrast, fingering, gravity segregation due to density difference and reduced relative permeability are minimized if not eliminated. CO_2 injection through CWI into an oil reservoir also requires lower compression, as the hydrostatic pressure of water makes injection of carbonated water much easier, and hence cheaper, than the conventional CO_2 gas injection. Burton and Bryant (2007) reported a lower wellhead injection pressure by about 400 psi to inject the carbonated water than to inject the CO_2 gas.

In comparison with the normal waterflood, secondary carbonated water flooding yields higher oil recoveries, and improved water injectivity as a result of oil viscosity reduction and oil swelling through chromatographic transfer of CO_2 from the flood water to the oil (de Nevers, 1964). The residual oil saturations of $\leq$2.86 cP viscosity oil after waterflooding were reported to have been reduced from 8% to almost 50% by carbonated waterflood (McFarlane et al., 1952; Hickok et al., 1960; Holm, 1963).

The high cost associated with the capture of CO_2 from the power or industrial plants, its pressurization and transport (Bachu, 2008) and a location that is normally far from the oil fields is unlikely to make CO_2 EOR using anthropogenic CO_2 economical in oil reservoirs which would otherwise be suitable candidates for EOR and CO_2 storage. This is particularly the case for the North Sea Continental Shelf (NSCS) reservoirs where despite having significant potential in increasing the oil recovery, CO_2 EOR could not be implemented, for the lack of low cost CO_2 and the non-conducive oil-price regime (Hadlow, 1992).

CWI, which requires less CO_2 as compared to conventional CO_2 injection, yet results in significant oil recovery, as will be shown later, offers an alternative injection strategy for CO_2 EOR to those candidate reservoirs. There are smaller and cheaper sources of CO_2 such as those separated from natural or associated gas from nearby oil and gas fields that may be located closer to the candidate fields that may be exploited for CWI.

CWI could also be beneficial to watered-out oil reservoirs in which high water saturations adversely affects the conventional CO_2 injections. The presence of mobile water has been reported to cause reduced displacement efficiency in pore- and core-scale tertiary flooding due to oil trapping where the oil is blocked from the injected solvent gas by a water layer (Stalkup, 1970; Shelton and Schneider, 1978; Tiffin and Yellig, 1983). Carbonated water, on the other hand, can spread and mix much easily with the in-situ water thus distributes the CO_2 more

uniformly to the trapped oil.

CWI was first introduced as an improved secondary oil recovery process by the Oil Recovery Corporation, known as ORCO flood (Martin, 1959). The first commercial field implementation of CWI was to augment the waterflooding in the K&S project in Oklahoma. After a few successful applications in the Texas and Oklahoma oil fields, the process unfortunately fell out of favour as the then high CO_2 cost from the liquefaction plant rendered it uneconomic. At residual oil saturation, large volumes of carbonated water, and thus CO_2, were required to bring about sufficient reduction in oil viscosity for favourable flow. The extra oil produced was not commensurate with the high cost of CO_2 gas obtained from the liquefaction plant (Holm, 1987). No field application of tertiary CWI has been reported. However, with the increasing availability of anthropogenic CO_2 and the drives to reduce its concentration in the atmosphere, the cost of CO_2 may no longer be the limiting factor.

With the relatively high solubility of CO_2 in water, CWI could also serve as an injection scheme for storing CO_2 in depleting oil reservoirs. The risk of buoyancy-driven leakage, as in the case of CO_2 bulk phase injection (Burton and Bryant, 2007) would be minimized in CWI, since CO_2 is in solution rather than a free phase. The weak carbonic acid formed in the aqueous phase increases the aqueous phase density that could bring about a gravitational and convective effect to the fluid flow: the heavier carbonated water will slump towards the bottom of the reservoir (Hebach, 2004), further securing storage. Monitoring would be less than what is required with the bulk phase injection, thus reducing the cost of monitoring the stored CO_2.

CWI has also been reported to have improved water injectivity and consequently accelerated the oil production (Ramsay and Small, 1964). Despite the concerns that carbonic acid may cause localized corrosion of steel (Browning, 1984), no evidence of further corrosion, apart from the normal waterflood corrosion, was reported in the K&S carbonated waterflood project (Hickok et al.,1962). In this particular case, the CO_2 injection lines were even re-used several times during the staging of the CO_2 injection. It was hypothesized that the limited proportion of CO_2 formed sufficient amounts of alkali and alkali earth carbonates and bicarbonates that act as buffers which prevent the corrosion of the steel (Martin, 1951). Corrosion has nevertheless been reported to be a common problem in many CO_2 EOR projects, particularly in the wet CO_2 portion of the injection system such as in meter runs, wellheads and tubing.

With the extensive experience in CO_2 EOR worldwide, materials for combating corrosion, such as the corrosion-inhibitor, corrosion-resistant alloys, stainless steel and anticorrosive equipment (Jarrel et al., 2002) have already been established with reasonable cost and thus this should not be a major issue.

Despite its potential for CO_2 EOR and storage, this injection mode has not been very much studied. In this thesis, the oil recovery and CO_2 storage benefits of secondary and tertiary CWI, as compared to plain (conventional) waterflood, were investigated experimentally through a series of high pressure, high temperature coreflood experiments. Water-wet and mixed-wet Clashach sandstone cores and a core from a North Sea oil reservoir were used in the experiments. The tests were carried out using light oil (n-decane), refined mineral oil of 81 cP and a 145 cP North Sea stock tank crude oil at test pressures and temperature typical of real reservoir conditions. The behaviour of the dissolved CO_2 that affects the effectiveness of CWI as an oil recovery method was also examined by observing the CO_2 front propagation throughout the tests.

The purposes of the experiments were to extend our understanding of the CWI mechanisms, quantify the additional oil recovery and the amount of the CO_2 stored from the process and to investigate the effects of oil viscosity, rock wettability and brine salinity on the oil recovery by CWI. Coreflood investigation of the CWI process on medium viscous oils in this study is relatively novel in the industry, as the available information in the literature thus far is only on light oil. The potential of this injection scheme for CO_2 storage which, to the best of the author's knowledge, has never been experimentally investigated before was also looked into. The experimental results presented here are essential to validate the simulation model, details of which are given in Chapter 4.

3.2. Experimental facilities and procedures

3.2.1. Coreflood rigs

A high-pressure high-temperature coreflooding rig was used in the displacement tests. Two setups of the equipment were employed; the difference being the conditions at which the effluent was collected and the size of the core holder. In both setups, the core holder was

mounted horizontally.

In both setups, the pressure transducers used were Quartzdyne DSB301-10-C85, rated to 10000 psi and 85 ^{o}C (http://www.quartzdyne.com/). The transducers were initially calibrated by the manufacturer and they were regularly checked in the lab prior to the tests by connecting them to a dead weight tester and applying a variety of pressures to see if they were reading the pressure correctly. The dead weight tester was in turn serviced and calibrated yearly by an instrumentation calibration service provider. The pressure readings from the transducers were logged to Labview 8.6 software.

Flow controls were provided by the Quizix C 5000-5K pumps; rated to 5000 psi and maximum flow rate of 2000 cc/hr (http://www.chandlerengineering.com). The injection volumes were calibrated by comparing the injected volume on the Quizix pump and the volume recovered, by both weight and test tube method.

The first equipment setup is schematically shown in Figure 3.1. The dual-cylinder pump system was connected to a Proserve transfer vessel, which was used to deliver the fluids into the core. The core effluent was carried through a backpressure regulator where the pressure drops to atmospheric pressure and hence any dissolved gas would be liberated. The separated liquid would then be collected in a graduated cylinder while the gas in a Chandler 2331D gasometer (http://www.chandlerengineering.com). The standard conditions at which the effluent volumes were measured in these tests were 60 ^{o}F and ambient pressure.

In another setup, schematically shown in Figure 3.2, four pumps were each connected to a transfer vessel. Two pumps were for injecting brine and oil at the desired flow rate and pressure to the entry side of the core holder. The other two pumps; also one for the brine and the other for the oil, were for retrieving the fluid through a sight glass with a calibrated viewing lens. The retrieving pump rate was held constant and similar to the injection rate, to ensure constant average pressure throughout the test.

The fluid withdrawn (either oil or brine) depends on the main fluid being produced, so as to ensure the fluid interface is within the preferable viewing range of the sight glass. The interface level of the fluids in the sight glass was monitored and recorded throughout the test, which was later used to calculate the amount of each fluid produced at the test conditions.

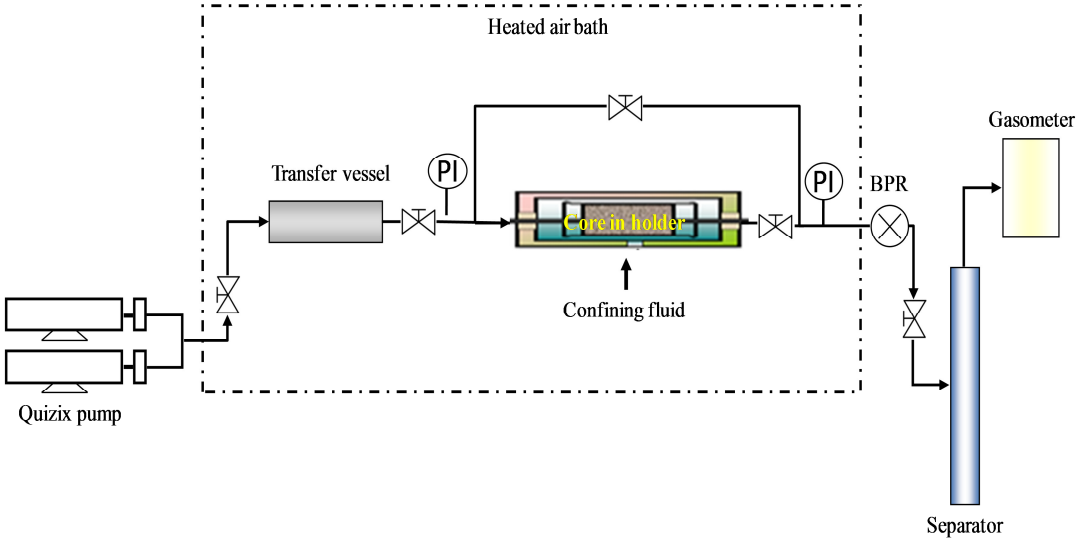

Figure 3.1: Schematic of the coreflood rig with effluents volume measured at the standard conditions.

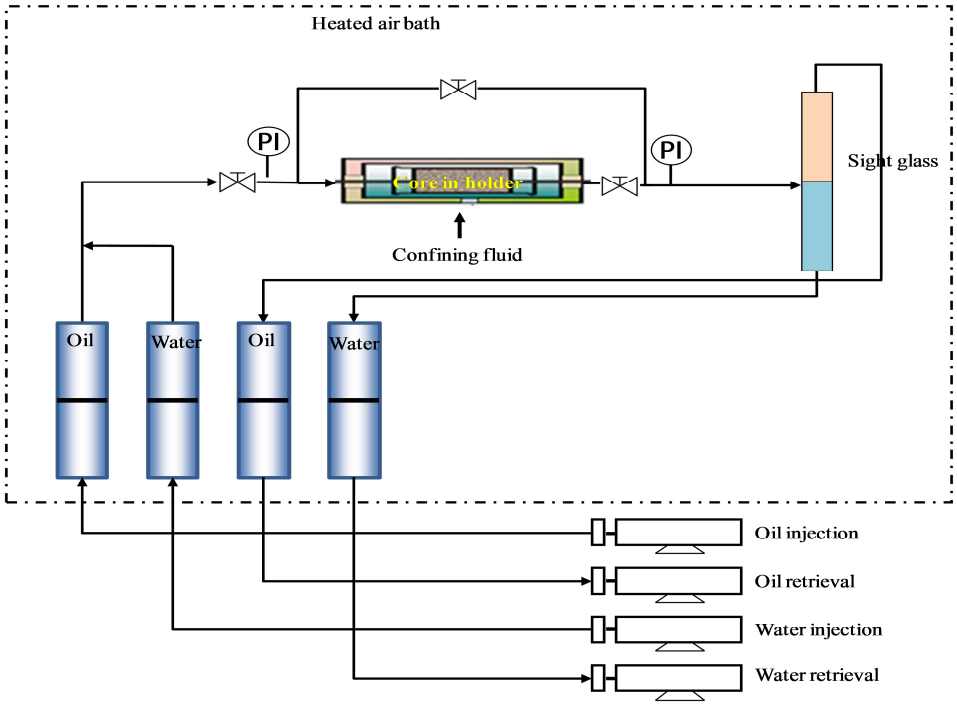

Figure 3.2: Schematic of the coreflood rig with effluents volume measured at the test conditions.

Both coreflood rigs are capable of operating at pressures up to 6000 psi and temperatures as high as 300 ^{o}F. The coreflood tests reported in this thesis were carried out at 2000 - 2500 psig and 100.4 ^{o}F. Pressure and temperature at the inlet and outlet end of the core holder are displayed continuously on the computer, which has a built-in data acquisition system. Temperature is maintained by keeping the apparatus inside a temperature-controlled enclosure. All the valves, fittings and pipework were made of a mixture of Hastelloy C276 to enable handling wet CO_2.

3.2.2. Core samples

Three types of cores were used in the coreflood tests i.e., a reservoir core and two Clashach sandstone cores, one with its natural water-wettability (water-wet) whereas the other was made mixed-wet by ageing it in a crude oil. The ageing procedures followed has long been developed and established in our lab, which resulted in the initially preferentially water wet core became mixed wet. Since the same ageing procedures were followed for the core used in this study, it was hence assumed that the aged core became mixed wet following the ageing process.

The Clashach core is a pale yellow buff, non-calcareous, medium grained sandstone from the Permean age. The environmental scanning electron microscope (ESEM) analysis shows that it is composed mainly of quartz (about 75 weight %), calcium carbonate, feldspar and traces of clay mineral (illite). The reservoir core was sampled from a North Sea sandstone oil reservoir. It is relatively friable with the sand particles on the surface of the core disintegrating rather easily upon friction, but by appropriate preparation, as will be described later, the core was able to withstand the test flow and pressure without collapse. No measurement of the core compressive strength was, however, made.

The porosity of the cores was determined by a helium porosity test while the pore volume of each core was determined as the total volume of fluid used to saturate the system minus the dead volumes of tubing connecting the core to the rest of the system.

The permeability of the core was first measured using methane, at the test pressure and temperature followed by measurement using the brine or oil sample at the same conditions.

Measurements were repeated at least three times, to ensure reliability. For the Clashach core, permeability measured using methane was found to be very rate-dependent, while those measurements using the oil sample (decane) were very stable and repeatable. Therefore, the effective permeability to oil was used to represent the Clashach core permeability. For the reservoir core, the average measured base permeability to brine was 4580 mD while that to methane was 16% lower. Instability of differential pressure readings at high flow rates when using methane introduced some uncertainties in the calculated permeability values. The base permeability to brine was therefore taken to represent the permeability of the reservoir core. During these repeated permeability measurements using brine, no fines were observed in the effluent. The dimensions and properties of the cores used are given in Table 3.1.

Table 3.1: Dimensions and properties of the cores used in the flow tests.

Core Name	Length, cm	Diameter, cm	Porosity, fraction	Absolute k, mD	Wettability
Clashach 1	33.20	4.99	0.185	1300	Water-wet
Clashach 2	61.30	4.99	0.165	850	Mixed-wet
Reservoir core	8.14	3.72	0.350	4580	Water-wet

3.2.3. Fluid samples

For the tests reported here, three oil samples and two brines were used. The oil samples were high purity n-decane ($C_{10}H_{22}$), a refined mineral oil and a stock-tank (dead crude) oil sample from a North Sea reservoir. Decane is miscible with CO_2 at the test temperature and pressure of 100.4 ^{o}F and 2000 psig, respectively. The relatively heavier refined oil and crude oil contain mainly C20+ components, as shown in Table 3.2 and 3.3 respectively, and are immiscible with CO_2 at the test conditions. The viscosities and densities of the oil samples are shown in Table 3.4.

Table 3.2: The extended compositions of the refined mineral oil.

Component	Mole%	Component	Mole%	Component	Mole%	Component	Mole%
C20s	0.17	C28s	5.20	C36s	4.86	C44s	2.05
C21s	0.28	C29s	5.96	C37s	4.17	C45s	1.11
C22s	0.73	C30s	6.13	C38s	4.30	C46s	1.29
C23s	1.62	C31s	5.72	C39s	3.61	C47s	0.78
C24s	2.99	C32s	5.28	C40s	3.57	C48s	0.71
C25s	4.11	C33s	5.22	C41s	3.22	C49s	0.58
C26s	5.55	C34s	5.57	C42s	2.14	C50+	1.62
C27s	5.13	C35s	4.46	C43s	1.87	TOTAL	100.00

Table 3.3: The extended compositions of the stock tank oil.

Component	Mole%	Component	Mole%	Component	Mole%	Component	Mole%
C3	0.06	C8s	2.96	C15s	5.06	C22s	2.77
iC4	0.06	C9s	2.29	C16s	4.78	C23s	2.31
nC4	0.07	C10s	2.95	C17s	3.94	C24s	2.35
iC5	0.18	C11s	3.01	C18s	4.09	C25+	37.31
nC5	0.09	C12s	3.86	C19s	3.71	TOTAL	100.00
C6s	0.53	C13s	4.52	C20s	3.27		
C7s	1.90	C14s	4.92	C21s	3.01		

Table 3.4: Properties of the oils used at 100.4 ^{o}F.

Sample	Properties	Value	Source
Decane	Viscosity at 2000 psig, cP	0.832	Lemmon et al. (2008)
	Density at 2000 psig, lb/ft^3	45.44	Lemmon et al. (2008)
Refined mineral oil	Viscosity at 2000 psig, cP	81	Measured
	Density at 2000 psig, lb/ft^3	57.12	Calculated (PREOS)
Dead crude oil	Viscosity at 2000 psig, cP	145	Measured
	Viscosity at 2500 psig, cP	158	Measured
	Density at 2000 psig, lb/ft^3	58.07	Calculated (PREOS)

The first brine used was synthetic brine made of degassed distilled water with 10,000 ppm salinity containing 0.8 wt% sodium chloride (NaCl) and 0.2 wt% calcium chloride hexahydrate ($CaCl_2.6H_2O$). The second brine used was of higher salinity representing typical injection brine (seawater) in the real field waterflood. It contains 2.6 wt% of sodium chloride (NaCl) and 0.6 wt% of calcium chloride hexahydrate ($CaCl_2.6H_2O$) with a total dissolved solid of 35,380 ppm. The ionic contents of the second brine are given in Table 3.5. Hereafter, the

low and high salinity brines are referred to as Brine 1 and Brine 2, with the corresponding carbonated brine as Carbonated Brine 1 and Carbonated Brine 2, respectively. Throughout this chapter, the terms carbonated water and carbonated brine are used interchangeably to refer to carbonated brine. The same brine was used for the connate water as well as the injected water in the tests.

To make up the carbonated brine, 99.9% purity CO_2 was mixed with brine in a pressure cell until saturation. The brine was first degassed by vacuum pump to remove air. It was then mixed with CO_2 in a rocking cell at the required carbonation pressure and 100.4 ^{o}F. The mixture was agitated to facilitate mixing until the pressure was stabilised, indicating that the fluids inside the cell were at equilibrium. The equilibrium fluid was then transferred into the storage vessels and stored at the test pressure and temperature. Properties of the brine samples are given in Table 3.6. All the viscosities of the brine and carbonated brines were measured. The density of Brine 1 was assumed as that of fresh water density, taken from National Institute of Standard (NIST) database (Lemmon et al., 2008), whereas the densities of the carbonated brines were extrapolated from data measured by Garcia (2001), Figure 3.3.

Table 3.5: Ionic content of the synthetic seawater (Brine 2).

Ion	ppm	Ion	ppm
Na	11700	Li	2.2
Ca	1170	Cl	18200
Mg	326	SO_4	3180
K	123	Br	34
Sr	31	HCO_3	0

Table 3.6: Properties of the brine used at 100.4 ^{o}F.

Sample	Pressure, psi	Viscosity, μ, cp	Density, ρ, g/cc	CO_2 solubility, sm^3/m^3	
				Calculated	Ave. Measured
Brine 1	2000	0.68	1.000	-	-
Carbonated Brine 1		0.69	1.011	31.1	29.9
Brine 2	2500	0.65	1.000	-	-
Carbonated Brine 2		0.85	1.030	29.3	28.2

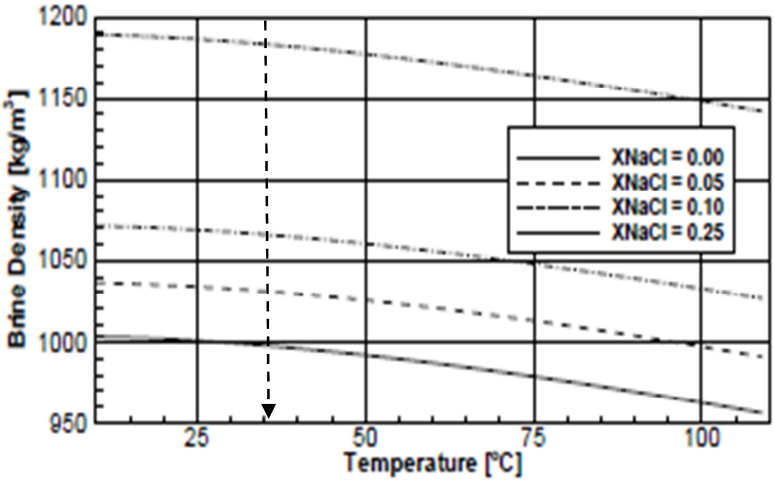

Figure 3.3: Density of NaCl solutions for salt mass fraction (XNaCl) from 0 to 0.25 (Garcia, 2001).

The CO_2 solubility in water (R_{sw}) was calculated by the Chang et al. correlation (1998), which is used in E300 simulator (ECLIPSE 2007.1). Details of the correlations are given in Appendix A3.1. The solubility was then corrected for the effect of brine salinity using Equation 3.1:

$$\log\left(\frac{R_{sb}}{R_{sw}}\right) = -0.028 S.T^{-0.12} \tag{3.1}$$

where R_{sb} is the CO_2 solubility in brine of salinity S in scf/stb, R_{sw} in scf/stb, S is the salinity in weight% of solid and T is temperature in °F.

At 2000 psig and 100.4 °F, R_{sw} was estimated at 31.1 sm^3/m^3 whilst at 2500 psig and 100.4 °F, R_{sw} was calculated to be 45.1 sm^3/m^3 (184.3 scf/stb), which was then reduced to 29.3 sm^3/m^3 (165 scf/stb) after correction, due to brine salinity. A good agreement was observed between the calculated and measured CO_2 solubility, as shown in Table 3.6.

3.2.4. Test preparation and procedures

The core was first cleaned by at least two cycles of methanol and acetone, and subsequently put in the oven at 149 ^{o}F (65 ^{o}C) to dry. The core was then wrapped in aluminium foil before being put into a sleeve and mounted horizontally in a high-pressure core holder. For the reservoir core which is relatively friable, a heat shrink was applied after wrapping the core with the foil to ensure the core did not disintegrate under the test flow and pressure. Brine was placed in the annular space between the core and the core holder and pressurized to provide a confining pressure. As the reservoir core was not preserved, there is a possibility that it might be oxidised. The effect of the possible oxidation on the results reported here was however not quantified.

Different displacement rates were used for different core sizes; 20 cc/hr (0.25 m/day) for the Clashach cores and 1 cc/hr (0.44 m/day) for the much shorter reservoir core. The rates were chosen such as to ensure that the displacement rate was within typical displacement rates at the reservoir scale of 0.1 to 1 m/day. The calculated viscous/gravity ratio, $R_{v/g}$, for the experiments using Equation 2.5 (in Chapter 2) are shown in Table 3.7. Except for the coreflood involving the viscous mineral oil in the Clashach core, $R_{v/g}$ values of the experiments are relatively low, indicating the flow is dominated by gravity. In order to minimize the impact of gravity segregation of the fluids inside the core, the core holder was rotated during the experiments.

Table 3.7: The calculated viscous/gravity ratio for the coreflood experiments.

Core	Length, cm	Diameter, cm	k, mD	Injection rate, cc/hr	Oil sample	$R_{v/g}$
Clashach 1	33.20	4.99	1300	20	Decane	5
					Mineral oil	1412
Clashach 2	61.30	4.99	850	20	Decane	13
Reservoir core	8.14	3.72	4580	1	Stock tank oil	34

Two sets of coreflood tests were carried out:

1. Secondary carbonated waterflood (without preceding water injection) at 100.4 ^{o}F and 2000 psig, using Clashach cores with no initial water saturation, S_{wi}.

2. Secondary and tertiary (post-waterflood) CWI performed using the reservoir core with crude oil at S_{wi}.

The **first** set of the coreflood tests were performed in the core rig shown in Figure 3.2 with effluent volumes measured at the test conditions, involving decane, refined viscous oil, Brine 1 and Carbonated Brine 1. Excluding any pre-existing water in the core for this set of tests enables us to accurately monitor the flow of the injected carbonated water and the manner in which the dissolved CO_2 is transported within the porous medium.

In the secondary process, the displacing fluid (water or carbonated water) was injected to displace the oil in the core without a preceding water injection. After saturating the core with the oil, plain water was injected until no oil was produced to quantify the oil recovery from the core by water injection (WI). The displacement was stopped when no change in the volume of the collected oil in the measuring cylinders was observed as the injection continued. At this stage, the oil production volume reduced from 1 PV per pore volume injected (PVI) to a very low value of 0.02 PV oil/PVI. In other words, the production rate was dropping from being equal to the injection rate at the beginning to 2% of that when the injection stopped. Prior to the subsequent secondary CWI, the core was cleansed with many pore volumes of acetone and methanol in order to remove any residual water or oil from the preceding waterflood test. The core was then again saturated with the oil under the same conditions, followed by the carbonated water displacement.

The **second** set of coreflood tests were performed using the reservoir core with crude oil sample in the core rig shown in Figure 3.1. All the coreflood tests in the reservoir core were performed at S_{wi} in order to closely mimic the presence of irreducible water in the reservoir. The coreflood displacements with Carbonated Brine 1 and Carbonated Brine 2 were carried out at 2000 and 2500 psig, respectively. The steps involved in the test with the S_{wi} are flowcharted in Figure 3.4.

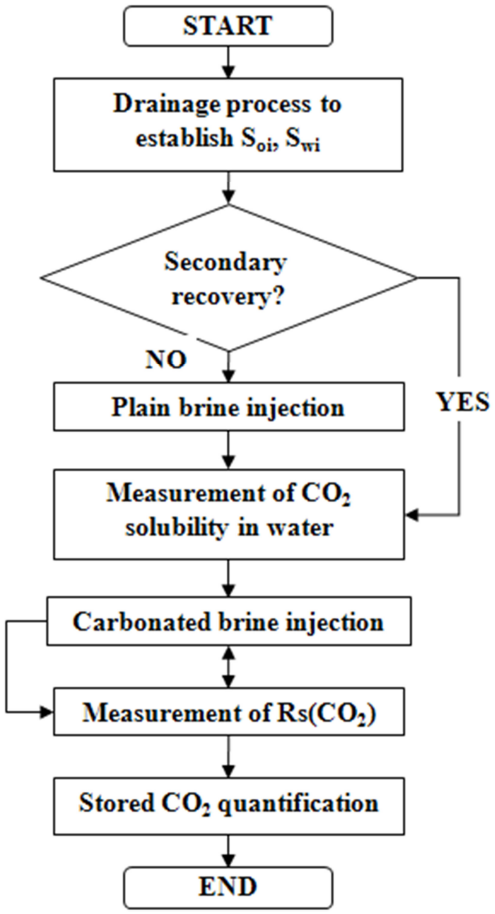

Figure 3.4: General work flow of the coreflood tests in the reservoir core at initial water saturation, S_{wi}.

The initial oil and water saturations were first established in the core. This was done by injecting oil through the brine-saturated core until the brine production came to a plateau. In the secondary CWI, the CO_2 content of the injected carbonated water was then measured to confirm no leakage of CO_2 from the carbonated water during transfer, followed by the carbonated waterflood. For the tertiary CWI, after establishing the initial fluid saturations in the core, plain water was injected until no measureable amount of oil was produced. Then the CO_2 content in the injected carbonated water was measured, followed by the carbonated waterflood.

The volume of the oil, gas and water produced, the differential pressure (ΔP) across the core, as well as the ratio of CO_2 gas produced to carbonated water injected, designated as Rs(CO_2),

were monitored and recorded throughout the tests. This ratio was compared with the initial CO_2 content in the carbonated water. This is to check whether the fluid inside the core was still taking up the CO_2 from the injected carbonated water. If it was, then the ratio showed an increasing trend. On the other hand, if the ratio started to level off, it indicated the fluid inside the core was almost saturated with CO_2. Although it is desirable to stop the test when the residual oil in the core is almost saturated with CO_2, practically, this would take many more pore volumes of carbonated water injections, and thus an impractically long experimental time. In this study, the tests were stopped when the $Rs(CO_2)$ has at least started to stabilize. When the coreflood test had stopped, plain water was flushed through the core and the CO_2 produced was measured to quantify the amount of the CO_2 stored in the core at the end of the coreflood test.

3.3. Experimental results and discussion

The displacement tests carried out in this study are shown in Figure 3.5. The test numbers mentioned in the subsequent text in this chapter refer to the test numbers shown in this plot. The effect of oil viscosity, core wettability, brine salinity and the recovery mode on CWI performance was investigated. In certain tests, the amount of the injected CO_2 being stored was also quantified. The behaviour of the dissolved CO_2 was examined by observing the CO_2 front propagation, as this affects the effectiveness of CWI as an oil recovery method.

As can be seen later, for the coreflood tests in the reservoir core, the S_{wi} established at the beginning of the tests vary slightly from one test to the other. In order to avoid these different initial conditions from influencing the analysis of the results, comparison was also made with the oil recovery expressed as a fraction of initial oil saturation, S_{oi}, instead of pore volume (PV).

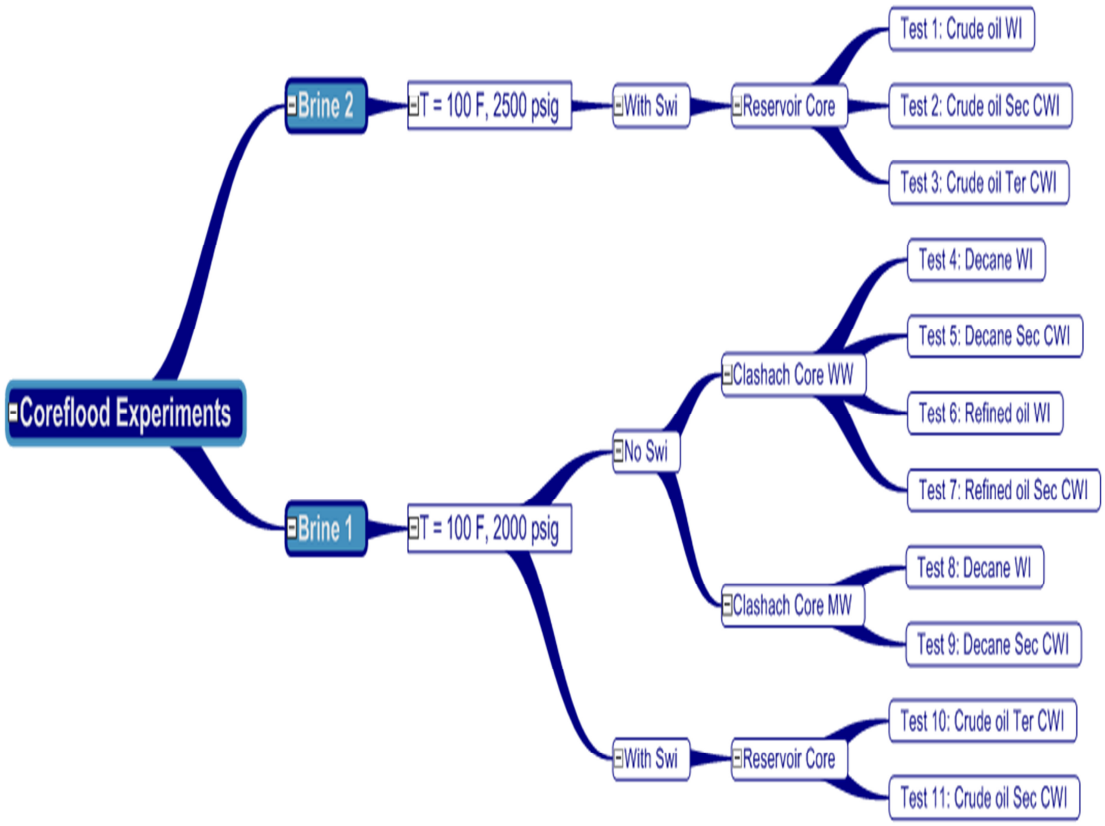

Figure 3.5: List of coreflood experiments reported.

3.3.1. Secondary versus tertiary CWI

In the secondary recovery mode, carbonated water was injected to displace the oil in the core (with or without S_{wi}) whereas in the tertiary recovery mode, CWI into the core started consecutively after plain water has been injected until close to waterflood residual oil saturation has been achieved. The comparison here is made between the coreflood test results in the reservoir core using crude oil and Carbonated Brine 2 (Tests 2 and 3). The CWI performance was compared with that of WI coreflood test carried out chronologically closest to it, to ensure that comparison is made at reasonably similar core properties. CWI has been reported to have caused permeability alterations in sandstone cores due to dissolution of rock minerals by the carbonic acid (Ross et al., 1983; Sayegh et al., 1990; Tang et al., 1999).

The crude oil was first injected into the brine-saturated core, whereby S_{wi} of 10.6 %PV was

established. Plain Brine 2 was then injected (Test 1) at 1 rcc/hr and stopped at 0.8 PVI where the rate of the oil production dropped to about 0.013 PV or 0.4 cc of oil produced per PVI. With this very low amount of oil produced, it was taken that continuing the brine injection would not produce any measurable amount of oil. 41.6 %PV (46.5 $\%S_{oi}$) oil recovery was recorded from this WI. The rather high residual oil saturation may have been contributed to by the relatively high viscosity of the oil used.

The core was next thoroughly cleaned by two cycles of toluene and methanol to prepare for the secondary CWI (Test 2). The initial oil and water saturation in the core were again established and this time S_{wi} of 7.2 %PV was obtained. Before injecting the carbonated water into the core, 4 PV of the carbonated water was first allowed to flow through the bypass line and the CO_2 produced was measured. The CO_2 in the brine was recorded at 27.7 sm^3/m^3, which was in reasonable agreement with the theoretical value of 29.3 sm^3/m^3. Having verified the CO_2 content, the carbonated water was then injected through the core at 1 rcc/hr.

At a certain stage during the injection, the water and oil effluent appeared emulsified with sediment-like materials produced (Figure 3.6), which was not observed during the preceding brine injection. In order to confirm the effluent volume, the cylinders containing core effluent were settled in an oven at 122 ^oF (50 ^oC) to allow separation of phases. 60.6 %PV (65.2 $\%S_{oi}$) of oil was recovered at the end of this secondary carbonated waterflood. No analysis was done to identify the sediment. However, the analysis of the water effluent using an Inductively Coupled Plasma (ICP) spectrometer showed the presence of Fe, Al and Si which were not present in the fresh carbonated brine. Due to the relatively friable nature of the core used, the sediment could possibly be fines which had migrated out of the core due to the flooding. Dissolution of the carbonate cementing material of the core could also possibly have occurred. Measurement of the core permeability after the test revealed that the permeability had increased by 17% to 5360 mD.

Figure 3.7 shows the ratio of CO_2 produced to the volume of carbonated water injected recorded during the secondary CWI (Test 2). Initially, all the CO_2 in the injected carbonated water was dissolved in the oil and in-situ water. The $Rs(CO_2)$ ratio increased gradually until it slowly levelled off at about 77 % of the initial value. At this point, the fluid in the core was minimally taking up the CO_2 in the injected carbonated water. The amount of CO_2 injected, produced and left in the core at any particular time during the displacement is plotted in Figure

3.8.

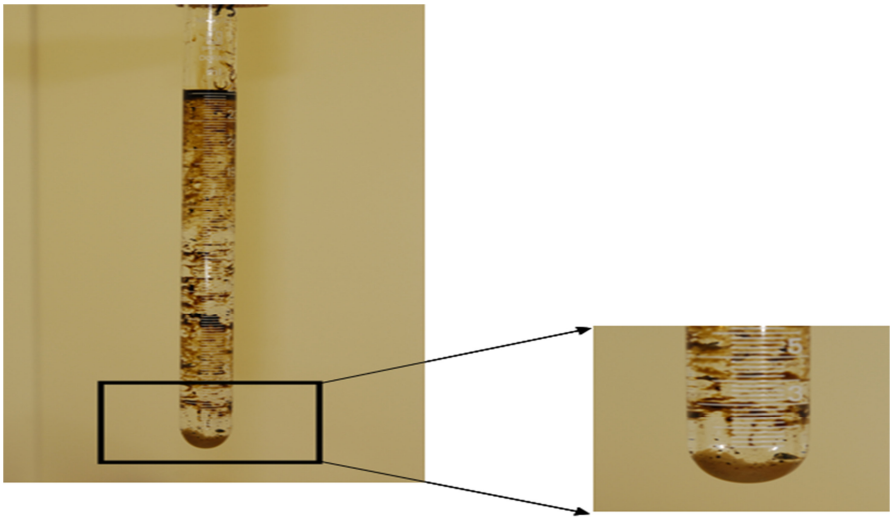

Figure 3.6: Example of sediment formed at the bottom of the measuring cylinder in the collected effluents.

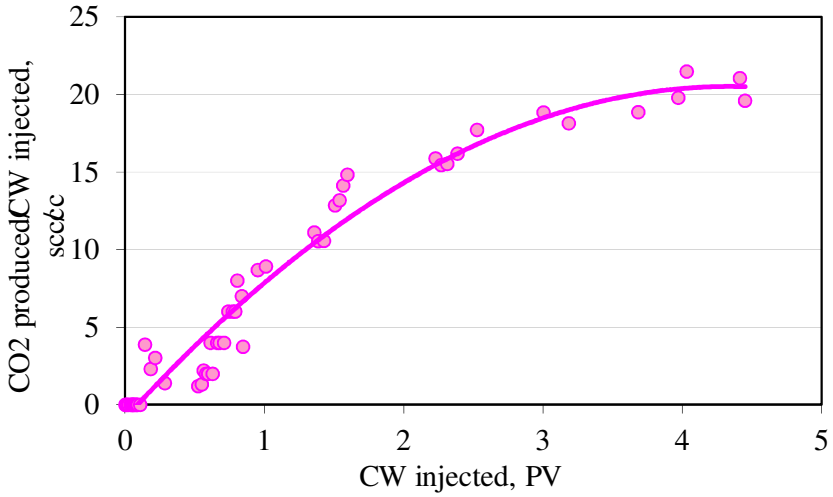

Figure 3.7: The ratio of the cumulative CO_2 produced to the volume of carbonated water injected during secondary CWI, crude oil in reservoir core at 100.4 ^{o}F, 2500 psig (Test 2).

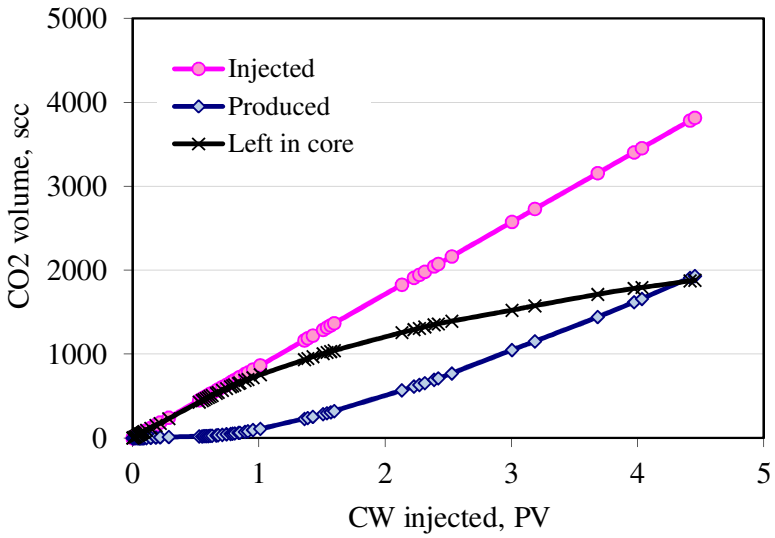

Figure 3.8: The cumulative CO_2 injected, produced and left in the core during secondary CWI, crude oil in reservoir core at 100.4 ^oF, 2500 psig (Test 2).

The tertiary CWI (Test 3) was carried out to quantify the level of increase in the oil recovery by CWI after a plain WI. S_{wi} was first established in the core, which was 12.7 %PV, following the same procedure described for Test 1. In order to simulate conventional water flooding, plain brine was then injected until up to 2.86 PV, by which time no further oil recovery was observed. 58.4 %PV (66.9 $\%S_{oi}$) of oil was recovered by the waterflood, leaving 28.9 %PV of residual oil. This much higher oil recovery from WI as compared to that from Test 1 is consistent with the increase in permeability of the core after Test 2. The carbonated water, which contained 28.7 sm3 of CO_2 per m^3 of brine for this test, was then injected into the core at 1 rcc/hr. The CO_2 produced was monitored throughout the test and after 5.26 PVI, the Rs(CO_2) reached 23.5 sm^3/m^3, as shown in Figure 3.9. At this point, no measurable amount of oil was produced and the CWI was stopped with 67.6 %PV (77.4 $\%S_{oi}$) of total oil recovered. Figure 3.10 shows the cumulative CO_2 injected, produced and left in the core.

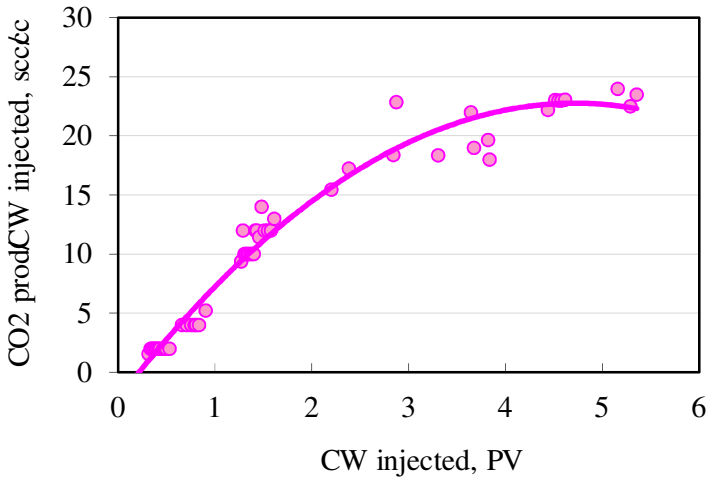

Figure 3.9: The ratio of the CO_2 produced to the carbonated water injected during tertiary CWI, crude oil in reservoir core at 100.4 ^{o}F, 2500 psig (Test 3).

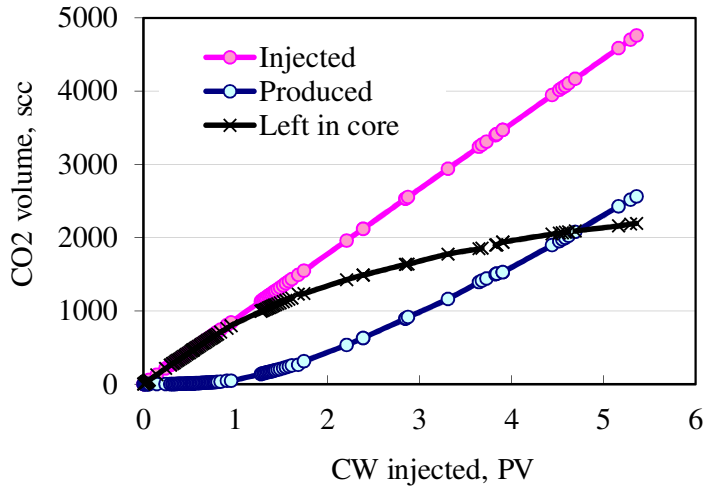

Figure 3.10: The cumulative volume of CO_2 injected, produced and left in the core during tertiary CWI, crude oil in reservoir core at 100.4 ^{o}F, 2500 psig (Test 3).

The oil recovery profiles of the secondary and tertiary CWI are shown in Figures 3.11 and 3.12, respectively. In the secondary CWI (Test 2), prior to breakthrough, the carbonated water flood has the same curve as the plain waterflood (Test 1). As shown in Table 3.8, the secondary CWI recovered 19 %PV (18.8 $\%S_{oi}$) more oil than the plain WI while 9.2 % PV (10.5 $\%S_{oi}$) incremental oil was produced from the tertiary process (Test 3). These results

clearly show that CWI has a promising potential as an EOR injection strategy in both secondary and tertiary recovery modes with higher recovery in the former than the latter. The results also serve as evidence that tertiary CWI can re-mobilize part of the oil that had been trapped in the preceding water injection period.

Table 3.8: The incremental oil recovery from the secondary and tertiary CWI.

Process	S_{wi}, % PV	Oil recovery		Incremental oil recovery	
		% PV	% S_{oi}	% PV	% S_{oi}
WI	10.6	41.6	46.5		
Secondary CWI	7.2	60.6	65.2	19.0	18.7
WI	12.7	58.4	66.9		
Tertiary CWI		67.6	77.4	9.2	10.5

For an ideal comparison, both secondary and tertiary experiments had to be conducted on the same piece of rock having the same properties. However, as mentioned above, the secondary CWI has resulted in the change of the core permeability giving higher oil recovery from the subsequent WI prior to the tertiary CWI. This inevitably raises a question as to what the actual incremental oil recovery for the tertiary CWI is for the unmodified core.

The author hypothesizes that without the change in the core permeability the tertiary CWI will still increase the oil recovery above that of WI and the incremental oil recovery maybe even higher than 9.2 %PV but not exceeding the 19% recorded by the secondary CWI. The fluid mobility in the core maybe slightly reduced but the remaining oil to be recovered by the CWI would be much more as compared with that with the higher permeability core.

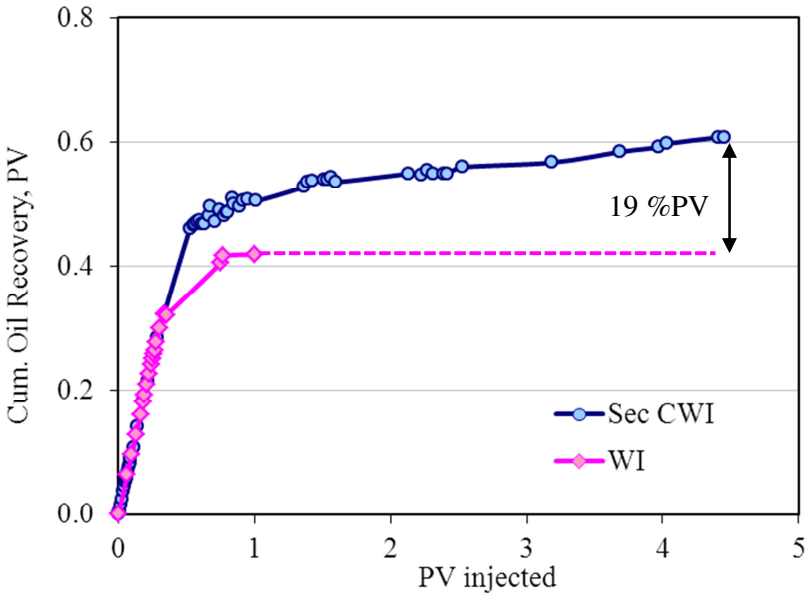

Figure 3.11: The cumulative oil recovery from secondary CWI using Carbonated Brine 2 in the reservoir core, at 100.4 ^{o}F, 2500 psig (Test 2).

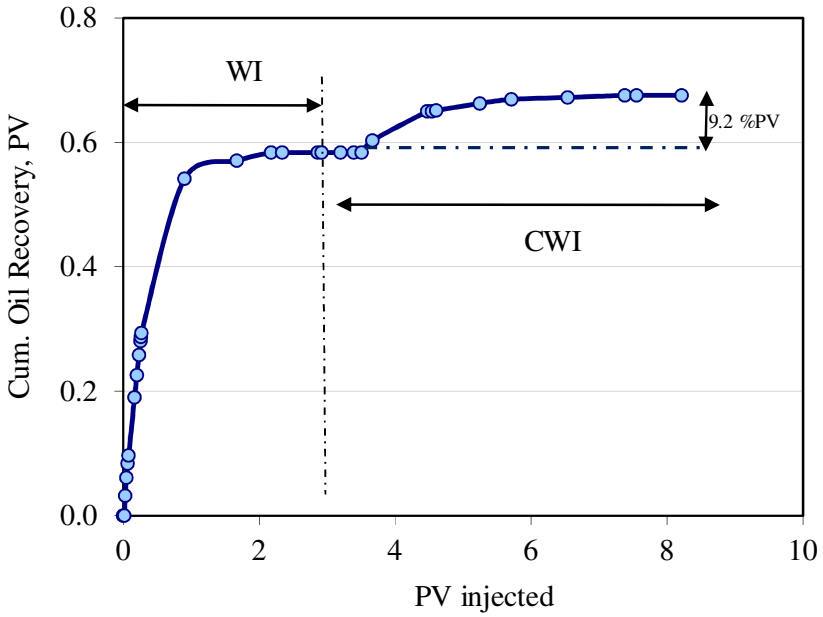

Figure 3.12: The cumulative oil recovery from the tertiary CWI using Carbonated Brine 2 in the reservoir core, at 100.4 ^{o}F, 2500 psig (Test 3).

3.3.2. Effect of oil viscosity

In order to investigate the effect of oil viscosity on the CWI performance, the secondary CWI in the water-wet Clashach core using decane (Test 4 and 5) and refined viscous oil (Test 6 and 7) were compared. For both tests the water and carbonated water was injected at 20 rcc/hr. At the test temperature and pressure, the refined oil viscosity of 81 cP is about two orders of magnitude higher than that of decane (0.82 cP).

The cumulative oil recovery and differential pressure across the core for decane and the refined viscous oil are shown in Figure 3.13 and Figure 3.14, respectively. Prior to water breakthrough, the rate of oil recovery equalled the rate of the carbonated water injection. Both WI and CWI broke through at about the same time, after which the oil production rate slowed down significantly. CWI gives higher additional oil recovery with decane than with viscous oil. With a favourable viscosity ratio of 1.2, closer to piston-like displacement with sharper breakthrough was observed for decane. Oil production took place mainly before the water breakthrough during which 64 %PV of oil was produced. At the end of the injections, a total of 71 %PV of decane was recovered by WI, while CWI produced 7.6 % more.

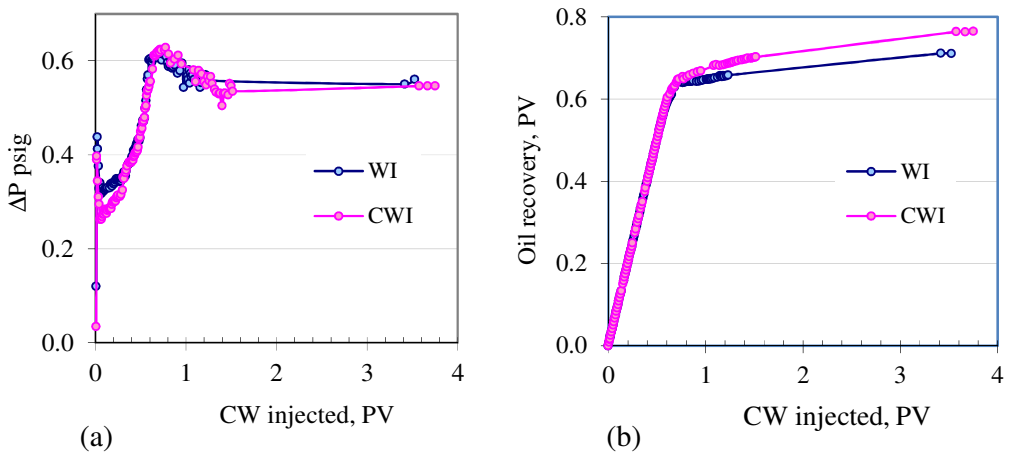

Figure 3.13: Comparison between the measured (a) differential pressure across the core and (b) cumulative oil recovery for WI and CWI, decane, water-wet core at 100.4 ^{o}F, 2000 psig (Tests 4 and 5).

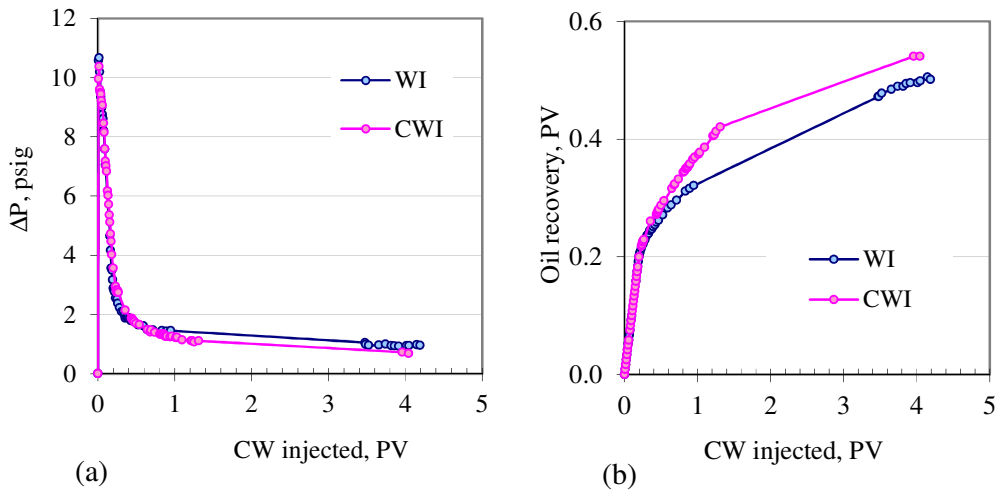

Figure 3.14: Comparison of measured (a) differential pressure across the core and (b) cumulative oil recovery between WI and CWI, refined viscous oil, water-wet core at 100.4 ^{o}F, 2000 psig (Tests 6 and 7).

In addition to a very favourable mobility ratio, the oil recovery in CWI of decane was also enhanced by the miscibility of decane with CO_2. Decane exhibited unlimited swelling with CO_2, which enhanced the oil production despite the fact that carbonated water is immiscible with decane. Sohrabi et al. (2009) observed in their micro-model experiments on tertiary CWI, using decane and 16.5 cP viscous oil at the same temperature and pressure as used in this study, that significant oil swelling took place during CWI: up to 105% for decane as compared to 23% for the viscous oil.

On the contrary, the high viscosity ratio of 119 and high viscous/gravity ratio (Table 3.7) between carbonated water and the more viscous oil strongly indicate unstable front displacement. This is evident by a much lower oil recovery from waterflooding of only 50.2 %PV as compared to 71 %PV for decane. A significant amount of oil was produced after the water breakthrough, i.e. 21.8 %PV in the plain waterflooding and 25.8 %PV in the CWI unlike decane displacement, where most of the oil was recovered prior to breakthrough. After 4 PV of total injections, 50.2 and 54.1 %PV of oil was recovered from WI and CWI, respectively. This is equivalent to 7.8 % higher oil recovery than from the plain WI.

The trend in differential pressure in both tests is also very different. For decane, the

differential pressure across the core was just a fraction of 1 psi, which increased gradually to a peak value at breakthrough, before gradually stabilizing as more carbonated water was injected. However, the more viscous oil requires much higher differential pressure to displace the oil as shown by a sharp declining ΔP trend in Figure 3.14. The slightly lower differential pressure than those of WI after the breakthrough demonstrate a more efficient displacement by the carbonated water despite the fact that more oil was produced.

3.3.3. Effect of wettability

The reservoir wetting state or wettability has been widely reported to affect the pore displacement mechanism and theh fluid distribution. Among the factors that affect wettability are oil and water composition, te mineralogy of the rock, the initial water saturation, and the temperature (Bobek et al., 1958; Buckley et al., 1989; Buckley and Liu, 1998).

The impact of core wettability on CWI performance was assessed by comparing the oil recovery and differential pressure of the WI and CWI for decane in the water-wet core as shown in Figure 3.13 and mixed-wet core. For the mixed-wet core, as can be seen in Figure 3.15, the additional oil recovery from CWI took place at breakthrough i.e., much sooner than in the water-wet core, in which the additional oil recovery took place gradually, after the breakthrough. Again, a much more efficient displacement in CWI is evident from much lower pressure drops across the core yet higher oil production than in WI. The difference in the differential pressure of WI and CWI is also much larger in the mixed-wet core.

For more or less the same pore volume injected, oil recovery from WI is lower in the mixed-wet core (58.5 %PV) than in the water-wet core (71.0 %PV). This is due to the fact that in the water-wet core, water occupies the small pores and forms a thin film over the rock surfaces while oil occupies the centres of the larger pores (Donaldson et al., 1971). During waterflooding, water will tend to imbibe into small-sized pores and displaces the oil into the centre of the large pores, which results in efficient oil recovery.

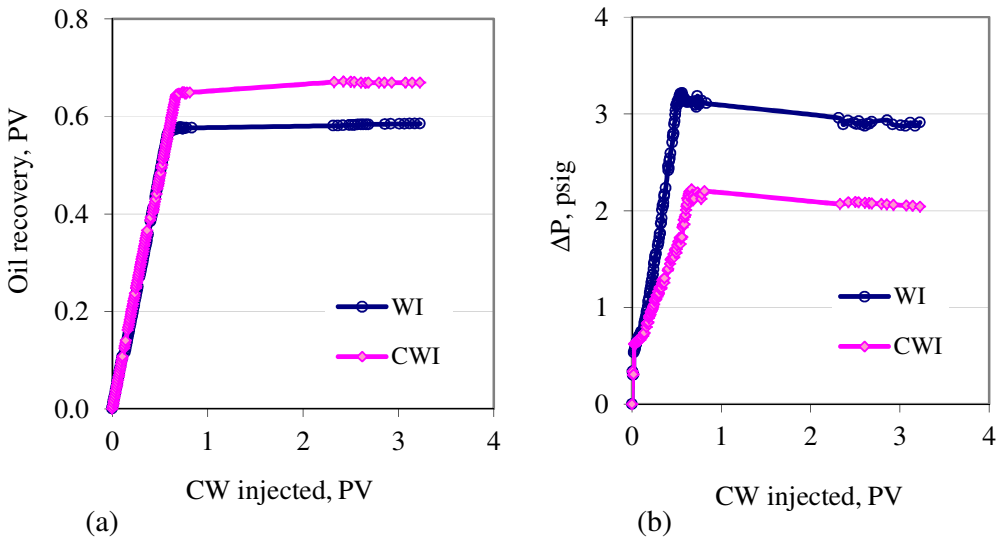

Figure 3.15: Comparison of measured cumulative oil recovery (left) differential pressure (right) across the core and between WI and CWI, decane, mixed-wet core at 100.4 ^{o}F, 2000 psig (Tests 8 and 9).

The improvement of oil recovery by CWI (relative to that of WI) is, however, higher in the mixed-wet core i.e. by 11.8 %, as opposed to only 7.6 % in the water-wet core. It was postulated that there is formation of continuous oil-wet paths of appreciable length through the mixed-wet rock, which gives rise to better connectivity and film flow of oil along the wetting phase even at low oil saturation (Salathiel, 1973). The connectivity is further enhanced by oil swelling, leading to better oil recovery. These observations are significant for CWI potential, since it is generally accepted now that many oil reservoirs are mixed-wet (Morrow, 1990; Jerauld and Rathmell, 1997). This encouraging observation was verified by another test with recovery measured at standard conditions (not reported here).

3.3.4. Effect of brine salinity

CO_2 solubility in brine is a function of pressure, temperature and brine salinity (Klins, 1984). It increases with pressure but decreases with temperature and water salinity. In order to examine the impact of brine salinity on CWI recovery, the results of the secondary and tertiary carbonated seawater (Carbonated Brine 2) flooding of the crude oil in the reservoir core with

those using low salinity carbonated brine (Carbonated Brine 1) were compared. It should however be noted that the latter was performed at 2000 psig, 100.4 ^{o}F with estimated CO_2 solubility of 31 sm^3/m^3. The CO_2 solubility in Carbonated Brine 2 at 2500 psig, 100.4 ^{o}F was around 29.3 sm^3/m^3. Only relative comparison in the oil recovery trend could be made, due to this difference in the test pressure.

As can be seen in Figure 3.16, at the same PV injected after breakthrough, the oil recovery from the secondary low salinity CWI is slightly higher than that of high salinity (Carbonated Brine 2). A similar trend was observed with the plain WI where the Brine 1 flooding (Test 10) yields higher oil recovery (48 %PV) than that obtained from Brine 2 injection (41.6 %PV) (Test 1). On the other hand, the incremental oil recovery for the tertiary CWI was higher in the high salinity Carbonated Brine 2 (Figure 3.17). The incremental oil recoveries from these coreflood tests are summarized in Table 3.9.

Table 3.9: The measured incremental oil recovery from the secondary and tertiary CWI using Carbonated Brine 1 and Carbonated Brine 2.

Process	Brine	S_{wi}, % PV	Incremental Oil recovery	
			% PV	% S_{oi}
Secondary CWI	Carbonated Brine 1	14.5	18.8	22.0
Secondary CWI	Carbonated Brine 2	7.2	19.0	20.5
Tertiary CWI	Carbonated Brine 1	15.4	6.6	7.8
Tertiary CWI	Carbonated Brine 2	12.7	9.2	10.5

3.3.5. Displacement front propagation

CWI as an EOR method relies on CO_2 contact with the resident oil. CO_2 solubility in the oil, through diffusion and dispersion mechanisms results in the oil viscosity reduction, vaporization of lighter hydrocarbon in crude oil and oil swelling that expels the oil from the rock matrix. This swelling effect results in much less residual oil left in the reservoir after flooding and the reduction in oil viscosity increases the fluid mobility thus increasing the local displacement efficiency. The immiscible CO_2 EOR process also benefits from these mechanisms.

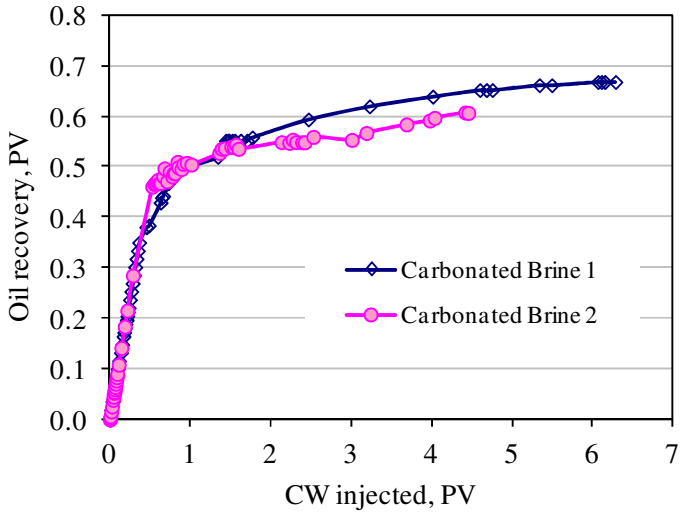

Figure 3.16: The cumulative oil recovery for secondary CWI using Carbonated Brine 1 and Carbonated Brine 2, crude oil in reservoir core (Tests 2 and 11).

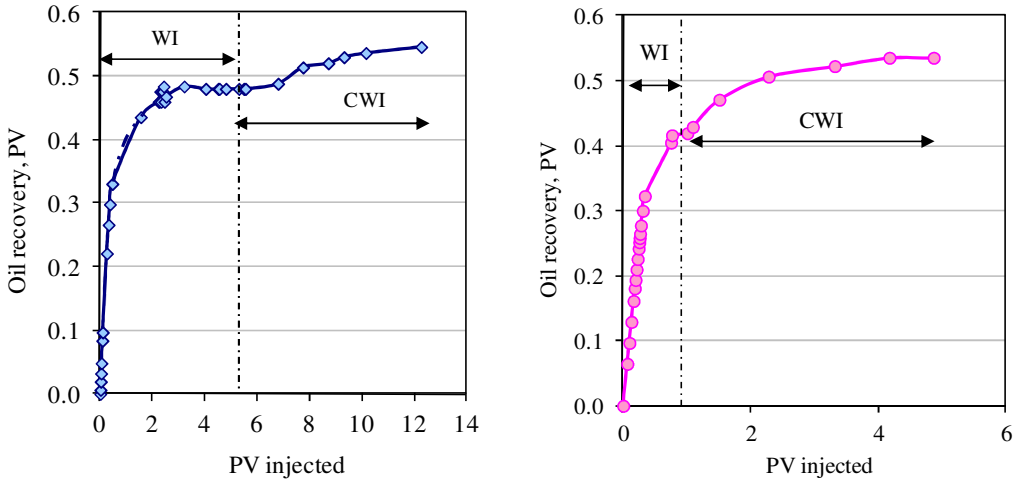

Figure 3.17: Comparison of oil recovery from tertiary CWI using (left) Carbonated Brine 1 (Test 10) and (right) Carbonated Brine 2 (Test 1), crude oil in reservoir core.

One of the main concerns in CWI is the deliverability of CO_2 by carbonated water to the oil ahead of the displacement front. If the carbonated water front is completely deprived of its CO_2 early and moves forward as plain water, its performance would be adversely affected and

would approach that of plain WI. To improve the oil recovery, CWI should be able to deliver the dissolved CO_2 to the oil, to result in the required changes of the oil physical and flow properties, such as the oil swelling and oil viscosity reduction. Larger improvement in oil mobility would be achieved if the carbonated water front is not deprived of its CO_2 early and travels a longer distance in the reservoir. Longer residence time of CO_2 in the reservoir is favourable for CO_2 storage, too.

The brine and CO_2 breakthrough times were thus closely observed and compared during the coreflood experiments. Figure 3.18a shows the early time production of brine and CO_2 in the secondary CWI experiment with decane in the mixed-wet core with recovery measured at the standard condition. CO_2 broke through after 0.64 PVI whereas brine broke through at 0.7 PVI. The same behaviour was also observed during the secondary Carbonated Brine 2 injection of the crude oil in the reservoir core (Test 2), with an even larger gap between CO_2 and brine breakthrough time. The CO_2 from the injected carbonated water had departed from the carbonated water, dissolved into the oil and was produced together with the oil ahead of the water, as shown in Figure 3.18b.

This small yet noticeable difference shows that the carbonated water front had not been depleted of its CO_2 content instead the CO_2 has moved ahead of the carbonated water front. This serves as evidence of the diffusion and dispersion of CO_2 from the carbonated water into the oil i.e. as a result of the CO_2 transfer from the carbonated water into the oil. This is an important finding because it proves good delivery of CO_2 by the carbonated water front to the oil as opposed to the behaviour of the carbonated water flood front predicted by the Buckley-Leveret method (de Nevers, 1964), in which the carbonated water loses its CO_2 completely into the oil to become plain water and moves faster than the CO_2.

A closer look at the gas production trend in Figure 3.19 also reveals that there were two distinct phases of gas production. During the first phase, the rate of gas production was more gradual indicating that the CO_2 gas slowly being produced; consistent with the CO_2 diffusion into and produced together with the oil. The gas production would have increased drastically after breakthrough if it was merely gas coming out of solution. The pressure data across the core given in Appendix A3.4 also shows that the inlet and outlet pressures were consistently close to the reported test pressure i.e. there was no unexpected pressure drop that could trigger gas evolving out of the solution prior to the gas breakthrough.

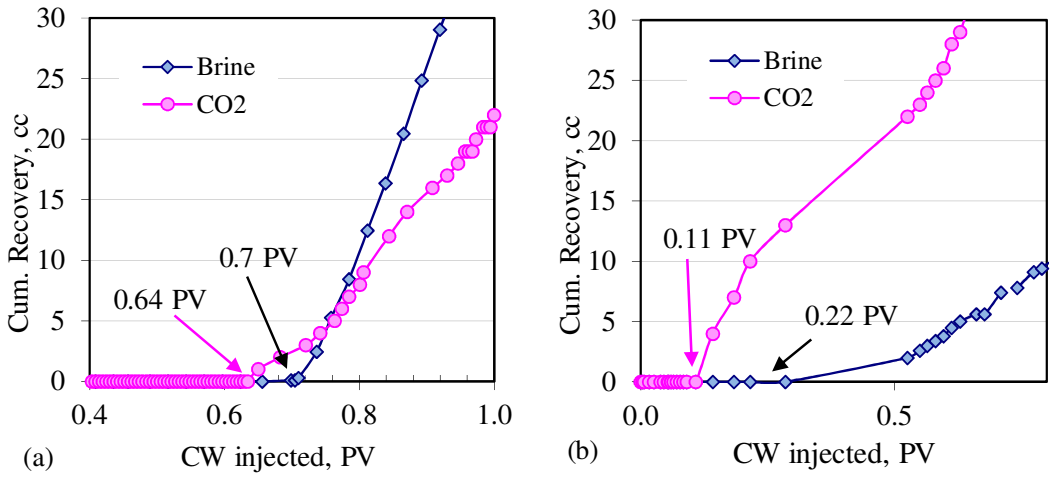

Figure 3.18: Early production of CO_2 and brine during secondary CWI of (a) decane in mixed-wet core and (b) crude oil in the reservoir core.

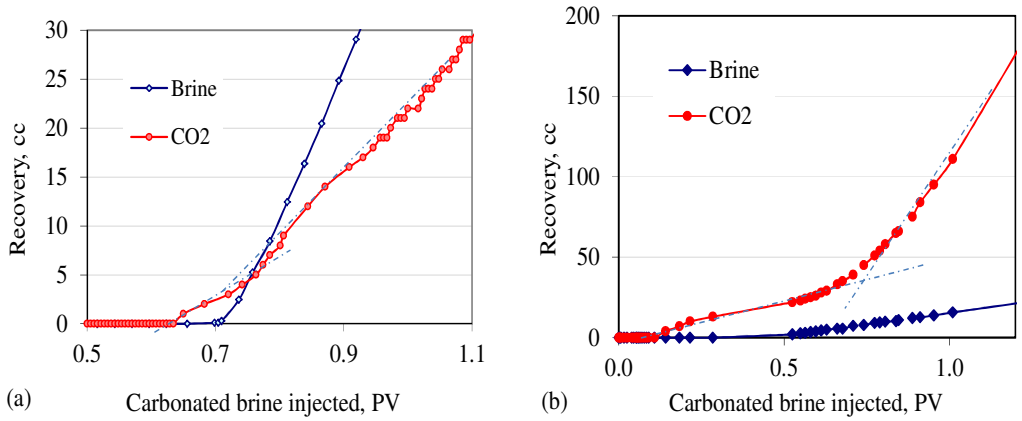

Figure 3.19: Early production of CO_2 and brine during secondary CWI of (a) decane in mixed-wet core and (b) crude oil in the reservoir core, showing two distinct gas production phases (shown by two dotted lines).

This process is somewhat analogous to the process of mass transfer and mixing that can lead to multiple-contact miscibility during some gas injections. As the injected carbonated water contacts the resident oil, a mixing zone is formed. This mixing zone, which is made of a mixture of oil and CO_2, moves ahead of the carbonated water front and its size increases with

time as it moves forward into the reservoir. This important observation helps us to understand the behaviour of the dissolved CO_2 and its interactions with the oil and water inside the reservoir as the CWI progresses, which impacts the effectiveness of CWI as an oil recovery method.

3.3.6. CO_2 storage through CWI

In CWI, part of the CO_2-diluted oil will be recovered. However, a large part of the transferred CO_2 will remain dissolved in the remaining oil, which is important for CO_2 storage. Taking the coreflood results of the stock tank oil in the reservoir core (Tests 2 and 3) as examples, about 45 and 51% of the injected CO_2 was stored in the secondary and tertiary CWI respectively, after about 4.5 PV of carbonated water injections (Table 3.10).

Table 3.10: The measured amount of CO_2 stored in the secondary and tertiary CWI using the stock tank oil in the reservoir core and Carbonated Brine 2 at 2500 psig, 100.4 ^oF.

Process	CO_2 injected, scc	CO_2 stored		Oil produced, cc	Retention factor, scc/cc
		scc	% CO_2 injected		
Secondary	3857	1743	45	18.78	93
Tertiary	4000	2048	51	2.76	742

Retention factor is defined as the standard volume of CO_2 left in the reservoir per stock tank volume of oil produced. In order to get an idea how these retention factors compare with those of the conventional immiscible CO_2 flooding, the author refers to the study by Klins and Farouq (1981) on conventional immiscible CO_2 flooding as an EOR method. They reported that for 100 cP oil at 100 ^oF, the retention factor varies from 181.6 scf of CO_2 per barrel of produced oil (32 scc/cc) for a reservoir with 70% S_{oi} to 1147.3 scf of CO_2 per barrel of produced oil (204 scc/cc) for a reservoir with 40% S_{oi}. Extrapolating this retention factor-S_{oi} relationship (Figure 3.20), the retention factor of the immiscible continuous CO_2 injection was estimated at 25 scc/cc and 382 scc/cc for 92.8% and 28.9% S_{oi}, which was the S_{oi} for the

secondary and tertiary CWI in this study, respectively. As shown in Table 3.9, much higher retention factor of 93 scc/cc and 742 scc/cc was obtained in the secondary and tertiary CWI processes, respectively. This could be contributed by the uniform distribution of CO_2 in the reservoir in CWI as compared to that in the immiscible continuous CO_2 injection.

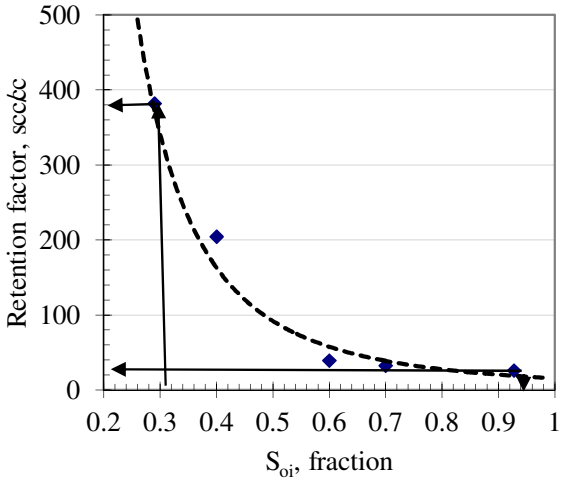

Figure 3.20: CO_2 retention factor for 100 cP oil in immiscible CO_2 injection as a function of S_{oi} (from Klins and Farouq, 1981).

3.4. Overall discussion

The results of a series of carbonated water coreflood experiments have been presented and discussed. Three different cores with different properties and states of wettability, three different oil samples and two different brines were used in the experiments with the main aims of determining experimentally the oil recovery and CO_2 storage by CWI and to further understand the mechanisms of the CWI process. Even though only one set of experiment for each process and sample was reported, the displacement tests were repeated at least twice and some trends were also checked for other samples used as well.

As a water-based oil recovery method, CWI performance has been compared with conventional waterflood, instead of direct CO_2 injection. At typical reservoir conditions, carbonated water dissolves 5 to 7 percent CO_2, thus direct comparison between CWI and (100%) CO_2 injection is difficult.

The experimental results clearly show that both secondary and tertiary CWI can improve the oil recovery above that of plain waterflooding. Secondary CWI gives higher and earlier incremental oil recovery than the tertiary CWI process as would usually be obtained for other oil recovery methods as well. In tertiary recovery, the remaining oil is more likely to be disconnected and exists in the form of isolated or by-passed patches, which are more difficult to remobilise. In the coreflood using the stock tank oil in the reservoir core reported here, secondary CWI reduces the waterflood oil saturation (S_{orw}) by 35%. It is interesting to note that this value falls within the 33-48% reduction of S_{orw} reported by McFarlane et al. (1952) from their carbonated water coreflood experiments, using much lighter Bradford crude ($\leq$ 2.86 cP) at 750 psig, 75 ^{o}F. The 40% improvement in oil recovery above the original estimates of conventional waterflood potential is also in good agreement with the 43% increase of oil recovery in the K&S secondary CWI project in Oklahoma reported by Hickok et al. (1962).

The tertiary CWI process in this study reduced the waterflood residual oil saturation by 31%. McFarlane et al. (1952) reported 8-47% reduction of the waterflood residual oil saturation by the tertiary carbonated coreflood of Bradford crude. It seems as if the oil viscosity does not strongly influence the reduction in the S_{orw} by CWI even though large difference in incremental oil recovery was observed between lighter and more viscous oil in terms of %PV.

The same trend was also observed in the case of decane (Tests 4 and 5) and viscous mineral oil (Tests 6 and 7) in the secondary CWI using the Clashach core, in which the additional oil recovery due to CWI of the more viscous oil, above that of WI, is more or less the same as that of decane, despite the former having the disadvantage of viscous fingering and much lower CO_2 solubility (lesser oil swelling) than decane. This infers that other mechanisms other than oil swelling due to CO_2 diffusion from carbonated water into the oil are also playing their roles.

It is believed that the more viscous oil benefits more from the oil viscosity reduction due to CO_2 diffusion into the oil than the lighter oil. For example, while, for decane, oil swelling and miscibility are the key recovery mechanisms, for the viscous refined oil, the viscosity reduction plays a greater role than the oil expansion. De Nevers (1964) in his simulation studies reported that "*carbonated water flooding will not be economical for crudes which swell strongly on carbonation but which do not have a significant viscosity reduction"*. As reported by Miller and Jones (1981), when contacted by CO_2, a larger percentage reduction

occurs in the viscosity of more viscous crudes. Macfarlane et al. (1952) demonstrated that CWI could result in more oil recovery than that theoretically possible by an oil volume expansion (oil swelling) alone. They reported reductions in oil viscosity of up to 50%. They also observed a similar trend of negligible difference in oil recovery when the viscosity of the Bradford oil used in their CWI coreflood tests was reduced from 2.86 cP to 1.42 cP by mixing it with heptane, at 750 psig and 75 ^{o}F. These comparisons highlight one of the important advantages of CWI: it brings comparable incremental oil recovery for light oil as well as for intermediate viscous oil. However, before this can be made a general conclusion, more coreflood experiments on a wider range of oil viscosities, densities and reservoir temperature and pressure are recommended to be carried out.

In addition to oil viscosity reduction, several mechanisms could have also contributed to the additional oil recovery by CWI. Sohrabi et al. (2009) and Riazi et al. (2009, 2010) studied the dominant pore scale mechanisms in secondary and tertiary CWI using decane and refined viscous oil through a series of two phase fluid flow experiments in a high pressure two dimensional glass micromodel. They concluded that swelling and remobilisation of isolated oil ganglia as a result of diffusion of CO_2 from carbonated water to oil as one of the most important mechanisms of oil recovery in CWI. They monitored the oil saturation in the micromodel versus time during CWI. Prior to the water breakthrough, oil recovery was mainly by displacement, as shown by the sharp drop in Figure 3.21. As more carbonated water was injected, CO_2 from the injected carbonated water diffused into the trapped oil left behind in the main displacement and swelled the oil. Over time, the isolated, swollen oil ganglia coalesced with each other and eventually produced. A similar observation was reported in the tertiary carbonated displacement in the micromodel (Riazi et al., 2009) but the level of swelling is less due to the presence of mobile water from the preceding waterflooding.

Another important mechanism is fluid redistribution or flow diversion. Oil swelling could cause fluid flow in some of the pores to become partially or completely restricted. In micromodel experiments using decane at 100 ^{o}F and 2000 psig, Riazi et al. (2009) observed that before CO_2 dissolution in the oil droplets, the carbonated water can flow through the sides of the pores (Figure 3.22a) but as the oil blobs swell (Figure 3.22b), some of the paths become partially or totally blocked. The carbonated water flow will be diverted and it contacts oil droplets in other areas that otherwise could have been bypassed, thus improving oil recovery.

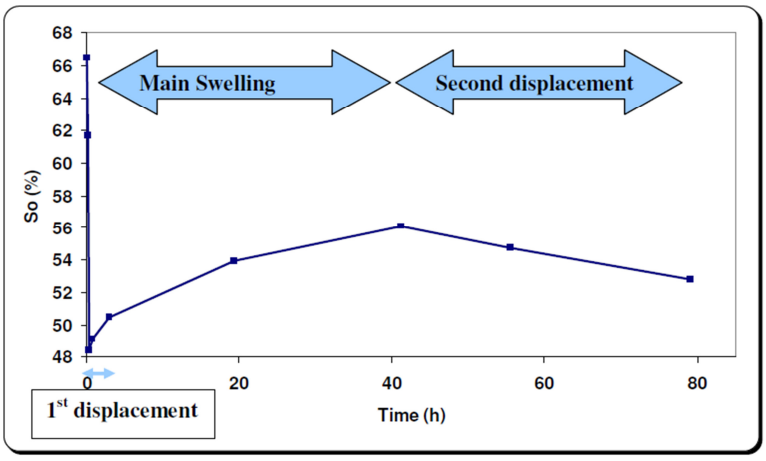

Figure 3.21: Oil saturation versus time, during CWI as a secondary recovery method in a micromodel (Sohrabi et al., 2008).

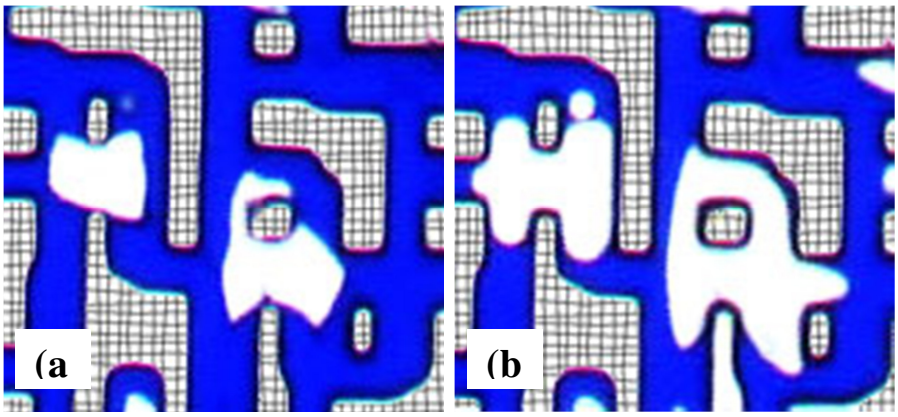

Figure 3.22: (a) Free oil droplets (white) surrounded by carbonated water (blue) (b) Swelled oil droplets as a result of dissolved CO_2 that block some of the fluid paths (Riazi et al., 2009).

Figure 3.18 earlier clearly shows that diffusion and dispersion of CO_2 is occurring during the core displacement in which much earlier CO_2 breakthrough time than that of the brine was recorded. The coreflood results also show that the native state of wettability of the rock is influential to the performance of CWI. This is further supported by the results from the CWI micromodel test on 16.5 cP mineral oil at 2000 psig and 100 ^{o}F (Figure 3.23), in which the oil/water interfaces show a more rounded shape after CWI (Figure 3.23b) than after WI (Kechut et al., 2010).

Change in oil-carbonated water interfacial tension could have also affected the recovery from CWI process. Johnson et al. (1952) reported a lowering of approximately 37% in interfacial tension between Bradford crude oil of 2.86 cP and carbonated water, at 750 psig, 75 ^{o}F. The carbonation level of the injected water, temperature, pressure, and reactivity of the crude oil have also been reported to affect CWI performance (Martin et al., 1951).

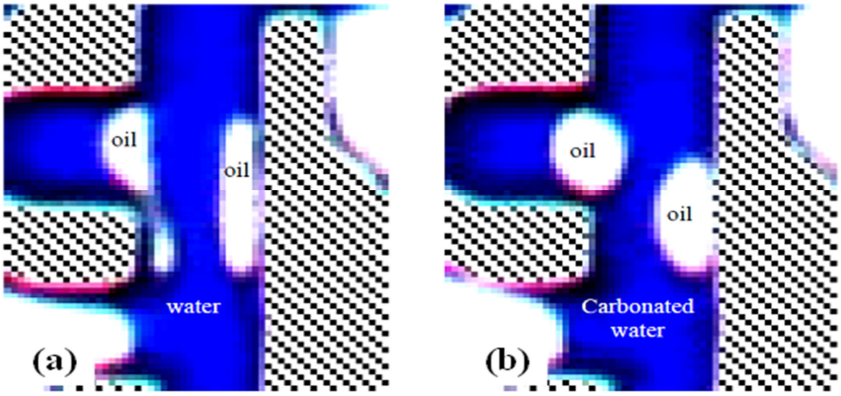

Figure 3.23: A magnified image of a section of the micromodel demonstrating different micromodel wettability: (a) more oil wet after WI (b) less oil wet after 15.8 hrs of CWI (Kechut et al., 2010).

This study emphasizes CWI as a CO_2-augmented waterflooding process to increase the oil recovery. But there is a potential to use this injection strategy for safe storage of CO_2 too. Many oil reservoirs in the world are approaching maturity and being waterflooded for pressure support and improving the sweep of the oil to the producer wells. Injecting CWI instead of injecting plain water could increase oil recovery and at the same time safely store part of the injected CO_2. Since waterflooding is normally carried out over a number of years, cumulatively CWI will provide quite a reasonable sized sink for CO_2 storage, and hence make a useful contribution to lowering the CO_2 emissions.

3.5. Potential of CWI application in UK North Sea oil reservoirs

The oil production from the North Sea as a whole is generally declining, even with infill drilling, as shown in Figure 3.24 (Energy Bulletin, 2010). The implementation of EOR seems to be one of the plausible ways to arrest further decline. Miscible hydrocarbon WAG injection has been successfully applied in some of the oil reservoirs in the North Sea, for example, WAG injection in the Ekofisk and Statfjord Fields.

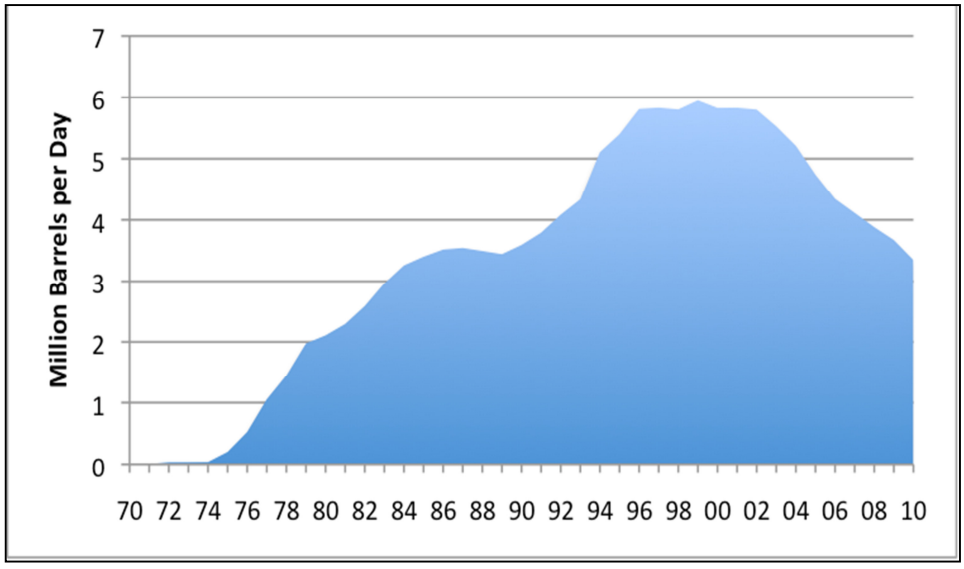

Figure 3.24: Oil production from the North Sea, based on EIA data (Energy Bulletin, 2010).

Many oil reservoirs in the North Sea are technically suitable for miscible CO_2 EOR, despite the engineering challenges posed by an offshore environment to the integration, logistics, operations, and maintenance of the complete CO_2-supply chain (Hustad et al., 2004). Mathiassen (2003) predicted that CO_2 injection could increase the oil recovery of 128 mature oilfields in the Norwegian Continental Shelf (NCS) from 240 to 320 million sm^3.

For the UK Continental Shelf (UKCS), 21 oilfields were screened to be suitable for CO_2 EOR; 14 of those with an estimated CO_2 storage capacity of >50 Mt (million tonne) are shown in Figure 3.25 (SCCS, 2009). However, limited CO_2 source and the lack of incentive for CO_2

EOR activities become the major economic deterrents for the process in the North Sea (Hustad et al., 2004). With exclusion of the cost for CO_2 purchase, the incremental capital and operating cost required to implement a CO_2-flood in the North Sea averages about 10 - 15% and 20% more than a similar water-flood project in the U.S. Permian Basin (Coleman et al., 2004).

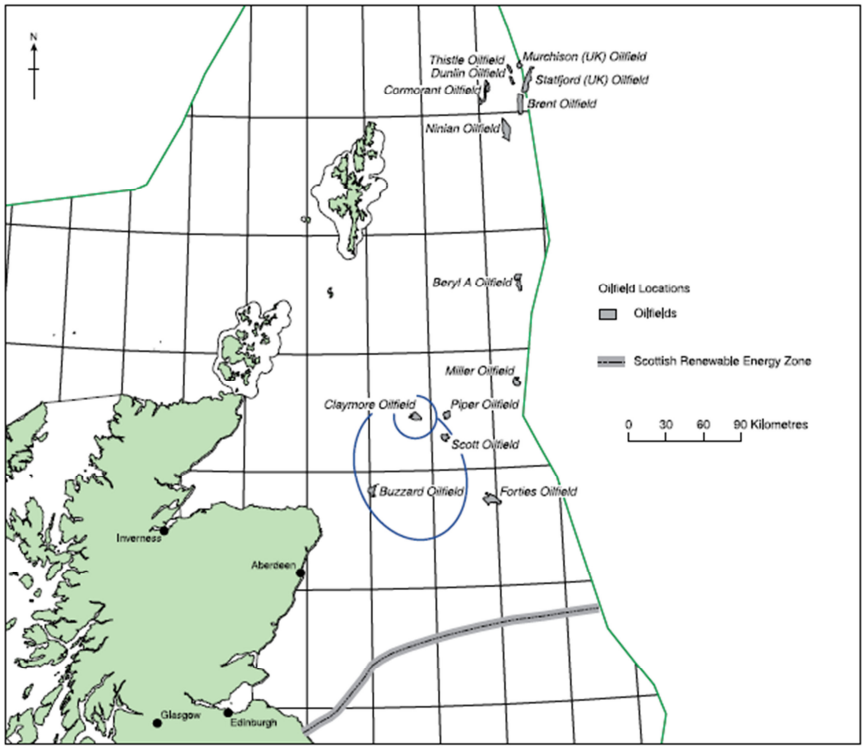

Figure 3.25: Oil fields suitable for CO_2-EOR. Blue ovals show the extent of the EOR study (SCCS, 2009).

In the North Sea area, waterflooding is the standard method of oil recovery with almost every reservoir is under waterflooding. The normally relatively long duration of wateflooding provides a huge potential to store this CO_2 through CWI and gain some additional oil at the same time. CWI can create an EOR opportunity in the UKCS offshore oilfields with small anthropogenic CO_2 sources, such as the CO_2 produced through the existing North Sea oil/gas production. As of 2010, the total amount of CO_2 from UKCS fields during production activities was estimated around 16.4 Mt (DECC, 2011).

Here, the author gives an estimate of the amount of CO_2 that can be stored in the 14 oil fields screened to be suited for CO_2 EOR in the UKCS through CWI. Table 3.11 shows the daily water injection rate of the fields based on the recent UK production Data Release (DECC, 2010). The average pressure and temperature of all these fields were assumed at 4598 psig and 213.8 ^oF, respectively, based on an average value for 55 waterflooded oil reservoirs in the North Sea reported by Akervoll and Bergmo (2010).

Table 3.11: The estimated amount of CO_2 injected and stored per year through CWI in UKCS oil fields at 4598 psig and 213.8 ^oF.

No	Field name	Water injection rate, kbpd	CO_2 injected, Mt per year	CO_2 stored, Mt per year
1	Beryl A	33.40	0.13	0.07
2	Brent*	61.70	0.25	0.12
3	Buzzard	196.00	0.79	0.39
4	Claymore	102.00	0.41	0.21
5	Cormorant	146.00	0.59	0.29
6	Dunlin	38.90	0.16	0.08
7	Forties	127.00	0.51	0.26
8	Miller*	4.73	0.02	0.01
9	Murchison (UK)*	4.47	0.02	0.01
10	Ninian	133.00	0.54	0.27
11	Piper	10.40	0.04	0.02
12	Scott	171.00	0.69	0.35
13	Statjord (UK)*	9.00	0.04	0.02
14	Thistle	125.00	0.50	0.25
	Total	**1160.00**	**4.68**	**2.34**

*Mt = million tonne kbpd = thousand barrel per day

CO_2 solubility in water at 4598 psig and 213.8 ^oF, calculated using the Chang et al. correlation, as given in Appendix A3.1, was 204.4 scf/stb or 6.94 lb CO_2 /100 lb water. For the oil fields not currently under waterflooding (labelled with * after the field name), the injection rate was assumed as 1% STOOIP per year. It was assumed that the reservoir pressure does not exceed the fracture pressure of the reservoir throughout the flooding. It was estimated that about 4.68

Mt of CO_2 could be dissolved in the injected water per year. Assuming that the same 50% of the injected CO_2 as measured in the experiment could be stored, even though it was expected this to be slightly higher at the higher operating pressure assumed here, 2.34 Mt could have been stored per year through the tertiary CWI.

For a wider perspective, lets us look at all the waterflooded offshore oilfields in the UKCS. According to the data published by DECC (UK Department of Energy and Climate Change), in 2010 around 1124 million cubic feet of water was injected in the North Sea offshore reservoirs. Assuming CO_2 solubility of 6.94 lb CO_2/100 lb water, 12.4 Mt of CO_2 could have been injected, of which 6.2 Mt could have been stored in 2010 alone in the UKCS offshore reservoirs, had carbonated water been injected instead of plain water. This is a relatively small amount as compared to the current CO_2 emissions from large sources in the UK of some 250 Mt/yr but it would still contribute to the reduction of smaller anthropogenic CO_2 emissions in the North Sea region. Therefore, although we put forward CWI as an alternative CO_2 injection strategy for improving oil recovery from reservoirs too far from natural sources of CO_2, we believe that CWI projects can also collectively contribute to storing significant quantities of anthropogenic CO_2 separated from activities around the oilfields.

3.6. Conclusions

The following conclusions are drawn from the results of the CWI experiments presented in this chapter:

- For all the rock and fluid samples used in this study, the ultimate oil recovery by CWI was consistently higher than that of water injection in both secondary and tertiary recovery modes. This demonstrates the potential of CWI for increasing oil recovery from both virgin and waterflooded reservoirs.
- Secondary CWI resulted in higher and earlier incremental oil recovery than the tertiary CWI process, as would usually be obtained for other oil recovery methods as well. In tertiary recovery, the remaining oil is more likely to be disconnected and exists in the form of isolated or by-passed patches, which are more difficult to remobilise.

- For miscible systems, CWI presents a great advantage in terms of efficient displacement in which very large oil swelling (infinite) could be achieved, as in the direct CO_2 injection despite the fact that only a fraction of the injected fluid is CO_2.
- The core wettability considerably affects the oil recovery by CWI. Significant difference in the oil production profile was observed particularly in the timing of the additional oil recovery between CWI in the water-wet core with that in the mixed-wet core using the same oil sample at the same tests conditions. While incremental oil recovery in the water-wet core occurred mainly after breakthrough (behind the displacement front), the additional oil recovery in the mixed-wet core occurred at breakthrough itself i.e., at the displacement front.
- The oil viscosity affects the amount of oil recovery by CWI. In terms of %PV, higher oil recovery was obtained by secondary CWI in light oil than in viscous oil, as the more piston-like displacement pattern in the light oil is more favourable for oil recovery. Nevertheless, the oil improvement above that of waterflooding due to secondary CWI was more or less the same in both oils, suggesting other recovery mechanisms, such as oil viscosity reduction, are more dominant than the adverse effect of viscous fingering in the CWI of the viscous oil.
- The carbonated water front was not depleted of its CO_2 content and the CO_2 was moving ahead of the carbonated water front. This proves good delivery of CO_2 by the carbonated water front and the role of diffusion and dispersion of CO_2 in the recovery mechanism.
- CWI has potential as an injection strategy for combining oil recovery and CO_2 storage. A relatively high percentage of the total volume of CO_2 injected in the CWI (ca. 40-50%) was stored at the end of the secondary and tertiary CWI experiments.
- At the immiscible conditions under tertiary recovery mode, CWI is more favourable than continuous CO_2 injection in retaining CO_2 in the reservoir, for a given amount of oil produced.
- CWI has potential as a CO_2 EOR and storage injection strategy in the depleting oilfields in the North Sea where the CO_2 source is limited and most of the fields are waterflooded.

3.7. References

[3.1] Akervoll, I. and Bergmo, P.E.: CO_2 EOR From Representative North Sea Oil Reservoirs, SPE 139765, SPE International Conference on CO_2 Capture, Storage, and Utilization, New Orleans, Louisiana, USA, 2010.

[3.2] Bachu, S.: CO_2 storage in geological media: Role, Means, Status and Barriers to Deployment, Progress in Energy and Combustion Science, 34, 254-273, 2008.

[3.3] Bando, S., Takemura, F., Nishio, M., Hihara, E. and Akai, M.: Solubility of CO_2 in Aqueous Solutions of NaCl at (30 to 60) °C and (10 to 20) MPa, J. Chem. Eng. Data, 48, 576-579, 2003.

[3.4] Bando, S., Takemura, F., Nishio, M., Hihara, E. and Akai, M.: Viscosity of Aqueous NaCl Solutions with Dissolved CO_2 at (30 to 60) °C and (10 to 20) MPa, J. Chem. Eng. Data, 49, 1328-1332, 2004.

[3.5] Bobek J.E., Mattax, C.C. and Denekas, M.O.: Reservoir Rock Wettability - Its Significance and Evaluation, Petroleum Transactions, AIME, Vol. 213, 1958, 155-160, 1958.

[3.6] Burton, M. and Bryant, S.L.: Eliminating Buoyant Migration of Sequestered CO_2 through Surface Dissolution: Implementation Costs and Technical Challenges, SPE Annual Technical Conference and Exhibition. Anaheim, California, U.S.A, 2007.

[3.7] Buckley, J.S., Takamura, K. and Morrow, N.R.: Influence of Electrical Surface Charges on the Wetting Properties of Crude Oils, Soc. Pet. Eng. Formation Evaluation, 4, 240-332, 1989.

[3.8] Buckley, J.S. and Liu, Y.: Some Mechanisms of Crude Oil/brine/solid Interactions, J. Pet. Science and Engineering, 20, 155-160, 1998.

[3.9] Burton, M. and Bryant, S.L.: Eliminating Buoyant Migration of Sequestered CO_2 through Surface Dissolution: Implementation Costs and Technical Challenges, SPE Reservoir Evaluation & Engineering, Vol. 12, 3, 399-407, 2009.

[3.10] Chang, Y. B., Coats, B.K. and Nolen, J.S.: A Compositional Model for CO_2

Floods Including CO_2 Solubility in Water, SPE 33164, SPE Reservoir Evaluation & Engineering, Vol. 1, No. 2, 133-160, 1998.

[3.11] Department of Energy and Climate Change (DECC) UK, https:// www.og.decc.gov.uk/pprs/pprsindex.htm accessed in February 2011 and personal communication with Offshore Inspectorate of DECC, June 2011.

[3.12] De Nevers, N.: A Calculation Method for Carbonated Water Flooding, SPE 569, SPE Journal, 9-20, March 1964.

[3.13] Donaldson, E.C. and Thomas, R.D.: Microscopic Observations of Oil Displacement in Water-wet and Oil-wet Systems, SPE 3555, SPE Annual Technical Conference and Exhibition, New Orleans, 1971.

[3.14] Energy Bulletin, published Dec 21 2010 by *The Oil Drum*, accessed 15/3/2011 at http://www.energybulletin.net/.

[3.15] Garcia, J.E.: Density of Aqueous Solutions of CO_2, Paper LBNL-49023, Lawrence Berkeley National Laboratory, http://repositories.cdlib.org/ lbnl/LBNL-49023, 2001.

[3.16] Hebach, A., Oberhof, A. and Dahmen, N.: Density of Water + Carbon Dioxide at Elevated Pressures: Measurements and Correlation, Chemical Engineering Data, 49, 950-953, 2004.

[3.17] Hickok C.W. and Ramsay H.J.: Case Histories of Carbonated Waterfloods in Dewey-Bartlesville Field, SPE 333, SPE Secondary Recovery Symposium, Wichita Falls, Texas, 7-8 May 1962.

[3.18] Holm, L.W.: Evolution of the Carbon Dioxide Flooding Processes, Journal of Petroleum Technology, Vol. 39, 11, 1337-1342, 1987.

[3.19] Holm, L.W.: CO_2 Requirements in CO_2 Slug and Carbonated Water Oil Recovery Process, Producers Monthly, September, 1963.

[3.20] Hustad, C.W. and Austell, J.M.: Mechanisms and Incentives to Promote the Use and Storage of CO_2 in the North Sea in: Roggenkamp, M.M., Hammer, U. (Eds.), European Energy Law Report I, 355-380, 2004.

[3.21] International Energy Agency, Key World Energy Statistics 2009.

[3.22] Jerauld, G.R. and Rathmell, J.J.: Wettability and Relative Permeability of Prudhoe Bay: A Case Study in Mixed-Wet Reservoirs, SPERE, 58, 1997.

[3.23] Johnson, W.E., Macfarlane, R.M. and Breston, J.N.: Changes in Physical Properties of Bradford Crude Oil when Contacted with Carbon Dioxide and Carbonated Water, Producers Monthly, November 1952.

[3.24] Klins, M.A.: Carbon Dioxide Flooding Basic Mechanisms and Project Design, International Human Resources Development Corp., Boston, 1984.

[3.25] Klins, M.A. and Farouq Ali, S.M.: Oil Production in Shallow Reservoirs by Carbon Dioxide Injection, SPE 10374, SPE Eastern Regional Meeting, Columbus, 4-6 November 1981.

[3.26] Kechut N.I., Riazi, M., Sohrabi, M. and Jamiolahmady, M.: Tertiary Oil Recovery and CO_2 Sequestration by Carbonated Water Injection (CWI), SPE 139667, SPE International Conference on CO_2 Capture, Storage, and Utilization, New Orleans, Louisiana, USA, 10–12 November 2010.

[3.27] Lemmon E.W., McLinden M.O. and Friend D.G.: Thermophysical Properties of Fluid Systems in NIST Chemistry WebBook, NIST Standard Reference Database No. 69, 2005 (http://webbook.nist.gov).

[3.28] Linderberg, E., Bergamo, P. and Moen, A.: The Long-term Fate of CO_2 Injected into an Aquifer, 6th International Conference on Greenhouse Gas Control Technology (GHGT-6), Kyoto, Japan, 2002.

[3.29] Lohrenz, J., Bray, B.G. and Clark, C.R.: Calculating Viscosity of Reservoir Fluids from their Composition, J. Pet. Tech., 1171, 1964.

[3.30] Martin J.W.: Additional Oil Production through Flooding With Carbonated Water, Producers Monthly, July, 1951.

[3.31] Martin, J.W.: Process of Recovering Oil From Oil Fields Involving the Use of Critically Carbonated Water, Patent 2,875,833, March 3, 1959.

[3.32] Martin, F.D.: Enhanced Oil Recovery for Independent Producers, SPE/DOE Eighth Symposium on Enhanced Oil Recovery, Tulsa, Oklahoma, 1992.

[3.33] Mathiassen, O.M.: CO_2 as Injection Gas for EOR and Estimation of the Potential on the Norwegian Continental Shelf, Norwegian University of Science and Technology, 2003.

[3.34] McFarlane, R.M., Breston, J.N. and Neil, D.C.: Oil Recovery from Cores When Flooded with Carbonated Water and Liquid CO_2, Producers Monthly, 23-35, November 1952.

[3.35] Miller, J.A. and Jones, R.A.: A Laboratory Study to Determine Physical Characteristics of Heavy Oil after CO_2 Saturation, SPE 9789, SPE/DOE Second Joint Symposium on Enhanced Oil Recovery of SPE, Tulsa, April 1981.

[3.36] Morrow, N.R., Lim, H.T. and Ward, J.S.: Effect of Crude Oil Induced Wettability Changes on Oil Recovery, SPE 13215, SPE Formation Evaluation, Vol. 1, 1, 89-103, February 1986.

[3.37] Pollack, N.R., Enick R.M., Mangone, D.J. and Morsi, B.I.: Effect of an Aqueous Phase on CO_2/Tetradecane and CO_2/Maljamar-Crude-Oil Systems, SPE 15400, SPE Reservoir Engineering, Vol. 3, No. 2, 533-541, 1988.

[3.38] Ramsay, H.J. and Small, F.R.: Use of Carbon Dioxide for Water Injectivity Improvement, Journal of Petroleum Technology, 25, 1964.

[3.39] Riazi, M., Sohrabi, M., Jamiolahmady, M., Ireland, S. and Brown, C.: Oil Recovery Improvement Using CO_2-Enriched Water Injection, SPE 121170, EUROPEC/ EAGE Conference and Exhibition, Amsterdam, 8-11 June 2009.

[3.40] Rowe Jr., A.M. and Chou, J.C.S.: Pressure-Volume-Temperature-Concentration Relation of Aqueous NaCl Solutions, Journal of Chemical and Engineering Data, Vol. 15, 1, 1970.

[3.41] Ross, G.D., Todd, A.C., Tweedie, J.A. and Will, G.S.: The Dissolution Effects of CO_2-Brine Systems on the Permeability of U.K. and North Sea Calcareous Sandstones, SPE Enhanced Oil Recovery Symposium, Tulsa, Oklahoma, 4-7 April

1982.

[3.42] Salathiel, R.A.: Oil Recovery by Surface Film Drainage in Mixed Wettability Rocks, J. Pet. Technol. 1216, Trans., AIME, 255, October 1973.

[3.43] Sayegh, S. G., Krause, F.F., Girard, M. and DeBree, C.: Rock/Fluid Interactions of Carbonated Brines in a Sandstone Reservoir: Pembina Cardium, Alberta, Canada, SPE Formation Evaluation, Vol. 5, 4, 399-405, December 1990.

[3.44] SCCS, Opportunities for CO_2 Storage around Scotland; An Integrated Strategic Research Study, available at www.erp.ac.uk/sccs; accessed February 2011.

[3.45] Shyeh-Yung, J.G.J.: Mechanisms of Miscible Oil Recovery: Effects of Pressure on Miscible and Near-Miscible Displacements of Oil by Carbon Dioxide, SPE Annual Technical Conference and Exhibition, Dallas, Texas, USA, 1991.

[3.46] Sohrabi, M., Riazi, M., Jamiolahmady, M., Ireland, S. and Brown, C.: Carbonated Water Injection for Oil Recovery and CO_2 Storage, Sustainable Energy UK Conference: Meeting the Science and Engineering Challenge, Oxford, UK, 2008.

[3.47] Sohrabi, M., Riazi, M., Jamiolahmady, M., Ireland, S. and Brown, C.: Mechanisms of Oil Recovery by Carbonated Water Injection, SCA2009-26, International Symposium of the Society of Core Analysts, Noordwijk, The Netherlands, 27-30 September, 2009.

[3.48] Tang, G.Q. and Morrow N.R.: Influence of Brine Composition and Fines Migration on Crude Oil Brine Rock Interactions and Oil Recovery, Journal of Petroleum Science and Engineering, 24, 99-111, 1999.

[3.49] Tiffin, D.L., and Yellig, W.F.: Effects of Mobile Water on Multiple-Contact Miscible Gas Displacements, SPE 10687, SPE Journal, 447-55, 1983.

[3.50] UK Production Data available at https://www.og.decc.gov.uk/pprs/ pprsindex.htm; accessed 29/10/2010 and personal communication with Mr. Phillip Harrison from Department of Energy and Climate Change Energy Development Unit.

[3.51] Van der Meer, L.G.H. and van Wees, J.D.: Limitations to Storage Pressure in Finite Saline Aquifers and the Effect of CO_2 Solubility on Storage Pressure, SPE

103342, SPE Annual Technical Conference and Exhibition, San Antonio, Texas, USA, 24-27 September 2006.

Chapter 4

Numerical Simulation of CWI

4.1. Introduction

For any oil recovery method, an accurate reservoir model with the ability to reliably predict the consequences of implementing the process is vital for successful management of the reservoir. Appropriate modelling of the CWI process is crucial for assessing its feasibility, design and predicting its performance at various scales or conditions.

Injection of CO_2 into oil reservoirs involves several complex physical and chemical processes such as dissolution of CO_2 into reservoir fluids that results in swelling of the oil, change in the oil viscosity, change in interfacial tension, miscibility with the oil and chemical interactions between the fluids and the rocks. The ability to account for most of these physical phenomena makes compositional simulators more commonly used to model processes involving CO_2 injection.

This chapter describes the modelling of the carbonated waterflood process. Despite the existence of voluminous literature on modelling studies of CO_2 EOR, only limited attempts to specifically model CWI have been reported.

The main objective of this simulation study was first to evaluate whether the commercially available reservoir simulators were able to adequately model the physics of carbonated water core flood at the laboratory scale. 'Adequate' here means there was a reasonable match between the calculated and experimental values with the main mechanisms of the process accounted for. The capability to model the process at the laboratory experimental scale where the hard data were available will give the user confidence to use the selected simulator to predict the performance of the process under different conditions and scales. There has been no simulation study, reported in the literature, specifically on CWI using the currently

and commercially available compositional reservoir simulators that the author could evaluate in this study. The results of this study, therefore, would provide valuable insight into the suitability of the commonly used reservoir simulators to model CWI as well as to identify the appropriate method to model the process at the experimental scale.

4.2. Evaluation of reservoir simulators

Three commercial compositional reservoir simulators commonly used in the oil to model CO_2 injection process namely ECLIPSE 300 (E300) of version 2007.1 of Geoquest, and GEM and STARS, both of 2008 versions, of Computer Modelling Group (CMG), were first evaluated for their suitability to model the CWI process.

In this evaluation, the main objective was to look into the features relevant to the CWI process such as the CO_2 solubility in the aqueous phase, defining carbonated water in the injection well and the cross-phase CO_2 diffusion in each of the simulators. A 1D core model was used. The predicted results using the simulators were compared with each other to evaluate their similarities, differences, strengths and limitations in modelling CWI process so that the most suitable simulator for the subsequent simulation tasks can be selected.

4.2.1.1D model description

The 1D core model is of 33.5 cm long and 5 cm diameter (equivalent to a square with side of 4.42 cm). The grid size sensitivity results (Table 4.1) on simultaneous CO_2 and water injection using E300 reveal that varying the grid size in the X and Y direction from 0.1675 cm to 0.67 cm resulted only in up to 1.3 % difference in the predicted oil production. The model grid of 100 x 1 x 1 grid cells was later chosen.

The core was water-wet Clashach sandstone with homogeneous porosity and permeability of 18.5 % and 1300 mD, respectively. Measured oil/water relative permeability curves shown in Figure 4.1 were used. Unlike CO_2 gas injection into water, where some of the gas is trapped in the water due to the imbibition process, in CWI, the imbibition effect is assumed

negligible as all the CO_2 is dissolved in solution. Thus, no hysteresis was considered. The effect of capillary pressure and the effect of the CO_2 on relative permeability were also ignored in this simulation study.

Table 4.1: 1D model grid sensitivity results (200 gridblock model as reference case).

DX=DY, cm	NX=NY	Cumulative oil produced, cc	% Diff. in cumulative oil produced
0.1675	200	104.105	0.00
0.3350	100	103.550	0.53
0.6700	50	102.747	1.30

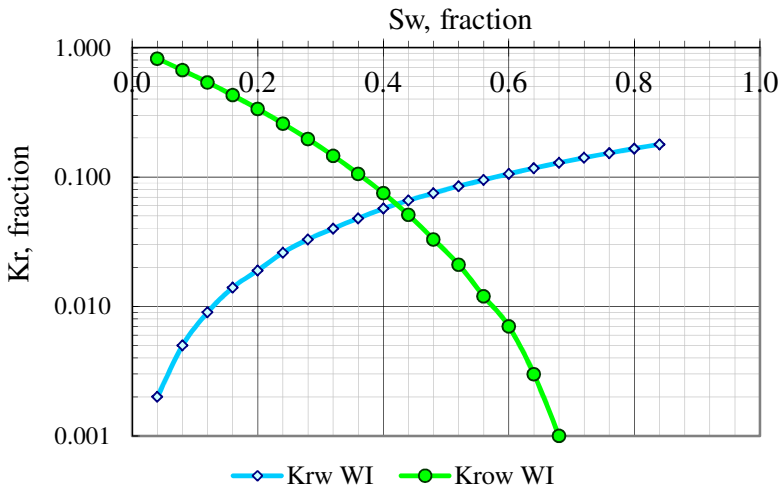

Figure 4.1: Measured oil/water relative permeability curves used in the model.

The production and injection wells were located at each end of the core. The injection rate of water and CO_2 gas was set at 18.5 and 554.8 cc/hr, respectively equivalent to a total injection of 20 cc/hr and are corresponding to the CO_2 solubility in water at the test temperature and pressure.

4.2.2. Fluid PVT data

The reservoir model was initialized at 2000 psig and 100.4 ^{o}F with decane ($C_{10}H_{22}$) used as the oil sample. PVTi and WinProp, the auxiliary EOS-based program for use in the E300 and GEM/STARS simulators, respectively, were used to characterize the fluid samples and generate the needed PVT data for the simulation. Unless otherwise stated, the three parameter Peng Robinson EOS (PREOS) was used to calculate the fugacity and density of components throughout the simulation study. Fluid viscosities were calculated using Lohrenz-Bray-Clark (LBC) method (1964) in PVTi and Jossi-Stiel-Thodos (JST) correlation (1961) in WinProp, both are basically according to the following functions:

$$\left[(\mu - \mu^{*})\xi + 10^{4}\right]^{0.25} = a_0 + a_1\rho_r + a_2\rho_r^{2} + a_3\rho_r^{3} + a_4\rho_r^{4} \qquad (4.1)$$

where μ is the oil or gas viscosity in cP or MPas, μ^* is the low-pressure viscosity in cP or MPas, $\xi = T_c^{1/6} M^{-1/2} P_c^{-2/3}$, is the viscosity-reducing parameter where critical temperature (T_c) is in K and critical pressure (P_c) is in atm, M is the molecular weight, ρ_r is the reduced molar density, $\rho/\rho_c = v_c/v$, $a_0 = 0.1023000$, $a_1 = 0.0233640$, $a_2 = 0.0585330$, $a_3 = -0.0407580$, and $a_4 = 0.0093324$.

The properties of decane and CO_2 measured by NIST (Lemmon et al., 2005) were used for comparison with the EOS-calculated values. In this exercise, only pure CO_2 was considered. In WinProp, the specific gravity, boiling point and molecular weight of decane were taken from Whitson (1982), while the critical properties were calculated using Kessler-Lee correlations (Winprop User Manual). In PVTi, the P_c, T_c and acentric factor are after Katz and Firoozabadi (1982). The difference in the corresponding values between the two sources of data was negligibly small. Figure 4.2 shows the phase plot of decane and CO_2 calculated by the PREOS. At 2000 psig and 100.4 ^{o}F, CO_2 is miscible with decane.

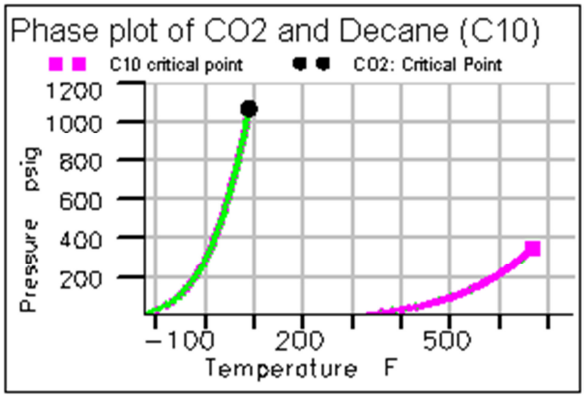

Figure 4.2: Phase plots of CO_2 and decane showing their critical points.

4.2.3. ECLIPSE 300 (E300)

E300 is a fully compositional reservoir simulator with cubic EOS, developed by Geoquest. PREOS was available to calculate the Z-factors, fluid densities and phase fugacities for defining the inter-phase equilibrium. E300 version 2007.1, the latest version available when the study started, was used throughout the study.

CO_2 dissolution into aqueous solution

In E300, there are several options to model the solubility of CO_2 in the water, depending on the site and operational conditions. CO2SOL feature, which allows hydrocarbons and CO_2 to exist in the oil and gas phases, while only CO_2 and water exist in the aqueous phase, was selected as the most suitable option and thus used in the study. Equilibrium between oil, gas, and water was assumed instantaneous and that water and hydrocarbon components are mutually insoluble. At equilibrium, the fugacity of CO_2 in the aqueous phase, which was constructed to match solubility data, equals that in the hydrocarbon phases.

The amount of CO_2 dissolved in water and the properties of the formed aqueous phase were defaulted to Chang, Coats and Nolen (1998) correlations, details of which are described in Appendix A3.1. Figure 4.3 shows the CO_2 solubility in water at 100.4 ^oF calculated using the correlations. At 2000 psig, 168.8 scf of CO_2 was dissolved per barrel of water.

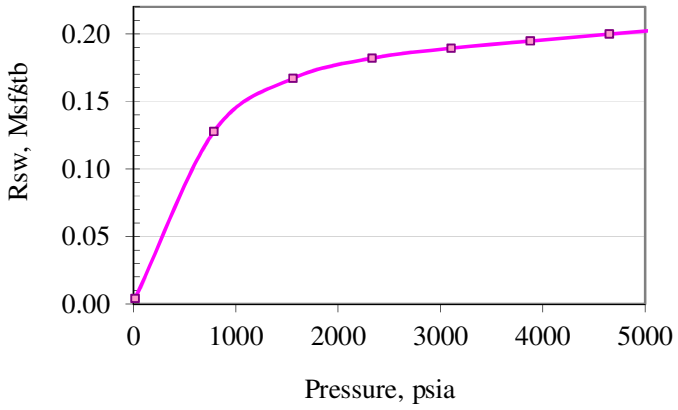

Figure 4.3: CO_2 solubility in fresh water, R_{sw}, as a function of pressure at 100.4 ^oF estimated by the Chang et al. correlation (1998).

Experimental studies, for instance, by Pollack et al. (1988), showed that the presence of water reduced the amount of CO_2 available for mixing with the hydrocarbons. E300 applies a sequential approach in modelling this effect. In a grid cell with CO_2, water and other hydrocarbon components, the moles of CO_2 dissolved in the aqueous phase were first determined through solving the CO_2/water fugacity constraint equation:

$$\omega_{CO2} * \phi_{CO2,w} = y_{CO2} * \phi_{CO2,v} \qquad (4.2)$$

where subscripts w and v denote the aqueous phase and CO_2-rich phase, respectively. y_{CO2} is the mole fraction of CO_2 in the CO_2-rich phase, ϕ_{CO2} is the fugacity coefficient of pure CO_2 and ω_{CO2} is the mole fraction of CO_2 in the aqueous phase. ω_{CO2} at the prevalent temperature and pressure was computed from the input CO_2 solubility in water for a saturated binary CO_2/water system as described earlier. Assuming the water vapour pressure is small relative to the total pressure and CO_2 vapour pressure at typical CO_2 flood conditions, (i.e., $y_{CO2} \sim 1$), the fugacity coefficient of CO_2 in the aqueous phase can be approximated as:

$$\phi_{CO2,w} \approx \frac{\phi_{CO2,V}^{EOS}}{\omega_{CO2}} \tag{4.3}$$

where $\phi_{CO2,v}^{EOS}$ is the fugacity coefficient of pure CO_2 in the vapour phase computed by the EOS. Nevertheless, the $\phi_{CO2,w}$ computation is applicable for a binary CO_2/water system only since it is a function of pressure and temperature but not composition. $\phi_{CO2,v}^{EOS}$ is for pure CO_2 and ω_{CO2} is for the binary CO_2/water system. The error introduced by the assumption should nevertheless be insignificant since the amount of CO_2 dissolved in the aqueous phase within the typical range of CO_2 EOR pressures is normally small (Chang et al., 1998).

Having solved for the CO_2/water fugacity constraint equation, a phase-stability test was sequentially run to establish the number of phases in the hydrocarbon phase and accordingly determine the compositions of each phase. At equilibrium, the oil and gas phase fugacities for each hydrocarbon component, and CO_2 fugacities in the hydrocarbon phase(s) and the aqueous phase are equal.

E300 simulation results

E300 does not have an explicit keyword to assign the composition of a single phase carbonated water in the injection stream at the surface.

Co-injecting CO_2 gas and water at the same location in proportions corresponding to CO_2 solubility in water at the test pressure and temperature, was probably the best way to define CWI in the model. This can be done either through the use of a multiphase injector or two normal injectors at the same location. This method does not create a single phase of carbonated water in the wellbore, but with the inherent instantaneous equilibrium and complete mixing assumptions, once the fluid enters a grid block the equilibrium flash calculations will determine thermodynamically stable mixture. From a simulation point of view, it makes no difference whether CO_2 and water have arrived from separate sources or arrived already mixed in the grid block, as long as their proportion is the same, pressure and

temperature is maintained and CO_2 is fully dissolved. In this case, it was found that using a dummy cell in the model to allow mixing before it gets into the actual core grid blocks gave exactly the same results as those without the dummy cell.

With the injection rates of CO_2 gas and water corresponding to the solubility of CO_2 in the aqueous phase at 2000 psig, 100.4 ^oF, E300 predicted an incremental oil recovery of 15.9 %STOOIP from the secondary CWI process.

4.2.4. GEM

GEM is an advanced general EOS compositional simulator by CMG; developed to simulate three phase, multi-components compositional effects of reservoir fluid during primary and EOR processes.

CO_2 solubility in water in GEM

GEM models the CO_2 solubility in the aqueous phase with Henry's Law (Li and Nghiem, 1986). For a component sparingly soluble in the aqueous phase, Henry's Law states that:

$$f_{iw} = y_{iw} H_i \qquad \text{i} \neq \text{water} \tag{4.4}$$

$$lnH_i = H_i^o + v_i^\infty (p - p_i^o)/RT \tag{4.5}$$

where f_{iw} is the fugacity of component i in the aqueous phase, y_{iw} is the mole fraction of component i in the aqueous phase, H is the Henry's constant with 'o' referring to the reference conditions, p is pressure, v_i^∞ is the partial molar volume of component i in the aqueous phase at infinite dilution, computed from the correlation by Lyckman et al. (Equation 4.6):

$$\left(\frac{p_{ci} v_i^\infty}{RT_{ci}}\right) = 0.0095 + 2.35\left(\frac{Tp_{ci}}{CT_{ci}}\right) \tag{4.6}$$

where T_{ci} and p_{ci} are critical temperature and critical pressure of component i, respectively, C is the cohesive energy density of water, R is the gas constant and T is temperature (GEM User Guide, 2008). To account for the effect of temperature and water salinity on Henry's constant of CO_2 Harvey's correlation (1996) was used. At 2000 psi, Henry's constant was calculated to be 2344.42. As shown in Figure 4.4, CO_2 solubility in pure water, calculated by Henry's Law (GEM), was slightly higher than that by the Chang et al. correlation (E300). At 2000 psig, Henry's Law and the Chang et al. correlation give CO_2 solubility in water of 0.19 and 0.17 Mscf/stb, respectively. (Note: throughout this thesis, Mscf refers to thousand standard cubic feet)

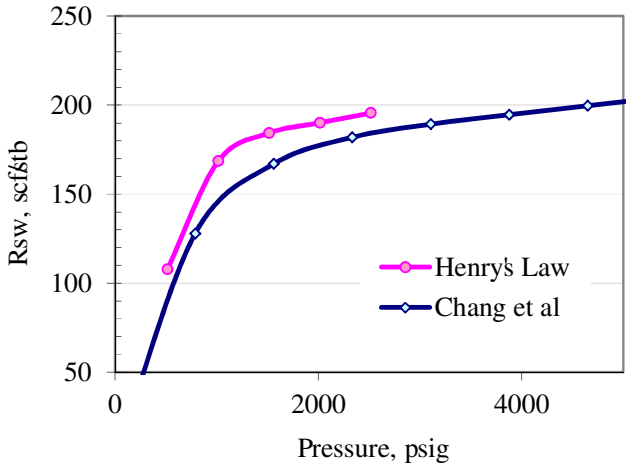

Figure 4.4: CO_2 solubility in fresh water calculated using Henry's Law and the Chang et al. correlation at 100.4 ^{o}F.

GEM simulation results

Similar to E300, there is no specific keyword to assign carbonated water in the injection well, thus simultaneous water and CO_2 injection as used in E300 case, was also employed here. No free gas was formed throughout the simulation run. Comparison of the predicted WI and CWI recovery is shown in Figure 4.5, where an incremental oil recovery of 9.7 %STOOIP was predicted.

4.2.5. STARS

Unlike E300 and GEM, STARS is a K-value compositional simulator. It is claimed to be ideally suited for advanced modelling of recovery processes involving the injection of steam, solvents, air and chemicals (STARS User Guide, 2008).

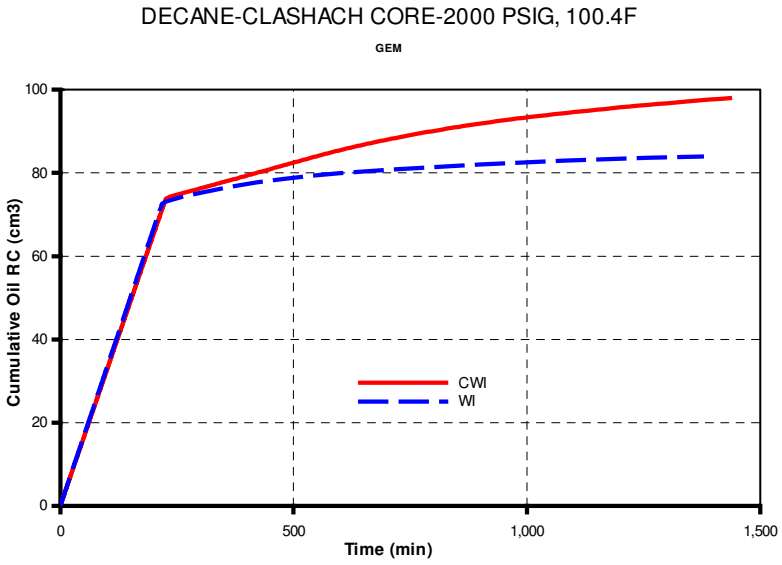

Figure 4.5: Predicted oil recovery from waterflooding and CWI by GEM.

The K-value or equilibrium ratio is the ratio of the concentration of a component in phases which are in thermodynamic equilibrium with each other. This can be a Liquid-Liquid or Gas-Liquid system. The water Gas-Liquid (GL) K-value is defined as the ratio of the gas phase mole fraction of water to the aqueous phase mole fraction of the component (Equation 4.7) while the Liquid-Liquid (LL) K-value is defined as the aqueous phase mole fraction of the component divided by the oil phase mole fraction of the component (Equation 4.8).

$$K_{iv} = x_{iv}/x_{il} \tag{4.7}$$

$$K_{iw} = x_{iw}/x_{il} \tag{4.8}$$

where xi is the mole fraction of component i. The subscripts v, l and w denote the gas, oleic and aqueous phases, respectively (WinProp User Guide 2008).

STARS fluid properties

In addition to the basic PVT properties such as the molar density, viscosity and molecular weight, STARS requires K-values of the components in the oil and aqueous phases to be inputted in the tabulated format. As a K-value compositional simulator, STARS did not use an exact EOS flash at all possible pressure and temperature, and compositions. Mixing rules and the K-value tables were instead used in order to allow stability and reasonable simulation time. The fluid physical properties from the EOS and STARS were reconciled at a reference pressure, temperature and feed composition and extrapolated to other values by the mixing rules. Pure component viscosities were calculated using the two-parameter corresponding states model of Teja and Rice (WinProp User Guide 2008).

In calculating the GL and LL K-values, the hydrocarbon and light gas components were all assumed to be oleic. Water was characterized as an aqueous component with K_w assumed to be unity. The GL and LL K-value tables were generated simultaneously using the Oil-Gas-Water flash process, which modelled the aqueous phase with Henry's Law and the vapour and liquid phases with the EOS, as described earlier. K-values are defined and calculated directly if a stable oil-gas-water system existed at the specified pressure and temperature (WinProp User Guide 2008). As depicted in Figure 4.6, the LL K-values for CO_2 are relatively small and increase slightly with pressure. In the model, decane was insoluble in water and water was not allowed to vaporize or be in the oil phase, thus there was zero LL K-value for both.

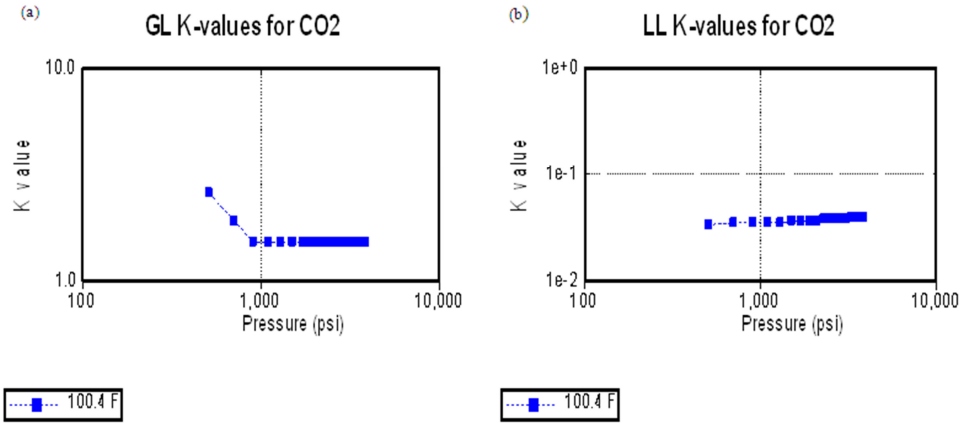

Figure 4.6: WinProp-generated CO_2 GL (left) and CO_2 LL (right) K-values for 0.5 mole fraction of decane and 0.5 mole fraction of CO_2 at 100.4 ^oF.

STARS simulation results

The CO_2 gas was co-injected with water through two injectors at the same locations, with the CO_2 injection rate similar to those used in GEM case, while the water injection rate was changed accordingly by the simulator to maintain the pressure. No free gas saturation was detected throughout the simulation confirming the CO_2 remained in the liquid phase. Figure 4.7 shows the oil recovery profile of WI and secondary CWI calculated by STARS, where an additional oil recovery of 7.3% STOOIP above that of water flooding was predicted.

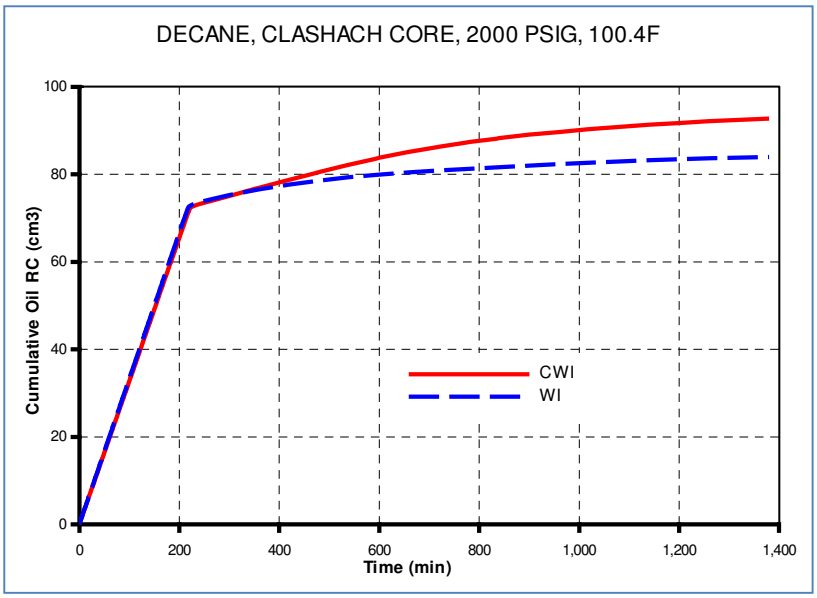

Figure 4.7: The cumulative oil recovery of WI and CWI predicted by STARS.

4.2.6. Comparison of simulation results

All three compositional simulators evaluated, as a default, assumed instantaneous equilibrium and complete mixing between phases and components. The flash calculations were used to determine the equilibrium phase compositions and amounts at a given pressure, temperature and an overall composition. At thermodynamic equilibrium, the fugacities in the liquid, aqueous and vapour phases, calculated directly from the EOS, are equal for each component.

Figure 4.8 compares the predicted incremental oil recovery from the secondary CWI by the three simulators. The slightly lower CO_2 solubility in water given by the Chang et al. correlation in E300 compared with that by Henry's Law in GEM and STARS may contribute to the difference in the predicted recovery. In spite of more or less the same total amount of CO_2 per barrel of water injected, E300 predicted a 62% and 21% higher incremental oil recovery than that predicted by STARS and GEM, respectively.

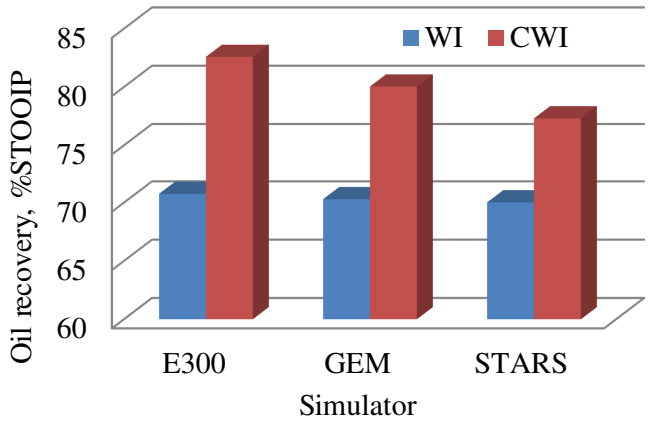

Figure 4.8: Comparison of the predicted oil recovery from WI and CWI by the three simulators.

The difference in the calculated oil viscosity could have also contributed to the difference in the incremental oil recovery. Figure 4.9 shows the calculated oil viscosity in a gridblock as a function of the mole fraction of CO_2 in oil. The higher the amount of CO_2 in the oil, the lower is the oil viscosity. We can see that the extent of the oil viscosity reduction of the three cases is consistent with the incremental oil recovery predicted. The oil viscosity reduction in STARS, which was calculated using the two-parameter corresponding states model of Teja and Rice, has a very different trend and is much less than that in E300 and GEM, which explains the smaller incremental oil recovery by the simulator.

Figure 4.10 shows the calculated amount of CO_2 in the oil and water phases in grid block (50,1,1) of the model. Giving the highest oil recovery, E300 has the highest CO_2 concentration in the oil phase whilst STARS, with the lowest oil recovery, has the highest

CO_2 concentration in the water phase. The difference in the incremental oil recovery is therefore mostly due to the solubility of CO_2 in both oil and water phases, which in turn are due to the different ways the K-values were generated.

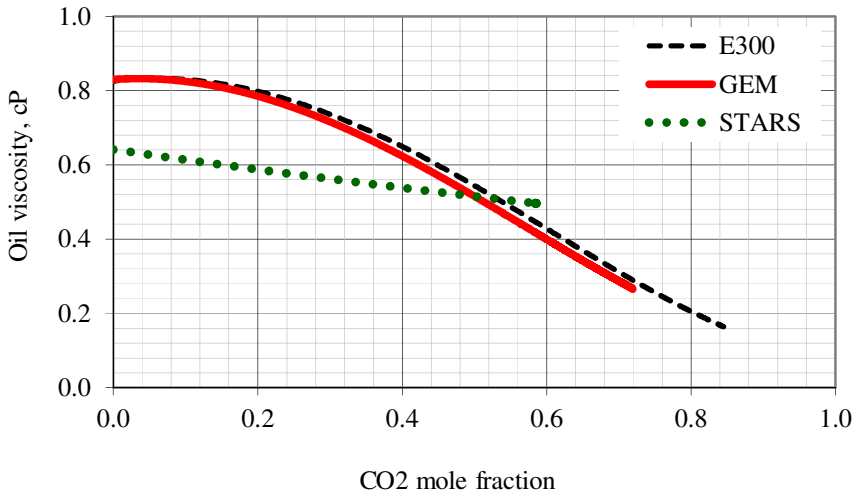

Figure 4.9: Variation of the calculated oil viscosity and CO_2 mole fraction in oil with time in grid block (50,1,1).

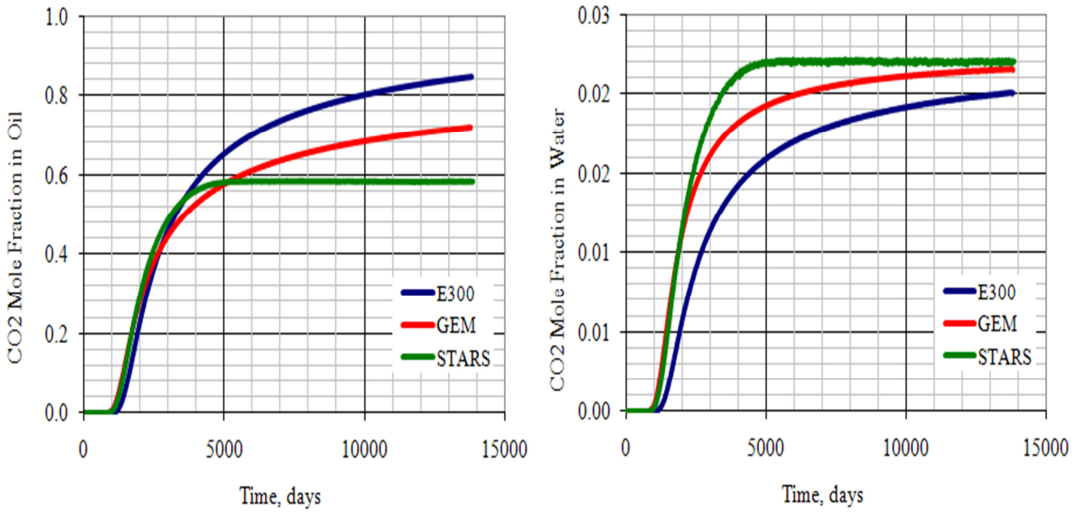

Figure 4.10: The calculated CO_2 content in oil (left) and in water (right) versus time in grid block (50,1,1).

Unlike E300 and GEM, which use EOS to determine the K-values at each temperature, pressure and overall composition, K-values in STARS were interpolated from the table inputted, which, in turn, was generated using the EOS at a certain reference of CO_2 mole fraction. The ultimate amount of CO_2 that dissolved in the oil and water phase, regardless of the amount of carbonated water injected, was limited by these K-values. Since the basic K-values are functions of pressure and temperature only, a certain amount of error might be introduced when the system is moving away from the reference point, such as where there is a strong compositional effect during the process.

It is anticipated that if the CO_2 content in each phase in all those three simulators as well as the viscosity correlation is made the same, more or less the same predicted oil recovery would be obtained, except for small differences due to numerical dispersion and different solution methods. It is thus concluded that none of the three simulators is more suitable to model the CWI process than the others. Being more widely used in the industry, the E300 simulator was used for the subsequent assessment.

4.3. Compositional modelling of the coreflood experiments

A more detailed modelling of the CWI coreflood experiments was next carried out using the E300 simulator with the oil/water relative permeability curves derived from the experimental WI data. Four sets of experimental data, consisting of WI and the corresponding CWI core displacements, were used to validate the model. They were WI and secondary CWI of decane in the water-wet and mixed-wet Clashach cores, and WI, secondary and tertiary CWI of the stock tank crude oil in the reservoir core.

4.3.1.1D model

The numerical core model used was one-dimensional (1D) in Cartesian coordinates. A linear model eliminates sweep effects, enabling the displacement efficiency to be studied more closely. The model had homogeneous porosity and permeability. The number of grid blocks necessary to eliminate numerical dispersion was determined from grid size sensitivity

simulations performed on the water injection and CO_2 injection processes. Taking grid sensitivity results on the reservoir core as an example, the oil recovery started to converge at 1/Nx of 0.01 or Nx=100, as depicted in Figure 4.11. The grid block dimensions for each of the core models are given in Table 4.2.

Table 4.2: Properties and dimensions of the core models and the injection rates used.

Core	Length, cm	Absolute k, mD	Porosity, fraction	No. of gridcells, Nx	DX=DY, cm	Qinjw, scc/hr	Qinjg, scc/hr
Clashach WW	33.20	1300	0.185	200	0.166	18.45	554.80
Clashach MW	61.30	850	0.165	200	0.332	18.45	554.80
Reservoir core	8.14	4580	0.350	100	0.081	0.94	27.49

In the simulation, the CO2SOL feature was invoked to account for CO_2 solubility in water. Carbonated water was obtained by co-injecting water and CO_2 in proportions corresponds to the CO_2 solubility measured for the experiments at the test temperature and pressure. The relatively small pressure drops during the coreflood tests allowed CWI to be modelled without free gas being created.

The production and injection wells were located at each end of the core. The injection rate of water and carbonated water in the laboratory varied according to the core size as per Table 3.7. In the simulation model, the injection rate of the carbonated water was represented by co-injection of the CO_2 gas and water corresponding to the measured solubility of CO_2 in water at the test temperature and pressure, as given in Table 4.3. The production well was set to operate at constant BHP, which was the test pressure.

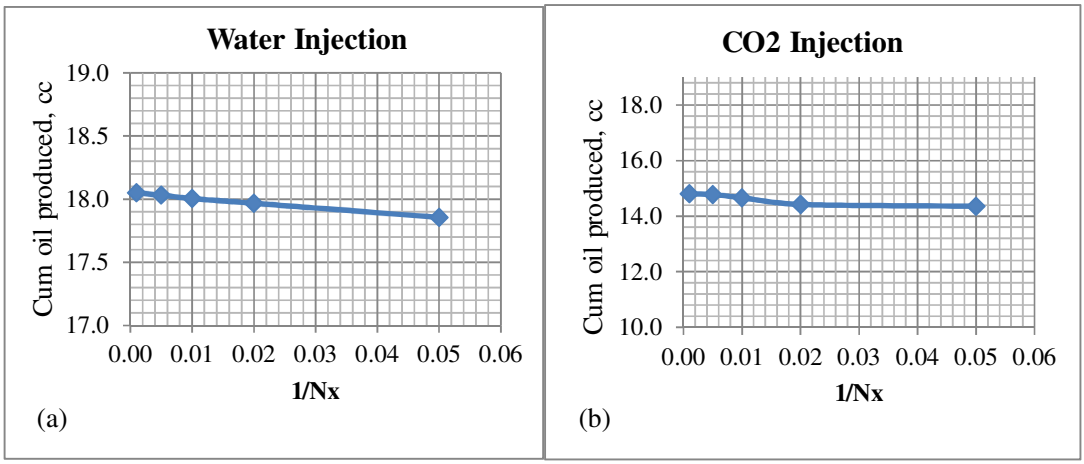

Figure 4.11: Grid sensitivity performed on (a) WI and (b) secondary CO_2 injection in the reservoir core on stock tank crude oil at 2000 psig, 100.4 ^oF.

4.3.2. Fluid PVT data

The PREOS model was used to characterize the oil samples used, which were decane and the stock tank crude oil and generate the PVT input data for the simulation. For decane and CO_2, the PVT data were as described earlier. The stock-tank crude oil properties are as given in Tables 3.3 and 3.4 of Chapter 3. It contains mainly C20+ components and is immiscible with CO_2 at the test pressure and temperature.

There were no measured PVT data available for the stock tank oil other than its compositions and viscosity. The constant composition expansion (CCE) and CO_2 swelling tests data of the original reservoir fluid (RF), from which the stock tank oil was sampled, were however, available. Also, neither SARA (Saturates, Aromatic, Resins and Asphaltene) nor TAN (Total Acid Number) information of the crude was available. As the original reservoir fluid did not exhibit any presence of asphaltene even when in contact with a high percentage of CO_2, the same was assumed for the dead crude oil.

The required PVT data for simulation for the stock tank oil were prepared, following the approach shown in Figure 4.12. The EOS model for the original reservoir fluid was first set up. It was then tuned to the available PVT data, details of which were given in Appendix A4.1, where a reasonable match was obtained between the experimental and simulated values, as shown in Figure 4.13. The tuning involved adjustment of the physical properties

of C8, C9 and C10+ fraction, which include the critical pressure and temperature, P_c, T_c, Omega A, Omega B, accentric factor, ZCrit and ZCrit(vis); the changes are all within 1-6% from the corresponding library values of the component except 10% change for Omega B parameter. The reservoir fluid was then numerically flashed from reservoir to standard condition of 60 ^oF and 14.7 psig. As shown in Table 4.3, the calculated oil compositions and viscosities reasonably agree with the measured values. The physical properties of the stock tank oil calculated by the EOS model for simulation are also given in Appendix A4.1.

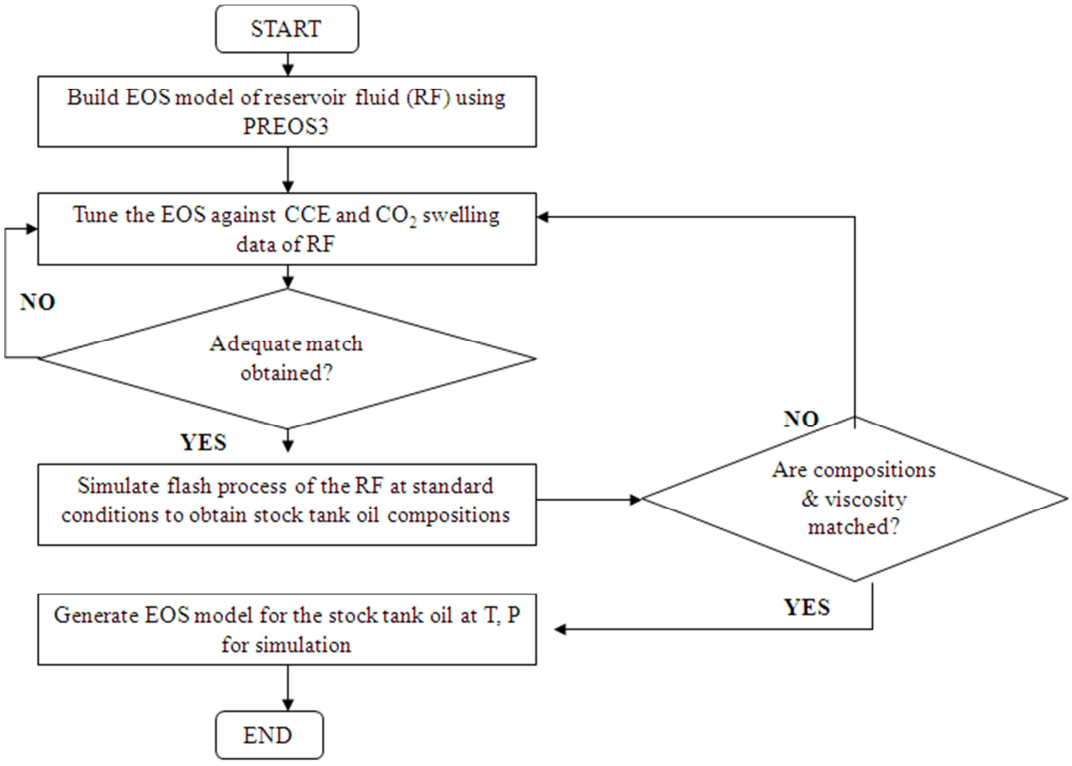

Figure 4.12: The approach to prepare the EOS model for the dead crude oil.

Table 4.3: Calculated versus measured stock tank oil composition and properties at 100.4 °F.

Component	Mole%	
	Measured	Calculated
C2-C4	0.19	1.37
C5-C7	2.71	2.68
C8-C9	5.25	3.94
C10+	91.85	92.01
Total	100.00	100.00
Mol. Weight of the stock tank oil	325	323
Oil surface density, lb/ft^3	58.8	52.7
Oil viscosity at 2000 psig, cP	145	145.6
Oil viscosity at 2500 psig, cP	158	163.6

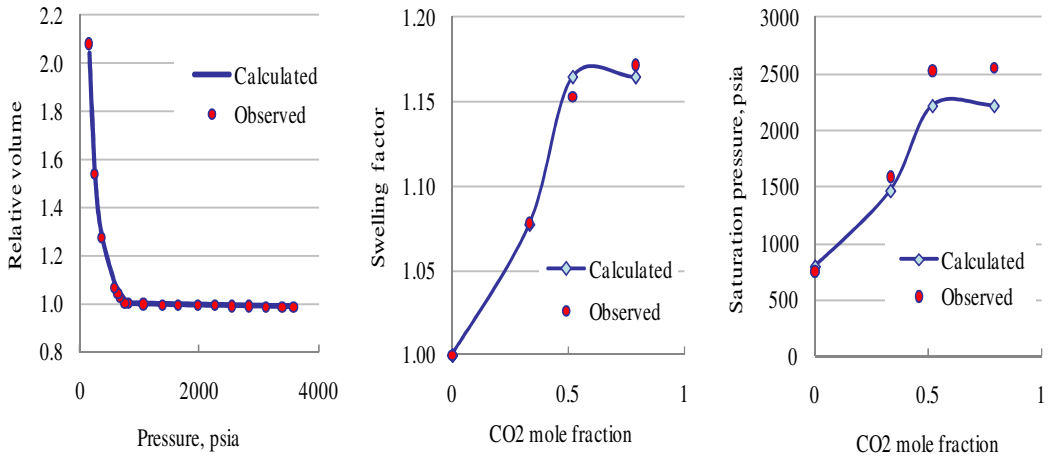

Figure 4.13: Comparison of experimental and calculated (left) oil relative volume (middle) swelling factor and (right) CO_2 saturation pressure of the original reservoir fluid, from which the stock tank oil used in this study was obtained.

4.3.3. Saturation functions

Relative permeability

In this study, relative permeability was estimated from the coreflood experiments, all of which were carried out under unsteady state conditions. The inverse problem approach was applied to obtain estimates of the relative permeability functions based on the experimental results of the displacement tests. Using a 1D core model of the same grid size shown in

Table 4.2 and a black oil core simulator, SENDRA©, the waterflood process was simulated and the oil-water relative permeability curves were obtained by history matching the experimental recovery and pressure drop data with relative permeability curves following a Corey-type correlation (Equation 4.9 and 4.10). The oil and water exponents (n_{ow}, n_w) and the vertical endpoints ($k_{rw(Sor)}$ and $k_{ro(Swi)}$) were varied until a reasonable match of fluid recoveries and the ΔP across the core was obtained.

$$k_{rw} = k_{rw(Sor)}(S_w^*)^{nw} \tag{4.9}$$

$$k_{ro} = k_{ro(Swi)}(S_w^*)^{now} \tag{4.10}$$

$$S_w^* = \frac{S_w - S_{wi}}{1 - S_{or} - S_{wi}} \tag{4.11}$$

where S_w* is the normalized water saturation, k_{rw} and k_{ro} are relative permeability of water and oil, respectively; $k_{rw(Sor)}$ is the relative permeability of water at residual oil saturation, S_{or} and $k_{ro(Swi)}$ is the relative permeability of oil at irreducible water saturation, S_{wi}.

The matches between the calculated and experimental oil and water recoveries, as well as the ΔP for each of the oil and core samples are given in Appendix A4.2 with the summary of the endpoints values and exponents (n_o and n_w) given in Table A4.2. The resulting oil/water relative permeability curves are shown in Figures 4.14-4.16. The relative permeability curves shown start at $S_w = 0$ on the left end since the core was fully saturated with oil to start with (i.e. no S_{wi} established in the core prior to water displacement). The assumption that S_o is almost 1.0 in this experiment is not unreasonable considering the core preparation procedure that was followed, where the core was flushed with at least two cycles of methanol and acetone, and subsequently put in the oven at 65 ^oC to dry, as described in Chapter 3. The procedure will leave an inconsequential amount of immobile water volume, if at all.

These relative permeability curves were subsequently used in simulating both the waterflood and the corresponding CWI. The test numbers mentioned in this section correspond to the tests described in Chapter 3.

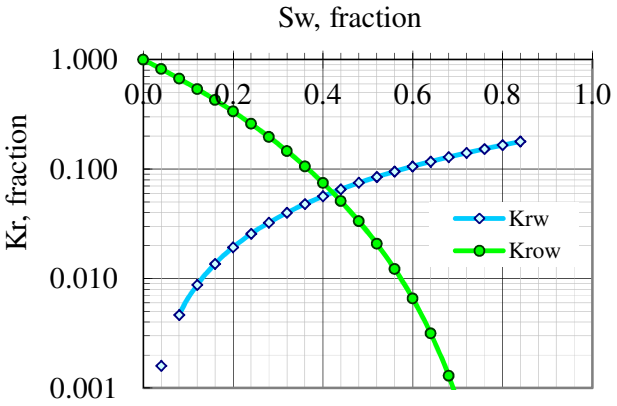

Figure 4.14: The estimated oil/water relative permeability curves from WI of decane in Clashach water-wet core (from Test 4 as in Chapter 3).

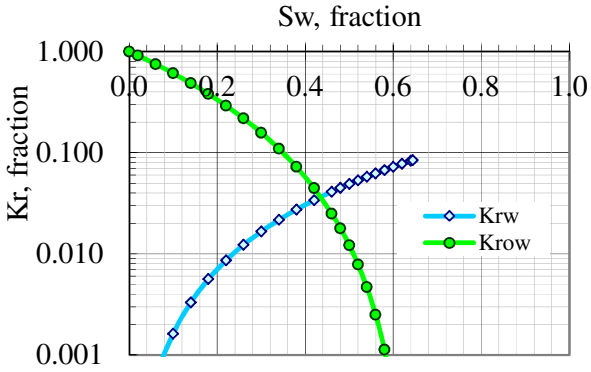

Figure 4.15: The estimated oil/water relative permeability curves from WI of decane in Clashach mixed-wet core (from Test 8 as in Chapter 3).

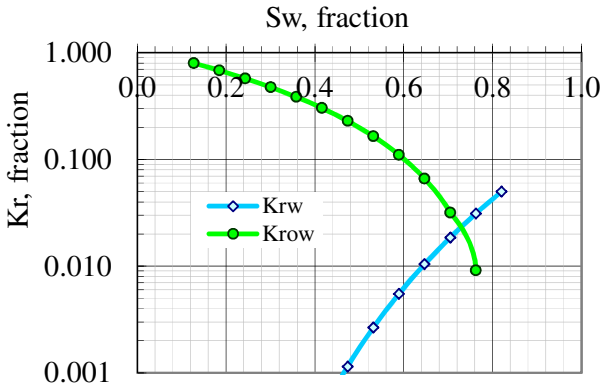

Figure 4.16: The estimated oil/water relative permeability curves from WI of stock tank crude oil and Brine 2 in reservoir core (from Test 1 as in Chapter 3).

The $k_{rw}@S_w=1-S_{or}$ in Figure 4.16 is relatively low. The curves were nevertheless selected because they gave the best match between the experimental and calculated ΔP and oil recovery. If we look at the oil recovery plot in Figure A4.3, the final saturation may have not been reached (the plateau is not totally flat) thus it is highly likely that the obtained $k_{rw}@S_w=1-S_{or}$ did not represent the actual endpoint.

Capillary pressure

The oil/water capillary pressure, Pc, was not measured for both the reservoir and Clashach cores used in the displacement tests. However, for the reservoir core, analogy was made on Pc data measured on a core from the same reservoir, shown in Figure 4.17.

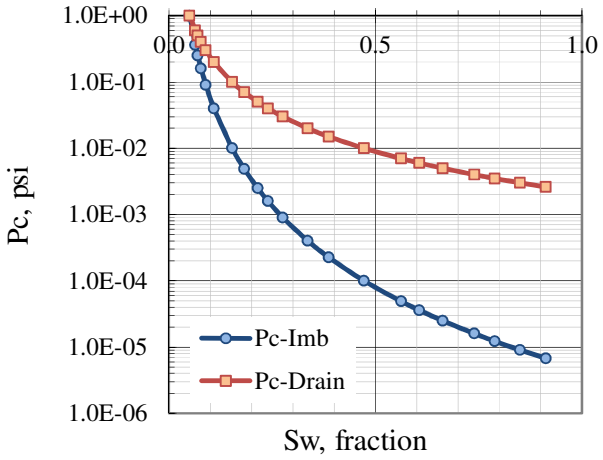

Figure 4.17: Measured Pc of a core taken from the same reservoir with that used in the experiments.

As we can see, the Pc is very small as compared to the ΔP recorded during the coreflood for a wide range of water saturation, as what would be expected for a high permeability core. The Pc effects may induce insignificant errors, and hence it was ignored in the simulation.

4.3.4. Simulation results

Secondary CWI: Decane in water-wet core (Tests 4 and 5)

The WI simulation results are given in Appendix A4.2. Using the oil/water relative permeability curves shown in Figure 4.14, the model predicted 12.4 %PV of additional oil recovery from the secondary CWI, as opposed to 5.4%PV obtained experimentally, as compared in Figure 4.18 and Table 4.4. The predicted oil recovery from CWI was corrected to the test pressure and temperature by assuming the calculated amount of CO_2 in the produced oil at any given time to be the same as the CO_2 content in the gridblock containing the producer. This estimation possibly introduced small errors in the predicted recovery.

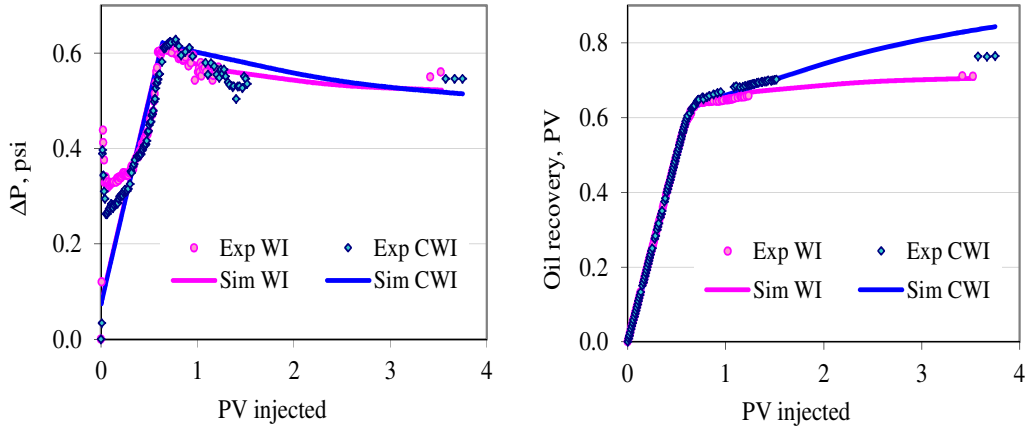

Figure 4.18: Comparison between measured and calculated ΔP across the core (left) and cumulative oil recovery (right) for WI and CWI, decane, water-wet Clashach core at 100.4 ^{o}F, 2000 psig.

Table 4.4: The experimental and predicted oil recoveries, WI and secondary CWI, water wet core, decane, 2000 psig, 100.4 ^{o}F.

Test No.	Process	Oil Recovery, % PV		Incremental Recovery, % PV	
		Experiment	Simulation	Experiment	Simulation
4	WI	71.0	70.7	-	-
5	CWI	76.4	83.1	5.4	12.4

Secondary CWI: Decane in mixed-wet core (Tests 8 and 9)

Oil/relative permeability curves in Figure 4.15 were used in the simulation of this test. The simulated oil recovery at the test conditions was calculated in the same manner as that described earlier for the water-wet core case. The match for the CWI was generally very poor. The predicted incremental oil recovery, Table 4.5, was almost twice as high as the experimental value. As shown in Figure 4.19, the ΔP trend as well as the CWI recovery profile at breakthrough time could not be modelled at all.

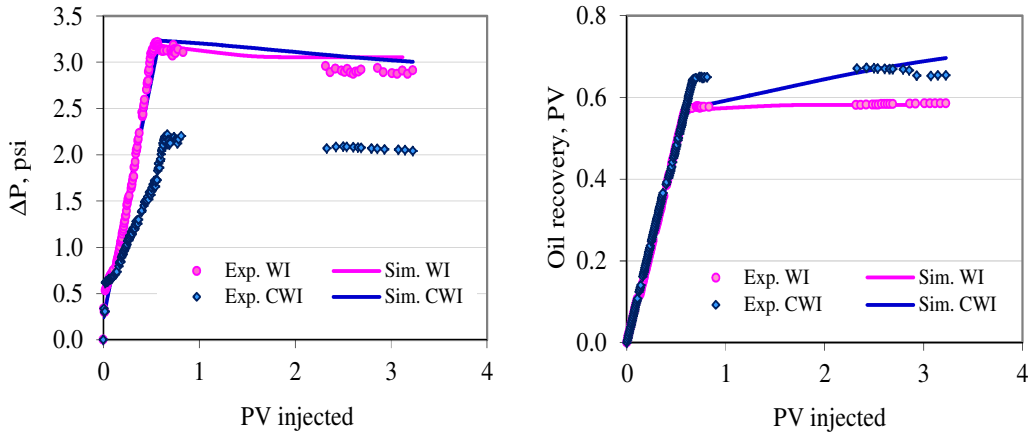

Figure 4.19: Comparison between measured and calculated (left) ΔP across the core and (right) cumulative oil recovery for WI and CWI, decane, mixed-wet Clashach core at 100.4 ^{o}F, 2000 psig.

Table 4.5: The experimental and predicted oil recoveries for WI and secondary CWI, mixed wet core, decane, 2000 psig, 100.4 ^{o}F.

Test No.	Process	Oil Recovery, % PV		Incremental Recovery, % PV	
		Experiment	Simulation	Experiment	Simulation
8	WI	58.5	58.2	-	-
9	CWI	65.4	71.6	6.9	13.4

Secondary CWI: Stock tank crude oil in reservoir core (Tests 1 and 2)

These are the simulation results for the secondary CWI with Brine 2 using oil/water relative permeability curves shown in Figure 4.16. The incremental oil recovery from CWI was over estimated by 16% (Table 4.6). From Figure 4.20, we can see that, despite a reasonable

match in the cumulative oil produced, the oil recovery match between the breakthrough time and the end of the experiment was quite poor. The brine recovery was modelled adequately but for the CO_2 gas, a much later breakthrough time and higher recovery was predicted, as shown in Figure 4.21.

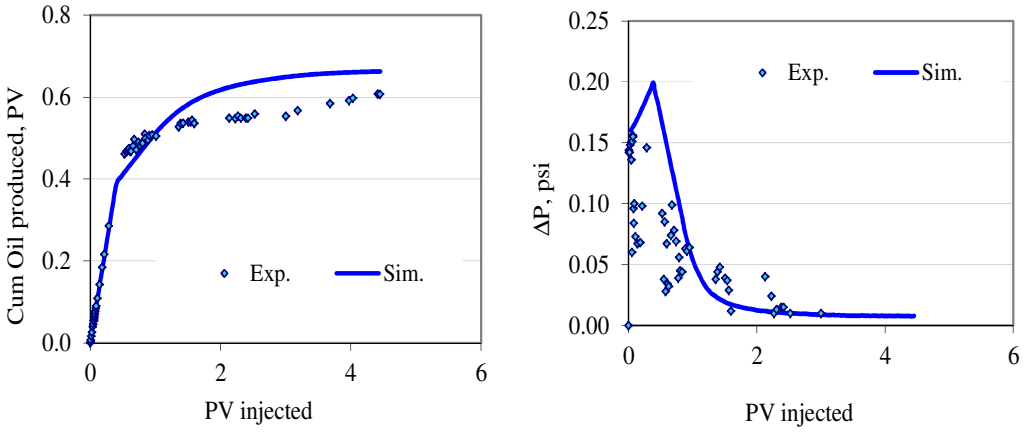

Figure 4.20: The oil recovery (right) and ΔP across the core (left) from secondary CWI in the reservoir core at 100.4 ^{o}F, 2500 psig (Test 2) and the simulator match of the coreflood.

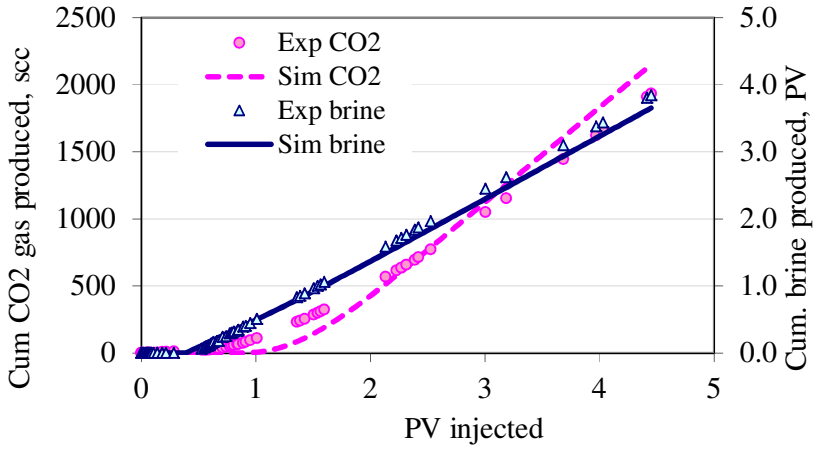

Figure 4.21: Brine (blue) and CO_2 gas (magenta) recovery from secondary CWI in the reservoir core at 100.4 ^{o}F, 2500 psig (Test 2) and the simulator match of the coreflood.

Table 4.6: The experimental and predicted oil recoveries from WI and secondary CWI of stock tank crude oil in reservoir core, 2500 psig, 100.4 ^{o}F.

Test No.	Process	Oil Recovery, % PV		Incremental Recovery, % PV	
		Experiment	Simulation	Experiment	Simulation
1	WI	41.6	40.6	-	-
2	CWI	60.6	62.7	19.0	22.1

Tertiary CWI: Stock tank crude oil in reservoir core (Test 3)

Table 4.7 shows that experimentally, 58.4 % PV was produced by WI and an additional of 9.2 % PV by the subsequent CWI, for this stock tank oil. The model, however, predicted 3.2% PV or 35% higher additional oil recovery than actual, Figure 4.22.

The plain brine was injected until up to 2.86 PV then followed by the carbonated brine up until 8.2 PV was injected in total. The water breakthrough during the WI period occurred after about 0.9 PV of plain brine had been injected (evident time lag in the water production curve in Figure 4.23). After breakthrough, the water production gradually increased as the flooding continued as shown by the straight line portion of the curve. When carbonated brine was injected, the mobile water behind the waterflood front continued to be swept towards the producer. The CO_2 then broke through after about 0.06 PV of carbonated brine (or a total of 2.92 PV since the flooding started) was injected. As we can see in Figure 4.22, during the plain brine displacement, the ΔP trend was declining rather smoothly. When the carbonated water was injected, initially there was an increase in ΔP most probably due to more resistance to flow due to the carbonated water viscosity being slightly higher than the plain water viscosity. The ΔP then gradually decreased as the total mobility decreases. The ΔP during CWI was much lower than that of during plain waterflood indicating the displacement is more efficient by carbonated water than by plain water. These however cannot be matched adequately. We can nevertheless see in Figure 4.23 that the brine and CO_2 gas production were adequately modelled.

Table 4.7: The experimental and predicted oil recoveries from WI and tertiary CWI of stock tank crude oil in reservoir core, 2500 psig, 100.4 °F.

Test No.	Process	Oil Recovery, % PV		Incremental Recovery, % PV	
		Experiment	Simulation	Experiment	Simulation
3	WI	58.4	58.1	-	-
	CWI	67.6	70.5	9.2	12.4

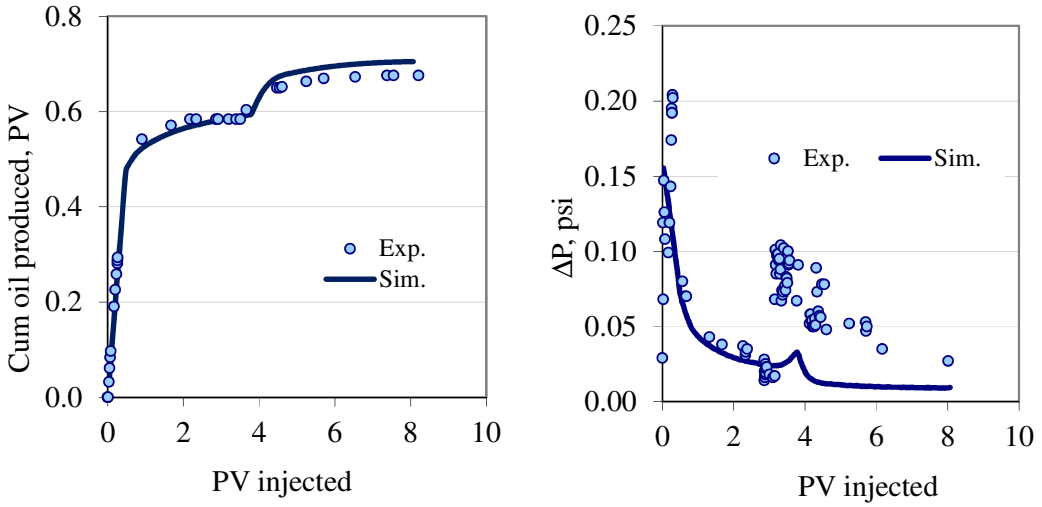

Figure 4.22: The oil recovery (left) and ΔP across the core (right) from WI and tertiary CWI in the reservoir core at 100.4 °F, 2500 psig (Test 3) and the simulator match of the coreflood.

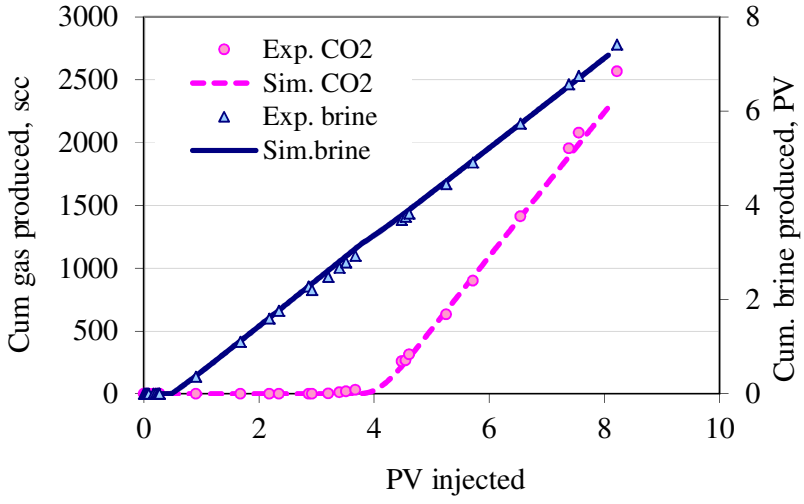

Figure 4.23: Brine (blue) and CO_2 gas (magenta) recovery from tertiary CWI in the reservoir core at 100.4 °F, 2500 psig (Test 3) and the simulator match of the coreflood.

In summary, taking experimental errors into consideration, it was generally observed that the cumulative oil recovered in the corefloods was much less than that in the calculations. The disagreement between the experimental and predicted incremental oil recovery from the CWI of the same oil sample was more pronounced for the tertiary than the secondary process, as demonstrated by the displacement test results of the dead crude oil.

The simulator calculations assumed instantaneous equilibrium and complete mixing between oil, gas and water within each grid block. The CO_2 is transferred from the carbonated water to oil and reaches equilibrium instantaneously with no dispersion or bypassing in the grid blocks. These assumptions are strongly believed to be one of the main reasons for the mismatch between the experimental and calculated results and will be looked into in more detail in the next section.

4.3.5. The effect of dispersive mixing at core scale

Non-equilibrium phenomena, such as bypassing, both at macroscopic and microscopic level, are probable reasons why the experimental oil recoveries were lower than calculated values.

Viscous fingering is a form of macroscopic bypassing which normally occurs due to high mobility contrast between the displaced and displacing fluid, reservoir heterogeneity, large transverse extent and high displacement rates (Gardner and Ypma, 1984). At the pore level, dispersive mixing and/or capillarity-induced bypassing could occur. Dispersive mixing, which includes molecular diffusion and mechanical dispersion, determines the extent to which a solvent will mix with the oil to promote mass transfer or miscibility under favourable conditions, thus affecting the oil recovery (Perkins and Johnston, 1963). Bypassing prevents complete mixing of components.

Molecular diffusion takes place solely due to the concentration gradient, with or without motion. Earlier researchers have reported the importance of molecular diffusion in determining the displacement efficiency in secondary and tertiary CO_2 floods (e.g. Grogan, et al., 1987, 1988; Campell, et al., 1985, Bijeljic, et al., 2002). Grogan and Pinczewski (1987) found that the transport of CO_2 through the water phase is the rate-controlling step of swelling a residual oil droplet separated by a water film. The presence of a water layer

separating the oil and CO_2 phases has been shown to reduce the CO_2 flood displacement efficiency at the core scale (Shelton et al., 1978; Tiffin et al., 1983). This effect of water blocking is significant, especially in water-wet conditions in which molecular diffusion through water films is the dominant mechanism for the solvent gas to reach, swell and reconnect isolated droplets.

Mechanical dispersion occurs due to the distribution of pore sizes, hence creating a distribution of path lengths and velocities where contact time is limited at the pore junction but longer in the pores. These distributions lead to incomplete mixing at the pore junction. Bypassing from mechanical dispersion is influenced by flow rate but not by core length (Stern, 1991).

Capillarity-induced bypassing only occurs in the tertiary displacement where solvent must displace water to mobilize the oil (Campbell and Orr, 1985) and is greatly influenced by the wettability of the rock. In a water-wet rock, for example, the solvent displaces water in the larger pores first and creates preferred high conductivity paths, bypassing small pores. This bypassing effect is reduced by reducing the capillary pressure forces, such as by increasing the flow rates and solvent viscosity (Stern, 1991).

Bypassing is, however, unlikely to play significant role in the displacement if the critical wavelength of instability, λ_c (Equation 4.14) is larger than the diameter of the core, since the fingers are eliminated by transverse dispersion.

$$\lambda_c = 2^{5/2}\pi \frac{\mu_o+\mu_s}{\mu_o-\mu_s}\frac{D_T}{\bar{v}} \tag{4.14}$$

where μ is viscosity with subscript o and s denotes oil and solvent, respectively, D_T is the transverse dispersion, which can be calculated by Equation 4.15 and $\bar{v} = Q/A\phi$ is the average velocity (Chandrasekhar, 1961 as quoted in Gardner and Ypma, 1984).

$$D_T = \frac{D_o}{F\phi} + 0.0157\bar{v}d_p\sigma \tag{4.15}$$

D_o is the diffusion coefficient of CO_2 in oil, F is the formation resistivity factor and σ is the inhomogeneity factor of the rock.

In order to gauge whether the displacement was stable for the coreflood in this study, λ_c was estimated. D_o was calculated using McManamey and Woolen's correlation (1973) while F was calculated using Archie's equation ($F = a/(\phi)^m$) with *m* and *a* assumed to equal 1.0. As no measured data was available, the rock inhomogeneity factor for all the cores was assumed to be 0.03; a value used by Gardner and Ypma (1984) for a system more or less similar to decane in the water-wet core of this study.

As we can see from Table 4.8, λ_c is smaller than the core diameter for all the tests, indicating viscous fingering might have affected the displacement process to certain extent. For the more friable reservoir core, there was nonetheless high uncertainty in the assumed inhomogeneity factor, hence the estimated λ_c.

Table 4.8: The estimated critical wavelength of instability of the coreflood tests.

Core	Diameter, cm	Porosity, fraction	Ave velocity, v, cm/s	D_T, cm^2/s	λ_c, cm
Clashach 1	4.99	0.185	1.536E-03	1.092E-05	1.00
Clashach 2	4.99	0.165	1.722E-03	1.057E-05	0.86
Reservoir core	3.72	0.350	7.302E-05	1.303E-06	0.32

Clear evidence of diffusion and dispersion of CO_2 during the core displacement was nevertheless observed from the much earlier CO_2 breakthrough time than that of the brine. As the author has already discussed and shown in Figure 3.18 in Chapter 3, for decane, the CO_2 broke through after about 0.64 PVI, while water broke through 0.06 PVI later. For the stock tank crude oil, the CO_2 and water broke through after 0.11 and 0.22 PVI, respectively. The model, on the other hand, predicted a much delayed gas breakthrough than that of brine, demonstrating the inappropriate distribution of CO_2 in the model calculated by the simulator.

Figure 4.24 shows the simulated profile of water saturation (SWAT) and mole fraction of CO_2 in the water phase (AMF1) and oil (decane) phase (XMF1) along the core at about breakthrough time. From this model output we can see how fast the CO_2 is moving in relation to the water front. The simulation results show that the water front was totally deprived of CO_2 i.e., the CO_2 concentration in the water phase reduces to zero, after travelling a certain distance through the core. The CO_2 concentration in the water phase dropped very rapidly as the carbonated water came in contact with the oil. As can be seen in

Figure 4.25, at breakthrough, the model predicted that the CO_2 in the carbonated water was partitioning into the oil at 0.007 gmole per cm of the core travelled and getting lesser as the flooding continues. The fresh supply of CO_2 from the injected carbonated water contacted more oil behind the front.

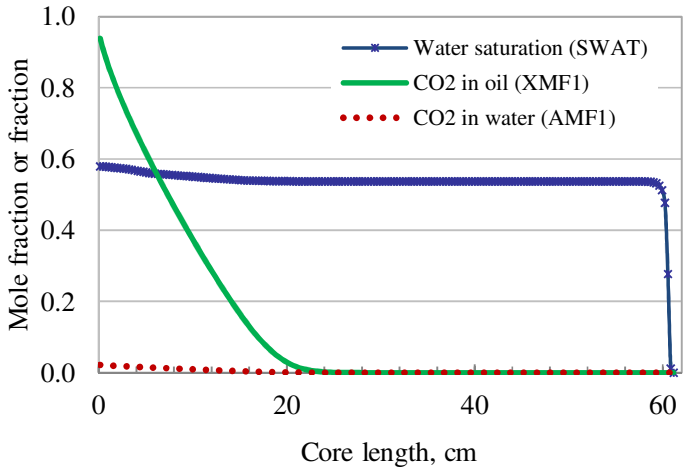

Figure 4.24: Simulated profiles of water saturation (SWAT) and CO_2 mole fraction in water (AMF1) and oil (decane) phase (XMF1) along the core at water breakthrough time.

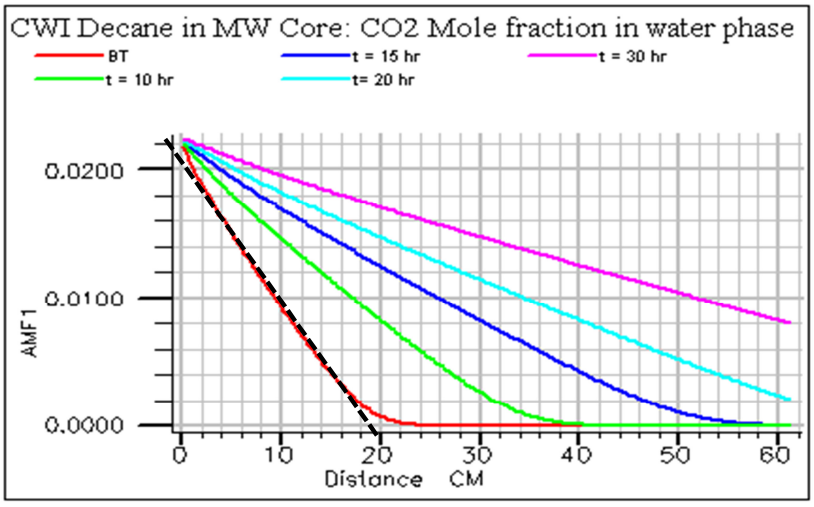

Figure 4.25: Simulated profiles of CO_2 mole fraction in the water phase along the MW core at different times for decane CWI.

Similar trend in the simulated profiles of water saturation, mole fraction of CO_2 in the water and oil phase was observed for the secondary CWI of the stock tank crude oil, Figure 4.26. The carbonated water displacement front totally deprived of CO_2, moved ahead of oil and broke through faster than CO_2 gas.

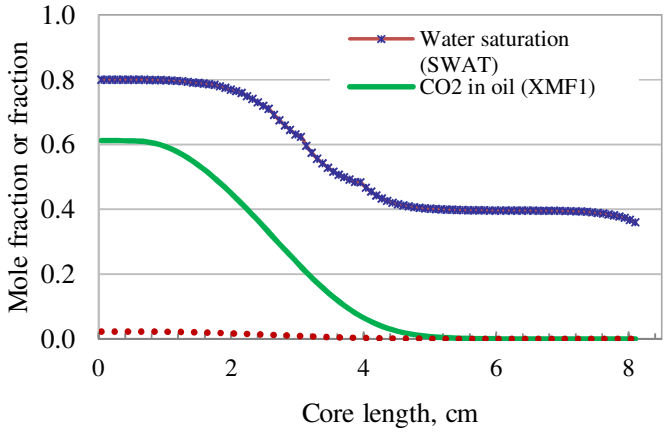

Figure 4.26: Simulated profiles of water saturation (SWAT) and CO_2 mole fraction in water (AMF1) and oil phase (XMF1) along the core at water breakthrough time (Test 2).

Figure 4.27 shows the corresponding plots of water saturation, oil saturation, CO_2 solubility in water and CO_2 mole fraction in oil phase along the core close to water breakthrough time while the composition of some components as they were produced in the producer and their variation along the core at a particular time are plotted in Figures A4.6-A4.8 (Appendix A4.3). The predicted CO_2 in both water and oil propagated equally with a larger portion of CO_2 transferred into the oil than into the water reflecting CO_2 solubility in both phases.

The predicted CO_2 amount in each phase is however not quite realistic especially at the scale involved. This is because, in reality, some diffusion and dispersion of CO_2 from the carbonated water into the oil phase take place thus at any given time it is hypothesized that the amount of the CO_2 should be smaller than what is calculated based on the instantaneous equilibrium assumptions. Whilst the simulation predicts that the carbonated water front was totally deprived of CO_2 and moving ahead as plain water, the experiment showed earlier breakthrough of CO_2 than water (Figure 3.31) confirming that the displacement font was not totally deprived of its CO_2.

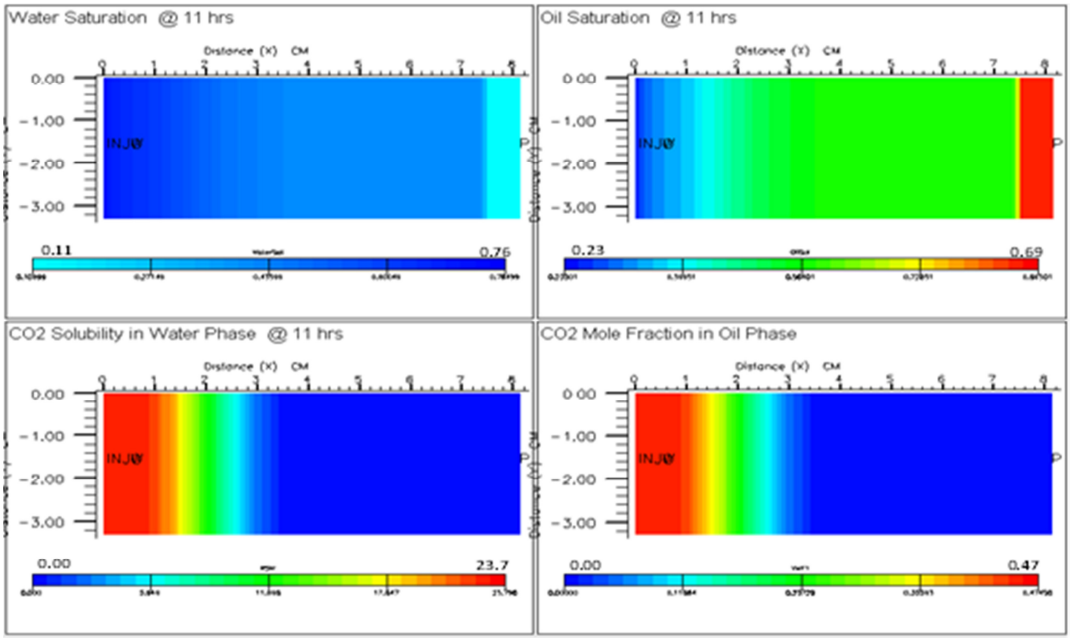

Figure 4.27: From top left clockwise:Simulated saturation plots of water, oil saturation, CO_2 solubility in water and CO_2 mole fraction in oil phase along the core close to water breakthrough time.

Experimentally for decane, the CO_2 broke through after about 0.64 PV of carbonated water was injected while water broke through 0.06 PV later. For the stock tank crude oil, CO_2 and water broke through after 0.11 PV and 0.22 PV of carbonated water had been injected, respectively. These observations serve as evidence of the inappropriate distribution of CO_2 by the simulator and that the equilibrium assumption is less reliable for modelling this process at the core scale.

Further evidence of the diffusion process in CWI was reported by Riazi et al. (2009). They reported the swelling of a 0.25 cm oil (decane) ganglion with time during carbonated water flooding in a water-wet micro model at 2000 psig and 100 ^{o}F, shown in Figure 4.28. CO_2 from the carbonated water diffused into the oil, resulting in the swelling of the oil and it took a definite amount of time for the system to reach equilibrium, where the oil volume came to a plateau. The diffusion equilibrium time, which is defined as the time for the oil to swell to 95% of its equilibrium volume, in this case was about 167 hrs.

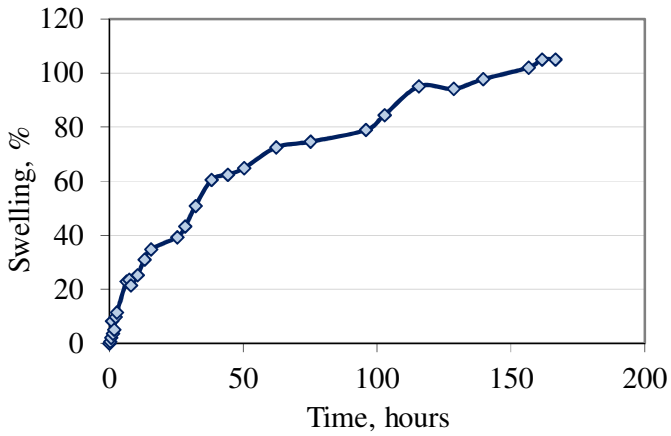

Figure 4.28: Swelling of the 0.25 cm decane ganglion during CWI in the micromodel experiment at 100 °F, 2000 psig (Riazi et al., 2009).

A wide range of diffusion path lengths, between 100 μm to the core diameter size, could, however, exist in the real porous media (Chatzis et al., 1983). The diffusion time, t, is correlated with the oil length, L_o, by Equation 4.16 (Grogan and Pinczewski, 1987):

$$t \sim \frac{(L_o)^2}{D_{i,o} S_{i,o}} \tag{4.16}$$

where L_o is the oil thickness in m, $D_{i,o}$ is the diffusion coefficient of CO_2 in oil in m^2/s and $S_{i,o}$ is the solubility of CO_2 in oil in mole/mole.

For the same oil-CO_2 system where the degree of oil swelling is assumed to be the same for all the oil sizes, the diffusion time for two different oil ganglion sizes can be calculated as:

$$\frac{t_1}{t_2} = \frac{(L_1)^2}{(L_2)^2} \tag{4.17}$$

Based on the known equilibrium time for the 0.25 cm oil ganglion size, the diffusion equilibrium time (in seconds) of various oil thicknesses were calculated and shown in Figure 4.29. In the simulation model, an oil ganglion size can be assumed to be equivalent to half of the grid block size, which was 0.083 cm in the decane case. From Figure 4.29, a contact

time in the order of 6.6E04 seconds (ca. 18 hours), where the diffusion was taking place at 1.26E-06 cm/s (≡ 0.083 cm/6.6E04 s), was required for the oil ganglion of this size to swell 100%. With the displacement of carbonated water at 2.845E-04 cm/s (20 cc/hr), there was not enough time for the displaced oil ahead of or behind the front to fully swell or reach equilibrium volume. Nonetheless, some swelling of the oil took place especially for the oil behind the front that was continuously receiving a fresh CO_2 supply from the injected carbonated water, so that some of the swollen oil blobs behind the front were large enough to coalesce and eventually be produced.

If the average oil size in the core was assumed to be the same as in the micromodel, based on Figure 4.28, at breakthrough time (4.55 hrs), the oil was estimated to have swelled by about 15% and by 35% at the end of the coreflood experiment (i.e., at 22.5 hrs). However, as shown in Figure 4.30b, the model predicted an oil swelling of 55% with average CO_2 content in the oil of up to 72 mole% (Figure 4.30a). This led to much larger oil viscosity reduction, hence more optimistic prediction of oil recovery.

This comparison between the calculated and experimental results shows that the local equilibrium was not achieved during the carbonated water displacement in the core, hence, the instantaneous equilibrium and complete mixing assumptions are less reliable for modelling the process. By the instantaneous equilibrium assumption, once the carbonated water contacted the oil in the grid cell, the CO_2 instantaneously partitioned itself between the oil and water, according to the solubility and fugacity equilibration.

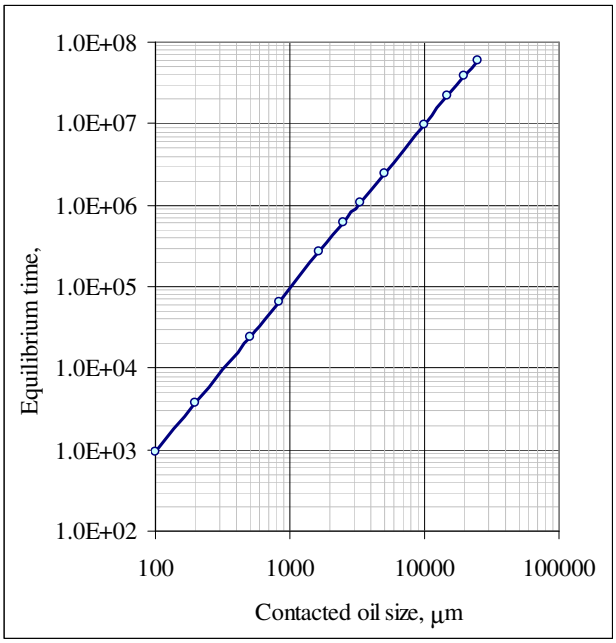

Figure 4.29: Diffusion equilibrium time (in seconds) by directly contacting decane with carbonated water for varying oil sizes, calculated using Equation 4.17.

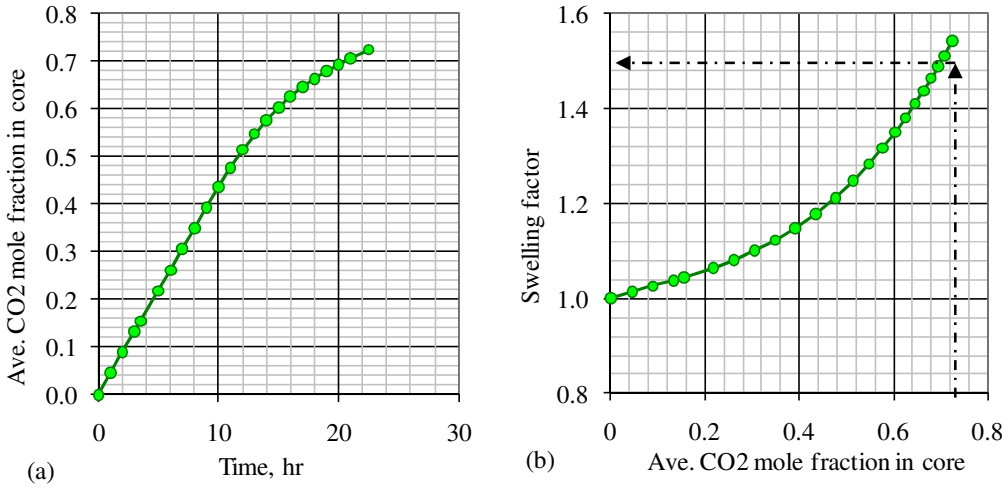

Figure 4.30: The calculated average CO_2 mole fraction in the oil phase in the core (left) and the EOS-calculated swelling factor versus CO_2 mole fraction in the oil (right), for CWI of decane at 100.4 ^oF, 2000 psig in the water wet core.

The author found that by merely incorporating the molecular diffusion of CO_2 within both

the oil and the gas phases in the model did not significantly alter the simulation results. The author believes that it is the cross-phase molecular diffusion and dispersion that is more influential to the oil recovery of CWI at the core scale. At the time this study was undertaken, none of the compositional simulators evaluated has yet the capability to account for the cross phase diffusion of CO_2 from the water phase to the oil phase. In this study, the author has evaluated the use of transport coefficients to account for the dispersion effects in the model and this is discussed next.

4.3.6. Modelling CWI with transport coefficients

The recovery efficiency in a miscible gas displacement in a porous medium is affected by the viscous fingering, due to the adverse viscosity ratio when a more mobile (less viscous) gas displaces less mobile (more viscous) oil resulting in some oil by-passed at breakthrough. The component mixing at the pore scale, due to molecular diffusion and fluid velocity variations, can dampen down the growth of viscous and gravity fingers. The requirement for a direct solution of the convection-diffusion equation of a very fine grid model to simulate the fine scale structure of the fingers combined with the numerical dispersion inherent in finite difference models prohibit the accurate larger scale study of such displacement process.

In this study, the author evaluated the transport coefficients, termed as 'α- factors' to compensate for the dispersion and diffusion of CO_2 effects in the model. The α-factor can be incorporated into the E300 model to mimic the effect of non-equilibrium mechanisms such as diffusion and dispersion. The coefficients were originally introduced by Barker and Fayers (1994) for modelling sub-grid block phenomena, such as rapid variations in phase saturations and compositions as a result of viscous fingering, reservoir heterogeneity and the development of narrow fronts, to improve the accuracy of compositional simulations performed with coarse homogeneous grid blocks.

The α-factor modifies the mobility of component c in phase p (M_p^c), according to:

$$M_p^c = \alpha_p^c x_p^c k_{rp} \frac{b_p^m}{\mu_p} \tag{4.18}$$

where x_p^c is the mole fraction of component c in phase p, k_{rp} the relative permeability of phase p, μ_p the viscosity of phase p, b_p^m the molar density of phase p and α_p^c is the transport coefficient of the component in phase p. The factor was inputted as a function of CO_2 mole fraction i.e., it modifies the mobility of the CO_2 component as the concentration changes.

The pre-requisite of this approach is a fine grid model of suitable Representative Elements of Volume for the reservoir that is able to model the sub-grid block phenomena of interest. The α-factors are calculated from the results of fine grid simulations and introduced in the flow terms to relate the compositions of the fluids flowing out of a large gridblock to the average compositions of those fluids within the block. However, since there was no fine grid CWI model available to be used as the basis in calculating the α-factor in this study, the experimental data were used as a reference and the α-factor was tuned as a history matching parameter.

Simulation results

Table 4.9 shows the predicted oil recovery with and without the α-factor. A huge improvement in the oil recovery match for the secondary CWI of decane was obtained with α-factor of 30 (Figure 4.31). Significant improvement in the oil recovery match particularly after the breakthrough time until the end of the test was also observed for the stock tank oil, with α-factor of 20 (Figure 4.32). These relatively large α-factors could be due to the sharp fronts in the solution of the homogeneous 1D model. Barker and Fayers (1994) have reported similar magnitude of α-factor in 1D simulation of a lean gas injection. Heterogeneities and three dimensional effects are expected to smear the fronts, hence giving a much lower α-factor value.

The water recovery for the latter, shown in Figure 4.33, was satisfactorily matched and the breakthrough time of CO_2 was also significantly improved. More CO_2 retention in test than in the model was however observed. This could possibly be due to the tuning parameter that resulted in the match of the EOS model versus the actual PVT data. As can be seen in Figure 4.13, the EOS used in the model for this sample predicted about 5% lower CO_2 saturation pressure. Since lower saturation pressure means lower amount of CO_2 dissolved

in the oil, this indicates that at any given pressure, the model predicted more CO_2 gas been released rather than being dissolved in the oil i.e., more CO_2 retention in test than in the model.

Table 4.9: The α-factor for matching the carbonated coreflood.

Oil	Process	α factor	Recovery, % PV		Incremental recovery		
			Expt.	Sim.	Expt., %PV	Sim., %PV	Difference, %
Decane	WI	-	71.0	70.7	-	-	-
	Secondary CWI	-	76.4	83.1	5.4	12.4	129.6
		30	76.4	77.2		6.5	20.4
Stock tank oil	WI	-	41.6	40.6	-	-	-
	Secondary CWI	-	60.6	62.7	19.0	22.1	16.3
		20	60.6	60.4		19.8	4.2
	WI	-	58.4	58.1	-	-	-
	Tertiary CWI	-	67.6	70.5	9.2	12.4	34.8
		20	67.6	70.2		12.1	31.5

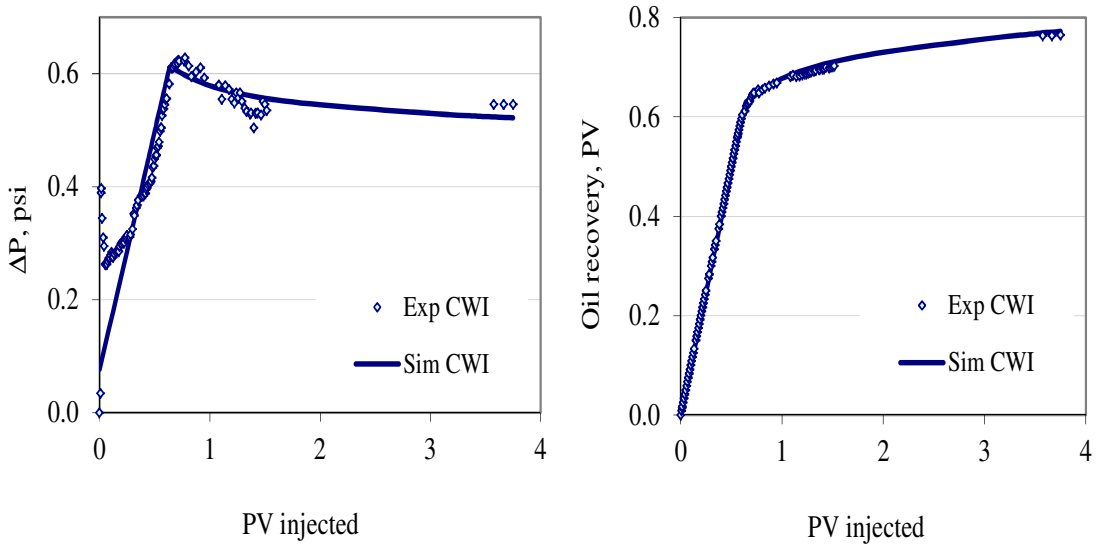

Figure 4.31: Comparison between measured and calculated ΔP across the core(left) and cumulative oil recovery (right) for secondary CWI, decane, water-wet Clashach core at 100.4 ^{o}F, 2000 psig, α-factor = 30.

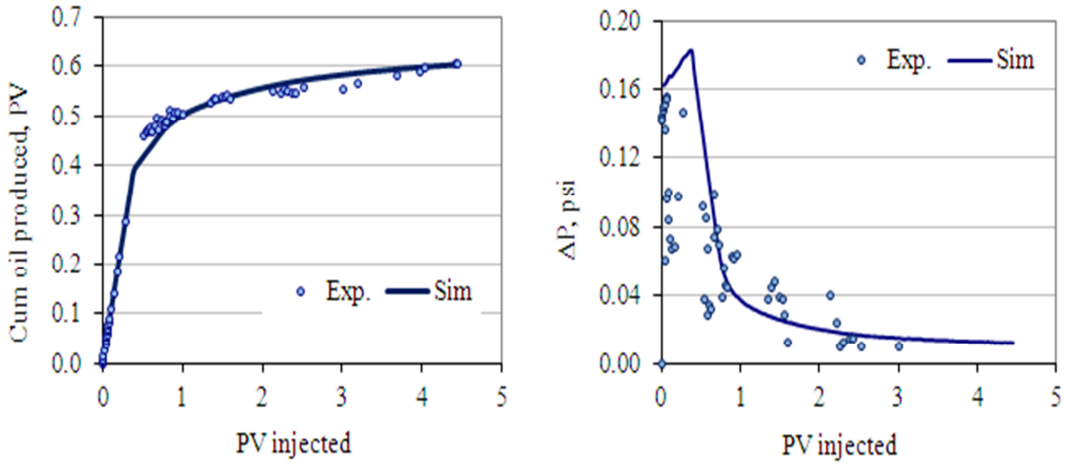

Figure 4.32: Comparison between measured and calculated cumulative oil recovery (left) and ΔP across the core (right) for the secondary CWI, stock tank oil, reservoir core at 100.4 ^{o}F, 2500 psig, α-factor = 20.

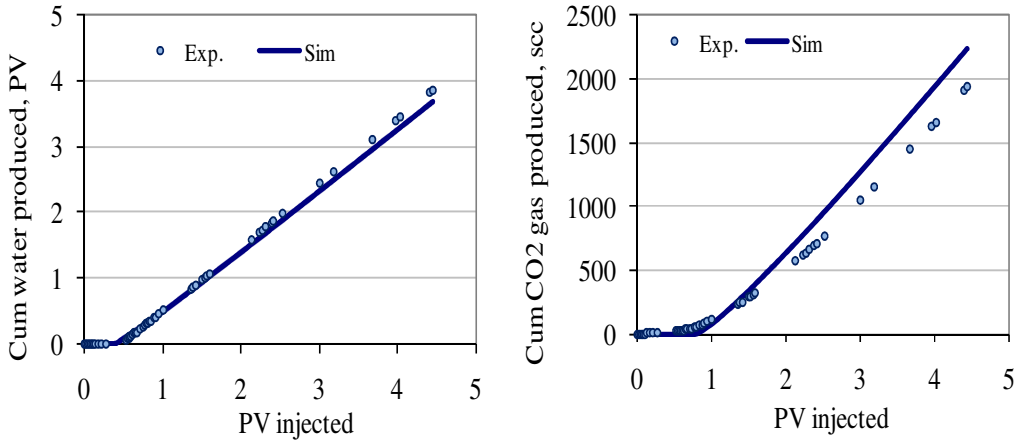

Figure 4.33: Comparison between measured and calculated cumulative brine recovery (left) and cumulative CO_2 produced (right) for the secondary CWI, stock tank oil, reservoir core at 100.4 ^{o}F, 2500 psig, α-factor = 20.

The comparison between the experimental and simulated results with the α-factor for the tertiary CWI is shown in Figures 4.34 and 4.35. As can be seen in Table 4.10, unlike the

secondary CWI, the predicted tertiary CWI recovery was not that sensitive to the α-factor. Incorporating a α-factor of up to 20 changed the predicted oil recovery by only 0.3 %PV. An unrealistically high α-factor could be required in order to get the same level of improvement as in the secondary CWI case, if obtained at all. The inadequacy of the α-factor for the tertiary CWI process is most probably because both oil and water phases were mobile in this mode of recovery, unlike in the secondary process, where oil was the only mobile phase in the core. Barker and Fayers (1994) reported the use of pseudo-relative permeabilities to correct the oil and gas fluxes (the two mobile fluids in their system) together with the use of the α-factors. The modification in the oil fluxes due to the α-factor and the presence of mobile water requires changes in the fluids' relative permeabilities. The correction in the relative permeabilities was however not examined in this thesis. Further investigation is recommended.

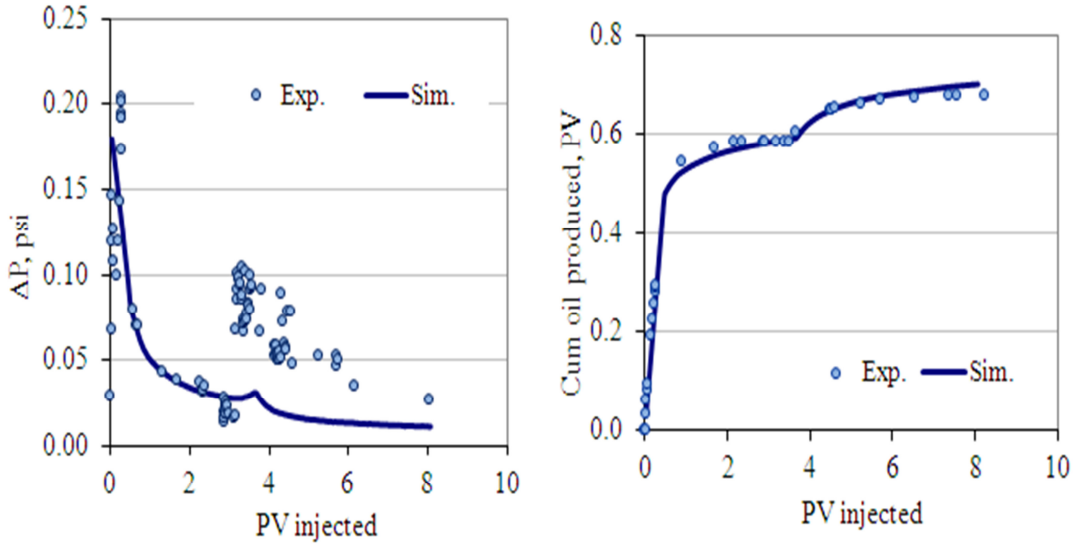

Figure 4.34: Comparison between measured and calculated ΔP across the core (left) and cumulative oil recovery (right) for the tertiary CWI, stock tank oil, reservoir core at 100.4 ^{o}F, 2500 psig, α-factor = 20.

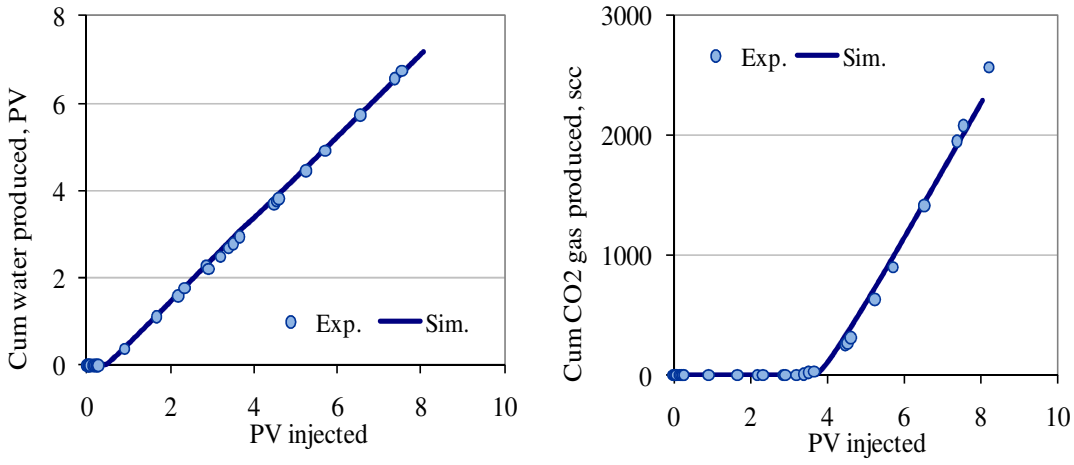

Figure 4.35: Comparison between measured and calculated cumulative brine recovery (left) and cumulative CO_2 produced (right) for the tertiary CWI, stock tank oil, reservoir core at 100.4 ^{o}F, 2500 psig, α-factor = 20.

Comparing the match in the oil recovery with and without the α-factor, for instance that for decane in the water-wet core in Figure 4.18 and 4.31, respectively; we can see that the α-factor significantly changes the match after the breakthrough time only. As such, this factor does not work satisfactorily for modelling the CWI in the mixed-wet core reported here since the mismatch in the oil recovery was also observed at the breakthrough point, Figure 4.19.

4.4. Alternative approaches in modelling CWI

The author has already discussed the shortcoming of the current simulator to model the CWI mechanisms and the use of the α-factor to represent the effect of dispersion in the model. Whilst the matches between the experimental and calculated results of the secondary CWI in the water-wet cores were improved when using the α-factor, the tertiary CWI prediction still needed improvement. The α-factor approach also cannot model the CWI in the mixed-wet core. Two other approaches using the available commercial simulators were examined, aiming to improve the match further.

4.4.1. Relative permeability approach using black oil simulator

In addition to displacement and molecular diffusion, interfacial tension (IFT) reduction and wettability alteration, which influence the relative permeability (kr), could also play a role in the oil recovery from CWI. This could probably explain the very different CWI recovery profile in the mixed-wet core than in the water-wet one. The recovery mechanisms by CWI process in the mixed wet core are vaguely understood. The approach of using the same oil/water relative permeability curves for modelling WI and CWI may not be appropriate for the mixed-wet core case leading to the significant mismatch.

The lower the IFT, the higher the capillary number, N_c, which in turn is the ratio of capillary to viscous forces (Equation 4.19) and has a significant effect on S_{or}, such that as N_c increases, S_{or} is reduced (Shen et al., 2006).

$$N_c = \frac{\mu_w V_w}{\sigma_{wo} \emptyset} \tag{4.19}$$

where μ_w is the viscosity of the displacing phase, V_w is the flow rate of the displacing phase, ϕ is the effective porosity and σ_{ow} is the IFT for the oil/water system. In CWI, there will be a discernible reduction in the IFT, thus S_{or}. This study has shown through the coreflood tests that secondary CWI can bring about 31% reductions in S_{orw} for a crude oil. To the author's knowledge, as far as the E300 simulator is concerned, incorporating the IFT changes is only possible through the use of a fully coupled ODD3P model, which incorporates hysteresis and miscibility effects for both relative permeability and capillary pressure for a three phase system. As there was no gas involved, there was no three-phase relative permeability data from the CWI tests. Since the three-phase data are the required input data to turn on the ODD3P feature, this method is therefore not applicable.

In this simulation approach, CWI was modelled as plain waterflood in an E100 black oil simulator and using the oil/carbonated water relative permeability curves. The 1D compositional models described earlier were converted to the E100 black oil model by changing the PVT input data to the required tabulated black oil format. The relative permeability acts as 'a factor' to account for all the important physics of the CWI process. A similar approach to that used in obtaining the WI relative permeability curves mentioned in

Section 4.3.3 was used to obtain the relative permeability from the experimental CWI tests. However, since several parameters (the exponents and end points) of the Corey's correlation were sensitized simultaneously to match the experimental data, non-unique solutions, in which a few different sets of relative permeability curves result in an acceptable match, were frequently obtained. In order to further constrain the solutions, the approach shown in Figure 4.36 was followed.

The oil/water relative permeability curves from the WI data were first estimated. Since the changes in the relative permeability to water, k_{rw}, between the WI and CWI processes were expected to be small, k_{rw} for CWI, $(k_{rw})_{CWI}$, was initially assumed to be the same as that of corresponding WI, $(k_{rw})_{WI}$. The endpoints and the exponent of the relative permeability to oil for CWI $(k_{row})_{CWI}$ curve were then adjusted until a reasonable match in the experimental data was obtained. For discussion purpose, only results for decane are shown here.

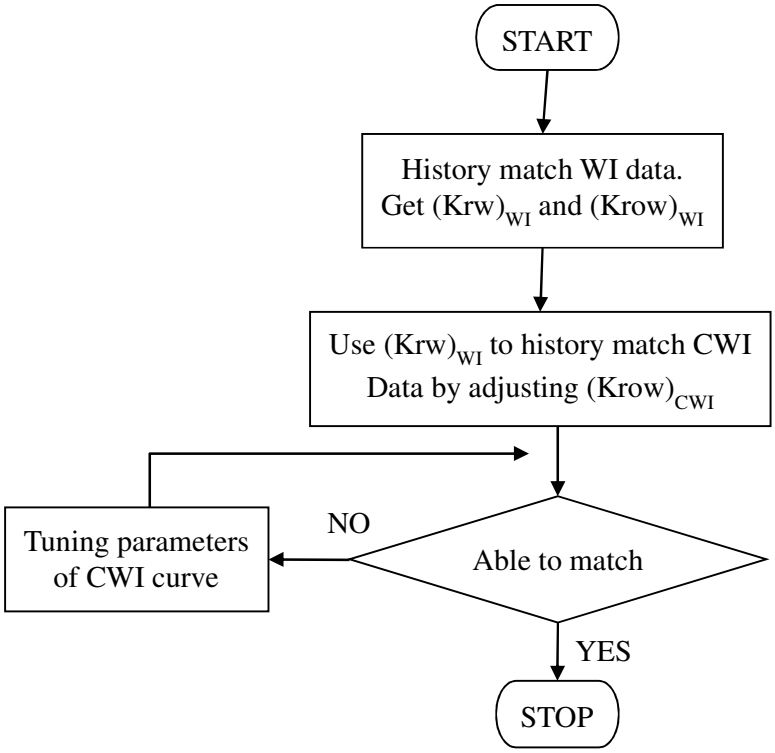

Figure 4.36: The approach in history matching the displacement tests data in obtaining the carbonated water/oil relative permeability curves.

Results and discussion

For decane in water-wet Clashach core (Tests 4 and 5), good agreement was obtained between the experimental and the calculated oil recovery and ΔP, as shown in Figure 4.37 and summarised in Table 4.10. The resulting relative permeability curves from WI and CWI are displayed in Figure 4.38. The $(k_{row})_{CWI}$ is slightly higher than $(k_{row})_{WI}$, which explains the additional oil recovery. The water relative permeability curve for CWI has slightly lower S_{or} and $k_{rw(Sor)}$ than WI. Since the WI recovery was already high, only a small reduction of S_{or} and a small increase in k_{row} as compared to WI were required to bring about the 5.4 %PV incremental oil recovery from the secondary CWI in this core.

Table 4.10: Relative permeability approach - Comparison of the simulated and experimental coreflood recovery of decane in water-wet Clashach core.

Test	Process	Recovery, % PV		Incremental Recovery, % PV	
		Experiment	Simulation	Experiment	Simulation
4	WI	71.0	71.3	-	-
5	CWI	76.4	75.6	5.4	4.3

For CWI of decane in the mixed-wet Clashach core (Tests 8 and 9), slightly higher $k_{rw(Sor)}$ and lower S_{or} in CWI were required as compared to WI to get the match shown in Figure 4.39. The significant differences in the ΔP and oil recovery trends in this mixed-wet core as compared to those in the water-wet core are also reflected in the differences in the relative permeability curves obtained where the difference between $(k_{ro})_{CWI}$ and $(k_{ro})_{WI}$ for the former is much larger. Table 4.11 compares the experimental and predicted oil recovery. The resulting relative permeability curves are shown in Figure 4.40.

Table 4.11: Relative permeability approach - Comparison between the simulated and experimental coreflood recovery of decane in the mixed-wet Clashach core.

Test	Process	Recovery, % PV		Incremental Recovery, % PV	
		Experiment	Simulation	Experiment	Simulation
8	WI	58.5	58.5	-	-
9	CWI	65.4	66.5	6.9	8.0

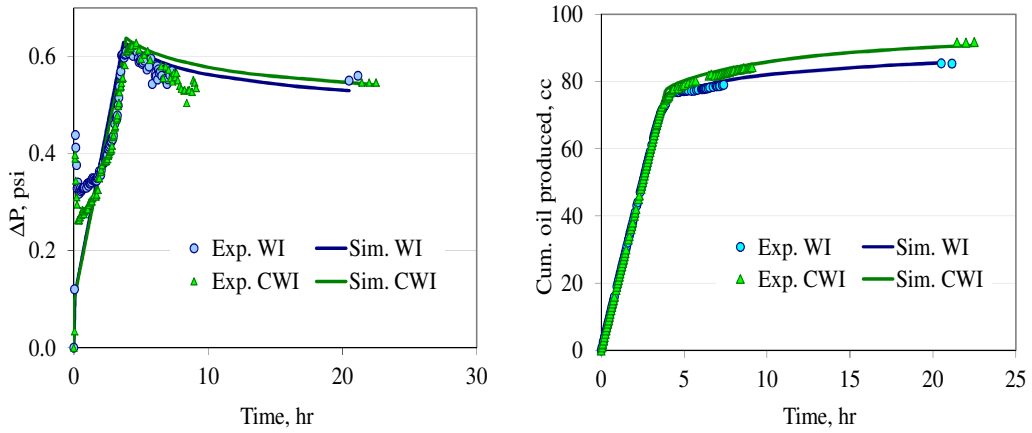

Figure 4.37: Comparison between measured and calculated ΔP across the core (left) and cumulative oil recovery (right) for the secondary CWI, decane, water-wet Clashach core at 100.4 ^{o}F, 2000 psig.

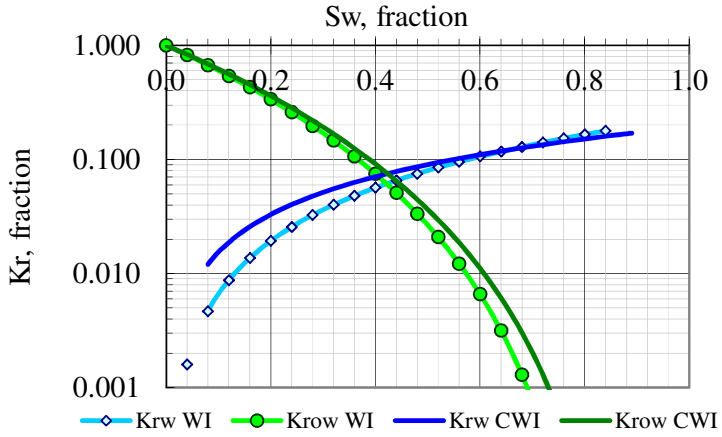

Figure 4.38: The estimated oil/water relative permeability curves for WI and CWI of decane in water-wet Clashach core.

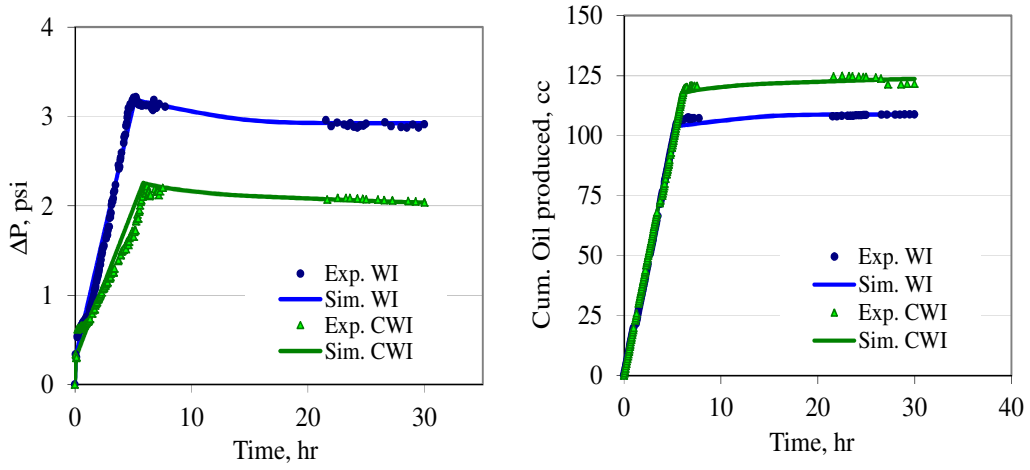

Figure 4.39: Comparison between measured and calculated ΔP across the core (left) and cumulative oil recovery (right) for the secondary CWI, decane, mixed-wet Clashach core at 100.4 °F, 2000 psig.

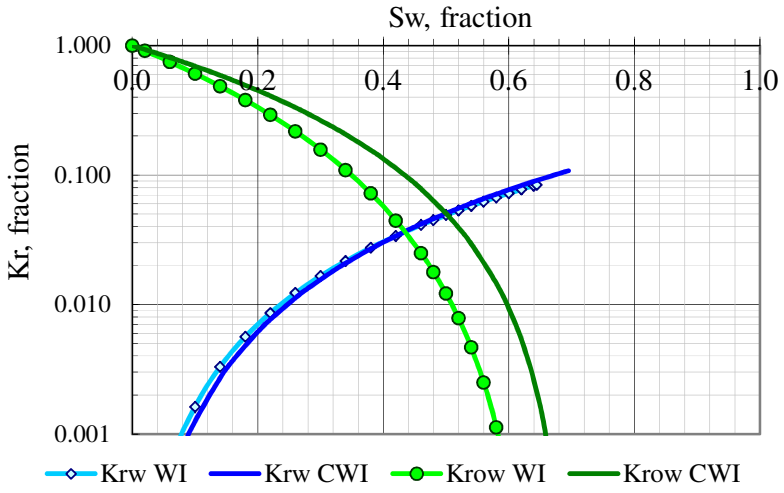

Figure 4.40: The estimated relative permeability curves for WI and CWI of decane in mixed-wet Clashach core.

Summary and conclusions

In this approach, one would need to have the measured carbonated water/oil relative permeability curves of the sample and use black oil simulator to model the CWI process

rather than using the oil/water relative permeability curves in the compositional simulator. Relative permeability curves were estimated from the experimental data by history matching the ΔP and recovery from the plain water and carbonated water displacement tests.

This approach is an easy-to-use method in predicting the performance of the CWI. However, the method is rather limited in application for several reasons. Firstly, it is applicable to model the process within the fluid saturation range involved in the experiments only, in view of the fact that the relative permeability used in the simulation was obtained by matching the experimental data within that saturation range. Nevertheless, the total injection in the core experiments is normally many more PV than the total fluid injection in the field; thus, the range of average saturation in the field can easily be within the saturation range involved in the experiments.

Since relative permeability was used as the history matching parameter, there is nonetheless a question as to which macroscopic flow effect is included in the relative permeability data. The approach might be inappropriate for modelling CWI at a larger scale without a proper up-scaling, be it at the same or different reservoir and flow conditions. This can only be verified if we have the performance data of CWI at the larger scale of interest. The up-scaling of the obtained relative permeability for the use at larger scale is beyond the scope of this thesis.

This approach is also only good to predict the fluid recovery until the breakthrough time, beyond which the oil recovery can be calculated but not the CO_2 gas production, since CWI was modelled as 'plain' waterflood to start with. Although, theoretically, the amount of CO_2 recovery and storage can be roughly estimated based on CO_2 solubility and concentration in both produced and remaining oil and water, no such information was available from a black oil simulation output. For prudent reservoir management especially for an integrated CO_2 EOR and storage project, reliable prediction of CO_2 gas production and retention is essential, therefore making this simulation approach unbefitting.

4.4.2. Todd-Longstaff model

The Todd and Longstaff (TL) model is one of the best known empirical models to represent

the effects of viscous fingering in a miscible displacement using a black oil simulator (Todd-Longstaff, 1972). In the TL model, viscous fingering is represented by the modification of the viscosity and density calculations, without having to reproduce the fine structure of unstable frontal advance or going to the expense and complexity of using a compositional model. The author evaluated this empirical model to simulate the CWI process at the core scale with the mixing parameter, ω, as the 'tuning' parameter representing what is in reality the effect of CO_2 diffusion and dispersion during the process. Coreflood tests of decane in the water-wet core and the stock tank oil in the reservoir core were used as case studies.

The TL model was originally developed for first-contact miscible gas floods, in which the solvent gas and reservoir oil components are miscible in all proportions thus only one hydrocarbon (non-wetting) phase exists in the reservoir. An empirical mixing parameter, ω, between 0 and 1, is used to represent the size of the dispersed zone or degree of fluid mixing within each grid cell. When the hydrocarbon components in each cell are fully mixed, ω equals 1 whereas ω equals 0 when the mixed zone is negligible with respect to the size of the grid cell. In practical applications the ω was normally chosen such that the resulting fluid density and viscosity reflect the effective fluid property averaged over the entire grid block. Details for the empirical model are given in Appendix A4.3. All the method does is basically calculating the effective oil and gas viscosity and density, based on the mixing parameter, ω, and does not attempt to describe the thermodynamic and transport phenomena that determine the details of the local fluid composition and flow characteristics.

The model

The 3-parameters TL model of E100 was used. The same black oil model as used in the relative permeability simulation approach described earlier was again employed, with relevant keywords and data added. Since there was no associated gas in the oil or free gas in the system, the PVT data for the gas was taken to be that of CO_2 but without allowing the CO_2 to be treated as dissolved gas at any pressure. The oil/water relative permeability curves from the corresponding WI coreflood as mentioned before were used while the gas/oil relative permeability curves for the decane case were taken from Chukwudeme and Hamouda (2009).

The carbonated water flood was modelled as simultaneous water and CO_2 gas injection at rates corresponding to the experimental amount of CO_2 that was dissolved to make up the carbonated water at the test pressure and temperature. A total injection rate of 20 cc/hr was used for decane and 1 cc/hr for the stock tank oil. The mixing parameter was initially assumed at 0.67; a value recommended by Todd and Longstaff (1972) for miscible flood performance in a laboratory sand pack, and later sensitized to get a better match of the experimental coreflood results.

Simulation results and discussion

As shown in Figure 4.41, the predicted oil recovery for decane matched the experimental results satisfactorily at ω of 0.4. The mixing parameter only modifies the effective density and viscosity of the oil-gas mixture, thus it has negligible impact on water recovery. As the effluents during this test were collected at the test pressure and temperature, no measured CO_2 gas production data was available for comparison with the simulated values.

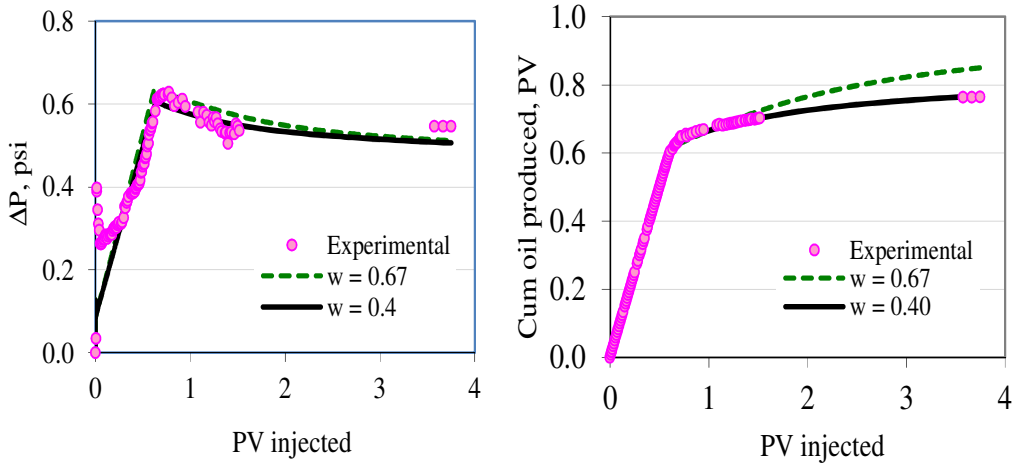

Figure 4.41: The experimental ΔP across the core (left) and oil recovery (right) for secondary CWI, decane, water-wet core and the simulation match by TL model.

For the secondary CWI of the stock tank oil, a relatively fair match was obtained for the ΔP and the oil and gas production at ω = 0.69 and the S_{or} at the maximum water saturation of the

test reduced by 30% of the actual value, Figure 4.42. The oil recovery was underestimated by 15% around the breakthrough time. While the calculated gas recovery was higher than the measured values by up to 30%, the water recovery was predicted adequately, Figure 4.43.

The experimental results and the best simulation match for the tertiary CWI of the same oil were obtained with $\omega = 0.67$, Figures 4.44 and 4.45. The match in the brine recovery was very good and quite reasonable for the cumulative oil produced. However, the match of ΔP especially at the start of CWI and the CO_2 recovery was very poor. The inability of the model to account for the compositional effect of the process could have contributed to the mismatch. Even though there is a solvent option of the TL method in which 4 components (water, oil, solvent and lean gas) can be defined within the reservoir, it is not applicable since the solvent needs to be a second gas phase. Defining the carbonated water as 'solvent gas' will result in no water production, instead huge amount of gas will be produced. This does not realistically represent CWI process.

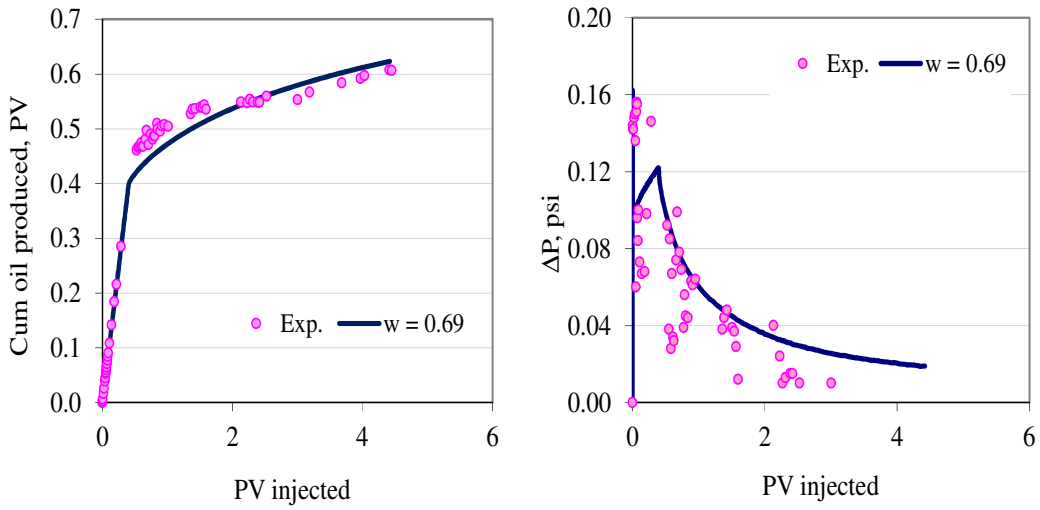

Figure 4.42: The experimental oil recovery (left) and ΔP (right) for secondary CWI in the reservoir core with stock tank crude oil and the simulation match by TL model at $\omega = 0.69$.

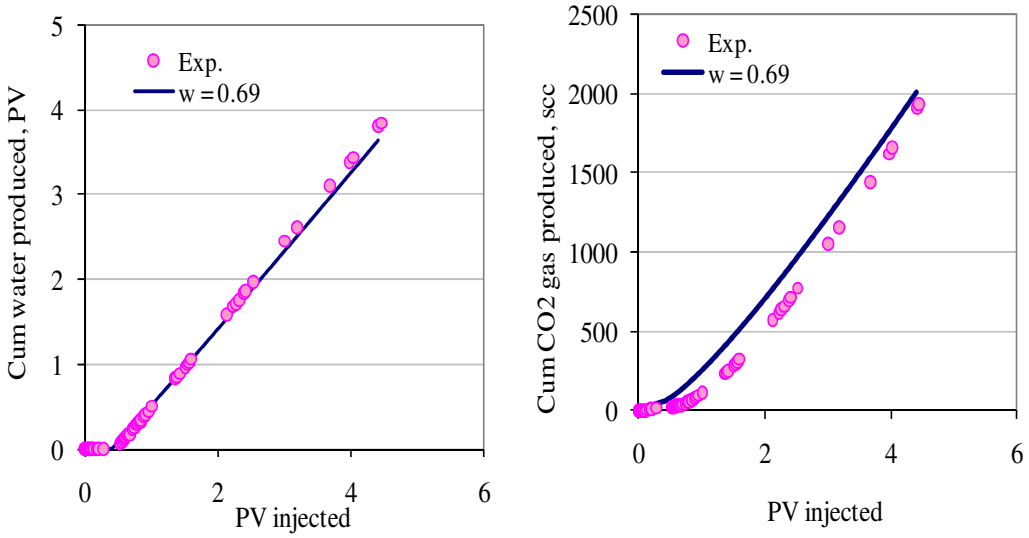

Figure 4.43: The experimental water (left) and CO_2 (right) recovery for secondary CWI in the reservoir core with stock tank crude oil and the simulation match by TL model at ω = 0.69.

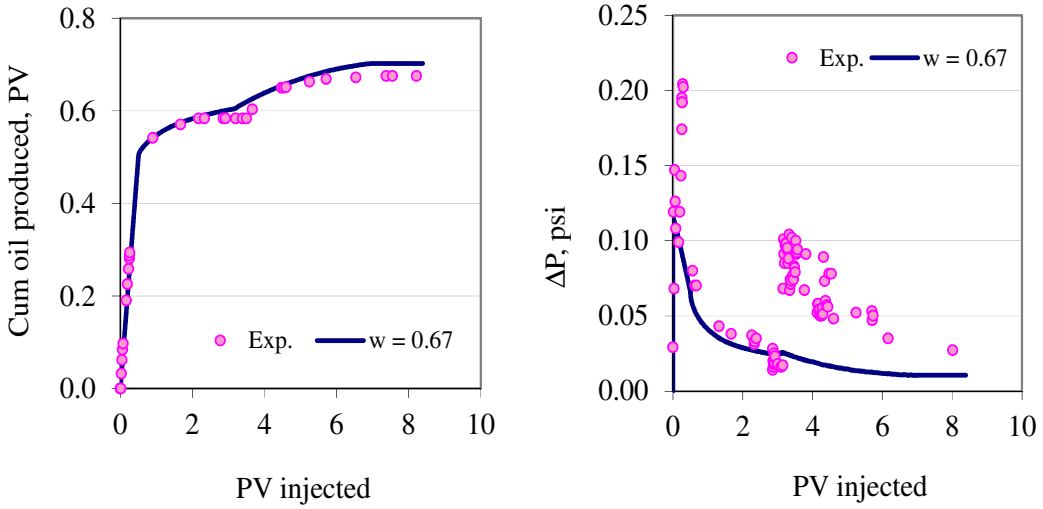

Figure 4.44: The experimental oil recovery (left) and ΔP (right) for tertiary CWI in the reservoir core with stock tank crude oil and the simulation match by TL model at ω = 0.67.

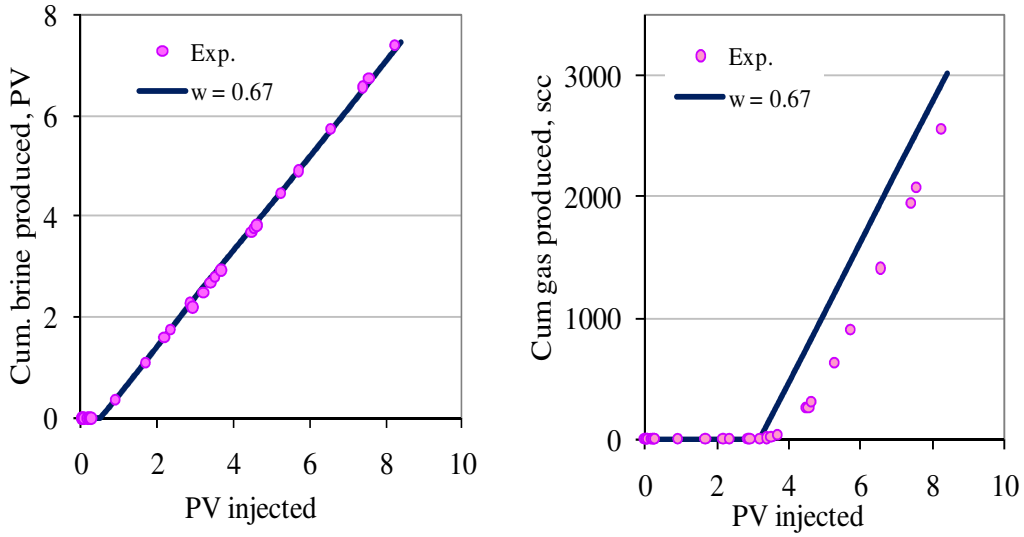

Figure 4.45: The experimental oil (left) and CO_2 (right) recovery for tertiary CWI in the reservoir core with stock tank crude oil and the simulation match by TL model at $\omega = 0.67$.

Summary and conclusions

The simulation results show that it is possible to get a reasonable to good match in the oil recovery, with appropriate tuning of the mixing parameter, ω, for both light and more viscous dead crude oil and for secondary and tertiary recovery modes of the case studies. Similarly to the use of transient coefficients (α-factor) in the compositional model described earlier, the application of TL model is also limited, since each displacement needs to be calibrated. Different ω was required to match the experimental data of different types of oil and recovery methods. It is not known how representative is the core scale ω to the field scale application. Todd and Longstaff (1972) suggested ω of 1/3 for simulating full-scale displacements as opposed to 2/3 (or 0.67) for matching the laboratory sand pack results.

Since the TL approach was developed for a first contact miscible system (i.e., no mass transfer effect), yet the carbonated waterflood of the crude oil was not first contact miscible, the resultant mixing parameter in this case would not only account for the viscous fingering but also the immiscibility of the process. The much higher predicted CO_2 gas production is not surprising since CO_2 was injected as free gas, without its solubility into the water accounted for, which means CO_2 gas and water were not bound in their movement through

the reservoir and flowed independently. Despite the limitation, this simulation approach could be useful as first-order approximation of CWI performance when the use of compositional model is not possible.

The difficulty in defining the carbonated water as a'gas solvent' and the inability to model water production properly renders the extended 4-parameter Todd-Longstaff method or the solvent option inappropriate to be used for simulating the CWI process.

Comparison between the alternative models for secondary CWI and tertiary CWI of decane and the stock tank oil at the core scale is shown in Figures A4.10-A4.14.

4.5. Overall discussion

Simulation studies were performed to investigate whether the available compositional simulators can properly model the CWI process. The features of three commonly used compositional simulators namely E300 (ver. 2007.1), GEM (ver. 2008.1) and STARS (ver. 2008.1) were first compared for their suitability to model the process. It was found that none of the simulators has an explicit keyword to assign carbonated water composition as a single phase in the injection stream. CWI was consequently simulated as co-injection of CO_2 and water at the same location, in proportion corresponding to the experimental CO_2 solubility in the aqueous phase at the test pressure and temperature. This co-injection approach, while it works adequately in a 1D core model, is suspected not amenable for modelling saturated carbonated water injection in a 2D and not also likely in a 3D model, as free CO_2 gas would be evolved out of the solution when there was a slight drop in the local pressure. If this happened, the displacement results would be masked by the effects of direct CO_2 injection. This problem however will not arise if the operating pressure is much higher than the carbonation pressure.

All the three simulators assume instantaneous equilibrium and complete mixing of components and phases in the grid blocks. However, the predicted incremental oil recovery per volume of carbonated water injected was different among the simulators and this was due to the difference in the CO_2 solubility in water, the equilibrium constant (K-values) and

correlations to calculate the fluid viscosities. Better agreement between the simulators' results could have been achieved if these differences were minimized. This comparison reveals that none of the three simulators are better than the other to model the CWI process. Being more widely used in the industry, E300 was subsequently used for the more detailed simulation of CWI at the core scale.

One main finding from the core scale CWI simulation using E300 is that the local equilibrium assumption was not appropriate to model the process as equilibrium was not actually achieved in the core during the displacement. The compositional model over-predicted the incremental oil recovery from CWI for all the tests carried out in this study. The supposition that the commercially available simulator can model CWI at the experimental scale has therefore proven not to be true.

The inaccuracy of the fluid characterization is very unlikely to be the main reason for the mismatch, since over-prediction was also exhibited in the case of decane, which is a single carbon number with established properties. Compelling evidence of CO_2 diffusion and dispersion in the oil recovery by CWI was observed through the experimental front propagation where CO_2 broke through faster than the water. This can only happen if the CO_2 in the injected carbonated water diffused and dispersed into the oil ahead of the front and produced earlier than the CO_2-deprived carbonated water. The lower estimated oil swelling during the displacement based on the equilibrium time, thus lower CO_2 content in the oil, as opposed to the simulator prediction, further corroborates the role of dispersive mixing in the CWI process. The instantaneous equilibrium and complete mixing between oil, gas, and water within each grid block of the simulator, on the other hand, resulted in a faster and higher amount of CO_2 from the carbonated water to be partitioned into the oil. A large viscosity reduction was consequently predicted, that resulted in optimistically higher incremental oil recovery.

The simulation results, however, may at first appear to be counter-intuitive. One may argue that if the carbonated water front was totally deprived of its CO_2 and moved forward as plain water, how then could the predicted oil recovery be higher than the experimental values? One possible reason is that the model predicted the CO_2 from the carbonated water affected the oil behind the front more than that ahead of it. From the predicted oil recovery profiles, for example, in Figure 4.18 and 4.20, we can clearly see that the over-prediction of the

incremental oil recovery from the CWI was after the breakthrough time. In the model, the carbonated water front 'lost' its CO_2 immediately to the oil upon contact and moves forward as plain water. The oil recovery up to breakthrough was thus purely due to displacement. Meanwhile, the oil behind the front dissolved more and more CO_2 from the injected carbonated water as the flooding continued. The amount of CO_2 dissolved in the oil at any given time was much higher than actual, due to the instantaneous equilibrium and complete mixing assumption of the model, resulting in higher production of the oil behind the front.

The three simulators evaluated can model molecular diffusion of CO_2 within the oil and gas phase but none can account for the CO_2 diffusion from the carbonated water to the oil phase (cross-phase diffusion), which the author believes is more influential to the recovery process along with the dispersive mixing.

The author has shown that the use of an adjustable transient coefficient or the α-factor in the compositional model, an approach developed by Barker and Fayers (1994) to model sub-grid block phenomena in coarse, homogeneous grid block compositional simulations, can be used to predict the experimental CWI results with reasonable accuracy especially for the secondary process. The simulation results show that the coreflood displacements can adequately be matched by adjusting this coefficient. This simulation approach incorporates the compositional effects, CO_2 solubility in the aqueous phase and lends itself to simulating the CWI process at a larger scale. It was nevertheless found to be less effective for simulating the tertiary process in this study and more investigations are recommended. If the use of compositional model is not possible, an alternative simulation method using the Todd and Longstaff model in black oil simulator could estimate the oil recovery from CWI by adjusting the mixing parameter, even though calculated gas production might be unreliable.

Despite its significance in CO_2 injection at the core scale, there are however, debates on the effect of the molecular diffusion and dispersion at the field scale. Any fluid injections at the field scales are subject to large scale oil by-passing resulting from channelling, gravity segregation and reservoir heterogeneity. Molecular diffusion perpendicular to the direction of flow could sharpen the flood front i.e. reduce the by-passing. But it is difficult to ascertain that diffusion is a significant mechanism over the by-passing effects, as it is difficult to know the actual length scales of the by-passing at the field scale. Grogan and Pinczewski (1987) estimated that the contact times required for CO_2 in the tertiary floods to contact and swell

the oil over metres of diffusion-path lengths was of the order of 8-80 years. For the typical field life of 20-50 years, diffusion of this scale may have significant impact, yet there is considerable uncertainty about typical lengths over which diffusion must operate in the field scale displacements. In their studies, Warner (1977) and Todd et al. (1982) deduced that it is quite unlikely that molecular diffusion will be significant in reducing the adverse effects of large-scale bypassing in the field. Muller and Lake (1991), in their numerical modelling of the water blocking effect in miscible flooding also concluded that water blocking (which is related to diffusion of CO_2 through the water barrier) apparently has no significant impact on recovery at the field scale.

There might be other factors contributing to the mismatch between the measured and calculated CWI performance, other than the dispersive mixing, such as the use of inappropriate relative permeability curves and the change in rock wettability or interfacial tension, all of which if present, were not accounted for in the model used. For example, in the case of decane in the mixed-wet core, in Figure 4.19, the additional oil recovery took place at breakthrough, whilst in the water-wet core the additional oil recovery took place gradually, after the breakthrough. The difference in the differential pressure of WI and CWI was also much larger in the mixed-wet core. The predicted incremental oil recovery values from CWI by the simulators for the water-wet and mixed-wet core were, however, very close to each other, despite each model using the respective oil/water relative permeability curves. This suggests that the simulator mainly accounts for the compositional effects only, which was the same in both cases, but not that of the rock wettability. Having different ΔP and breakthrough time, the use of the same oil/water relative permeability curves for both WI and CWI for the mixed-wet core proved to be inappropriate. The relative permeability approach seems to be adequate to model the oil recovery but unable to predict the gas production. Further research is required to obtain more experimental data of CWI in mixed-wet cores and subsequently find the appropriate approach to model the process in these cores.

4.6. Summary and conclusions

From the simulation studies presented in this chapter, it can be concluded that:

4.6.1. Evaluation of compositional simulators

- None of the evaluated simulators has an explicit keyword to assign a single phase carbonated water composition in the injection stream at the surface. Thus CWI was simulated by co-injecting CO_2 and water at the same location in proportion corresponding to the CO_2 solubility in water at the test conditions.
- For the 2D model used, a slightly under-saturated carbonated water was necessary to sustain single phase CWI.
- All the three compositional simulators assume instantaneous equilibrium and complete mixing between phases, such that the fugacities of CO_2 in the oil and aqueous phase are bounded by its individual solubility in these two phases.
- For a given ratio of cumulative CO_2 injected to total water injected (FGIT/FWIT), E300 predicted the highest incremental oil recovery of 14.5 %STOOIP while STARS predicted the lowest incremental recovery of 9.2% STOOIP.
- CO_2 solubility in water by the Chang et al. correlation in E300 is lower than that by Henry's Law in CMG and STARS. At 2000 psig, 100.4^{o}F, the former estimated 12% lower CO_2 solubility than the latter.
- The difference in the incremental oil recovery is mostly due to the difference in viscosity calculation and the solubility of CO_2 in both oil and water phases, which in turn is due to the difference in assigning the K-values in those simulators. It is believed that if all these factors are made the same, the incremental oil recovery would be more or less the same too.
- A high amount of CO_2 was dissolved from the carbonated water into the oil as CWI continues. A large viscosity reduction and consequently high incremental oil recovery was predicted by the simulators.
- None of the three simulators is better suited to model CWI than the others.

4.6.2. Coreflood simulations

- The local equilibrium was not achieved during the CWI in the core, thus rendering the simulators with the instantaneous equilibrium assumption inappropriate for modelling CWI process at the scale studied. The supposition that the commercially

available simulator can model CWI at the experimental scale has therefore proven not to be true.

- At the core scale investigated, the compositional simulator over-predicted the oil recovery for both secondary and tertiary CWI.
- The simulator does not simulate the partition of CO_2 between water and oil realistically. The model predicted that the CO_2 in the carbonated water front partitioned very quickly into the oil behind the front and that the displacement front was totally deprived of CO_2 after travelling a certain distance through the core. Conversely, in the experiment, CO_2 was produced earlier than water signifying the dispersive mixing (diffusion and dispersion) of CO_2 into the oil at the displacement front.
- The dispersive mixing effect was adequately modelled by the transport coefficient (α-factor) in the compositional model for the secondary CWI process but less effective for the tertiary CWI process.
- The Todd-Longstaff model with mixing parameter as tuning parameter can give first-order approximation of CWI performance at the core scale without the use of a compositional model.
- For the mixed-wet core, the oil/water relative permeability curves from the WI coreflood were demonstrated to be inappropriate for the CWI due to the different oil recovery and ΔP trends of both processes.
- Further study is recommended on the effects of wettability and the IFT changes during CWI and the appropriate way to model CWI particularly in mixed-wet cores.

4.7. References

[4.1] Barker, J.W. and Fayers, F.J.: Transport Coefficients for Compositional Simulation with Coarse Grids in Heterogeneous Media, SPE 22591, SPE Advanced Technology Series, Vol.2, No. 2, 103-112, 1994.

[4.2] Bijeljic, B.R., Muggeridge, A.H., and Blunt, M.J.: Effect of Composition on Waterblocking for Multicomponent Gas Floods, SPE 77697, SPE Annual Technical Conference and Exhibition, San Antonio, Texas, 29 Sep.-2 Oct. 2002.

[4.3] Campbell B.T. and Orr, Jr F.M.: Flow Visualization for CO_2/Crude-Oil Displacements, SPE 11958, SPE Journal, Vol. 25, No. 5, 665-678, October 1985.

[4.4] Chang, Y. B., Coats, B.K. and Nolen, J.S.: A Compositional Model for CO_2 Floods Including CO_2 Solubility in Water, SPE 33164, SPE Reservoir Evaluation & Engineering, Vol. 1, No. 2, 133-160, 1998.

[4.5] Chatzis, I., Morrow, N.R. and Lim, H.T.: Magnitude and Detailed Structure of Residual Oil Saturation, SPE 10681, SPE Journal, 23 (2), 311-326, April 1983.

[4.6] Chukwudeme, E.A. and Hamouda, A.A.: Enhanced Oil Recovery (EOR) by Miscible CO_2 and Water Flooding of Asphaltenic and Non-Asphaltenic Oils, Energies, 2, 714-737, 2009.

[4.7] CMG GEM User Manual, 2008.

[4.8] CMG STARS User Guide, 2008.

[4.9] CMG WinProp User Guide 2008.

[4.10] Cullick, A.S. and Mathis, M. L.: Densities and Viscosities of Mixtures of Carbon Dioxide and n-decane from 310 to 403 K and 7 to 30 MPa, J. Chem. Eng. Data, 29(4), 393-396, 1984.

[4.11] ECLIPSE 2007.1 Simulation Software Manual, Schlumberger.

[4.12] Fussell, L.T. and Fussell, D.D.: An Iterative Technique for Compositional Reservoir Models, SPE 6891, SPE Journal, Vol. 19, No. 4, 211-220, 1979.

[4.13] Gardner, J.W. and Ypma, J.G.J.: An Investigation of Phase Behaviour-Macroscopic Bypassing Interaction in CO_2 Flooding, SPE Journal, Vol. 24, No. 5, 508-520, 1984.

[4.14] Grogan A.T. and Pinczewski W.V.: The Role of Molecular Diffusion Processes in Tertiary CO_2 Flooding, SPE 12706, Journal of Petroleum Technology, Vol. 39, No. 5, 591-602, May 1987.

[4.15] Harvey, A.H.: Semi-empirical Correlation for Henry's Constants over Large Temperature Ranges, AIChE J, Vol. 42, No. 5, 1491-1494, May 1996.

[4.16] Katz, D.L. and Firoozabadi, A.: Predicting Phase Behaviour of Condensate/ Crude Oil Systems Using Methane Interaction Coefficients, Journal of Petroleum Technology, 1649-55, November 1978.

[4.17] Kechut N.I., Riazi, M., Sohrabi, M. and Jamiolahmady, M.: Tertiary Oil Recovery and CO_2 Sequestration by Carbonated Water Injection (CWI), SPE 139667, SPE International Conference on CO_2 Capture, Storage, and Utilization, New Orleans, Louisiana, USA, 10–12 November 2010.

[4.18] Lemmon E.W., McLinden M.O. and Friend D.G.: Thermophysical Properties of Fluid Systems in NIST Chemistry Webbook, NIST Standard Reference Database No. 69, Eds. P.J. Linstrom and W.G Mallard, June 2005, National Institute of Standards and Technology (http://webbook.nist.gov).

[4.19] Li, Y.K. and Nghiem, L.X.: Phase Equilibria of Oil, Gas and Water/Brine Mixtures for a Cubic Equation of State and Henry's Law, Can. J. Chem. Eng., Vol. 64, 486-496, 1986.

[4.20] Lohrenz, J., Bray, B.G. and Clark, C.R.: Calculating Viscosity of Reservoir Fluids from their Composition, Journal of Petroleum Technology, 1171, 1964.

[4.21] McManamey, W.J. and Woolen, J.M.: The Diffusivity of Carbon Dioxide in Organic Liquids at 25 ^{o}C and 50 ^{o}C, AIChE J. 19, 3, 667-69, May 1973.

[4.22] Muller T. and Lake L.W.: Theoretical Study of Water Blocking in Miscible Flooding, SPE 20206, SPE Reservoir Engineering, Vol. 6, No. 4, 445-451, 1991.

[4.23] Nghiem L.X., Sammon, P., Grabenstetter, J. and Ohkuma, H.: Modelling CO_2 Storage in Aquifers with a Fully-Coupled Geochemical EOS Compositional Simulator, SPE/DOE Symposium on Improved Oil Recovery, Tulsa, Oklahoma, 17-21 April 2004.

[4.24] Perkins, T.K. and Johnston, O.C.: A Review of Diffusion and Dispersion in Porous Media, SPEJ, 70-80, March 1963.

[4.25] Pollack, N.R., Enick R.M., Mangone D.J. and Morsi B.I.: Effect of an Aqueous Phase on CO_2/Tetradecane and CO_2/Maljamar-Crude-Oil Systems, SPE 15400,

SPE Reservoir Engineering, Vol. 3, No. 2, 533-541, 1988.

[4.26] Riazi, M., Sohrabi, M., Jamiolahmady, M.: Experimental Study of Pore-Scale Mechanisms of Carbonated Water Injection (CWI), Journal of Transport in Porous Media, DOI 10.100.47/s11242-010-9606-8.

[4.27] Riazi, M., Sohrabi, M., Jamiolahmady, M., Ireland, S. and Brown, C.: Oil Recovery Improvement Using CO_2-Enriched Water Injection, SPE 121170, Proceedings of the 2009 SPE EUROPEC/EAGE Annual Conference and Exhibition, Amsterdam, The Netherlands, 8-11 June 2009.

[4.28] Sendra 2007 User Guide, Petec Software & Services.

[4.29] Shelton, J.L. and Schneider, F.N.: The Effects of Water Injection on Miscible Methods Using Hydrocarbons and Carbon Flooding Dioxide, SPE 4580, SPE Journal, Vol. 15, No. 3, 217-226, 1978.

[4.30] Shen, P., Zhu, B., Li, X.B. and Wu, Y.S.: The Influence of Interfacial Tension on Water/Oil Two-Phase Relative Permeability, SPE 95405, SPE/DOE Symposium on Improved Oil Recovery, Tulsa, Oklahoma, USA, 22-26 April 2006.

[4.31] Standing, M.B.: Notes on Relative Permeability Relationships, Division of Petroleum Engineering and Applied Geophysics, The Norweigan Institute of Technology, The University of Trondheim, August 1974.

[4.32] Stern, D.: Mechanisms of Miscible Oil Recovery: Effects of Pore-Level Fluid Distribution, SPE 22652, SPE Annual Technical Conference and Exhibition, Dallas, Texas, 1991.

[4.33] Tiffin, D.L. and Yellig, W.F.: Effects of Mobile Water on Multiple-Contact Miscible Gas Displacements, SPE 10687, SPE Journal, Vol. 23, No. 3, 447-55, 1983.

[4.34] Timmerman, E.H.: Practical Reservoir Engineering, Vol. 2, PennWell Books, 1982.

[4.35] Todd, M.R. and Longstaff, W.J.: The Development, Testing and Application of a Numerical Simulator for Predicting Miscible Flood Performance, SPE 3484, Journal

of Petroleum Technology, July 1972.

[4.36] Todd, M.R., Cobb, W.M. and McCarter, E.D.: CO_2 Flood Performance Evaluation for the Cornell Unit, Wasson San Andres Field, SPE 10292, Journal of Petroleum Technology, Vol. 34, No. 10, 2271-2282, October 1982.

[4.37] Warner H.R Jr.: An Evaluation of Miscible CO_2 Flooding in Waterflooded Sandstone Reservoirs, SPE 6117, Journal of Petroleum Technology, Vol. 29, No. 10, 1339-1347, October 1977.

[4.38] Whitson, C.H.: Characterizing Hydrocarbon Plus Fraction, SPE Journal, 683-694, 1982.

Chapter 5

Numerical Simulation of Various CO_2 Injection Strategies for Coupled EOR and Storage

5.1. Introduction

Generally, the CO_2 EOR process aims to sweep the oil to the producing wells by channelling CO_2 gas into previously by-passed areas. In conventional CO_2 EOR projects, the purchase of CO_2 gas is one of the highest operating costs (Jarrell et al., 2002) therefore, the project design always aims for this cost to be reduced by maximising the oil recovery with the minimum possible injection of CO_2. On the contrary, in the CO_2 storage projects, the objective is to safely store as much CO_2 as possible in the reservoir. In coupled EOR and storage process, both oil recovery and CO_2 storage are to be maximized economically. The significantly different objectives for storing CO_2 with EOR inevitably call for different engineering design from CO_2 EOR or CO_2 storage process alone.

In the previous two chapters, the potential of the water-based CO_2 EOR method in enhancing oil recovery and storing CO_2 has been discussed. This chapter deals with the storage of CO_2 in depleting oil reservoirs through gas-based CO_2 injection techniques, which include the conventional WAG, SSWAG, TAPWAG and HWAG injections, descriptions of which are given next. The continuous CO_2 flooding (CO2I) and plain water injection (WI) serve as the limiting case of zero and infinite WAG ratio, respectively. The author also looked at a possibility of applying a new injection strategy for the said purpose. The technical evaluation of several CO_2 injection strategies through numerical simulations is presented. The motivation for this work is to find a CO_2 injection scheme that can simultaneously

increase oil recovery and the amount of CO_2 stored in the reservoir.

5.1.1. CO_2 injection schemes

Continuous CO_2 gas injection (CO2I)

In this injection scheme, CO_2 gas is compressed to the required pressure before it is continuously injected into the reservoir, until about 20-40% HCPV (hydrocarbon pore volume) has been injected, followed by chase water or lean gas to drive the solvent bank through the reservoir. CO_2 gas has better local displacement efficiency than water, especially in miscible flooding and it benefits from early production response, better injectivity and minimum water blocking. Successful CO_2 flooding could increase the ultimate oil recovery by 8 to 14% OOIP (Hadlow, 1992).

However, high mobility of CO_2 as compared to the displaced oil (i.e., high mobility ratio) gives rise to severe gravity-tonguing and viscous fingering (Perkins et al., 1965; Juanes and Blunt, 2007). The injected CO_2 bypasses much of the oil in the reservoir leading to poor sweeps efficiency that is further exacerbated by reservoir heterogeneity and density differences between gas, oil and water.

Several CO_2 injection strategies have been proposed and applied in the field to improve the sweep efficiency, such as CO_2 slug followed by water, water alternating CO_2 gas injection (WAG), simultaneous WAG (SWAG) injection, carbonated water injection (CWI) and soak-alternating-water injection. Water is used to reduce the overall mobility of the displacing fluid thus increase sweep efficiency.

Water-Alternating-Gas injection (WAG)

Water-alternating-gas (WAG) injection was initially designed to overcome the problem of high CO_2 mobility that greatly reduces the effectiveness of CO_2 flooding (Christensen et al., 2001). In WAG injection, gas and water are injected sequentially through the same well at pre-determined size of gas and water slugs. Typical slug size is from about 1 to 30 or 40%

HCPV (Chen et al., 1984; Sanchez, 1999) with a WAG ratio typically range from 1:4 to 5:1.

The CO_2 gas trapped by the alternating water reduces the CO_2 mobility and helps to stabilize the displacement front, thus yielding greater volumetric conformance and improved sweep efficiency (Champion and Shelden, 1989). The combination of the high microscopic displacement efficiency of the oil during the gas cycle and the better volumetric sweep efficiency of water during the water cycle increase the oil production over a plain waterflood or gasflood alone. As compared with CO2I, WAG requires a smaller volume of CO_2. Successful WAG applications have been reported to produce an additional 5 to 10% OOIP oil recovery (Christensen et al., 2001).

In addition to the factors affecting the continuous CO_2 flooding, WAG injection was also reported to be influenced by hysteresis, three-phase relative permeability effects, that lead to reduced gas injectivity (Rogers and Grigg, 2000; Awan, 2008), half-cycle-slug size i.e., the amount of non-condensable gas injected prior to switching to water, total solvent slug size, WAG ratio (Attanucci et al., 1993; Surguchev et al., 1992; Christensen et al., 2001) and factors affecting gravity segregation such as fluid density and viscosities. Away from the injection wells, gravity segregation could lead to a large bypassed zone attributed to gas over-ride and water under-ride (Blackwell, 1960). As compared with CO2I, WAG takes longer time to inject the required volume of CO_2 and has a tendency to suffer from the water-shielding effect by high water saturations. The presence of mobile water has been reported to cause reduced displacement efficiency in pore and core-scale tertiary flooding due to oil trapping, where the oil is blocked from the injected solvent gas by the water layer (Shelton and Schneider, 1978; Stalkup, 1983; Tiffin and Yellig, 1983)

In order to further improve the WAG performance technically and economically, several variants of WAG injection have been applied, such as simultaneous WAG (SWAG), Hybrid-WAG (HYWAG), tapered WAG (TAPWAG), and cyclic WAG.

Simultaneous WAG (SWAG) injection

In simultaneous WAG (SWAG) injection, water and gas slugs are injected simultaneously. Using the same mechanisms as WAG, SWAG offers the additional advantage of reducing

the capillary entrapment of oil, thus providing better mobility control of the gas (van Lingen, 1996). Laboratory models showed that the sweep efficiency of SWAG injection could be as high as 90% compared with 60% for gas alone (Caudle and Dyes, 1958). The injection fluids can be injected at the same perforation intervals or at selective perforations such that the water slug is injected up-dip while the gas is injected down-dip. Laboratory and simulation studies (Ma et al., 1995; van Lingen et al., 1996), reported that SWAG with selective injection intervals (referred to as SSWAG hereafter) performs much better than SWAG with gas and water injected at the same perforation layers. Due to gravity, water will flow downwards, impeding the vertical upward flow of the gas. The CO_2 conformance is improved and results in more steady gas production. For these reasons, only SSWAG injection was evaluated in this study.

SWAG injection has been implemented in the Siri Field in the North Sea (Quale, 2000) and the Joffre Viking field (Stephenson et al., 1993). Water and gas are simultaneously injected in waterflood lines. This reduces the capital and operating costs since there is no need for separate water and gas injection and lines to the injection sites and gas distribution systems (Ma et al., 1995).

Hybrid WAG (HWAG) injection

Hybrid WAG injection combines the best features of WAG and CO2I injection in which a large slug of gas is injected followed by small slugs of water and gas. It benefits from the faster oil response associated with continuous gas injection and the higher ultimate oil recovery and more efficient CO_2 utilization characteristic of the WAG process (Hadlow, 1992). This process was patented by UNOCAL where a 9% pore volume (PV) of CO_2 was injected followed by the remaining 21% at 1:1 WAG ratio (Huang and Holm, 1986).

Tapered WAG (TAPWAG) injection

In the tapered WAG process, the WAG ratio is increased step-wise at predetermined solvent bank sizes (Hadlow, 1992), so that more water and less CO_2 are injected during any

complete WAG cycle. The objective is mainly to reduce the gas injection and gas production and therefore improve the overall economics of the process. This process was implemented, for example, in the Rangely Unit where the WAG ratio was increased from 1:1, until 30% HCPV of CO_2 had been injected, then increased to 2:1 until 40% of HCPV of CO_2 was injected (Attannuci, 1993).

The comparison of the benefits between these injection methods from the EOR perspective, based on experimental studies and field applications, is shown in Table 5.1.

Table 5.1: Comparison of benefits of different CO_2 injection schemes.

Injection scheme	Description	Advantages
Continuous CO_2 (CO2I)	CO_2 is injected continuously as gas or supercritical phase.	Early production response, better injectivity and minimum water blocking.
Water Alternating Gas (WAG)	CO_2 gas and water are injected sequentially through the same well at pre-determined size of gas and water slugs.	Controlled CO_2 gas mobility thus improved sweep efficiency, more efficient CO_2 utilization.
Simultaneous WAG (SWAG)	Water and CO_2 gas slugs are injected simultaneously at the same perforation intervals.	More efficient CO_2 utilization, reducing the capillary entrapment of oil, thus providing better mobility control of the gas.
Selective SWAG (SSWAG)	Water slug is injected at the bottom perforation intervals while the gas is injected at the top perforation intervals.	As for SWAG plus improved CO_2 conformance and more steady gas production.
Tapered WAG (TAPWAG)	WAG ratio is increased step-wise at predetermined solvent bank sizes.	Reduced costs since less gas injection and production.
Hybrid WAG (HWAG)	Large slug of gas is injected followed by small slugs of water and gas.	Early production response, higher ultimate oil recovery and more efficient CO_2 utilization.

5.1.2. Previous related studies

The field experience in storing CO_2 through EOR is still very limited. However, the scores of mature CO_2 EOR projects worldwide can provide information in terms of trapped CO_2 and benchmarks for incremental oil recovery versus pore volume of CO_2 injected from using this method.

A few simulation studies have reported the use of several CO_2 injection schemes for coupled CO_2 EOR and storage in the oil fields. Kovscek and Cakici (2005) carried out sensitivity studies on several CO_2 injection scenarios and used equal-weighted objective functions of oil recovery and reservoir utilization factor as co-optimization parameters. For maximizing the oil recovery and CO_2 stored, they recommended miscible solvent gas (CO_2 with C2 to C4) injection, which at an appropriate later time switched to CO_2 injection and combined with control of produced GOR to prevent excessive gas re-cycling. They also suggested WAG with a small slug size for a period of time, before ending the process with a large CO_2 slug for increased CO_2 storage without affecting the oil recovery.

Other relevant studies are mainly focused on optimizing the design parameters of certain CO_2 injection schemes. Using reservoir simulation, Malik and Islam (2000) evaluated the use of horizontal wells to increase oil recovery and CO_2 storage in the reservoir through straight CO_2 gas injection in the Weyburn field. Ravagnani et al. (2007) assessed the technical and economic feasibility of continuous CO_2 gas injection under the Brazilian fiscal regime for EOR and sequestration using dynamic system or life-cycle approach. They took into account the project cash flow, the emissions and energy used in the process. Murray et al. (2001) studied the soak-alternating-gas (SAG) injection method whilst Qi et al. (2008) reported the sensitivity of WAG ratio to maximize CO_2 storage through the SWAG process. Simulation studies by Ghomian et al. (2008) and Forooghi et al. (2009) focus on optimizing the WAG design parameters for the integrated processes, using response surface and experimental design methodology.

In this thesis, the evaluation was extended to not only the conventional WAG process but also on other four commonly used CO_2 injection schemes as described earlier. Unlike the study by Kovscek and Cakici (2005) who considered only the oil recovery and the amount of CO_2 stored, this study took into account some main economic factors as well.

5.2. Overall approach

CO_2 injection into an oil reservoir is a complex process that depends on geologic, reservoir and operational factors. Therefore, designing, analyzing and mitigating the risk of the integrated CO_2 EOR and storage processes requires a thorough understanding of the importance of these factors to the performance of the processes, which calls for a systematic investigation.

The scope of the evaluation would be prohibitively wide if all CO_2 injection schemes, reservoir parameters and operational factors are to be studied simultaneously. Thus, in this study a practical approach shown in Figure 5.1 was developed and followed. In the first part, the oil recovery and CO_2 storage from several injection strategies suited for CO_2-flood EOR were evaluated and ranked to find the best strategy; results of which are presented in this chapter.

Then in the second part, parametric simulation was carried out to identify the influential factors on the oil recovery and CO_2 stored under the best injection strategy for coupled EOR and storage identified in the first part. These influential flood design parameters were then optimized to give maximum profit of the oil recovery and CO_2 storage. Design of Experiment (DOE) and the associated technique of Response Surface Model (RSM) were employed as the tools to make effective use of reservoir simulation for the sensitivity and optimization studies. Details of the parametric simulation and flood design optimization are given in Chapter 6.

The evaluation discussed in this chapter involved predicting the performances of several CO_2 injection strategies using a compositional reservoir simulator based on a set of assumed reservoir and operating parameters. The use of a compositional reservoir simulator is essential as it can better model two important aspects of oil recovery and storage, namely the compositional effects of CO_2-oil displacement and CO_2 solubility in the water phase. The geochemical effects on the rock minerals when CO_2 dissolves in water were, however not accounted for.

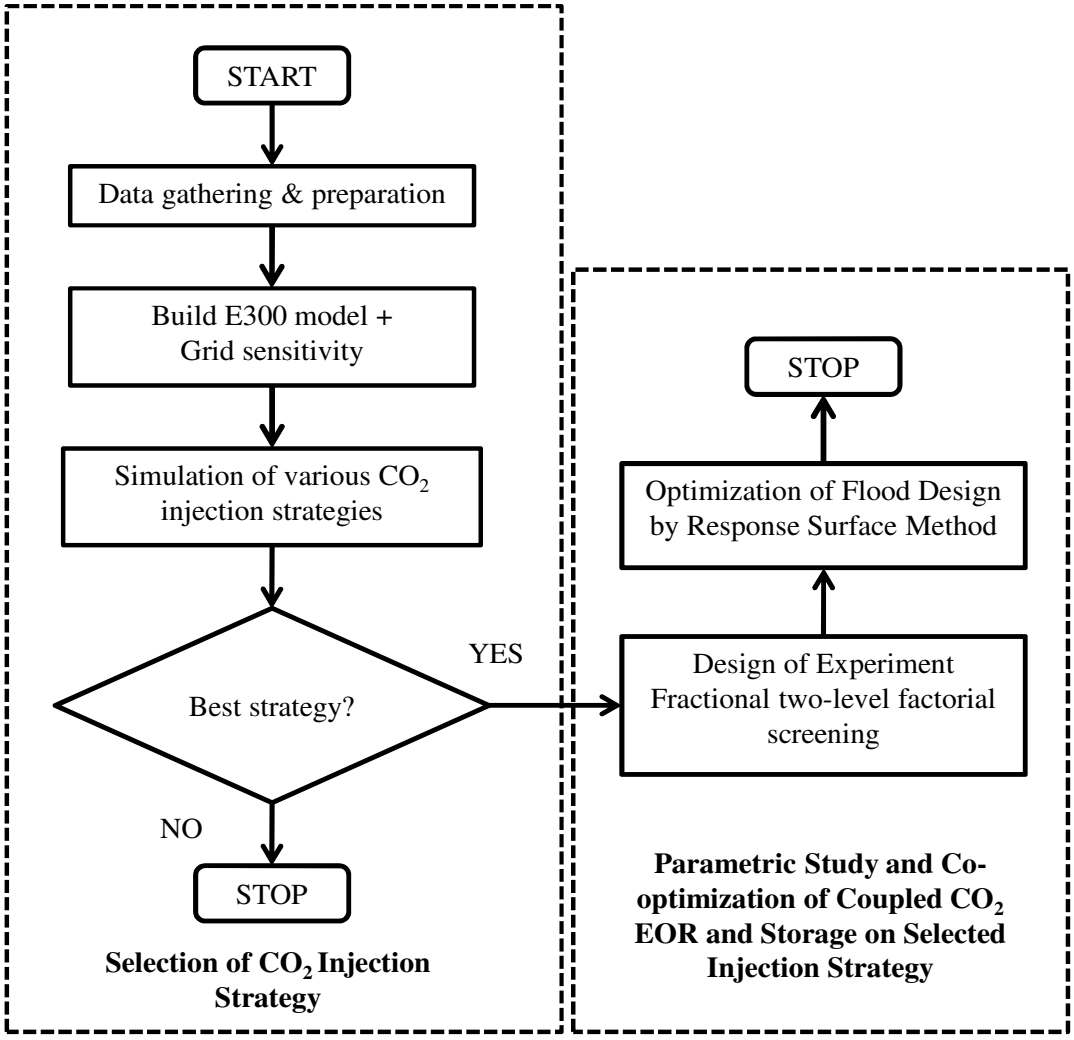

Figure 5.1: The overall approach in investigating the CO_2 injection strategies, parametric simulation study and co-optimization of the coupled CO_2 EOR and storage process.

In addition to CO2I, WI, WAG, SSWAG, TAPWAG and HWAG injection, a new injection scheme, named intermittent WAG or INTWAG, was also assessed. Conceptually, INTWAG injection involves alternating a CO_2 slug and water injection similar to that used in the WAG injection. However, apart from alternating the injected phases, the injection also alternates between locations. This injection method was examined to gauge the benefit of CO_2 diffusion to the oil recovery and CO_2 storage by shutting in some wells for certain period of time before switching to the other phase and also the benefit of the drainage-imbibition processes that occur as a result.

Due to the uncertainty in appropriately modelling the CWI process at the reservoir scale, as discussed in Chapter 4, CWI was not incorporated in this evaluation. Furthermore, as a water-based CO_2 EOR technique, the performance of CWI would be more appropriately compared to that of WI than that of the gas-based techniques.

It is more likely that the CO_2 injection for EOR and storage will be implemented as tertiary rather than a secondary recovery method, especially in the current economic situation with oil values higher than the CO_2 sequestration credits. 75% of the total CO_2 miscible projects in the US are in the tertiary flooding mode (Oil & Gas Journal, 2010). Nevertheless, according to the same reference, 18% of CO_2 miscible projects worldwide are in the secondary recovery phase. In this study, CO_2 injections were examined as both secondary and tertiary recovery methods and each for immiscible and miscible displacements (Figure 5.2).

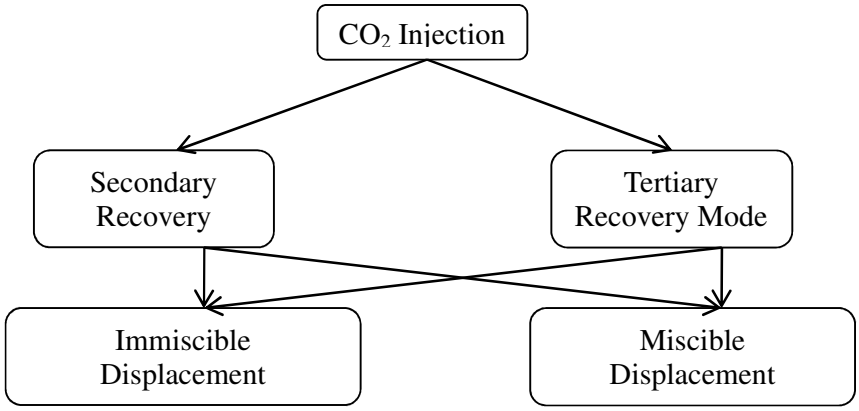

Figure 5.2: Recovery methods and production well controls evaluated.

The miscible and immiscible conditions were attained by the way the injection and production was controlled, which will be described later. CO_2 injection for pressure maintenance, which would typically be applied to oil reservoir gas caps (Holtz, 2009) is not considered in this study since it is assumed that in the interest of CO_2 storage one would want to inject as much CO_2 as possible, up to the maximum safe BHP.

The oil recovery and CO_2 stored from each of the injection strategies were then compared and ranked. Two approaches in ranking the processes were used; one was solely based on

technical criteria while the other incorporated the economic criteria as well. Previous researchers have used oil recovery (Kovscek and Cakici, 2005; Trivedi and Babadagli, 2005) and incremental oil recovery (Kulkarni et al., 2004; Forooghi et al., 2010) in ranking the performance of the injection schemes for EOR. For ranking the CO_2 storage, the amount of CO_2 stored in fraction of reservoir pore volume (Kovscek and Cakici, 2005) as well as CO_2 saturation in the model (Ghomian et al., 2008; Forooghi et al., 2010) have been applied.

In this study, for ranking based on technical criteria only, the approach by Kovscek and Cakici (2005) using weighted oil recovery factor, R, and a CO_2 storage factor, S, shown in Equation 5.1, was used.

$$f = w_1 \frac{N_p^*}{STOOIP} + w_2 \frac{V_{CO2}^R}{PV} \tag{5.1}$$

where

$$R = \frac{N_p^*}{STOOIP} \times 100 \tag{5.2}$$

$$S = \frac{V_{CO2}^R}{PV} \times 100 \tag{5.3}$$

w_1 ($0 \leq w_1 \leq 1$) and w_2 ($=1-w_1$) are weights, STOOIP is the original stock tank oil in place, V_{CO2}^R is the volume of CO_2 stored in the reservoir, and PV is the pore volume of the reservoir. R is the incremental oil recovery factor due to the CO_2 injection i.e. the amount of oil recovered during the CO_2 injection phase only but. N_p*, which is described in Equation 5.4, is the net production of oil during the CO_2 injection phase only, discounted by the amount of energy, E, needed to compress the produced gas to injection pressure for reinjection, Equation 5.5.

$$N_p^* = N_p - E \tag{5.4}$$

$$E = \frac{3.1815x10^{-7}}{\gamma} P_{in} Q_{in} \left[\left(\frac{P_{out}}{P_{in}} \right)^{\gamma} - 1 \right] t \tag{5.5}$$

where γ is the pump compression factor for CO_2, which equals 0.23, P is pressure (lbf/ft^2), Q is flow rate (ft^3/min) and the subscripts *in* and *out* refer to the low and high pressure sides of the compressor (Douglas, 1988). E has the unit of barrels of oil and *t* is time in days. For the tertiary CO_2 injection process R represents the oil recovery after the waterflooding duration, that is, $N_p = N_{pt}-N_{pw}$ where N_{pt} is the total cumulative oil produced and N_{pw} is the cumulative oil produced during waterflooding period. It was assumed in this simulation study that 95% of produced CO_2 was recycled. The gas enters the compressor at 250 psi and leaves the compressor at the average reservoir pressure at the time of injection. A sensitivity study on the inlet pressure between 100 to 400 psi indicates that the inlet pressure does not affect the ranking of the injection schemes.

The main economic incentive for any CO_2 EOR project is always the profit per barrel of oil (Hustad et al., 2004). When economic factors were considered, the net present value (NPV) per barrel of oil produced and CO_2 stored were therefore used as the objective functions in ranking the CO_2 injection schemes evaluated. This study also assumes equal importance of oil recovery and CO_2 storage in ranking the performance of injection strategies thus, equal w_1 and w_2 (i.e. $w_1 = w_2 = 0.5$) was applied. In reality, this might not be the case and the weight may need to be changed accordingly, depending on the main objective of the injection. Assigning $w_1 = 1$ means the objective is maximizing the oil recovery only, while $w_2 = 1$ when CO_2 storage is the only priority. Practically, weights will be chosen based on the revenue produced by both oil recovery and CO_2 sequestered. Sensitivity results on the weight used are also presented later in this chapter.

5.3. Reservoir simulation model

5.3.1. Model description

A hypothetical three dimensional (3D) model shown in Figure 5.3 was used for evaluating the CO_2 injection strategies. It represents part of a reservoir with nine oil producers and four injectors arranged in four inverted 5-spot well patterns. The main reason for using this multiple well patterns model is to enable the simulation of INTWAG injection that involves alternating CO_2 and water injection between patterns.

The reservoir was assumed as homogeneous water-wet sandstone and the model was run with no-flow outer boundary conditions. The reservoir is 3000 ft x 6000 ft x 270 ft with 1500 ft to 1700 ft well spacing. Initially, the model was discretized to 20x40x10 gridblocks with all the vertical layers having equal thickness. The reservoir was under-saturated at the initial pressure of 4000 psig and under vertical equilibrium conditions with oil-water contact at 7415 ftss. There is local bottom water that does not provide substantial water movement, in the last layer of the model. The injectors were perforated through all vertical gridblocks (layers), unless otherwise stated, while the producers were perforated only in the first eight layers.

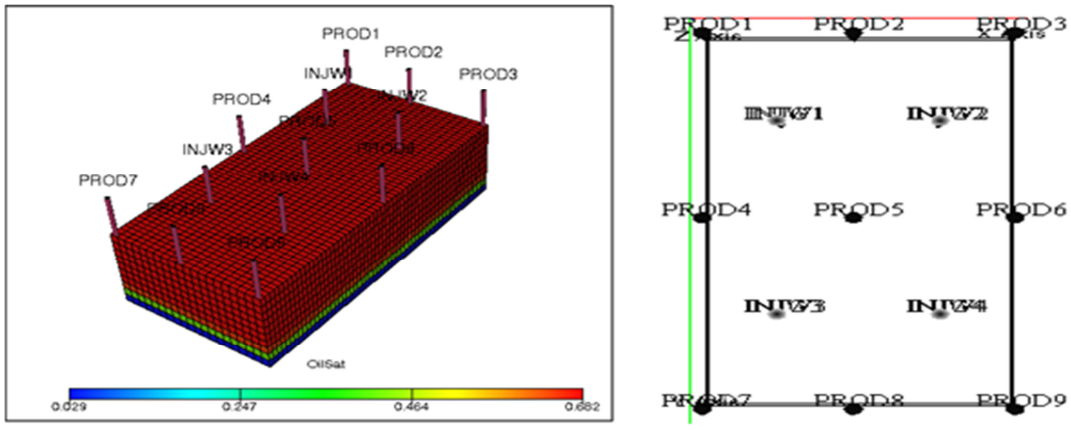

Figure 5.3: Well locations in the model.

ECLIPSE 300 (E300) compositional simulator that uses the EOS model to describe the reservoir fluid phase behaviour encountered during the CO_2 gas injection process was used in the simulation. The fundamental formulation of this compositional simulator is similar to that given in Appendix A2.1. Grid sensitivity analysis in the X and Y directions was then carried out with WI and tertiary WAG process to establish the grid resolution required. The WAG process started with 5% HCPV of CO_2 gas injection followed by water at WAG ratio of 1:1. The WAG cycle was repeated until the end of simulation, at 25 years.

Figure 5.4 shows the oil recovery of WI and WAG process at a varying number of gridblocks in the X (NX) and Y (NY) directions. Waterflooding recovery seems to be

insensitive to the NX and NY within the range sensitized. For the WAG injection, oil recovery also appears to be unaffected by NX but refining the grid size in the Y direction tends to improve recovery until an optimum size of 60 grid blocks is reached beyond which the recovery change becomes negligible. The grid dimension of 20x60x10 was then taken to be adequate to accurately resolve the flow and used in the subsequent simulations. The properties of this homogeneous model are given in Table 5.2.

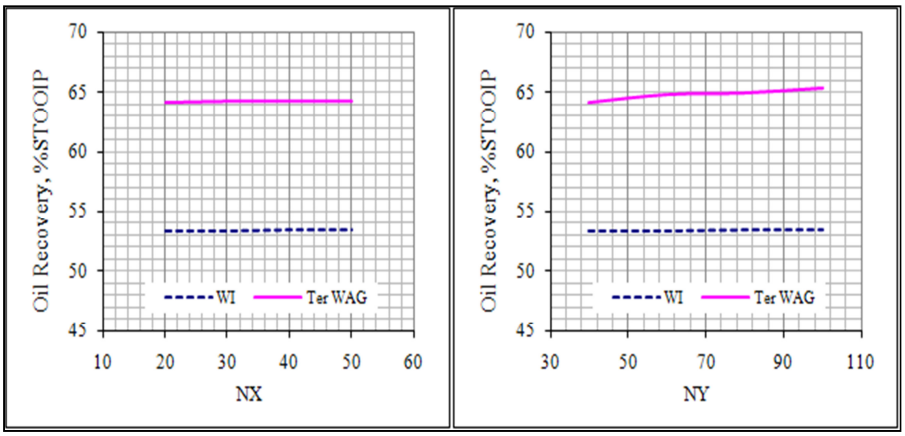

Figure 5.4: Grid size (NX and NY) sensitivity of WI and tertiary WAG injection at WAG ratio of 1:1.

Table 5.2: Average grid properties of the homogeneous 3D model.

Initial reservoir pressure, psig	4000
Reservoir temperature, ^{o}F	150
Grid size, ft	150x100x27
Connate water saturation, fraction	0.32
No of gridblocks	20x60x10
Porosity, fraction	0.25
Permeability, mD	800
k_v/k_h ratio	0.1

5.3.2. Fluid PVT data

The reservoir fluid data was based on Little Knife reservoir fluid reported by Thakur et al. (1984). Little Knife oil is a relatively light oil of 41 ^{o}API and 0.2 cP at its actual reservoir temperature of 245 ^{o}F and 2680 psig saturation pressure, which is quite similar to a typical North Sea reservoir oil. For this study, the reservoir fluid was slightly modified in that the small amount of CO_2 (1.2 mole%) was set to zero and the composition renormalized. This change was to facilitate the analysis of produced and stored CO_2 from the simulation results and has negligible impact on the phase behaviour of the oil. The three-parameter PREOS model was first tuned to match the available saturation pressure, differential liberation and swelling test data at 245 ^{o}F. Details of the match are given in Appendix A5.1. The original ten components were then lumped by mole fraction to four pseudo-components (PC) as shown in Table 5.3. The lumping has no effect on the already tuned EOS model, yet the smaller number of components greatly reduces the simulation time.

Generally, the higher the temperature, the higher is the CO_2 MMP (Klins, 1984). The original Little Knife reservoir temperature of 245 ^{o}F is considered to be on the high side of the favourable temperature range for CO_2 miscible flooding (NPC, 1976). Therefore, a reservoir temperature of 150 ^{o}F was instead used for this study. Using the tuned EOS model, the required PVT data for simulation at 150 ^{o}F were generated. The details are given in Table A5.1 of Appendix A5.1

Table 5.3: Compositions of the reservoir fluid used.

Component	Mole %	Pseudo Component	Mole %
N2	0.977	PC1	36.768
C1	35.792		
C2	10.574	PC2	17.724
C3	7.150		
IC4	1.449	PC3	12.958
NC4	4.133		
IC5	1.600		
NC5	2.104		
C6	3.672		
C7+	32.550	PC4	32.550
Total	100.000		100.000

At 150 °F, the reservoir fluid exhibits bubble point pressure of 2405 psig. The reservoir is under-saturated i.e., no free gas cap, at the initial reservoir conditions. At 150 °F and 4000 psig, CO_2 primarily exists as a gas-like supercritical phase. The EOS model predicts the CO_2 MMP of 3660 psi at 150 °F, which means the reservoir fluid is miscible with CO_2 at the initial reservoir pressure of 4000 psig. The CO_2 viscosity (0.07 cP) is, however, about nine times lower than the oil viscosity (0.584 cP) and 6 times lower than that of water (0.44 cP). While miscibility results in high local displacement efficiency, this unfavourable viscosity ratio between CO_2 and oil and also water may lead to low sweep efficiency due to unstable front displacement. Improving the sweep efficiency is therefore crucial when designing the injection/production strategy.

In the simulation model, hydrocarbons and CO_2 are allowed to exist in the oil and gas phases while only CO_2 and water exist in the aqueous phase. The CO_2 partitioning between the oil and gas phases was calculated using the fugacity equilibration method. The oil and gas phase densities and fugacities were calculated using the EOS while the CO_2 in the aqueous phase were modelled using algorithms by Chang, Coats and Nolen (1998), as described in Appendix A3.1. At 150 °F and 4000 psig, 176.7 scf of CO_2 dissolves in 1 barrel of water (Figure 5.5). For simplicity, the injected and in-situ water in this study were assumed as fresh water, thus no correction due to brine salinity on the CO_2 solubility was necessary.

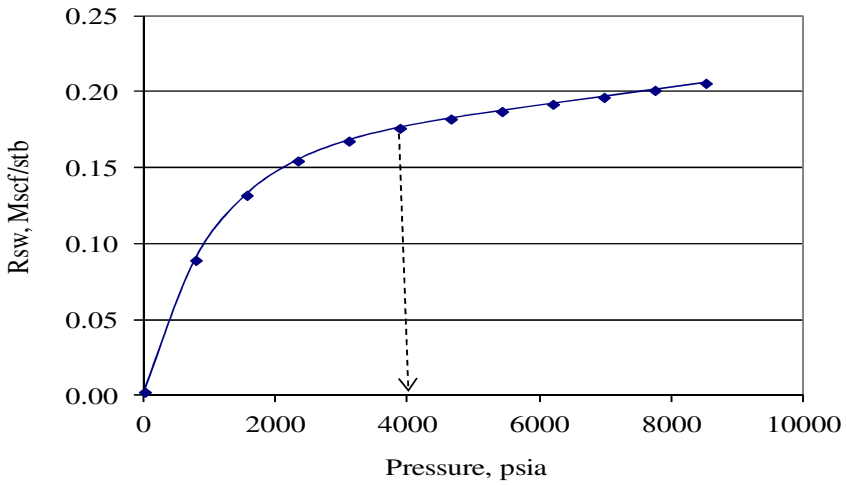

Figure 5.5: Calculated CO_2 solubility in water, R_{sw}, at 150 °F using the Chang et al. correlation (1998).

5.3.3. Saturation functions

Two-phase relative permeability

Multiphase flow and cyclic changes in fluid saturations, as in WAG injection, give rise to hysteresis phenomenon i.e., relative permeability and capillary pressure depend not only on the current saturation, but also on the history of the saturation (Carlson, 1981). In this simulation study, hysteresis was assumed in the relative permeability of the non-wetting phase only.

The oil/water and gas/oil relative permeability curves with the corresponding hysteresis data used were those for water-wet sandstone by Oak, as cited by Spiteri (2005), shown in Figure 5.6(a) and 5.6(b), respectively. Suffix *d* in the plots indicates drainage while suffix *i* indicates imbibition. The capillary pressure hysteresis was assumed negligible since its effects are believed to be relatively small during the production and injection phase of an EOR/storage project. The effect of capillary pressure hysteresis is important to account for the retardation of the buoyant transport of the CO_2 plume, which normally occurs after the injection of CO_2 has stopped (Altundas et al., 2010).

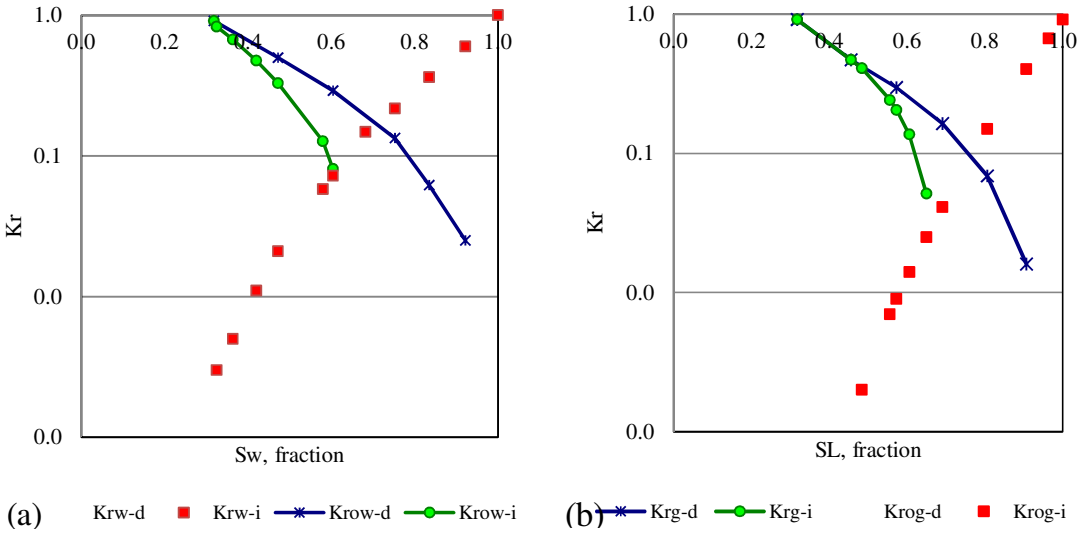

Figure 5.6: (a) Oil/water and (b) Gas/oil relative permeability curves used in the simulation of the homogenous sandstone model (Oak, 1990, as cited by Spiteri, 2005).

Relative permeability hysteresis was modelled by the Killough (1976) method. In this method, the critical gas saturation endpoints specified for the input gas imbibition function determine the trapped saturation and Land's parameter. The trapped critical saturation, S_{ncrt}, for the maximum non-wetting phase saturation reached in the run, S_{hy}, is given by:

$$S_{ncrt} = S_{ncrd} + \frac{S_{hy} - S_{ncrd}}{A + C(S_{hy} - S_{ncrd})} \tag{5.6}$$

$$A = 1 + a(S_{nmax} - S_{hy}) \tag{5.7}$$

where, C is Land's parameter, and S_{ncrd} is the critical saturation of the drainage curve, and A (Equation 5.7) is the modification factor to overcome unphysical behaviour at very small S_{hy} (ECLIPSE, 2007). S_{nmax} is the maximum non-wetting phase saturation value while *a* is defaulted to 0.1. Stone 2 method (Aziz and Settari, 1979, as quoted in the Eclipse User Manual, 2009) was used to estimate the three-phase relative permeability since this method can better model the mixed wet system, which is relevant to the current simulation study.

Two-phase capillary pressure

The capillary pressure, Pc, used in the model was calculated using the approach reported by Ghomian et al. (2008), where Pc is defined in terms of the Leverett J-function (Equation 5.8):

$$Pc = \sigma cos\theta \sqrt{\frac{\emptyset}{k}} J \tag{5.8}$$

where ϕ is the porosity, k is the permeability, θ is the contact angle and σ is interfacial tension between water-oil. The J-function was calculated as:

$$J = S_1^{-n} + J_e - 1 \tag{5.9}$$

where S_1 is the wetting phase saturation as a fraction, J_e is the entry value of the J-function and was assumed as 0.4 for the sandstone (Ghomian et al., 2008), and *n* is the pore size distribution index. *n* = 2 was assumed for a relatively well-sorted sandstone. Poorly-sorted

rock has lower *n* value. Since no measured value of σ was available, a value of 26 was assumed based on the data measured by Yang et al. (2005) at 38 °C and 4000 psig.

The model has a pore volume of 216.4 MMrb and an average initial oil saturation of 0.62 with 83.6 MMstb and 101 MMscf oil and gas originally in place, respectively.

5.3.4. Well operating conditions

General well control

All the processes were assumed to take place at isothermal (constant reservoir temperature) conditions. Model predictions were made for 25 years. The well economic limits for the producers were set at a minimum oil rate of 5 stb/day, maximum water-cut of 99% and a maximum gas-oil ratio (GOR) of 20 Mscf/stb. On reaching any of these economic limits, the most offending layer was automatically closed. However, in the interest of maximizing CO_2 storage, the CO_2 injection continued until the average reservoir pressure reached the maximum BHP or until the 25 years of the simulation period, whichever was earlier. This is different from the common practice in conventional EOR, where CO_2 was normally injected only up to a certain volume followed by a much cheaper chase fluid like water or lean gas.

The maximum allowable injection BHP was limited to 5860 psia based on an assumed 0.8 psi/ft fracture gradient at the datum depth of 7285 ftss. The injector wells were controlled by the injection rate. The total fluid injection rate for all scenarios corresponds to 12.9 %STOOIP per year with 7000 stb/day/well and 16,285 Mscf/day/well for water and gas, respectively (or equivalent to 7047 rb/day/well at 4000 psig, 150 °F). These rates are relatively high if compared with the typically used 3-10 %STOOIP per year in a real field operation. They were nevertheless used here to expedite the production, so that close to the ultimate oil recovery (EUR) could be attained by the end of the model prediction. Since the injection rate was fixed, the required reservoir pressure, whether above or below the MMP, was obtained by controlling the production wells as follows:

Fixed BHP mode

The default production was under a minimum BHP constraint of 2000 psi. A big pressure draw down occurred at the beginning of the production resulting in a very steep pressure decline and in impractically high oil production rates, albeit it might only be for a short period of time. For a more realistic value, the maximum oil production rate was capped at 8000 bbl/day/well, a typical maximum rate for a vertical well with $9\frac{5}{8}$ inch tubing. Throughout most of the flooding duration, the average reservoir pressure was below the MMP: thus, this well control mode represents the immiscible flooding conditions (low pressure flooding). Re-pressurisation of the reservoir occurred in some cases, as the injection was continued even with the economic limits already reached.

Fixed rate mode

This well control mode was to simulate the miscible conditions during the CO_2 injection. To attain average reservoir pressure above the MMP throughout the simulation period, the total fluid withdrawal at reservoir conditions was set at a rate 10% lower than the total injection rate of 28,190 rb/day (giving injection/production ratio of 1.1:1). This well control mode is also referred to in this thesis as the high pressure flooding mode.

5.3.5. CO_2 injection scenarios

Each of the evaluated injection strategies, the setting of which are given next, were simulated both as secondary and tertiary recovery methods. In the secondary recovery mode, CO_2 injection started from the first day of production. In the tertiary recovery mode, CO_2 injection started after seven years of waterflooding, at which the watercut was 54 and 86% for fixed rate and fixed BHP control, respectively.

WAG: The conventional WAG injection was carried out at WAG ratio of 1:1. This ratio has been reported in several studies to result in an optimum WAG performance (for example, Christensen et al, 1998). The injection started with 5% HCPV of a CO_2 slug,

followed by the same amount of water and the cycle repeated.

TAPWAG: The WAG ratio was initially set at 1:1 until 30% HCPV of CO_2 was injected. The WAG ratio was then increased to 2:1 until 40% HCPV of total injections and to 3:1 from 40 % of HCPV injections until the end of simulation.

HYWAG: In this injection scheme, the CO_2 slug was first injected continuously up to 20 %PV followed by WAG at 1:1 ratio with 5% HCPV half cycle until the end of simulation.

Selective SWAG (SSWAG): CO_2 gas and water were simultaneously injected at 1:1 ratio similar to that of WAG in two injection wells defined at the same location with the water injectors open to flow in the first top five layers (layers 1-5) whereas the gas was injected only through the bottom five layers (layers 6-10).

INTWAG: Figure 5.7 schematically illustrates the schedule of the injection and production wells in this injection scheme.

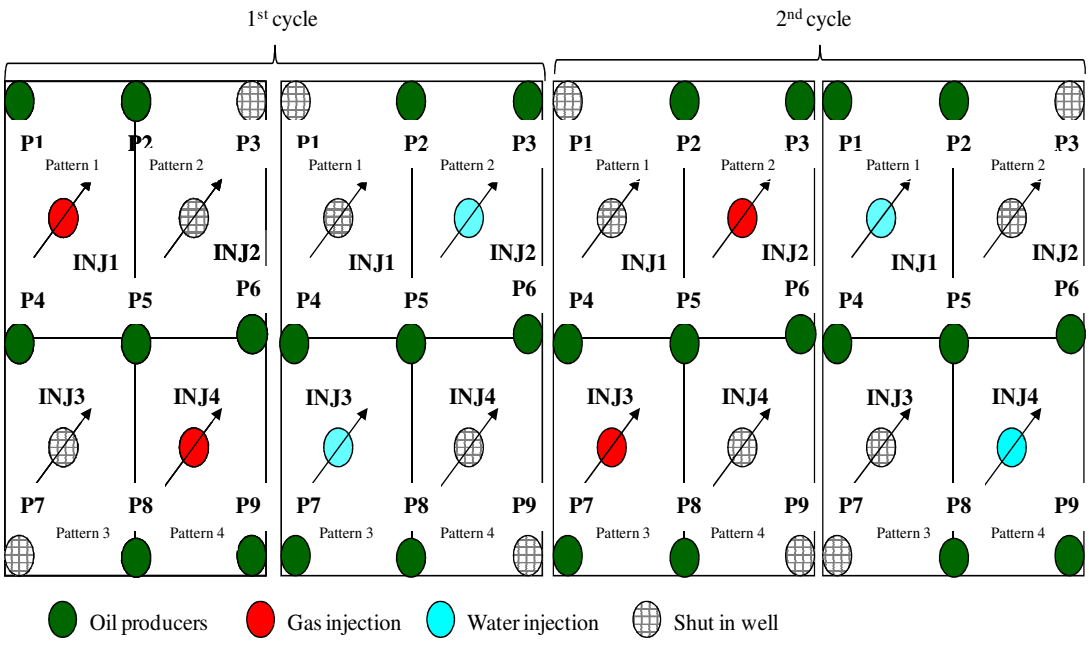

Figure 5.7: Injection/production wells schedule in INTWAG injection.

Generally, when the gas or water is injected in one pattern, the injector (INJ) and producer (P) dedicated to the pattern next to it are closed. In the first half cycle, the injectors in the second and third pattern (INJ2, INJ3) and the oil producer attached solely to those patterns (P3 and P7), are closed. At the same time, CO_2 gas slug is injected in the first and fourth pattern (INJ1 and INJ4) with the other producer wells open to flow. In the subsequent half cycle, INJ1, INJ4 and producers P1 and P9 are shut in while water is injected in wells INJ2 and INJ3. This completes the first full INTWAG cycle.

Having completed the first cycle, INJ2 and INJ3 are opened to CO_2 gas injection with the other wells remaining in the previous status. After the CO_2 slug is injected, wells INJ2, INJ3, P1 and P7 are shut in and water is injected in wells INJ1 and INJ4. The well schedule is then repeated until the end of simulation. The injection schedule is different from the conventional WAG in that in conventional WAG, gas and water are injected alternately in the same well and simultaneously in all patterns.

The injection rates in the active wells were doubled to maintain the same total injection rates as in the other injection strategies. In this particular case, the resulting injection rate per injector well might be impractically high (exceeding well capacity). In reality a more realistic injection rate may be chosen and a simulation to examine this effect was also run. This new injection schemes were further examined by sensitizing the effect of the WAG ratio as well as the slug size on the oil recovery and CO_2 stored; more detailed simulation results are presented in the next section.

5.4. Simulation results

Compositional simulations were successfully performed on WI and all the six CO_2 injection schemes as secondary and tertiary recovery methods under both well control modes. More detailed sensitivity study was carried out on the newly conceptualized INTWAG injection scheme in order to gain more understanding of its performance and benefit for CO_2 EOR and storage.

5.4.1. INTWAG injection

In the base case, WAG ratio of 1:1 was used with 5% HCPV of CO_2 slug, followed by the same amount of water. Water and CO_2 were injected according to the schedule as described in Figure 5.7. Diffusion of CO_2 in both oil and gas phases were turned on in the simulation. The molecular diffusion coefficient of CO_2 in the oil phase was estimated using correlation by McManamey and Woolen (1973):

$$D_{CO2,oil} = 1.41x10^{-10}\mu_{oil}^{-0.47} \quad (5.10)$$

where μ_{oil} is the viscosity of oil in Pas and $D_{CO2,oil}$ in m^2/s. The viscosity of oil used was 0.584 mPas at the reference reservoir temperature and pressure, giving a $D_{CO2,oil}$ of 4E-03 ft^2/day. Unfortunately, with oil present, the version of E300 used can only consider the CO_2 molecular diffusion in the hydrocarbon phase and not in the water phase (ECLIPSE, 2007).

The simulation results for all the INTWAG runs are summarised in Table 5.4. CO_2 utilization is defined as Mscf of CO_2 required to producing one barrel of incremental oil. The oil recoveries shown for the tertiary process are oil recovered during the INTWAG injection phase only.

The results show that INTWAG injection yields higher oil recovery than WI in both recovery methods. More oil was being recovered and more CO_2 stored in the secondary than in tertiary INTWAG injection. Figures 5.8a and 5.8b depict the oil recovery and CO_2 stored during the secondary and tertiary INTWAG injection, respectively.

Higher oil recovery was obtained from the miscible flooding (fixed rate control) than the immiscible one (BHP control) as expected. CO_2 was also used more efficiently to recover the additional oil in the miscible INTWAG processes as demonstrated by the lower CO_2 utilization factor. As Table 5.4 shows, there is a bigger improvement in oil recovery under miscible conditions in the tertiary than in the secondary recovery method. However, more CO_2 was stored per barrel of produced oil in the immiscible injection particularly in the tertiary recovery mode.

Table 5.4: The predicted oil recovery, CO_2 utilization and storage factor of INTWAG injections.

Recovery mode	Control mode	R, %STOOIP	S, %PV	CO_2 utilization, Mscf/bbl	CO_2 retention, Mscf/bbl
Secondary	BHP	60.5	37.5	47.7	2.5
Secondary	Rate	69.3	21.7	15.9	2.0
Tertiary	BHP	11.6	31.7	28.1	11.6
Tertiary	Rate	23.3	18.1	16.2	5.3

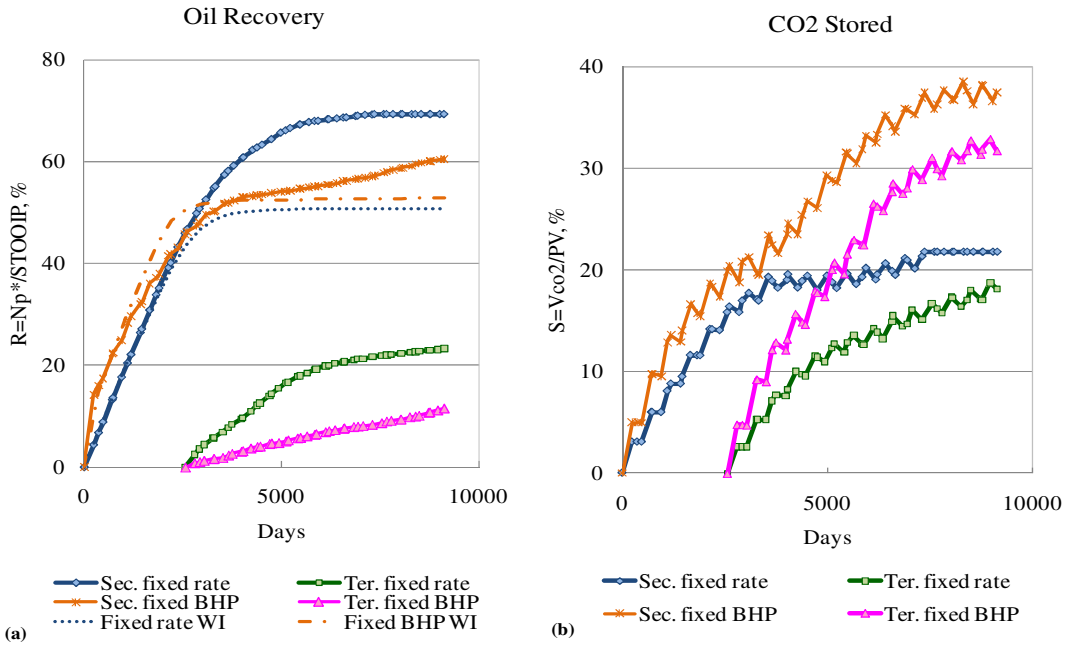

Figure 5.8: Predicted (a) oil recovery and (b) CO_2 storage from INTWAG injection under secondary and tertiary recovery methods.

In order to gauge its performance, INTWAG was compared with conventional WAG injection as shown in Table 5.5. Slightly higher oil recovery and CO_2 storage was generally observed for INTWAG as compared with WAG injection except in the secondary recovery method under miscible condition where both perform equally well. In the immiscible process, the secondary and tertiary INTWAG requires 24% and 8% less CO_2, respectively, to produce one additional barrel of oil than in the corresponding WAG scheme. For the

miscible tertiary INTWAG injection, the incremental oil recovery and CO_2 storage are higher than that of normal WAG.

The alternating shut-in (or soak) period of some wells during INTWAG injection could have given more time for CO_2 to dissolve deeper into the oil and through the mobile water barrier to contact the by-passed oil. This shut-in period depends on the slug size and the WAG ratio. The effect of these two parameters on INTWAG performance was further investigated using tertiary INTWAG injection and the results are given next.

Table 5.5: Comparison of oil recovery factor, CO_2 utilization and CO_2 storage between INTWAG and WAG injections.

Process	Recovery mode	Control mode	R, % STOOIP	CO_2 utilization, Mscf/bbl	S, % PV
INTWAG	Secondary	BHP	60.5	47.7	37.5
WAG			58.6	62.5	36.2
INTWAG	Secondary	Rate	69.3	15.9	21.7
WAG			69.3	14.9	21.0
INTWAG	Tertiary	BHP	11.6	28.1	31.7
WAG			10.0	30.7	29.4
INTWAG	Tertiary	Rate	23.3	16.2	18.1
WAG			21.2	14.6	14.1

Sensitivity study on CO_2 slug size

The slug size refers to the amount of CO_2 injected during the half cycle of the process, expressed as percentage of HCPV. With a WAG ratio of 1:1, the slug size was sensitized from 1 to 7 %HCPV. Figure 5.9 shows that, within the range sensitized, the incremental oil recovery for the production under the BHP constraint is not sensitive to the slug size. Since the larger the slug size, the longer the shut in period of the inactive pattern, these results also mean the oil recovery is not significantly affected by the diffusion of the CO_2 into the oil that might occur during the shut in period. Larger slug size means a larger amount of CO_2 injected per slug interval, thus a higher amount of CO_2 being stored, despite the same total amount of CO_2 was injected over the total injection duration. For the immiscible INTWAG,

increasing the slug size from 1 to 7 %HCPV, increases the CO_2 storage by 10% i.e., from 30% to 33%PV.

Conversely, the slug size is influential to both incremental oil recovery and CO_2 storage in the miscible INTWAG injection. The larger the slug size, the higher the oil recovery and CO_2 storage. Increasing the slug size from 1% to 7 %HCPV increases the oil recovery by 8%. Even though the amount of CO_2 stored at any given slug size is higher in the immiscible case, the rate of increase in the amount of CO_2 stored with the slug size is higher in the miscible cases in which increasing the slug size by 6 %HCPV increases the amount of CO_2 stored by 50%.

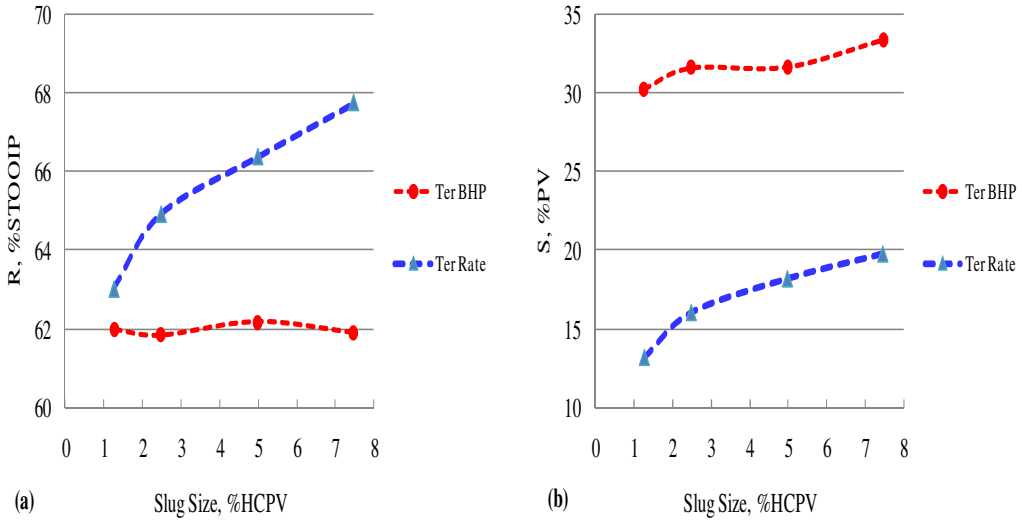

Figure 5.9: Variation of the (a) incremental oil recovery and (b) CO_2 storage with CO_2 slug size for tertiary INTWAG injections under both injection modes.

Sensitivity study on the WAG ratio

The WAG ratio, defined as the reservoir barrel of water slug to that of CO_2 slug in one cycle, was sensitized from 1:4 to 3.95:1. The effect of the WAG ratio on the oil recovery from the immiscible and miscible tertiary INTWAG is shown in Figure 5.10a and 5.10b, respectively. At a higher WAG ratio, less CO_2 was injected per any given cycle and also over the total injection duration, thus there was less CO_2 in contact with the oil. At a smaller WAG ratio,

the reverse is true. For example, at the lowest WAG ratio of 1:4, high gas production was predicted, even though the cumulative oil production was the highest for some duration of the injection. The high gas production escalated GOR to its limit, triggering the closure of producer wells and thus loss of production. There is an optimal WAG ratio that gives the highest oil recovery for both immiscible and miscible cases, which is 1:1 (1) and 1:3 (0.67), respectively.

Under both flooding conditions, CO_2 storage increases with decreasing WAG ratio, as illustrated in Figure 5.11. Higher CO_2 storage is, however, predicted under the immiscible conditions, with only about half as much in the miscible flooding mode. The lower average reservoir pressure at the beginning of the injection and the re-pressurization that occurred toward the end of the flooding period results in high CO_2 storage for low WAG ratio cases. Generally, lower oil recovery was obtained with higher WAG ratio (higher volume of water in each cycle) until an optimal point is reached.

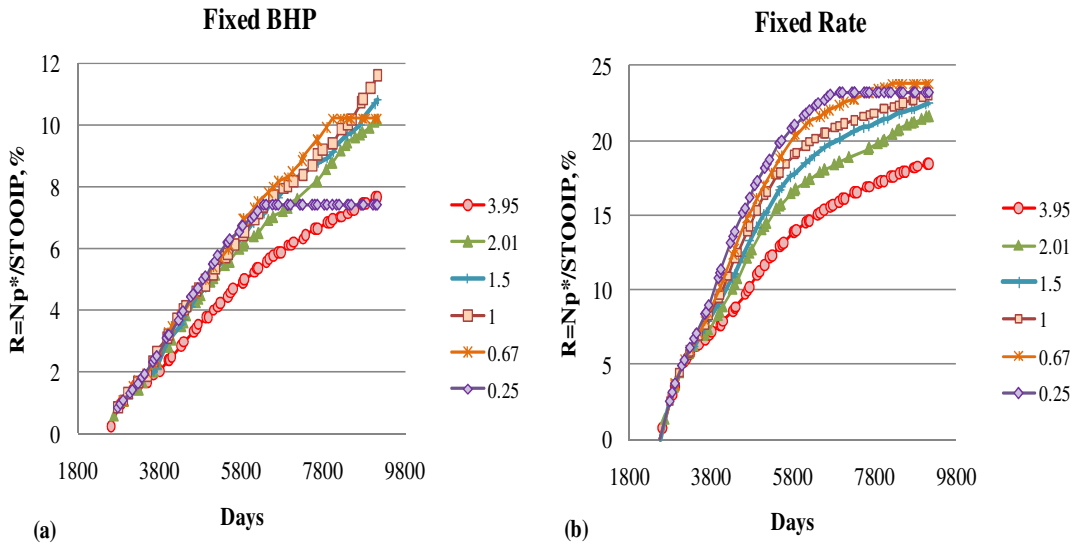

Figure 5.10: Variation of the oil recovery with the WAG ratio under (a) immiscible and (b) miscible tertiary INTWAG injection.

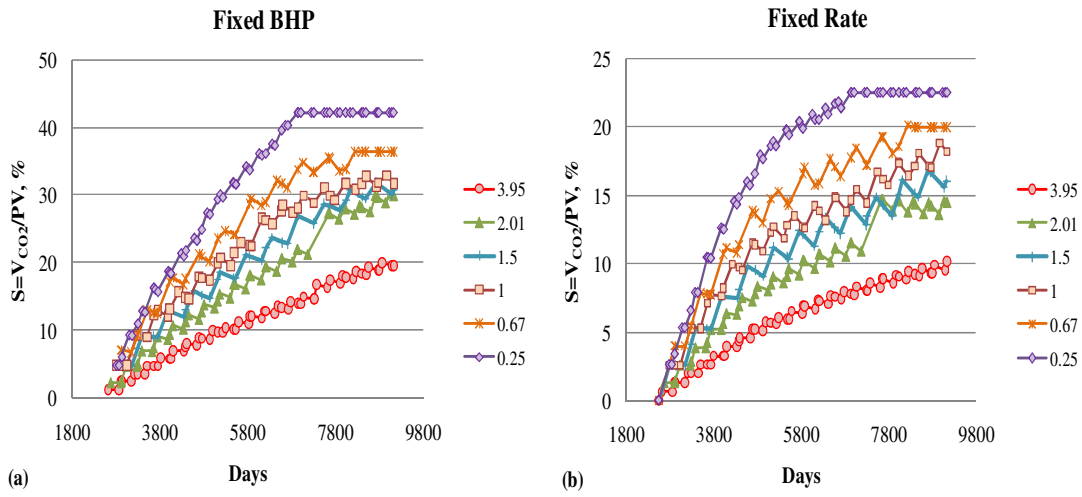

Figure 5.11: Variation of the CO_2 storage with the WAG ratio under (a) immiscible and (b) miscible tertiary INTWAG injection.

Effect of the injection rate

Since some wells are usually switched off, wells that are injecting are doing so at unrealistic rates in order to maintain the total production rate as the other injection schemes. To investigate the effect of the injection rate on the performance of this process, secondary INTWAG injection under fixed rate mode was simulated using more realistic injection rates i.e., 7000 bbl/day/well and 16285 Mscf/day/well for water and gas injection, respectively.

The results show that, for the same injection period, reducing the injection rates to half leads to significant loss of oil recovery, thus revenue. The cumulative oil recovery reduces to 52.5% STOOIP instead of 74.38 %STOOIP if the total injection was made the same as the other injection strategies. The CO_2 dissolution (as indicated by the CO_2 concentration) in the aqueous phase and gas saturation distribution, however, follow the same pattern as that of with the higher rates, the latter will be shown later, albeit much smaller area around the well was contacted by the injected CO_2.

Comparison of INTWAG injection performance with other injection schemes is given in the subsequent section.

5.4.2. CO_2 injection for maximizing oil recovery

Conventionally, increasing oil recovery is the main objective of CO_2 injection into the oil reservoirs. In order to screen for the most favourable CO_2 injection scheme for EOR only, only the oil recovery (R) was compared (or f with $w_1 = 1$ and $w_2=0$).

Figure 5.12 shows the secondary oil recovery profiles under both production constraints. It is evident that the incremental oil recoveries above that of WI for the immiscible process (Figure 5.12a) are relatively small (2.5 to 8.0 %STOOIP). INTWAG injection yields the highest oil recovery, followed very closely by WAG injection. Immiscible SSWAG, TAPWAG and HYWAG injections yielded more or less the same oil recovery while CO2I performed poorer than the waterflood. CO2I suffers from the unfavourable viscosity ratios between CO_2 and the oil at lower pressures below the MMP, due to reduced CO_2 viscosity, that leads to early CO_2 breakthrough.

In contrast to this, much higher incremental oil recoveries above that of WI were predicted for all the injection schemes under the miscible conditions (Figure 5.12b). Oil recovery from SSWAG injection is the highest, with 29 %STOOIP of additional oil recovery. Using this method, 10.6 Mscf of CO_2 was required to produce an additional barrel of oil. Although giving lower recovery than SSWAG, the other injection schemes also outperform WI with oil recoveries exceeding 70 %STOOIP, albeit there are some delays in the oil production for CO2I and HYWAG process during the intermediate times between 2000 and 8000 days. From the CO_2 gas consumption efficiency point of view, all WAG injections require only half or less of the CO_2 volume as does CO2I, which is 13-16 Mscf/bbl for WAG against 34.5 Mscf/bbl for CO2I. WAG is thus preferable if there is limited amount of CO_2 gas available for injection.

Similar trends to what was predicted for the secondary recovery were also observed for the tertiary recovery, Figure 5.13. The preceding waterflooding yielded 50.6 %STOOIP and 43.4 %STOOIP for the immiscible and miscible case, respectively. For the immiscible flooding mode, TAPWAG injection gives the highest oil recovery of 62.8 %STOOIP whereas for the miscible injection, SSWAG did better than the rest, with 71.5 %STOOIP of oil recovery.

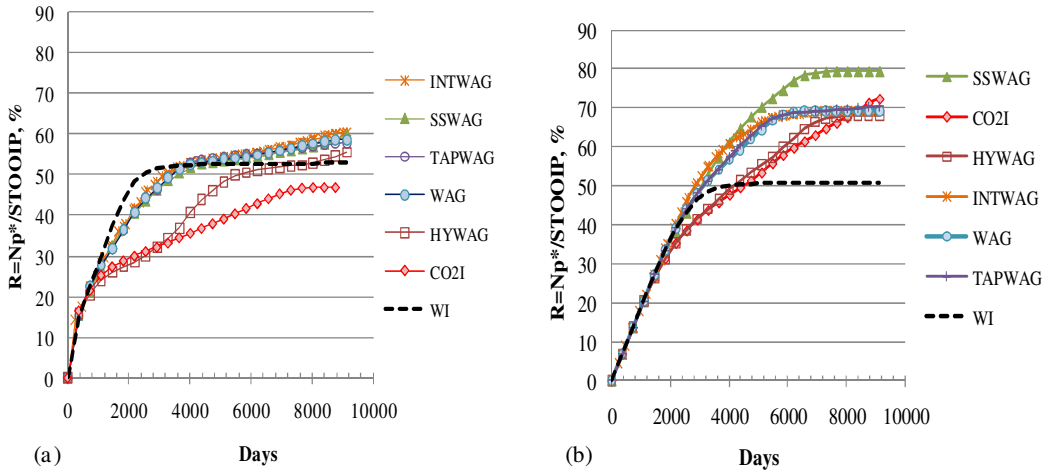

Figure 5.12: The oil recovery for secondary CO_2 injection strategies under (a) immiscible flooding and (b) miscible flooding.

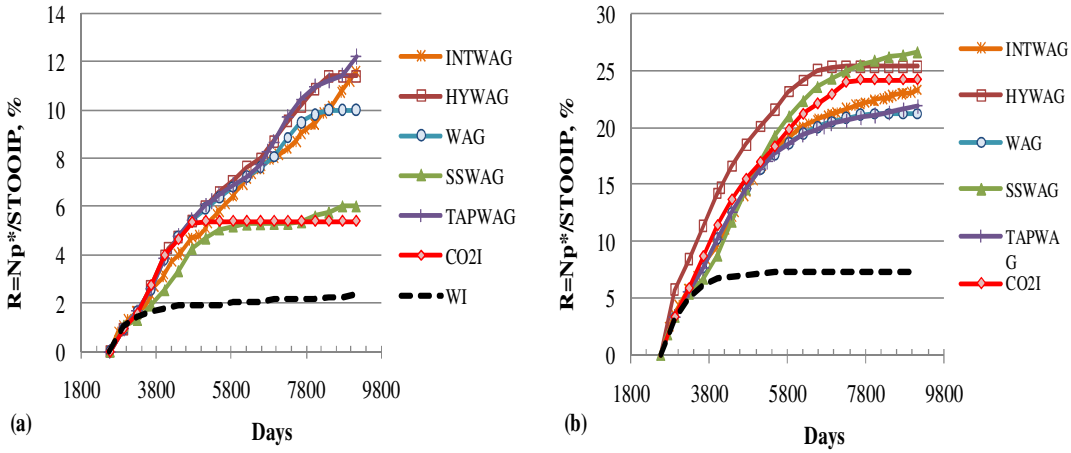

Figure 5.13: The incremental oil recovery for tertiary CO_2 injection strategies under (a) immiscible flooding and (b) miscible flooding.

5.4.3. CO_2 injection for maximizing storage

The CO_2 storage capacity of the reservoir includes both the CO_2 that remained in the reservoir at the end of EOR operation and any extra CO_2 that can be injected after the EOR project until the maximum allowable BHP or project duration of 25 years is reached,

whichever is earlier. When the main priority of the CO_2 injection was to maximize the CO_2 storage, comparison was done on S only (or *f* with $w_2 = 1$ and $w_1=0$).

Figures 5.14 and 5.15 show the percentage of pore volume occupied by CO_2 for the secondary and tertiary CO_2 injection, respectively. Unlike the oil recovery trend, the amount of CO_2 stored in the reservoir is higher in the immiscible flooding than in the miscible process for both secondary and tertiary injections. The summary of the CO_2 stored for all the injection cases is given in Table 5.6. It is interesting to note that the ranking of the injection schemes is the same in the secondary and tertiary recovery for the immiscible injection but not in the case of the miscible flooding. CO2I stores the highest amount of CO_2, in both flooding conditions and recovery methods, since only CO_2 is filling up the pore space created by production. In the tertiary recovery, some of the pore volumes have already been filled up with water from the preceding water injection, resulting in much lower CO_2 stored than that obtained in the secondary recovery.

The CO_2 retention factor is the highest in the immiscible CO2I despite the fact that no additional oil recovery was produced. In the tertiary process, the CO_2 storage is less as the injected CO_2 needs to displace both oil and water unlike in the secondary process where the injected CO_2 only needs to displace the oil. TAPWAG gives the lowest amount of the CO_2 stored as the injected volume of CO_2 is also the least.

In the tertiary CO_2 flooding, higher CO_2 storage of 43 %PV was achieved through immiscible CO2I as opposed to 33 %PV in the corresponding miscible case. Since CO_2 solubility in crude oils is typically five to six times higher than in water, the higher remaining oil saturation in the low pressure flooding case (which have lower oil recovery) than that of the miscible flooding, dissolves larger amount of CO_2. However, the main contributing factor to the high CO_2 storage in the immiscible flooding is the pressurization of the reservoir towards the end of the injection process. The lower starting average reservoir pressure greatly increases the capacity of CO_2 that can be injected and sequestered before the reservoir pressure reaches its maximum limit.

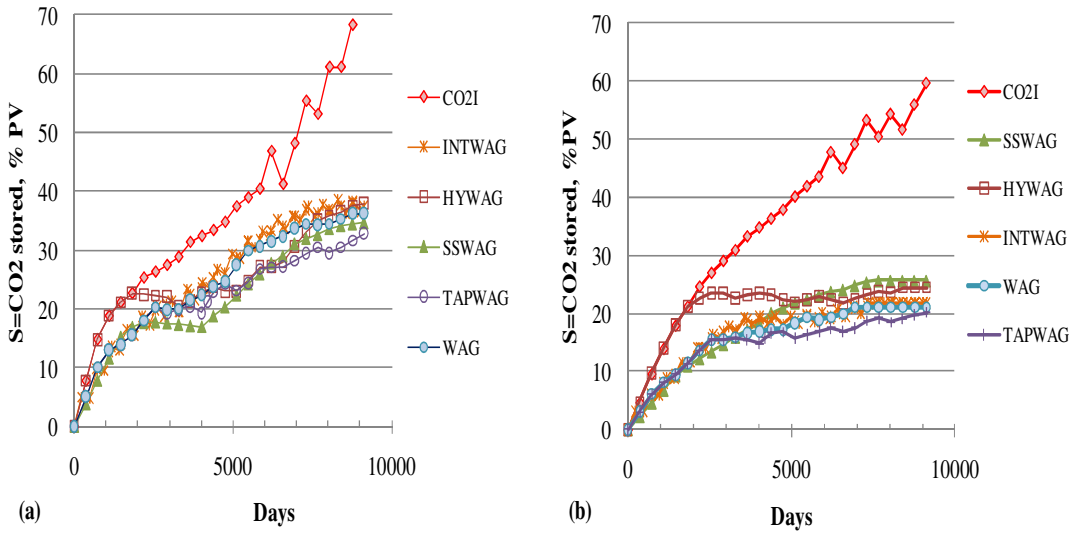

Figure 5.14: Percentage of reservoir pore volume filled by CO_2 for secondary CO_2 injection strategies under (a) immiscible flooding and (b) miscible flooding.

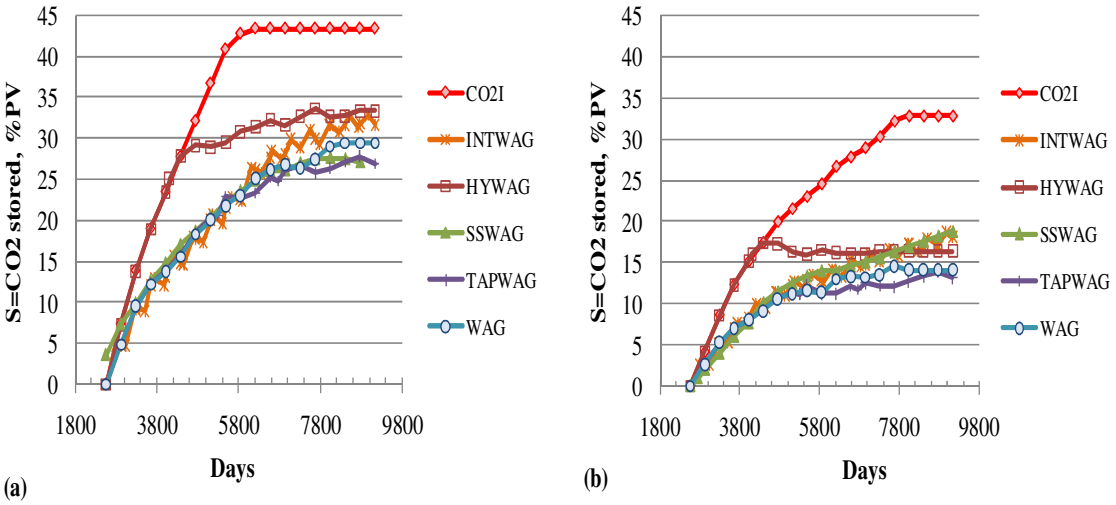

Figure 5.15: Percentage of reservoir pore volume filled by CO_2 for tertiary CO_2 injection strategies under (a) immiscible flooding and (b) miscible flooding.

Table 5.6: Summary of CO_2 storage and retention factor for all the injection schemes.

Process	CO_2 stored, %PV				CO_2 retention, Mscf of CO_2 stored/bbl of oil produced			
	Secondary recovery method		Tertiary recovery method		Secondary recovery method		Tertiary recovery method	
	Fixed BHP	Fixed Rate	Fixed BHP	Fixed Rate	Fixed BHP	Fixed Rate	Fixed BHP	Fixed Rate
CO2I	74.58	59.63	43.35	32.78	7.10	5.19	36.30	9.00
WAG	36.20	21.04	29.41	14.11	2.50	1.94	12.44	4.61
SSWAG	34.64	25.62	27.08	18.84	2.32	2.09	18.55	4.92
HWAG	37.92	24.45	33.31	16.41	2.72	2.21	11.93	4.95
TAPWAG	32.83	20.16	26.88	13.10	2.20	1.83	9.02	4.14
INTWAG	37.46	21.74	31.68	18.08	2.51	1.99	11.59	5.34

Effect of re-pressurization to CO_2 storage

In order to gauge the contribution of re-pressurization to the CO_2 storage, secondary injections under the fixed BHP well control mode were simulated without re-pressurisation. The average reservoir pressure for all injection strategies was generally low, as can be seen in Figure 5.16b. In these cases, the simulation was stopped once the economic limits were reached. Figure 5.16a shows the CO_2 stored from those runs, and if compared with Figure 5.14a, we can see that without re-pressurization, the CO_2 storage for CO2I is very much less, i.e., only about 48 %PV instead of 74.6 %PV, albeit still higher than what was stored in the other injection schemes, Table 5.7.

Table 5.7: Effect of pressurization after EOR on CO_2 storage, secondary CO2I with production under BHP constraints.

Secondary CO2I- BHP mode	R, %STOOIP	S, %PV
With pressurization	46.9	74.6
Without pressurization	43.1	48.2

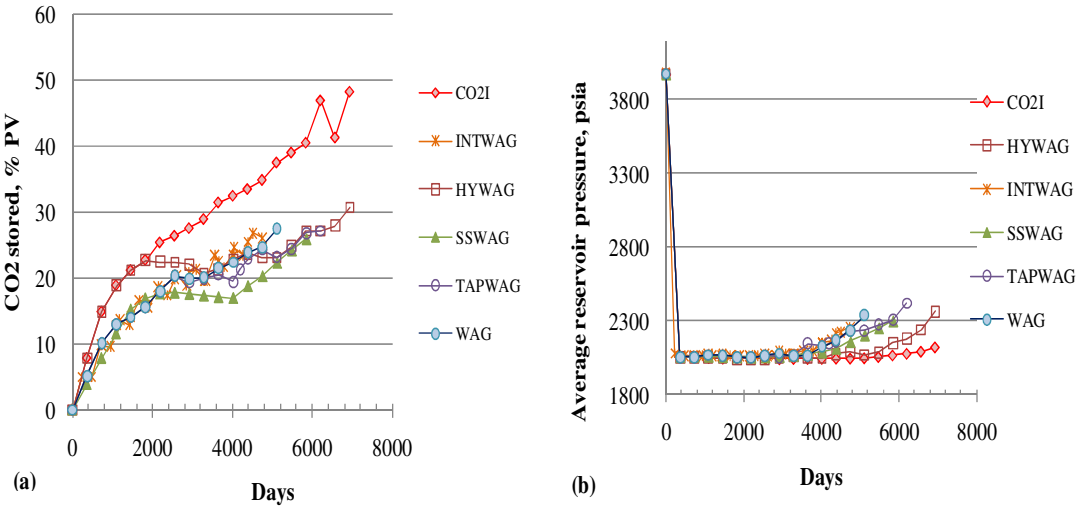

Figure 5.16: (a) Percentage of reservoir pore volume filled by CO_2 for secondary CO_2 injection strategies under BHP well control mode (b) Average reservoir pressure for the case without pressurization.

The relationship between R and S is shown in Figures 5.17 and 5.18 for secondary and tertiary CO_2 injections, respectively. In most cases, S increases with increasing R but the rate of increase varies between injection schemes. Notably for CO2I, S increases drastically with R towards the end of the injection period and at constant R during the pressurization period. For most of the immiscible WAG injections, S exhibits a levelling off trend with increasing R; consistent with the fact that the portion of the pores being filled with water is increasing and limiting the CO_2 storage capacity.

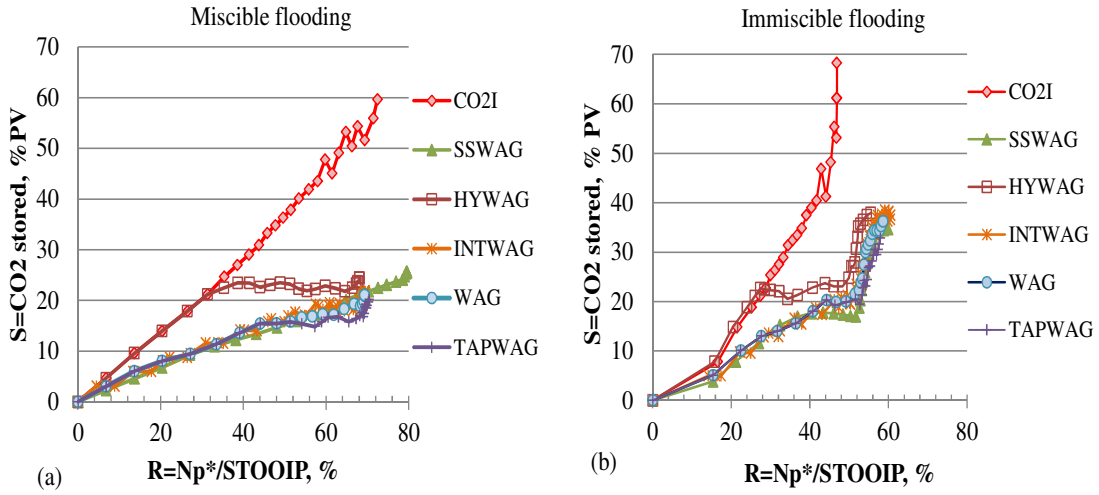

Figure 5.17: Cross-plots of S and R for the secondary CO_2 injections under (a) miscible and (b) immiscible flooding.

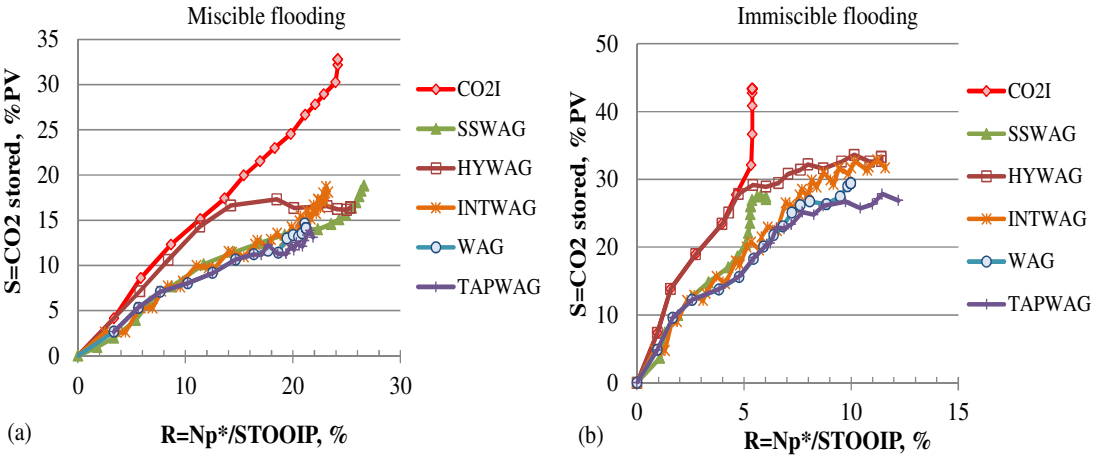

Figure 5.18: Cross-plots of S and R for the tertiary CO_2 injections under (a) miscible and (b) immiscible flooding.

5.4.4. CO_2 injection for EOR and CO_2 storage

Equal importance of EOR and CO_2 storage (w_1=w_2=0.5)

As we are interested in finding the CO_2 injection strategy that could optimize both oil recovery and CO_2 stored, the function *f* versus time (Equation 5.1) with weight $w_1 = w_2 = 0.5$ was plotted. The injection scheme with the most potential to co-optimize the oil recovery and CO_2 storage technically is the scheme with the highest *f* value, which, as can be seen in Figures 5.19 and 5.20, it is miscible CO2I for both secondary and tertiary recovery modes.

These results are based on the assumption that the compression cost (as a penalty on the oil production as defined by Equation 5.4 and 5.5), was only on the amount of recycled gas. But in reality, part of the injected gas could also come from other source other than the recycled gas. Sensitivity run results nevertheless indicate that accounting for the total CO_2 injected volume in compression, rather than only the 95% produced CO_2 gas, reduces the N_p^*(Equation 5.4) but has insignificant consequences on the ranking of the injection schemes.

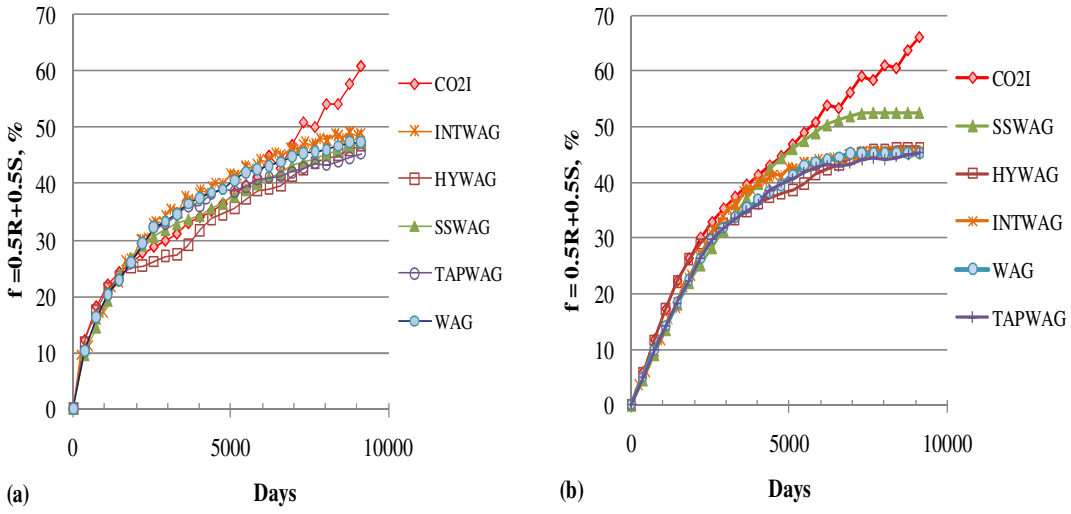

Figure 5.19: Function *f* with equal weight of oil recovery and storage (w_1=w_2=0.5) for secondary CO_2 injection strategies under (a) immiscible and (b) miscible flooding.

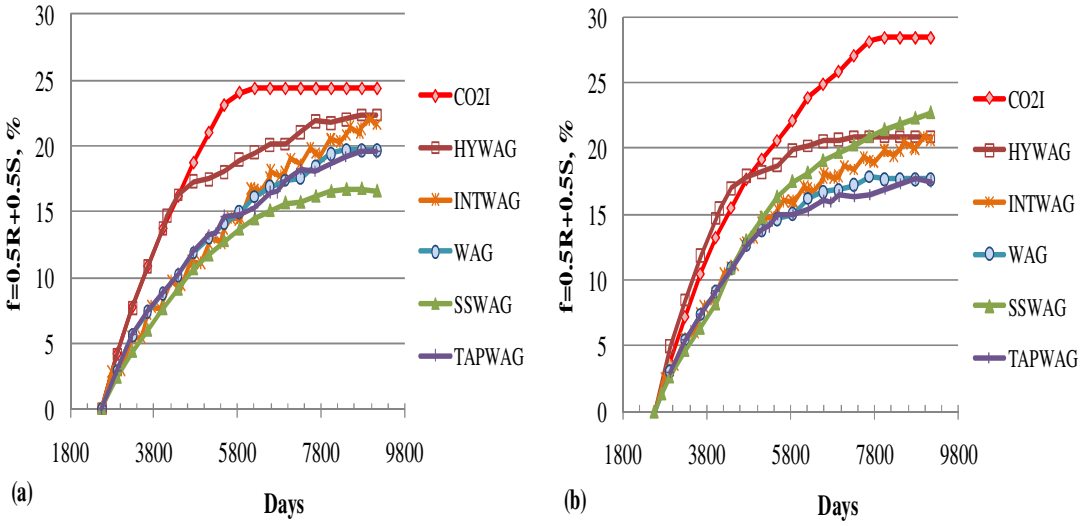

Figure 5.20: Function *f* with equal weight of oil recovery and storage (w_1=w_2=0.5) for various tertiary CO_2 injection strategies under (a) immiscible and (b) miscible flooding.

Higher importance on EOR than CO_2 storage (w_1=0.75; w_2=0.25)

As stated earlier, the weight, w_1 and w_2, in Equation 5.1 would depend on the main objective of the CO_2 injections. There could be a situation where the oil recovery has the higher priority yet the importance of CO_2 storage could not be totally ignored or the scenario where the oil recovery has a much higher value than the CO_2 storage. In order to evaluate this scenario, *f* was calculated with w_1=0.75 and w_2=0.25.

The resulting *f* versus time for the secondary and tertiary recovery is shown in Figures 5.21 and 5.22, respectively. We can clearly see a significant difference in the *f* trend for the fixed BHP (immiscible) mode, Figures 5.21a and 5.22a, in that CO2I is no longer the preferred injection strategy, instead, this is now the INTWAG and HYWAG injection, for the secondary and tertiary recovery, respectively. CO2I does, however, remain the preferable injection for the miscible tertiary recovery (Figure 5.22b), while one might want to opt for SSWAG for the secondary miscible flooding rather than CO2I as the latter is just marginally higher than the rest only towards the end of the injection period.

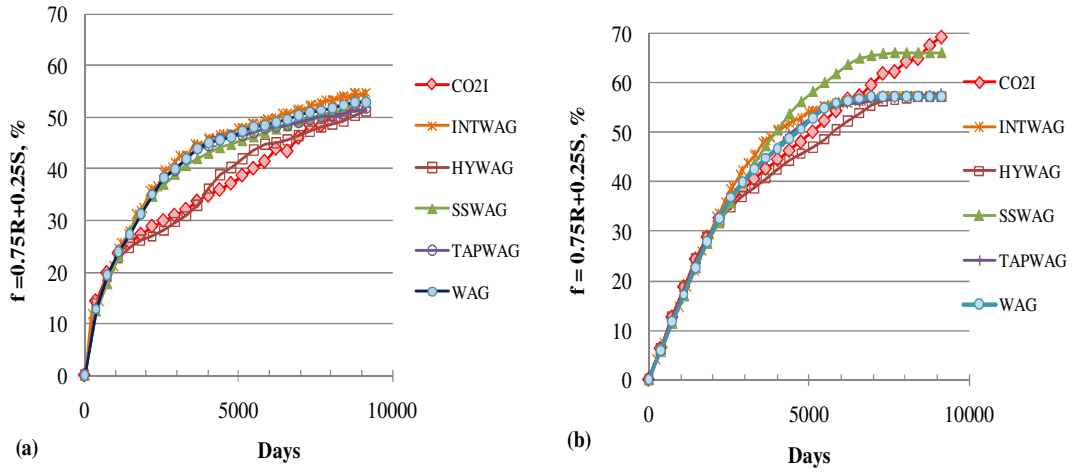

Figure 5.21: *f* profiles with higher priority to oil recovery (w_1=0.75 and w_2=0.25) for secondary CO_2 injection strategies under (a) immiscible and (b) miscible flooding.

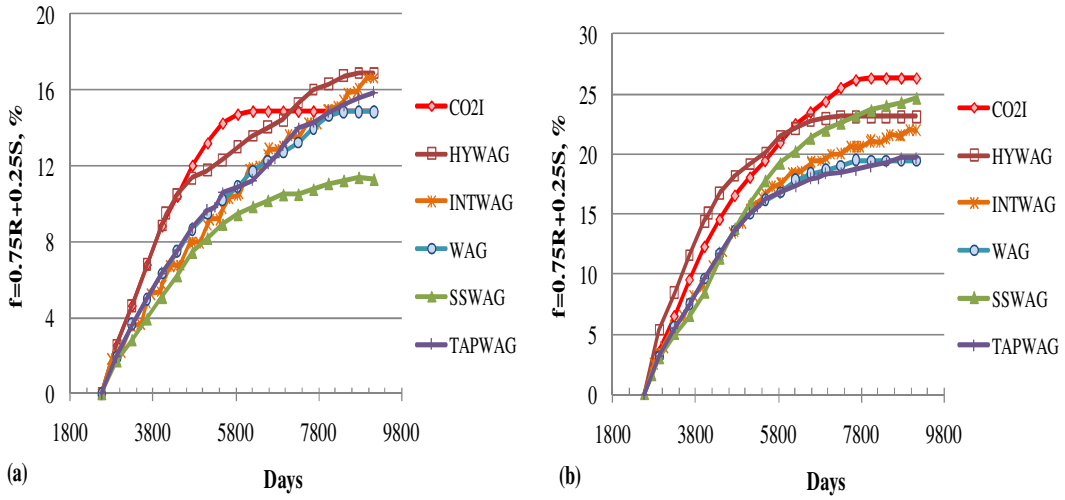

Figure 5.22: *f* profiles with higher priority to oil recovery (w_1=0.75 and w_2=0.25) for tertiary CO_2 injection strategies under (a) immiscible and (b) miscible flooding.

The *f* was plotted versus the weight w_1 in Figures 5.23 and 5.24 in order to determine how much the weight factor actually matters. w_1 = 0 means CO_2 storage is the objective of the injection while w_1 = 1 means enhancing oil recovery is the priority. For the secondary injection mode, CO2I exhibits the most drastic change in trend between miscible and immiscible processes, Figure 5.23. We can see here that the weight only maters beyond w_1 of about 0.75, else CO2I is always the most suitable injection strategy.

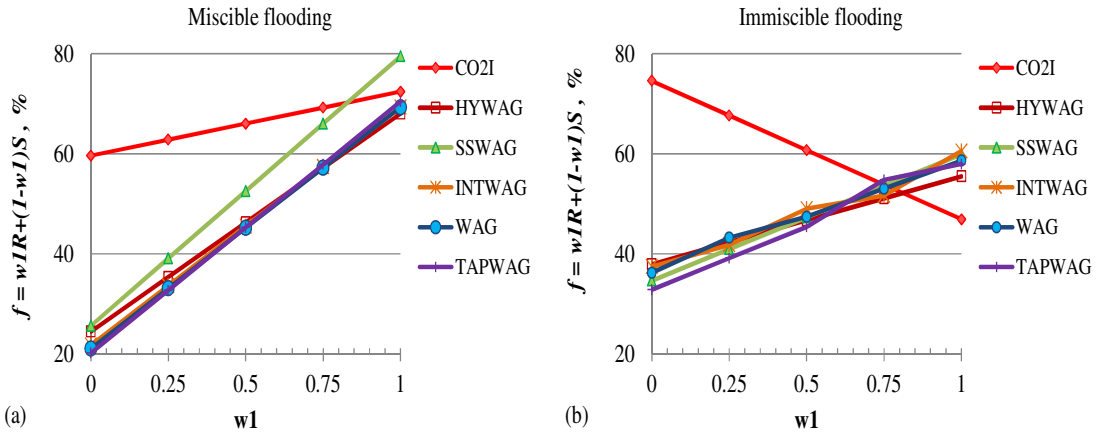

Figure 5.23: f versus w_1 for secondary CO_2 injection strategies under (a) miscible and (b) immiscible flooding mode.

Similar trend in f versus w_1 was observed for the miscible tertiary CO_2 injections where up to w1 of 0.85, CO_2 is the most suitable process. It is nevertheless interesting to see that the slopes of f versus w_1 plots are negative for the immiscible injections (Figure 5.24b) indicating that CO_2 storage contribution is more dominant than the oil recovery. The weight for ranking the immiscible tertiary injection schemes only matters when w_1 is smaller than 0.7.

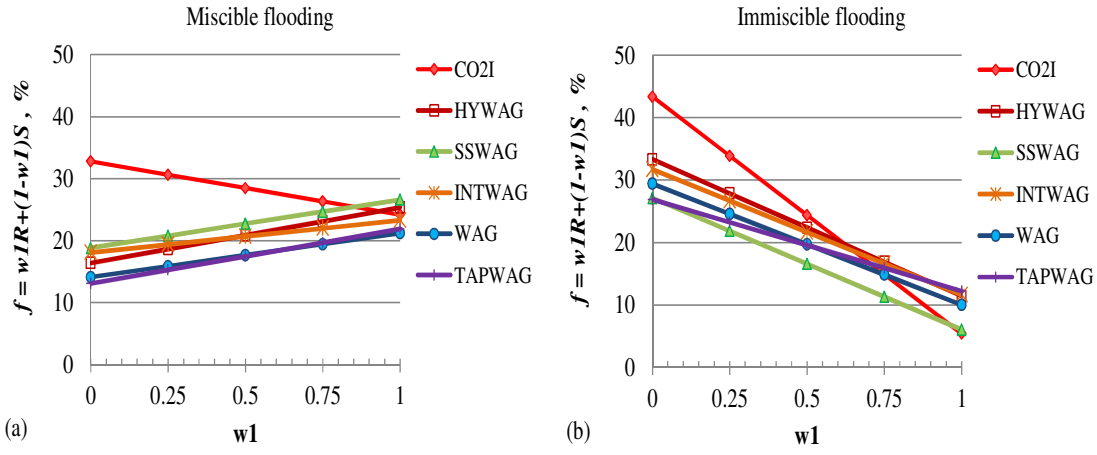

Figure 5.24: f versus w_1 for tertiary CO_2 injection strategies under (a) miscible and (b) immiscible flooding mode.

5.5. Economics associated with CO_2 EOR and storage

The results and discussions presented thus far are only based on the technical viability of the various gas-based CO_2 injection strategies for storing CO_2 through EOR. Yet CO_2 EOR projects are usually tied to high investments, which warrant comprehensive evaluation of the technical and financial uncertainties.

The cost of CO_2 EOR projects are influenced by many factors; the main ones include reservoir characteristics, rate of production, cost of capital, the future market price of crude oil, price of CO_2 at the field, CO_2 compression, recycling cost and inflation rates. Many of these are likely to fluctuate and have uncertainties. Integrating CO_2 storage as one of the injection objectives adds more elements to the economic model. As the cost of the anthropogenic CO_2 from the static sources is much higher than the CO_2 from natural sources, the cost of integrated CO_2 EOR and storage would inevitably be much higher too. Incentives such as CO_2 credits are being introduced to promote the implementation of this integrated process. However, it has not properly internalized yet by the industry and is also likely to vary from one country to another. The regulatory and tax structure for CO_2 sequestration are also unclear (Kuuskra et al., 2008).

Due to the complexity of the economic model for CO_2 EOR and storage, it is rather challenging to have a generic yet robust model for use during the screening stage. However, to get an insight on the effect of the economic factors on the ranking of the various CO_2 injection schemes evaluated, a simplified stand-alone project economics with discounted cash flow (DCF) in a spreadsheet format was prepared.

5.5.1. Discounted cash flow

DCF analysis is a method of valuing a project using the concepts of the time value of money where all future cash flows are estimated and discounted to give their present values (Equation 5.11). The net present value (NPV) is the sum of all future cash flows, both incoming and outgoing and is taken as the value of the project (Mian, 2002).

$$NPV = \sum_{t=0}^{N} \frac{FV_t}{(1+i)^t} \tag{5.11}$$

where FV is the future cash flow, i is the interest rate, which reflects the cost of tying up capital and may also allow for the risk that the payment may not be received in full.

Positive NPV shows the project is profitable whereas negative NPV indicates the project is making a loss. In this exercise, cash inflows are generated from the oil production while the outflows include the capital expenditure (CAPEX), operating expenditure (OPEX), cost of CO_2 gas injected and gas recycled. The assumed economic parameters used in the DCF analysis are shown in Table 5.8.

Table 5.8: Economic parameters for NPV calculations.

Parameter	Value	Unit	Reference
Oil price	50	$/bbl	Average value of the last decade http://forecasts.org/data
CO_2 price	2.38	$/Mscf	Ferguson et al., 2010
Escalation of Oil and CO_2 price	2	% per year	Assumed to be the same as the inflation rate
Total Operating Expenditure	3.1	$/stb of oil produced	Ferguson et al., 2010
Total Capital Expenditure	2.1	$/stb of oil produced	Ferguson et al., 2010
Recycled cost	0.75	$/Mscf	Assumed value
Escalation of all operating cost	2	% per year	Assumed to be the same as the inflation rate
Royalty	12.5	%	Assumed value
Discount rate	10	%	Mian, 2002

The CAPEX in all cases was assumed to be the same i.e., four injector wells at an estimated $10 million per well and a CO_2 recycling plant of $5 million for the CO_2 injections. The following additional assumptions were also made:

- The price of CO_2 used is inclusive of its transportation and compression.
- Water for injection is available at no cost.

- CAPEX incurred in the year the CO_2 injection starts.
- Cost of emitted CO_2 from the use of energy is not accounted for.
- Revenue from selling of produced gas is not considered.
- Neither EOR credit nor CO_2 credit is considered.
- Calculated NPV used is before tax.

Further description on the NPV calculations is given in Appendix A5.2.

The main economic incentive for any CO_2 EOR project is always the profit per barrel of oil (Hustad et al., 2004). For a coupled CO_2 EOR and storage project, the incentive would naturally be the combination of profit per barrel of oil, R^*, and profit per Mscf of CO_2 stored, S^*, which were used in ranking the CO_2 injection schemes evaluated:

$$R^* = \frac{NPV}{N_p} \tag{5.12}$$

$$S^* = \frac{NPV}{V_{CO2}^*} \tag{5.13}$$

where NPV is the net present value of the project, V_{CO2}^* is Mscf of CO_2 stored in the reservoir and N_p is the total oil produced during CO_2 injection period. For the tertiary process, the NPV used in Equation 5.12 and 5.13 was the overall project NPV minus that of the WI. Ghomian et al. (2008) had used more or less similar parameters but differed in some of the economic parameters and assumptions used.

5.5.2. Ranking of CO_2 injection schemes incorporating the economic factors

Table 5.9 shows the summary of the profits of oil produced and CO_2 stored as well as the equal-weighted function, *f*, for the secondary injection processes. The results clearly show that incorporating economic factors into the evaluation of the injection strategies changes the ranking. TAPWAG injection is now the favoured injection scheme that gives the highest profit per volume of CO_2 gas stored under miscible conditions. Immiscible TAPWAG brings the highest profit per barrel of oil produced and is most likely to co-optimize the oil

recovery and CO_2 storage economically.

For the tertiary injection mode, Table 5.10, oil recovery and CO_2 storage is generally more economic when carried out under miscible conditions. Whilst the best dollar value of CO_2 stored can be achieved with the miscible TAPWAG injection, the highest profit per barrel of oil is given by the miscible WAG injection and this injection scheme is also economically viable to co-optimize oil recovery and CO_2 storage.

Table 5.9: Profit of oil produced, CO_2 stored and f values, for secondary CO_2 injections.

Process	$R^*=NPV/N_{pt}$		$S^*=NPV/V_{CO2}$		$f = 0.5(R^*+S^*)$	
	BHP	RATE	BHP	RATE	BHP	RATE
CO2I	13.71	11.97	2.28	2.65	8.00	7.31
WAG	19.14	17.83	8.26	9.81	13.70	13.82
SSWAG	18.89	17.00	8.78	8.57	13.83	12.79
HWAG	15.98	15.25	6.53	7.69	11.25	11.47
TAPWAG	**20.10**	17.91	9.57	**10.39**	**14.83**	14.15
INTWAG	18.89	18.02	8.14	9.72	13.51	13.87

Table 5.10: Profit of oil produced, CO_2 stored and equally weighted R* and S* values, for the tertiary CO_2 injections.

Process	$R^*=NPV/N_{pt}$		$S^*=NPV/V_{CO2}$		$f = 0.5(R^*+S^*)$	
	BHP	RATE	BHP	RATE	BHP	RATE
CO2I	-12.46	9.78	-0.40	1.35	-6.43	5.57
WAG	3.04	**16.29**	0.31	4.13	1.68	**10.21**
SSWAG	2.38	14.10	0.33	3.28	1.36	8.69
HWAG	0.78	15.30	0.09	3.67	0.43	9.49
TAPWAG	3.27	15.92	0.42	**4.46**	1.84	10.19
INTWAG	1.64	14.35	0.18	3.21	0.91	8.78

The cross plot of R* and S* for the secondary injections in Figure 5.25 exhibits no clear trend especially for the miscible injections (Figure 5.25a) unlike that of the R - S plots in Figure 5.17. A much clearer trend between R* and S* can however be seen when these two are plotted against time, as presented in Figure 5.26. The NPVs were initially negative due to the capital expenditure for CO_2 injection (the scale of the plots, however, was set to start

from zero). The oil recovery profits, R*, were relatively high during the early years of injection since the oil production was the highest then gradually declined and levelled off. For CO2I, S* follows more or less the same trend as R*, while for HYWAG injection, S* is anti-correlated with R* such that S* increases when R* decreases. For the other injection schemes, S* was relatively low at the beginning, then gradually increased before declining as more and more oil was recovered and CO_2 stored without equivalent increase in NPV. Fluctuation in S* was observed for the injection schemes that involved periodic CO_2 injections.

The plots of f (= w_1R* + (1-w_1)S*) versus w_1 for the secondary injection schemes in Figure 5.27 confirms that TAPWAG injection tops the ranking regardless of the weight used. This shows that the R* and S* are quite robust as the ranking parameters.

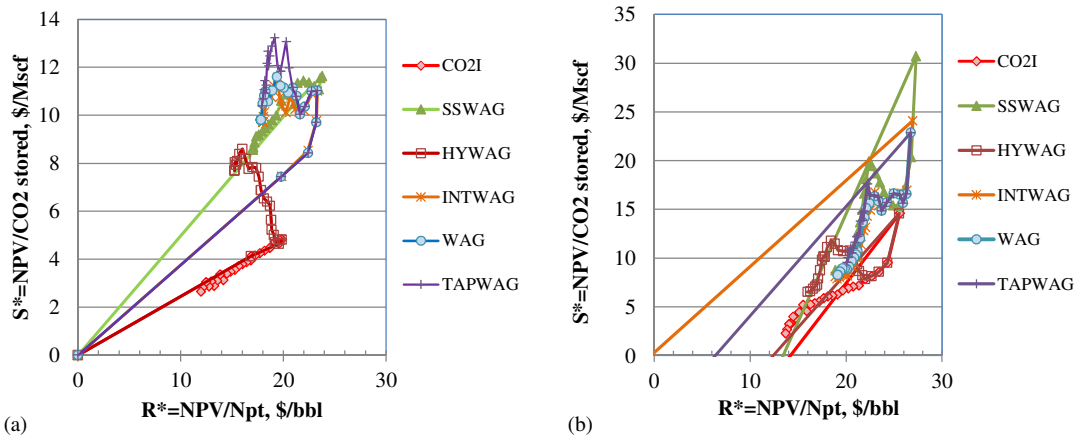

Figure 5.25: Cross-plots of S* and R* for the secondary CO_2 injections under (a) miscible and (b) immiscible flooding.

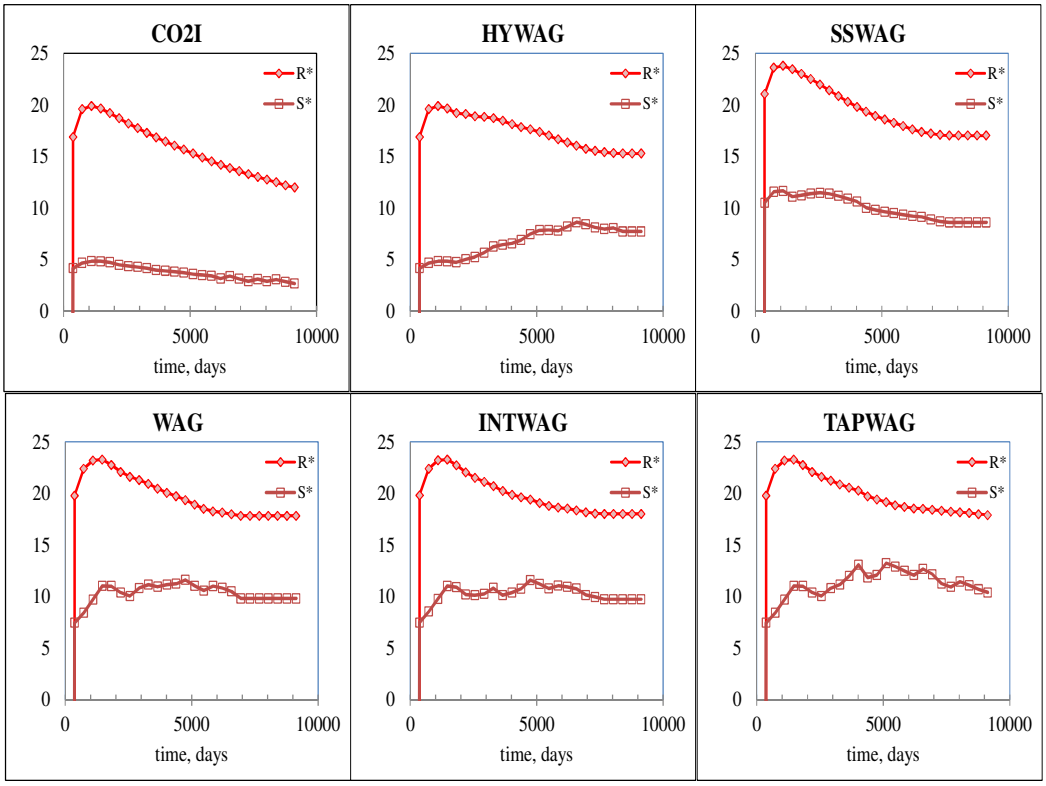

Figure 5.26: Plots of S* and R* aganst time for the miscible secondary CO_2 injections.

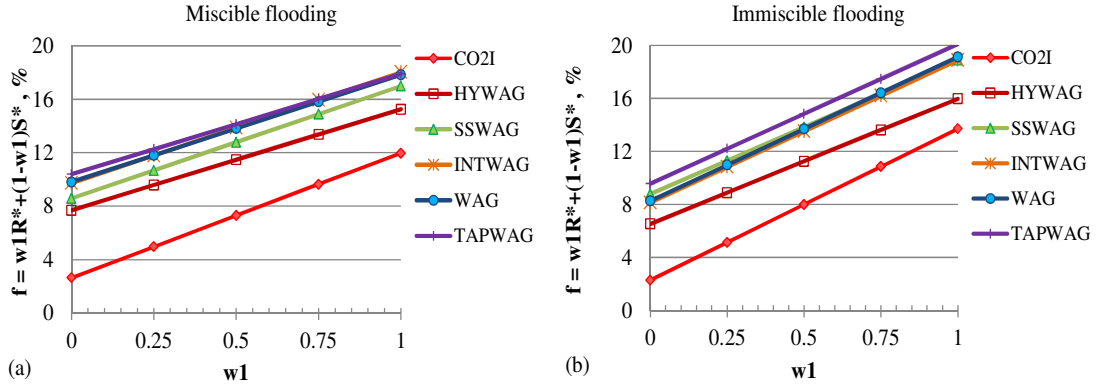

Figure 5.27: *f* (incorporating the economic factors) versus w_1 for secondary CO_2 injection strategies incorporating the economic factors under (a) miscible and (b) immiscible flooding.

Again, no clear trend between R* and S* was observed for the tertiary injections, Figure 5.28. At any given w_1, the miscible injections give higher *f* than the immiscible injection methods. The weight is immaterial in ranking the most profitable process. As shown in Figure 5.29, miscible WAG injection has the highest *f* values regardless of the w_1 used, closely followed by SSWAG injection.

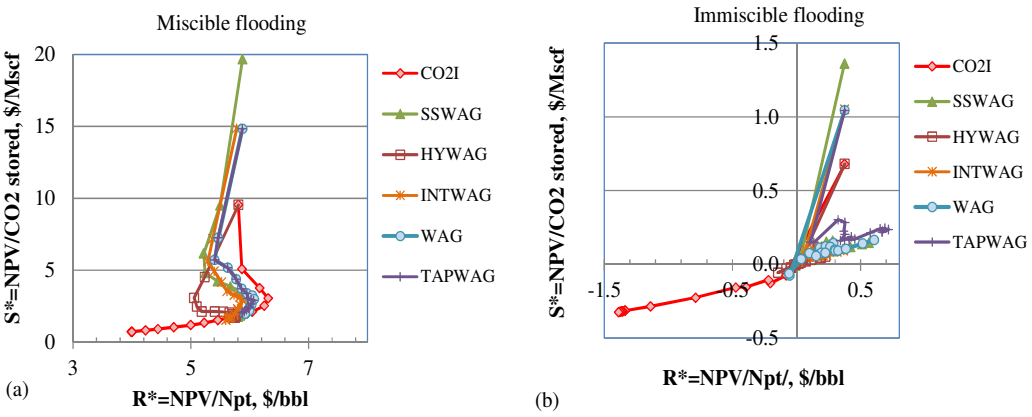

Figure 5.28: Cross-plots of S* and R* for the tertiary CO_2 injections under (a) miscible and (b) immiscible flooding.

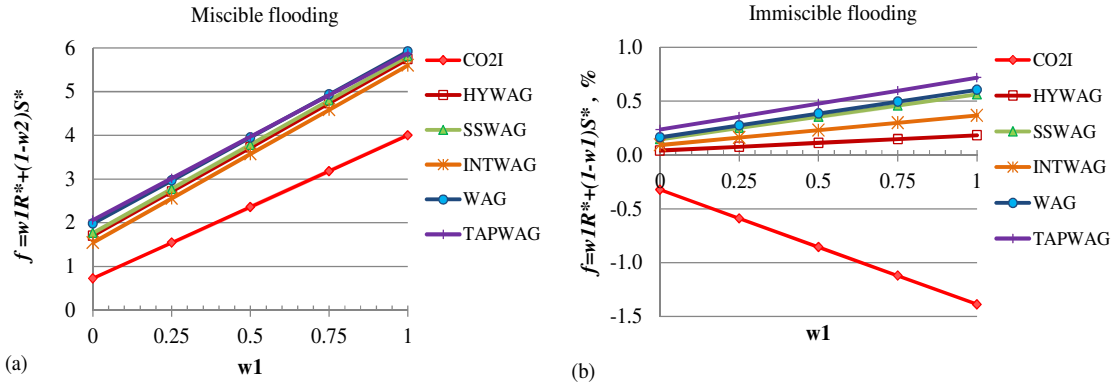

Figure 5.29: *f* incorporating the economic factors versus w_1 for tertiary CO_2 injection strategies under (a) miscible and (b) immiscible flooding.

5.5.3. Sensitivity study on different economic scenarios

The results presented thus far were based on the assumed constant economic parameters as given in Table 5.8. However, not only the economic parameters, such as the oil price, CO_2 price, inflation rate and OPEX, are susceptible to fluctuation and uncertainty, there are also different economic scenarios that may have huge influence on the viability of the coupled CO_2 EOR and storage projects.

One important economic scenario is the provision of carbon credits as a tax incentive for storing CO_2 to reduce the greenhouse gas emission in

to the atmosphere. Most of the active CO_2 EOR projects in the USA, for instance, are relying on the much cheaper natural CO_2 source. Without any tax incentives that can offset the incurred costs, it will be difficult to attract the oil producers to use the much more expensive anthropogenic CO_2 source for EOR or storage. Another scenario that affects the economics of the coupled process is the offshore versus onshore application. CO_2 injection into offshore reservoirs is expected to be significantly more expensive than into onshore reservoirs mainly due to higher drilling costs and the requirement of platform installation in the former.

A sensitivity study on selected economic parameters was carried out taking also into consideration the two economic scenarios described above. The main objectives were to quantify how much credit would make CO_2 sequestration through EOR process economical and also to examine the effect of uncertain economic parameters on the CO_2 credit. It is well understood that positive NPV means the project is profitable. From Table 5.10, only the immiscible CO_2 injection gives negative NPV without any incentives. As such, only this injection scheme was evaluated in the CO_2 credit sensitivity study.

Economic sensitivity study approach

The performance of the immiscible tertiary CO2I in the heterogeneous reservoir model was used as the case study to demonstrate the need for the CO_2 credit incentive. The effect of other uncertain economic parameters on the required credit was also studied. The

parameters and their range of uncertainty are shown in Table 5.11 with CO_2 credit required as the only response factor. The CO_2 credit required was estimated as the value that leads to project breakeven point or zero NPV. One can easily figure out that getting a CO2 credit higher than the required value will bring profit (positive NPV) to the project.

Table 5.11: Economic factors sensitized for the assessment of CO_2 credit requirement.

Factor	Name	Units	Type	Subtype	Minimum (-1)	Maximum (+1)
A	Oilprice	$/bbl	Numeric	Continuous	20	80
B	CO2price	$/Mscf	Numeric	Continuous	1.59	3.17
C	Inflation	%	Numeric	Continuous	2	4
D	Operation		Categoric	Nominal	Onshore	Offshore

For the offshore application, the costs of drilling of the injection well and recycling plant, the fixed OPEX (this is basically the maintenance cost of the equipment and hardware), variable OPEX and the recycling costs were assumed to be two times higher than the base case values (assumed for onshore application) given in Table 5.8. The uncertainty of the inflation rate, which was reflected in the escalation factor of the oil and CO_2 gas price and the OPEX, was also considered.

The conventional sensitivity study where one parameter is varied at a time (OFAT), keeping all other parameters at the base case value, not only suffers from being extremely inefficient as the number of runs could become prohibitively large, but more importantly, it cannot detect interactions of factors. In general, N parameters varying at p levels would results in p^N simulation runs. As in this study, full factorial for 11 parameters at 2 levels requires 2^{11} or 2048 simulations, which are too expensive to run.

In order to maximize the amount of unbiased information regarding the factors affecting the coupled CO_2 EOR and storage process by the CO2I injection but from minimum number of simulations, the design of experiment (DOE) approach was employed. DOE has been used in many areas of reservoir engineering, for example, by Damsleth et al. (1992), Egeland et al. (1992) and White et al. (2003) to study the effects of uncertain reservoir parameters on

production, by Oliveira et al. (2009) to evaluate heavy oil recovery and by Sifuentes et al. (2009) to study the influence of different physical properties on the effectiveness of CO_2 storage in aquifers. With this experimentation strategy, the same information as obtained with the OFAT method can be developed with a minimal number of simulation runs, without losing information (Damsleth et al., 1992). Moreover, as DOE examines all of the variables simultaneously, the interactions between factors can also be examined, which would otherwise not be possible when using the OFAT approach.

A specialized DOE software package, Design-Expert® version 8.0.6 (State-Ease Inc's software), was employed to determine the experimental design pattern and calculate the statistical results. Since the analysis involved both numeric and categoric parameters, the D-optimal experimental design was selected. The D-optimal criteria were developed to select design points in a way that minimizes the variance associated with the estimates of the specified model coefficients. More description on the D-optimal design is given in Appendix A5.3. A polynomial model with quadratic order of terms was found to give a high fraction (> 90%) of design space. 101 runs were identified, details of which are given in Table A5.3 of Appendix A5.3.

Sensitivity study results

Using the economic parameters in Table 5.8, the sensitivity study found that a CO_2 credit of \$4.2 and \$5.13 per Mscf of CO_2 stored is required to make the tertiary immiscible CO2I project to breakeven for the onshore and offshore project, respectively. The calculated CO_2 credits required for the range of economic parameters sensitized are summarized as a histogram in Figure 5.30 with details in Table A5.4 in Appendix A5.3. The absolute values of the CO_2 credit may not mean much as the reservoir model used is a hypothetical one, nevertheless, the results give a valuable insight on the effect of uncertain economic parameters on the CO_2 credit requirement in both onshore and offshore application of immiscible CO2I. As expected, the required CO_2 credit for the onshore project is generally lower than that required for the offshore project mainly due to the higher CAPEX and OPEX for the offshore operation.

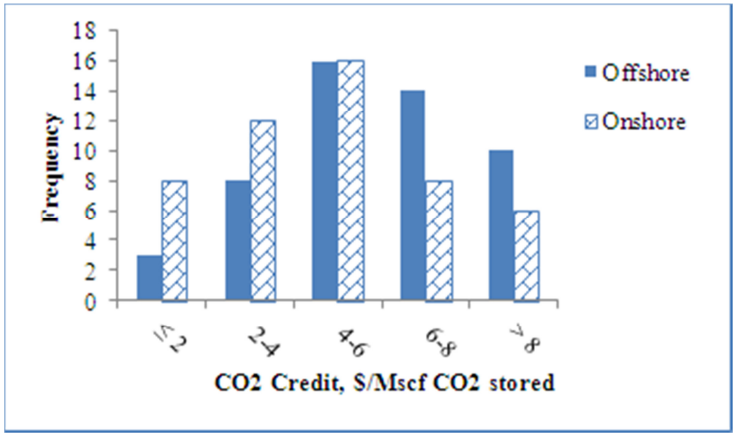

Figure 5.30: Range of CO_2 credits required for immiscible tertiary CO2I.

To build confidence with the statistical analysis of the data, the response models on the CO_2 credit was evaluated using analysis of variance (ANOVA). ANOVA is a statistical test using the F-distribution (probability distribution) function and information about the variances within each population and between grouping of populations to help decide if variability between and within each populations are significantly different. More description of the ANOVA is given in the Appendix A5.4.

Shown in Table 5.12 is the statistics for the model. As indicated by the R-squared value (a measure of the amount of variation around the mean explained by the model), 100% of the variation in the model has been described by the model. The predicted versus actual plot, i.e., the graph of the predicted response values versus the actual response values in Figure 5.31 also shows a 45° straight line indicating that all the response values are predicted by the model. This means, the resulting equation of the CO_2 credit, with coefficients of the actual factors as given in Table 5.13, can be used as a proxy model to calculate the CO_2 credit required for a given oil price, CO_2 price, inflation rate and onshore or offshore operation.

Table 5.12: Summary of the statistics for the model.

Std. Dev.	9.00E-03	R-Squared	1.0
Mean	5.3	Adj. R-Squared	1.0
C.V. %	0.17	Pred. R-Squared	1.0
PRESS	9.39E-03	Adeq. Precision	3248

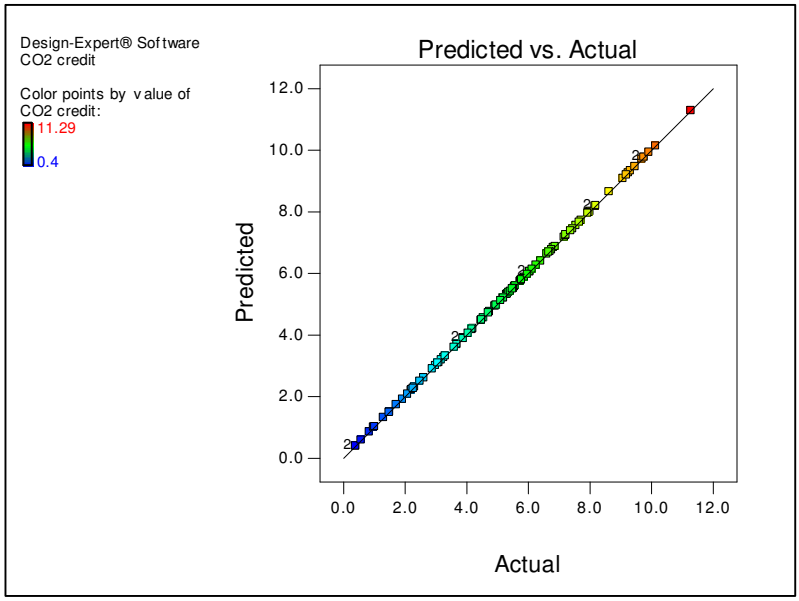

Figure 5.31: A graph of the actual versus predicted values of the CO_2 credit required for the tertiary immiscible CO2I process.

Table 5.13: Coefficients of the final equation of CO_2 credit required in terms of actual factors.

Factor	Constant	* Oilprice	* CO2price	* Inflation	* Oilprice * CO2price	* Oilprice * Inflation	* CO2price * Inflation	* Oilprice^2	* CO2price^2	* Inflation^2
Coefficient - Onshore	1.04917	-0.045556	1.92488	-0.13509	-1.27E-05	-6.78E-03	0.3472	2.11E-06	-4.76E-03	0.038743
Coefficient - Offshore	1.79411	-0.045596	1.92405	-0.03388	-1.27E-05	-6.78E-03	0.3472	2.11E-06	-4.76E-03	0.038743

Figure 5.32 shows the perturbation plot of the CO_2 credit. The perturbation plot of a response shows how it changes as each factor moves from the chosen reference point, with all other factors held constant at the reference value, and thus gives a perspective on the model. A steep slope or curvature in a factor shows that the response is sensitive to that factor. It is evident that the CO_2 credit is very strongly influenced by the oil and CO_2 price and not so much by the escalation factor. The perturbation plot for the onshore operation was found to be very similar.

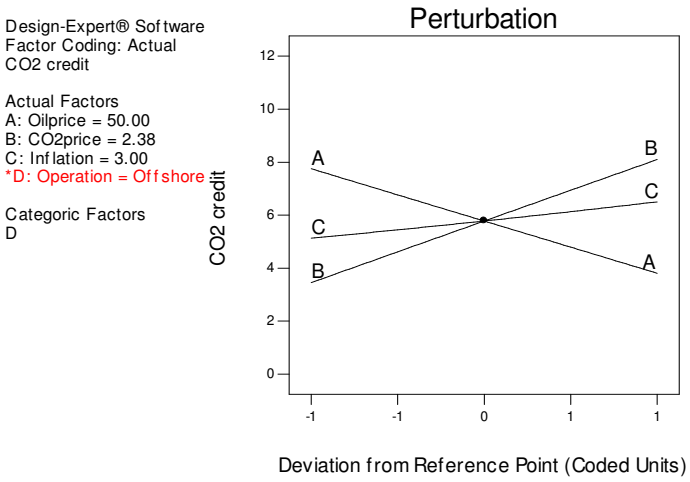

Figure 5.32: Perturbation plot for CO_2 credit for the tertiary immiscible CO2I injection offshore.

The oil and CO_2 price were subsequently selected as the axes in plotting the contour plot. The contour plot is a two-dimensional representation of the response across the select factors. In the case where there are more than two factors the 2D surface can be thought of a slice through the factor space. The contour lines represent the value of the CO_2 credit. The surface becomes red at higher response level, yellow in the middle, and green at lower level. As can be seen in Figure 5.33, relatively low CO_2 credit is required when the oil price is high and CO_2 price is low. Understandably, providing the same incentive to the other injection schemes, which originally show positive NPV even without any incentives, will make those processes more profitable.

5.6. Discussion

The evaluation of various CO_2 injection strategies in this study is helpful in increasing the understanding of CO_2 injection performance both as secondary and tertiary oil recovery methods, either solely for EOR or CO_2 storage or for coupled oil recovery and CO_2 storage, from the technical and economics point of view. The evaluation also gives some important insights on the potential of a newly conceptualised injection strategy, INTWAG injection, for EOR and CO_2 storage purpose.

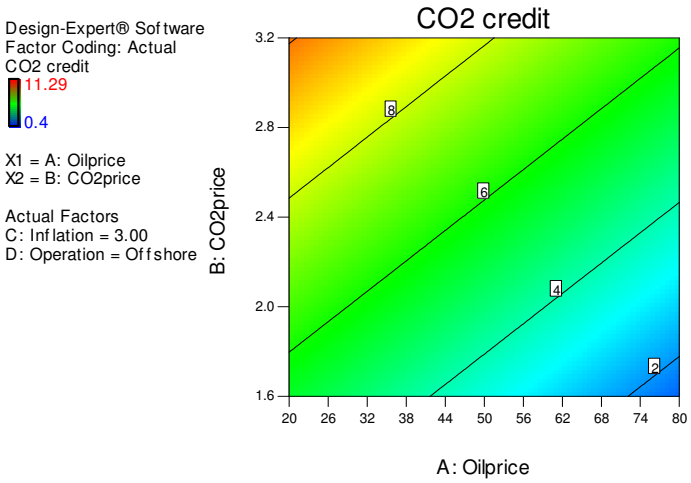

Figure 5.33: Contour plot of oil price (A) and CO_2 price (B) for CO_2 credit of the offshore tertiary CO2I process with the inflation set at 3%.

5.6.1. INTWAG injection

Shutting in the production wells after a period of CO_2 injection, during which CO_2 was dissolved in oil, has been reported to be beneficial to the oil recovery. In this study, INTWAG injection, which also involves shut-in period, was evaluated through numerical simulation, on its potential as CO_2 EOR and storage injection strategy.

INTWAG injection was proposed to benefit from two main CO_2 recovery mechanisms; the controlled mobility of gas by the alternate water injection as in the conventional WAG process and improved mass transfer between the oil and CO_2 during the soak period. When CO_2 gas is injected, it displaces the oil and water near the injection well (drainage process). When the well is shut in, natural imbibition would occur as the gas, water and oil phase redistributes itself within the well drainage area. The hysteresis process would result in some gas being trapped. This phenomenon is beneficial to CO_2 storage and induces low gas relative permeability, which increases the oil recovery through increase in the oil relative permeability. Figure 5.34 shows the saturation profiles of CO_2 gas (left column) and the CO_2 amount in the aqueous phase (right column) at various times in the YZ cross-section of the model passing through INJ1 and INJ3 injection wells (refer to Figure 5.3 for well locations). In the given plot, INJ1 is the well on the left while INJ3 is on the right.

By 237 days (topmost plot in Figure 5.34), 2.5% HCPV of CO_2 has been injected in INJ1. We can see that CO_2 has penetrated into the reservoir away from the injection well as indicated by a much larger area of CO_2 solubility in water (right column plot) than that of the gas saturation (left column plot). After a shut in period (shown in plots at time 474 and 711 days), the gas saturation diminishes and the CO_2 diffuses further away into the in-situ oil and water. The subsequent water injection (shown in plot at time 948 days) pushed the CO_2 even further away from the wellbore.

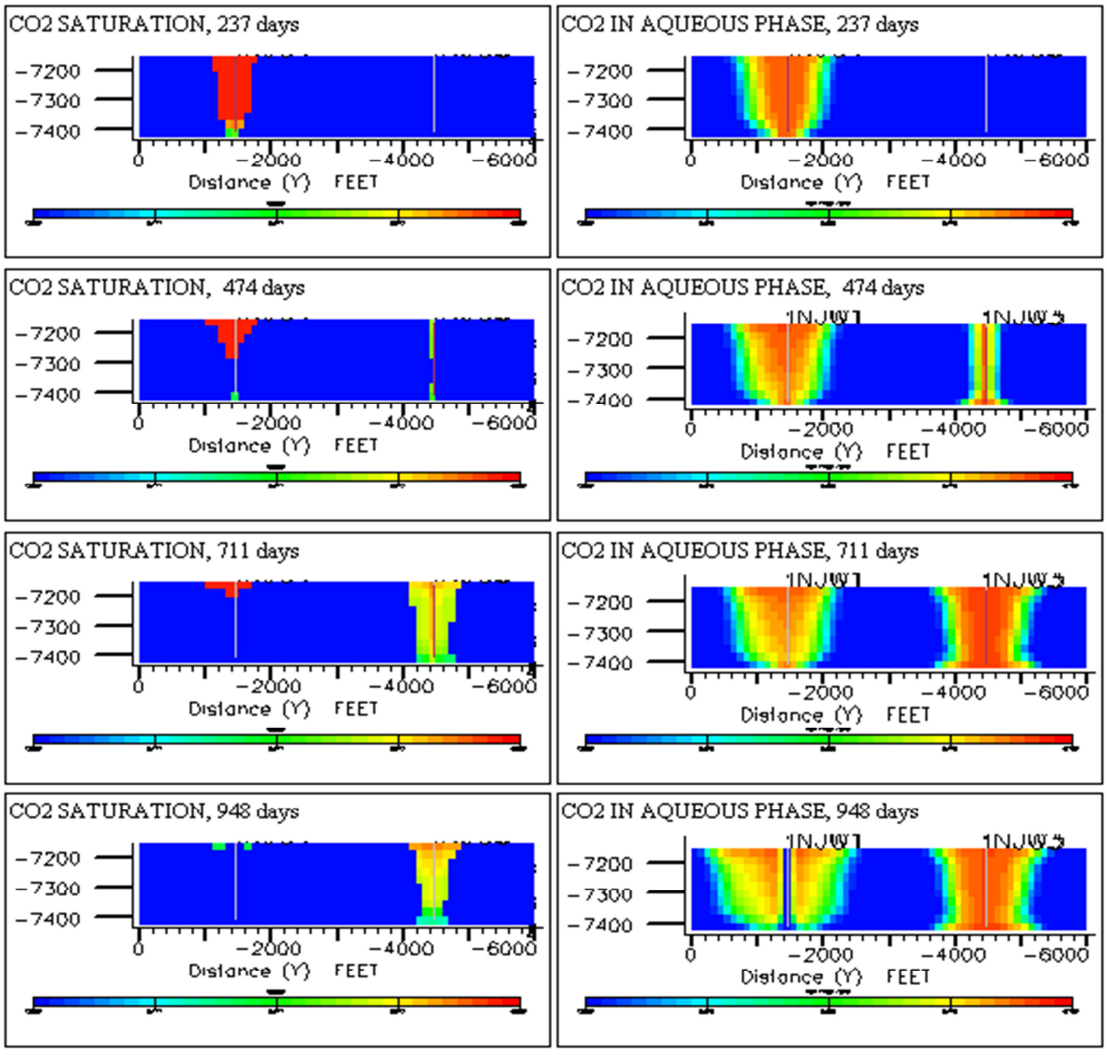

Figure 5.34: Saturation profiles for CO_2 gas (left column) and CO_2 solubility in the aqueous phase (right column) at various time, for miscible secondary INTWAG injection.

In continuous CO_2 injection, due to the adverse viscosity ratio between the oil and CO_2, bypassing of oil would occur behind the flood front, thus, more CO_2 is needed to contact more oil. In INTWAG injection, the shut in period is meant to give longer time for CO_2 to diffuse into the by-passed oil, particularly for the tertiary process, where mobile water is present. The diffusion dampens the transverse dispersion and consequently increases the mass transfer between the injected CO_2, without having to inject more CO_2. Oil swelling would increase, which favourably increases the oil relative permeability and oil viscosity reduction, which in turn improves the mobility of the oil to the producer wells. Miscible INTWAG performs better in terms of oil recovery. However, the reverse is true for the CO_2 storage where much higher CO_2 retention per barrel of oil produced was predicted under the tertiary recovery mode.

Parametric simulation results show that in INTWAG injection, larger slug size is favourable for CO_2 storage. The 'soak time' equivalent to 7% HCPV slug size increases oil recovery from miscible INTWAG injection by 8% but has little impact on the immiscible process. On one hand, a larger slug size injected means a longer soak time is required to reach equilibrium between the CO_2 and the fluids in place, but on the other hand, it also means a longer time is available for CO_2 diffusion in the pattern with the closed injector and producer. There is only a limited amount of CO_2 that can dissolve into the oil under immiscible condition, thus extending the soak time does not really bring in significant additional oil. There must be an optimum soak time beyond which incremental recovery is negligible. Conversely, in the miscible process, the CO_2 solubility in oil and the resulting oil swelling are much larger, thus a longer time available for diffusion leading to more oil recovery.

The sensitivity of the WAG ratio in INTWAG injection shows similar behaviour as that reported for the conventional WAG injection in that at very low WAG ratio (that is, too much gas is injected), oil recovery performance deteriorates. Gravity segregation causes the gas to tongue at the top of the reservoir and consequently reduces the gas sweep efficiency. Too much water, as at high WAG ratio, will lead to water underride which also reduces displacement efficiency.

In tertiary INTWAG injection, the higher water saturation reduces the amount of CO_2 that dissolves in oil. With a longer shut in period, apart from dissolving more CO_2 into the oil,

more CO_2 could be dissolved into the water too and increases the density of the water (Hebach, 2004). Part of the CO_2-diluted oil will be recovered, which contributes to the additional oil recovery. However, a large part of the injected CO_2 will remain dissolved in the remaining oil, which is important from the CO_2 storage perspective. It is believed that if the CO_2 diffusion into the water can be appropriately modelled (which the simulator used in this exercise could not do when the oil phase is present), more distinct results could have been observed when the soak time changes even in the immiscible INTWAG injection.

The evaluation concludes that INTWAG injection results in higher incremental recovery compared to waterflood and has potential as CO_2 EOR and storage injection strategy. It performs better than WAG injection under the immiscible conditions, in that it requires much less CO_2 per volume of incremental oil recovered and higher amount of CO_2 stored.

5.6.2. CO_2 injection for EOR and storage

Simulation results in this study clearly show that to maximize oil recovery requires a different injection strategy than that to maximize the CO_2 storage and both could also be different from the injection scheme that co-optimizes oil recovery and the amount of CO_2 stored. The control mode of the production, which affects the reservoir pressure and thus the miscibility between CO_2 and the oil, also strongly influences the performance of the integrated process.

Table 5.14 summarises the oil recovery, CO_2 stored and *f* factors with equal weight of oil recovery and CO_2 storage for all the simulated cases **without** the economic factors. Under the miscible conditions, secondary CO_2 injections resulted in higher and earlier incremental oil recovery than the tertiary process, as expected. In the secondary processes, CO_2 can easily contact the oil whereas the presence of the mobile water phase from the preceding waterflood in the tertiary recovery method hampers CO_2 from contacting the residual oil (Shelton et al., 1978; Tiffin et al., 1983). Several studies (for example by Grogan, et al., 1987, 1988; Campell, et al., 1985; Bijeljic, et al., 2002) have also shown that the presence of a water layer separating the oil and CO_2 phases adversely affects the CO_2 diffusion into the oil.

Table 5.14: Comparison of oil recovery factor, CO_2 storage and *f* function; secondary and tertiary CO_2 injection strategies.

Injection scheme	Fixed BHP production constraint (immiscible flooding)						
	R = Np*/STOOIP, %			S = V_{CO2}/PV, %		*f* = 0.5R+0.5S	
	Secondary	Tertiary		Secondary	Tertiary	Secondary	Tertiary
		Total	Post WI				
WI	52.97			-		26.61	
CO2I	44.56	55.97	5.39	**74.58**	**43.35**	59.57	24.37
WAG	58.60	60.57	9.99	36.20	29.41	47.40	19.70
HYWAG	55.50	61.99	11.41	37.92	33.31	46.71	22.36
SSWAG	59.89	56.61	6.03	34.64	27.08	47.26	16.56
TAPWAG	57.94	62.79	12.21	32.83	26.88	45.39	19.54
INTWAG	60.52	62.18	11.59	37.46	31.68	48.99	21.64
Injection scheme	Fixed rate production constraint (miscible flooding)						
	R = Np*/STOOIP, %			S = V_{CO2}/PV, %		*f* = 0.5R+0.5S	
	Secondary	Tertiary		Secondary	Tertiary	Secondary	Tertiary
		Total	Post WI				
WI	50.70			-		25.35	
CO2I	72.39	67.58	24.17	59.63	32.78	**66.01**	**28.48**
WAG	69.27	64.61	21.21	21.04	14.11	45.15	17.66
HYWAG	68.00	65.37	21.96	24.45	16.41	46.23	19.18
SSWAG	**79.45**	**70.02**	**26.61**	25.62	18.84	52.54	22.72
TAPWAG	70.39	65.27	21.87	20.16	13.10	45.27	17.48
INTWAG	69.29	66.69	23.28	21.74	18.08	45.51	20.68

Note: The 'Post WI' recovery shown for the tertiary process refers to the oil produced during the CO2 injection phase only.

It is also evident from the results that a significant loss in oil recovery would occur if the average reservoir pressure dropped below the MMP, as was the case for oil productions under the BHP constraints. In the immiscible flooding, CO_2 swells the oil and reduces the oil viscosity only to certain extent (Klins, 1984), but the residual oil saturation is not affected. As can be seen in Table 5.14, the total recoveries of the immiscible tertiary process are higher than those from the corresponding secondary injections, except for the SSWAG injection. Water has higher viscosity and better mobility control than gas thus WI gives higher recovery, particularly prior to breakthrough, than CO_2 gas injection.

For the reservoir and conditions used in this study, the best injection strategy, technically, for maximizing the oil recovery is miscible SSWAG injection while the highest CO_2 stored was obtained under immiscible CO2I with pressurization of the reservoir after EOR period. The most promising injection scheme to co-optimize oil recovery and CO_2 storage was found to

be the miscible CO2I.

The miscible SSWAG injection outperforms the other injection schemes in both secondary and tertiary recovery, with the lowest CO_2 utilisation. In the normal WAG and SWAG injection where the injectors are open to flow in all layers, water and gas encroachment in the bottom and top perforations of the producers, respectively, hastens gas and water breakthrough. The SSWAG injection effectively minimises the gravity segregation effects and gives much higher overall sweep efficiency by delaying breakthrough and increasing the contact area between the injected CO_2 and oil.

High pressure flooding and miscibility, however, work against CO_2 storage. This is evident by the much lower CO_2 storage under high pressure flooding mode. Low reservoir pressure at the start of the CO_2 injection provides more storage capacity for CO_2, and this is further enhanced by additional CO_2 injection after the production has ceased. Simulation results in this study indicate that re-pressurization accounts for about 35% of total CO_2 storage in the immiscible CO2I.

It is however worth mentioning that whilst the depth of the reservoir used in this evaluation (7285 ftss) is quite typical in an EOR project, it might be on the high side of the reservoir depths commonly encountered in CO_2 storage projects. The density of CO_2 beyond its critical pressure (approximately at depth of 800 m or 2500 ft) does not change very much thus injecting into deeper reservoirs would involve a much higher compression cost without much added benefit in terms of volume of CO_2 that could be stored.

Another main finding from this simulation study is that injection schemes that were traditionally designed for minimizing CO_2 utilization per incremental volume of oil produced, such as WAG, SSWAG and TAPWAG, are not, technically, performing so well in terms of CO_2 storage. Despite having the advantage of improved sweep efficiency from the controlled gas mobility by the alternate slug of water, the injected water in these injection schemes competes with the injected CO_2 for the pore space. This leads to only about half the CO_2 or less as in the CO2I being stored.

The ranking of the injection schemes however significantly changed when even simple economic factors are taken into account. The injection schemes that are traditionally

designed for minimizing CO_2 utilization per incremental volume of oil produced are still the most economic for the coupled CO_2 EOR and storage purpose. Immiscible CO2I process would have negative NPV (i.e. not economical) if no incentive for storing CO_2 with EOR is provided. Sensitivity study shows that the CO_2 credit required to making the CO2I injection economical for EOR and storage is greatly influenced by the oil and CO_2 price and whether the project is onshore or offshore. The ranking parameters, R* and S*, were also found to be quite robust such that the ranking was not influenced by the weight used.

5.7. Summary and conclusions

Storing CO_2 through EOR in an oilfield not only aims to increase the oil recovery but also to maximize the amount of CO_2 left behind at the end of the recovery. These objectives are significantly different from maximizing the oil recovery alone and require optimization. A practical work flow was developed for ranking and optimizing the injection strategies suited for CO_2-flood EOR and storage for a given reservoir.

The main features of the method include the evaluation of various CO_2 injection schemes through compositional reservoir simulation. Simulations calculate the incremental oil recovery and the amount of CO_2 sequestered in the reservoir. Two sets of ranking parameters were used in selecting the CO_2 injection method with the highest potential; an objective function f of equally weighted oil recovery and CO_2 storage and the equally weighted profit per barrel of oil produced and profit per Mscf of CO_2 stored. Ranking of the injection schemes by the f values incorporating the economic factors identifies the CO_2 injection strategy with the highest potential to co-optimize EOR and CO_2 storage economically. Different weights could be assigned to oil recovery and CO_2 stored, depending on the primary objective of the CO_2 injection.

A newly conceptualized INTWAG injection scheme, that involves alternating CO_2 and water injection between phases and well patterns, was also evaluated together with CO2I, WAG, HYWAG, SSWAG and TAPWAG injections.

From the simulation study, it was concluded that:

5.7.1. INTWAG injection

- INTWAG injection could increase the oil recovery above that of waterflooding.
- Under immiscible conditions, INTWAG requires much less CO_2 per incremental oil recovered and stores higher amount of CO_2 than normal WAG injection.
- Large slug size is beneficial to the CO_2 storage and oil recovery under miscible condition but has small impact on oil recovery under the immiscible process.
- There is an optimum WAG ratio corresponds to the highest oil recovery. Smaller WAG ratio is preferred for CO_2 storage using this injection scheme.

5.7.2. CO_2 injection strategies for oil recovery and storage

- The injection strategy to maximize the oil recovery is different from that to maximize CO_2 storage, which in turn is different from the injection scheme that co-optimizes both oil recovery and CO_2 storage.
- The injection schemes that traditionally designed for minimizing CO_2 utilization per incremental volume of oil produced are technically not performing well for CO_2 storage.
- The control mode of the production, which affects the reservoir pressure strongly influences the process performance. For maximum oil recovery and CO_2 storage, higher reservoir pressure which reaches miscible displacement should be targeted and maintained throughout the flooding.
- Miscible CO_2 injections give higher oil recovery than the corresponding immiscible process but the reverse is true for CO_2 storage.
- Based on the predicted performance only, the best injection strategy for maximizing the oil recovery is the miscible SSWAG injection while the highest CO_2 stored was obtained under immiscible CO2I with pressurization after EOR. The most promising injection scheme to co-optimize oil recovery and CO_2 storage is found to be the miscible CO2I.
- With the economic factors accounted for, immiscible TAPWAG and miscible WAG injections are found to be the most promising injection scheme for co-optimizing oil recovery and CO_2 storage for secondary and tertiary recovery, respectively.

- Providing incentive for sequestering CO_2 through EOR in the form of CO_2 credit could make more CO_2 injection strategies economical for the purpose. The CO_2 credit was found to be strongly influenced by the oil and CO_2 price.

The miscible WAG injection under the tertiary recovery mode was selected for the subsequent parametric study and co-optimization of the integrated process, which are detailed in the next chapter.

5.8. References

[5.1] 2010 Worldwide EOR Survey, Oil & Gas Journal, April 5, 2010.

[5.2] Abbaszadeh, M., Ohno, K., Okano, H., Morales, J. and Caraza, J.: Reservoir Characterization and CO_2-EOR Injection Studies in Chicontepec Turbidite Reservoirs, Mexico, SPE 12637, International Petroleum Technology Conference, Kuala Lumpur, Malaysia, 3-5 December 2008.

[5.3] Altundas, Y. B., Ramakrishnan, T. S., Chugunov, N. and de Loubens, R.: Retardation of CO_2 due to Capillary Pressure Hysteresis: A New CO_2 Trapping Mechanism, SPE International Conference on CO_2 Capture, Storage, and Utilization, New Orleans, Louisiana, USA, 10-12 November 2010.

[5.4] Anadarko, Enhanced Oil Recovery, Anadarko website, accessed in August 2010.

[5.5] Attanucci, V., Aslesen, K.S., Hejl, K.A. and Wright, C.A.: WAG Process Optimization in the Rangely Carbon Dioxide Miscible Flood, SPE 2662, SPE 68th Annual Technical Conference, 1993.

[5.6] Awan, A.R., Teigland, R. and Kleppe, J.: A Survey of North Sea Enhanced-Oil-Recovery Projects Initiated During the Years 1975 to 2005, SPE Reservoir Evaluation & Engineering, Vol. 11, 3, 497-512, 2008.

[5.7] Aziz, K. and Settari, A.: Petroleum Reservoir Simulation, Applied Science Publishers, London, 398, 1979.

[5.8] Bijeljic, B.R., Muggeridge, A.H., Blunt, M.J.: Effect of Composition on Waterblocking for Multicomponent Gasfloods, SPE 77697, SPE Annual Technical Conference and Exhibition, San Antonio, Texas, 29 September-2 October 2002.

[5.9] Blackwell, R.J., Terry, W.M., Rayne, J.R., Lindley, D.C. and Henderson, J.R.: Recovery of Oil by Displacements with Water-Solvent Mixtures, Petroleum Transactions, Vol. 219, 293-300, 1960.

[5.10] Campbell, B.T. and Franklin M. Orr Jr.: Flow Visualization for CO_2/Crude-Oil Displacements, SPE 11958, SPE Journal, Vol. 25, No. 5, 665-678, October 1985.

[5.11] Carlson F.M.: Simulation of Relative Permeability Hysteresis to the Non-wetting Phase, SPE 10157, SPE Annual Technical Conference and Exhibition, San Antonio, Texas, 4-7 October 1981.

[5.12] Champion, J.H. and Shelden, J.B.: An Immiscible WAG Injection Project in the Kuparuk River Unit, Journal of Petroleum Technology, Vol. 41, 5, 533-540, 1989.

[5.13] Chang, Y. B., Coats, B.K. and Nolen, J.S.: A Compositional Model for CO_2 Floods Including CO_2 Solubility in Water, SPE 35164, SPE Reservoir Evaluation & Engineering, Vol. 1, No. 2, 155-160, 1998.

[5.14] Chen, M.S., Allard, D.R. and Anli, J.: Factors Affecting Solvent Slug Size Requirements in Hydrocarbon Miscible Flooding, SPE 12636, SPE/DOE Fourth EOR Symposium Annual Meeting, Tulsa, 1984.

[5.15] Christensen, J.R., Stenby, E.H., Skauge, A.: Review of the WAG Field Experience, SPE 71203, SPE International Petroleum Conference and Exhibition of Mexico, Villhermosa, March 3-5, 1998.

[5.16] Damsleth, E., Hage, A. and Volden, R.: Maximum Information at Minimum Cost: A North Sea Field Development Study with an Experimental Design, SPE 23139, Journal of Petroleum Technology, 1350-1356, December 1992.

[5.17] Douglas, J. M.: Conceptual Design of Chemical Processes, McGraw-Hill, New York, NY, 153-156, 1988.

[5.18] ECLIPSE 2007.1 Simulation Software Manual, Schlumberger

[5.19] Egeland, T., Hatlebakk, E., Holden, L. and Larsen, E.A.: Designing Better Decisions, SPE 24275, SPE European Petroleum Computer Conference held in Stavanger, Norway, 25-27 May 1992.

[5.20] Enick, R.M. and Klara, S.M.: Effects of CO_2 Solubility in Brine on the Compositional Simulation of CO_2 Floods, SPE Reservoir Engineering, Vol. 7, 2, 253-258, 1992.

[5.21] Ferguson, R.C., Kuuskraa, V.A., Van Leeuwen, T.S. and Remson, D.: Storing CO_2 with Next Generation CO_2-EOR Technology, SPE 139717, SPE International Conference on CO_2 Capture, Storage, and Utilization, New Orleans, Louisiana, USA, 10-12 November 2010.

[5.22] Forooghi, A., Hamouda, A. and Eilertsen, A.T.: Co-optimization of CO_2 EOR and Sequestration in a North Sea Chalk Reservoir, SPE 125550, SPE/EAGE Reservoir Characterization and Simulation Conference, 19-21 October, Abu Dhabi, UAE, 2009.

[5.23] Ghomian, Y., Pope, G.A. and Sepehmoori, K.: Efficient Investigation of Uncertainties in Flood Design Parameters for Coupled CO_2 Sequestration and Enhanced Oil Recovery, SPE 139738, SPE International Conference on CO_2 Capture, Storage, and Utilization, 10-12 November, New Orleans, Louisiana, USA, 2010.

[5.24] Ghomian, Y., Pope, G.A. and Sepehmoori, K.: Hysteresis and Field-Scale Optimization of WAG Injection for Coupled CO_2-EOR and Sequestration, SPE/DOE Improved Oil Recovery Symposium, Tulsa, Oklahoma, 2008.

[5.25] Grogan A.T. and Pinczewski W.V.: The Role of Molecular Diffusion Processes in Tertiary CO_2 Flooding, SPE 12706, JPT May 1987.

[5.26] Hadlow, R.E.: Update of Industry Experience with CO_2 Injection, SPE 24928, 67th Annual Technical Conference and Exhibition of the Society of Petroleum Engineers, Washington DC, 1992.

[5.27] Haskin, H.K. and Alston, B.R.: An Evaluation of CO_2 Huff 'n' Puff Tests in Texas, SPE 15502, Journal of Petroleum Technology, Vol. 41, 2, 177-184, February 1989.

[5.28] Hebach, A., Oberhof, A. and Dahmen, N.: Density of Water + Carbon Dioxide at Elevated Pressures: Measurements and Correlation, Chemical Engineering Data, 49, 950-953, 2004.

[5.29] Holtz, M.H.: Geologic CO_2 Storage in Oil Fields: Considerations for Successful Sites, SPE 126198, SPE International Conference on CO_2 Capture, Storage, and Utilization, San Diego, California, 2-4 November 2009.

[5.30] Huang, E.T.S. and Holm, L.W.: Effect of WAG Injection and Wettability on Oil Recovery during Carbon Dioxide Flooding, SPE 15491, Annual Technical Conference and Exhibition, New Orleans, LA, Oct 5-8, 1986.

[5.31] IEA/CSLF Report to the Muskoka 2010 G8 Summit, Carbon Capture and Storage; Progress and Next Steps, 2010.

[5.32] Jarrell, P.M., Fox. C., Stein, M. and Webb, S.: Practical Aspects of CO_2 Flooding, SPE Monograph Series, 2002.

[5.33] Juanes, R., Spiteri, E.J., Orr, F.M. and Blunt, M.J.: Impact of Relative Permeability Hysteresis on Geological CO_2 Storage, Water Resources Research, 42, W12418, doi:10.1029/2005WR004806, 2006.

[5.34] Juanes, R. and Blunt, M.J.: Impact of Viscous Fingering on the Prediction of Optimum WAG Ratio, SPE Journal, Vol. 12, 4, 486-495, 2007.

[5.35] Killough, J.E.: Reservoir Simulation with History-dependant Saturation Functions, Petrol. Trans. AIME, 261:37-48, February 1976.

[5.36] Klins, M.A.: Carbon Dioxide Flooding Basic Mechanisms and Project Design, International Human Resources Development Corp., Boston, 1984.

[5.37] Klins, M.A. and Farouq Ali, S.M.: Oil Production in Shallow Reservoirs by Carbon Dioxide Injection, Paper SPE 10374, SPE Eastern Regional Meeting, Columbus, 1981.

[5.38] Kovscek, A.R. and Cakici, M.D.: Geological Storage of Carbon Dioxide and Enhanced Oil Recovery II. Cooptimization of Storage and Recovery, Energy Conversion & Management, 46, 13, 2005.

[5.39] Kulkarni, M.M. and Rao, D.N.: Experimental Investigation of Various Methods of Tertiary Gas Injection, SPE 90589, SPE Annual Technical Conference and Exhibition, Houston, Texas, USA, 26-29 September 2004.

[5.40] Kuuskraa, V. A. and Ferguson, R.: Storing CO_2 with Enhanced Oil Recovery, DOE/NETL-402/1312/02-07-08, February 7, 2008.

[5.41] Lemmon E.W., McLinden M.O. and Friend D.G., Thermophysical Properties of Fluid Systems in NIST Chemistry Webbook, NIST Standard Reference Database No. 69, Eds. P.J. Linstrom and W.G Mallard, June 2005, National Institute of Standards and Technology (http://webbook.nist.gov)

[5.42] Ma, T.D., Rugen, J. A., Stoisits, R. F. and Voungren, G. K.: Simultaneous Water and Gas Injection Pilot at the Kuparuk River Field, Reservoir Impact, SPE 30726, SPE Annual Technical Conference and Exhibition, Dallas, 22-25 October 1995.

[5.43] McCain Jr. and Cawley W.D.: Reservoir Fluid Property Correlations-State of the Art, SPE 18571, SPE Reservoir Engineering, Vol. 6, No. 2, 266-272, 1991.

[5.44] Mian, M.A.: Project Economics & Decision Analysis, Vol. 1: Deterministic Model, Pennwells book, ISBN: 978-0-87814-819-6, 2002.

[5.45] Moritis, G.: CO_2 Miscible, Steam Dominate Enhanced Oil Recovery Processes, Oil & Gas Journal, April 19, 2010.

[5.46] National Energy Technology Laboratory (NETL), U.S. Dept. of Energy, http://www.netl.doe.gov/technologies/carbon_seq/database/index.html, accessed in August 2010.

[5.47] NPC (National Petroleum Council), Enhanced Oil Recovery: An Analysis of the Potential for Enhanced Oil Recovery from Known Fields in the United States; Washington, DC, 231, 1976.

[5.48] Oak, M.J.: Three-Phase Relative Permeability of Water-Wet Berea, SPE 20183, SPE/DOE Enhanced Oil Recovery Symposium, Tulsa, Oklahoma, 22-25 April 1990.

[5.49] Oliveira, M.F., Barillas, J.L.M, Mata, W. and Dutra Junior: A Parametric Study of Solvent Injection as a Recovery Method for Heavy Oil and Bitumen Reservoirs, SPE 122040, SPE Latin American and Caribbean Petroleum Engineering Conference, Cartagena, Colombia, 31 May - 3 June 2009.

[5.50] White, C.D. and Royer, S.A.: Experimental Design as a Framework for Reservoir Studies, SPE 79676, SPE Reservoir Simulation Symposium, Houston, Texas, 3-5 February 2003.

[5.51] Perkins, T.K., Johnston, O.C. and Hoffman, R.N.: Mechanics of Viscous Fingering in Miscible Systems, SPE Journal, Vol. 5, 4, 301-317, 1965.

[5.52] Pollack, N.R., Enick, R.M., Mangone, D.J., Morsi, B.I.: Effect of an Aqueous Phase on CO_2/Tetradecane and CO_2/Maljamar-Crude-Oil Systems, SPE 15400, SPE Reservoir Engineering, Vol. 3, 2, 533-541, May 1988.

[5.53] Qi, R., La Force, T.C. and Blunt, M.J.: Design of Carbon Dioxide Storage in Oilfields, SPE Annual Technical Conference and Exhibition, Denver, Colorado, USA, 2008.

[5.54] Quale, E. A., Crapez, B. and Stensen, J.A.: SWAG Injection on the Siri Field - An Optimized Injection System for Less Cost, SPE 65165, SPE European Petroleum Conference, Paris, France, 24-25 October 2000.

[5.55] Sanchez, N.L.: Management of Water Alternating Gas (WAG) Injection Projects, SPE 53714, Latin American and Caribbean Petroleum Engineering Conference, Caracas, Venezuela, 1999.

[5.56] Sayegh, S.G. and Najman, J.: Phase Behavior Measurements of CO_2-SO_2-Brine Mixtures, Canadian J. of Chemical Engineering, 65, No. 2, 314, 1987.

[5.57] Shelton, J.L. and Schneider, F.N.: The Effects of Water Injection on Miscible Methods Using Hydrocarbons and Carbon Flooding Dioxide, SPE 4580, SPE Journal Vol. 15, 3, 217-226, 1978.

[5.58] Sifuentes, W., Blunt, M.J. and Giddins, M.A.: Modelling CO_2 Storage in Aquifers: Assessing the Key Contributors to Uncertainty, SPE 123582, SPE Offshore Europe Oil & Gas Conference & Exhibition, Aberdeen, UK, 8-11 September 2009.

[5.59] Spiteri E.J. and Juanes R.: Impact of Relative Permeability Hysteresis on the Numerical Simulation of WAG Injection, Journal of Petroleum Science and Engineering 50, 115-139, 2006.

[5.60] Spiteri, E.J., Juanes, R., Blunt, M.J. and Orr Jr. F.M.: Relative-Permeability Hysteresis: Trapping Models and Application to Geological CO_2 Sequestration, SPE 96448, SPE Annual Technical Conference and Exhibition, Dallas, Texas, 9-12 October 2005.

[5.61] Stalkup, F.I.: Displacement of Oil by Solvent at High Water Saturation, SPE Journal, Vol. 10, 4, 337-348, 1970.

[5.62] Surguchev, L.M. and Krakstad, O.S.: Screening of WAG Injection Strategies for Heterogeneous Reservoirs, SPE 25075, European Petroleum Conference, France, 1992.

[5.63] Thakur, G.C., Lin, C.J. and Patel, Y.R.: CO_2 Minitest, Little Knife Field, ND: A Case History, SPE 12704, SPE Enhanced Oil Recovery Symposium, 15-18 April 1984, Tulsa, Oklahoma, 1984.

[5.64] Tiffin, D.L. and Yellig, W.F.: Effects of Mobile Water on Multiple-Contact Miscible Gas Displacements, SPE 10687, SPE Journal, 447-55, 1983.

[5.65] Trivedi, J. J. and T. Babadagli, T.: CO_2 and Flue Gas Sequestration during Tertiary Oil Recovery: Optimal Injection Strategies and Importance of

Operational Parameters, Canadian International Petroleum Conference, Calgary, Alberta, Jun 7-9, 2005.

[5.66] Van Lingen, P.P. and Knight, S.: WAG Injection to Reduce Capillary Entrapment in Small Scale Heterogeneities, SPE 36662, SPE Annual Meeting, Colorado, October 1996.

[5.67] White, C.D. and Royer, S.A.: Experimental Design as a Framework for Reservoir Studies, SPE 79676, SPE Reservoir Simulation Symposium, Houston, Texas, 3-5 February 2003.

[5.68] Yang, D., Tontiwachwuthikul P., and Gu, Y.: Interfacial Tensions of the Crude Oil + Reservoir Brine + CO_2 Systems at Pressures up to 31MPa and Temperatures of 27 °C and 58 °C, Journal of Chemical Engineering Data, No. 50, 1242-1249, 2005.

Chapter 6

Parametric Study and Process Design Optimization of CO_2 Injection for Coupled EOR and Storage

6.1. Introduction

The factors affecting the performance of CO_2 WAG injection for EOR have been extensively studied and reported in the literature, for example by Chen et al. (1984), Champion and Shelden (1989), Sanchez (1999), Rogers and Grigg (2000) and Awan et al. (2008). However, there are very limited studies on factors influential to the performance and economic viability of WAG injection for both EOR and CO_2 storage purpose.

This chapter presents the parametric simulation and flood design optimization of the miscible WAG injection process. In the conventional CO_2 EOR projects, the main objective is maximizing the oil recovery with the lowest use of CO_2. The CO_2 produced is normally re-injected for an efficient and economic CO_2 utilization. Since the trapped CO_2 in the reservoir cannot be re-cycled, CO_2 sequestration is to be minimized as much as possible in EOR. However, in coupled CO_2 EOR and storage projects, in addition to maximizing the oil recovery, the other key objectives are also to maximize the amount of CO_2 stored in the reservoir at the end of the process and ensure that the CO_2 remains safely confined. For the integrated project to be technically and economically viable, it is essential that these two competing objectives co-optimized. Co-optimization here refers to getting the highest possible profit in terms of both oil recovery and CO_2 storage by applying the best combination of the influential design factors within a predefined range.

6.1.1 Relevant previous studies

There is a large volume of studies in the literature about the optimization of the CO_2 flood design for EOR (for example Ramirez et al., 1984; Rivas et al., 1994; Gharbi, 2001; Panda et al., 2009; Darvishnezhad, 2010). However, the number of published studies on the optimization of a coupled EOR and CO_2 storage process is still very limited.

Malik and Islam (2000) evaluated, through reservoir simulation, several CO_2 injection strategies using horizontal injection wells to optimize the oil production and CO_2 storage in Weyburn Field, Canada. They recommended injecting the CO_2 into the producing formation and re-pressurizing the reservoir after the end of the EOR phase to increase the CO_2 storage.

Controlling the produced GOR was also reported to effectively co-optimize CO_2 sequestration and oil recovery (Kovscek and Cakici, 2005; Pamukcu et al., 2008). A lower GOR limit resulted in significantly more CO_2 stored in the reservoir with only a slight adverse impact on oil recovery. This is further enhanced by combining this procedure with solvent injection that creates miscible displacement. Using a streamline-based simulation, Qi et al. (2008) sensitized the CO_2 reservoir volume fractional flow of CO_2 SWAG injection and concluded that injecting more water than the optimum WAG ratio can impede the movement of CO_2 to the production wells, thus leading to a higher amount of CO_2 storage.

These parametric studies seeking to understand the issues limiting the performance of the EOR process for CO_2 storage were based on a one-factor-at-a-time (OFAT) approach, which fail to take into account any interactions between the critical factors.

Much recently, Ghomian et al. (2008) and Forooghi et al. (2009) have reported the use of an experimental design and reservoir simulation to co-optimize oil recovery and CO_2 storage. The use of solvent gas, a horizontal injector and producer, and a high WAG ratio were found to be favourable for co-optimized performance.

In this chapter, the experimental design and the Response Surface Method (RSM) were used to effectively select the sensitivity runs for the simulation, find the statistically significant factors to the process and identify the window of operability where requirements of maximum oil recovery and CO_2 storage profit simultaneously meet the critical properties. The significant factors were first screened using a fractional factorial design, and then a

response surface model was used to fully model the effects, followed by a confirmation simulation run to verify the results.

6.2. Parametric simulation study of coupled CO_2 EOR and storage

6.2.1. Parametric study approach

Setting the objectives

The focus of the parametric study was to screen out the factors that are not critical to the profitability of the miscible CO_2 WAG injection (i.e. under fixed rate well control mode) in both the homogeneous and heterogeneous model. Only the post-waterflooding or tertiary WAG injection was evaluated, as it is a common practice in the industry that CO_2 EOR is implemented after the oil fields have been exploited by a combination of natural drive and secondary water or gas flood. Tertiary process is more relevant when CO_2 storage is also one of the objectives of the injection project. In this case, the depleted oil field would eventually be converted into a storage site, and this conversion process is irreversible if the storage is permanent (Stevens et al., 2000). In the tertiary injection, CO_2 is stored through dissolution in the remaining oil and water in the reservoir as well as occupying the pore space when the reservoir is further pressurised by CO_2 after the EOR period.

The WAG injection was first analysed through a sensitivity study of several reservoir and operational parameters to examine how these factors affect the amount of CO_2 retained in the reservoir and the oil recovery. This parametric simulation served to screen the important design variables for the subsequent optimization. The oil recovery profit (R^* as in Equation 5.12) and CO_2 storage profit (S^* as in Equation 5.13) were used as the response parameters.

Choosing the factors and levels examined

The selection of factors was made to reflect the most common reservoir characteristics and well operation conditions based on the literature review (for example Jarrel et al., 2002) and prior knowledge. A total of 11 factors, as listed in Table 6.1, were incorporated in the

sensitivity analysis. Geophysical aspects such as seals, faults and fractures and the geochemical reactions between CO_2, water and the rock minerals might also affect the CO_2 WAG injection process but were not considered in this study. Throughout this chapter, the abbreviations and factor labels will be used heavily, thus the readers are referred to Table 6.1 for the description.

Table 6.1: Factors evaluated (with abbreviation) and the range involved in parametric simulation of CO_2 WAG injection in the homogeneous reservoir model.

Factor Label	Description	Units	Low Level (-1)	High Level (+1)
A	Reservoir permeability (PERMX)	mD	20	2000
B	Reservoir porosity (PORO)	fraction	0.1	0.3
C	k_v/k_h ratio (KV/KH)	-	0.05	0.3
D	Relative permeability (RELP)	table number	1 (water-wet)	2 (oil-wet)
E	Oil viscosity (OILVIS)	cP	4	65
F	Maximum produced gas oil ratio (GOR)	Mscf/stb	10	50
G	Preceding waterflood duration (WFLD)	year	3	7
H	Injected CO_2 gas composition (CO2)	mole fraction	0.5	1
J	Gas injection rate per well (QINJ)	Mscf/day	8720	17445
K	Slug size (SLUG)	%HCPV	0.5	8
L	WAG ratio (WAGR)	-	0.25	3

* Letter 'I' was purposely excluded as it symbolizes the identity of the design matrix of the tool used.

The minimum and the maximum values of each parameter were chosen to be reasonably far apart, so that the effect was likely to be seen, but not exceeding the typical operating boundaries. For the purpose of the sensitivity analysis, all factors were assumed as not correlated, except for the capillary pressure, Pc, which changes with permeability and porosity of the system, as described in the next page. Pc was thus not defined as one of the factors: only permeability and porosity were.

Reservoir permeability (PERMX): Permeability influences the fluid flow. Heterogeneity in lateral and vertical directions affects the flow path and determines the well perforation intervals. The reservoir permeability was sensitized from 20 to 2000 mD for the

homogeneous model. For the heterogeneous model, more details on the model are given later, a global multiplier of 0.5 and 3 times the original permeability value was applied, with maximum permeability capped at 20000 mD. This gives average permeabilites of 180 and 1500 mD, respectively.

Reservoir porosity (PORO): Porosity determines the capacity of the reservoir and thus strongly influences CO_2 storage. Apart from reservoir depth and temperature, the fraction of the porosity that can be filled with CO_2, determines the amount of the CO_2 that can be sequestered. For the homogeneous model, the high porosity level was set at 30% whilst the low level was set at 10%. For the heterogeneous model, a global multiplier of 0.5 and 2 times the base case values, capped at 40% was applied giving 10% and 32% average porosity for the low and high level case, respectively.

Capillary pressure: Since the Pc is a function of the reservoir quality index $\left(\sqrt{\frac{k}{\phi}}\right)$, it was recalculated for each combination of permeability and porosity, using Equation 5.8 (of Chapter 5). The pore size distribution index and entry value of the J-function remain the same as those used in Chapter 5.

Vertical to horizontal permeability (k_v/k_h) ratio (KV/KH): The k_v/k_h ratio affects the vertical conformance of WAG injection, and thus CO_2 distribution in the reservoir. The high and low level in the sensitivity analysis were set at 0.05 and 0.3, respectively.

Relative permeability (RELP): Relative permeability governs the multiphase flow through the porous media and strongly affects the pressure and production response. It depends, among other factors, on the fluid saturation levels and wettability of the formation. In this parametric study, the relative permeability was to represent the wettability of the formation. The low level represents the relative permeability for the water-wet system (table 1) while the high level represents the relative permeability of an oil-wet system (table 2).

The relative permeability curves, shown in Figures 6.1 and 6.2, were generated using Corey-type correlation with assumed endpoints (Table 6.2) following Craig's rule in distinguishing between strongly water-wet and oil-wet systems (Craig, 1971). For a water-wet system, the oil relative permeability is characterised by an S_{or} of 30 % or higher, n_o of around 2 - 3 and

an end-point relative permeability $k_{ro,cw}$ of around 0.6 - 0.8. The corresponding water relative permeability is characterised by a Corey exponent n_w of around 4 - 6 and an end-point relative permeability $k_{rw,Sor}$ of around 0.1 - 0.4. For an oil-wet system, water and oil exchange places. Also according to Craig's rules, for the oil-wet system, the intersection of k_{rw} and k_{row} curves for an oil-wet system occurs at $S_w < 0.45$ whilst for the water-wet system, it is usually higher than 0.5. Corey's correlations were also used to create the oil/gas relative permeability curves in Figure 6.2. The assumed endpoints and exponents are given in Table 6.3.

Table 6.2: Assumed oil/water relative permeability endpoints.

Table	Wettability	S_{wc}	S_{orw}	$K_{rw}(S_{orw})$	$K_{ro}(S_{wc})$	n_o	n_w
1	Water-wet	0.25	0.33	0.35	1.0	2.5	5.0
2	Oil-wet	0.15	0.58	0.55	0.8	6.0	2.0

Table 6.3: Assumed oil/gas relative permeability endpoints.

Table	Wettability	S_{gc}	S_{org}	$K_{rg}(S_{org})$	$K_{rog}(S_{gc})$	n_o	n_g
1	Water-wet	0.03	0.1	1.0	1.0	4.5	3
2	Oil-wet	0.03	0.2	1.0	1.0	5.5	3

The hysteresis was assumed for the non-wetting phase for each oil/water and oil/gas system (k_{row} and k_{rg}). The scanning curve was calculated using the non-wetting phase hysteresis model by Land (1968) and Carlson (1981).

$$K_{rnw}^{imb}(S_o) = K_{rnw}^{drain}\left(S_{nwf}\right) \tag{6.1}$$

where

$$S_{nwf} = S_{nwc} + \frac{1}{2}\left\{(S_{nm} - S_{nwr}) + \sqrt{(S_{nw} - S_{nwr})^2 + \frac{4}{C}(S_{nw} - S_{nwr})}\right\} \tag{6.2}$$

$K_{rnw}^{imb}(S_{nw})$ and $K_{rnw}^{drain}\left(S_{nwf}\right)$ is the imbibition at the non-wetting phase saturation, S_{nw}, and the drainage of the non-wetting phase relative permeability at the corresponding free

non-wetting phase saturation, S_{nwf}, respectively. For the K_{row}, the Land's constant C was assumed to be 2.0 and the critical oil saturation S_{oc} = 0. For the K_{rg}, the trapped gas saturation, S_{gt}, was assumed to be 0.25 for both the water-wet and oil-wet systems.

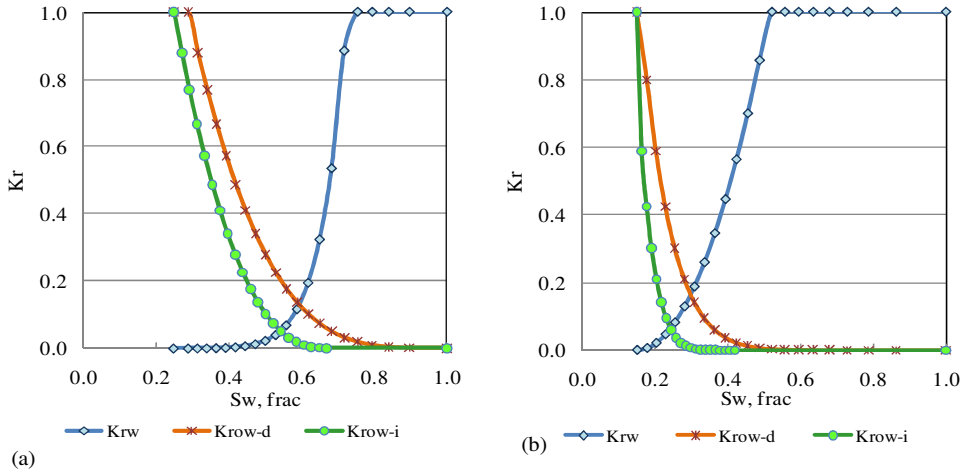

Figure 6.1: The calculated oil/water relative permeability curves with hysteresis for (a) water-wet and (b) oil-wet rock.

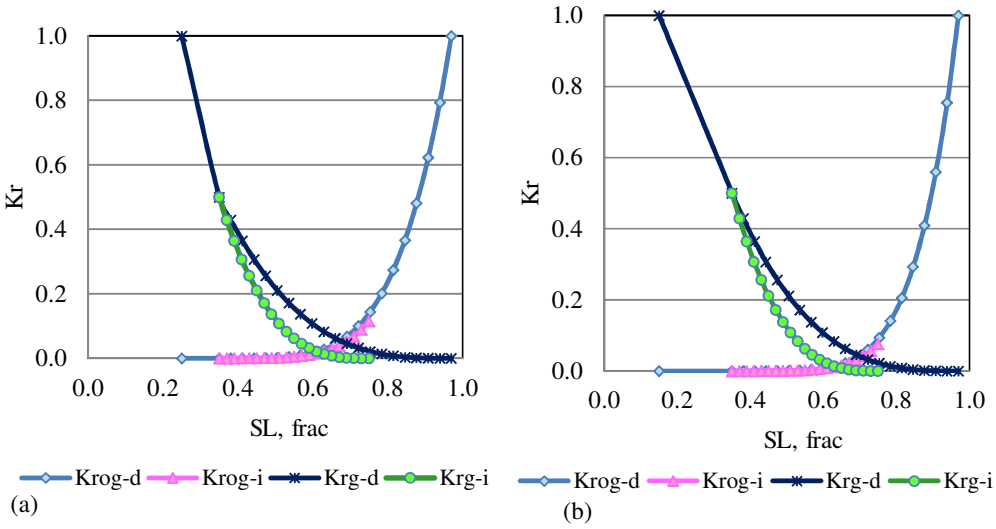

Figure 6.2: The calculated gas/oil relative permeability curves with hysteresis for (a) water-wet and (b) oil-wet rock.

Oil viscosity (OILVIS): Oil viscosity reduction due to CO_2 solubility into the oil is one of the main recovery mechanisms in CO_2 flooding (Miller and Jones, 1981; Klin, 1984). Oil viscosity also governs the mobility of the oil in the reservoir. Representing the low level viscosity oil was Little Knife oil, as used in Chapter 5, with 4 cP viscosity at standard conditions. Representing the high level was Little Knife oil with the same composition but with higher specific gravity and higher molecular weight of the C14+ fraction that gives a viscosity of 65 cP at the standard condition.

Injected gas composition (CO2): The injected gas composition has a significant impact on the effectiveness of CO_2 EOR, as it is very influential on the MMP (Jessen et al., 2005). In this study, the injected gas composition was sensitized between pure CO_2 and a gas mixture containing 50 mole% CO_2 and 50 mole% of C1 and N_2 mixture.

Gas injection rate (QINJ): The base case gas injection rate was 11630 Mscf/day, which is equivalent to 5000 bbl/day of water injection at 4000 psig, and 150 ^oF. This injection rate was chosen so as to get a reasonable amount of production within the simulated duration. The low and high levels were set at 8720 and 17445 Mscf/day/well, respectively.

Waterflood duration prior to WAG injection (WFLD): The timing to start WAG injection after waterflooding was also varied between 3 to 7 years, to reflect the different mobile water saturation, S_{wi}, at the time the CO_2 injection started.

WAG ratio (WAGR): The low level WAG ratio was set at 1:4 while the high level was set at 3:1.

Selecting the experimental design

The DOE method and the same tool Design-Expert® version 8.0.6 (State-Ease Inc.'s software) was again used to determine the number of runs and combinations of parameters for the sensitivity study. In the initial stage of screening for the factors critical to the process, the author chose the simplest but most powerful DOE tool: the standard two-level fractional factorial experimental design. This approach assumes that information on the main effects and low-order interactions may be obtained by running only a fraction of the complete

factorial experiments and that the higher order interactions are negligible (Montgomery, 1991). Mathematically, it is described as 2^{k-p}, where k refers to the number of factors and minus p excludes a fraction of the experiments (Box, 1961 as quoted in Anderson and Whitcomb, 2007), which equals 5 in this study. Each input variable is varied at high (+1) and low (-1) level as discussed earlier. $2^{11-5} = 64$ experiments (or simulation runs) were identified. R* and S* were again used as the response factors and will be described later.

Performing the simulation

Two similar compositional models, being different only in permeability and porosity, were used for the parametric simulations. The model is a quarter of the compositional model described in Chapter 5 with 10x30x10 grid blocks, representing an inverted five-spot pattern of an oil field. In addition to identifying the critical factors to the oil recovery and CO_2 storage profit, the results will also give an insight into whether the influential factors are the same for both homogeneous and heterogeneous reservoirs.

For the homogeneous model, the permeability and porosity are constant at 800 mD and 25%, respectively. The porosity and permeability values for the heterogeneous model were taken from a section of the SPE10 Model 2 (http://www.spe.org/web/csp/). The model consists of a prograding Tarbert formation at the top part and the fluvial Upper Ness formation in the lower part. The carved out section for this study however only involved the Tarbet formation where permeability variation is relatively large but smooth. The extracted properties of 10x30x10 cells from the fine SPE10 model were directly populated into the quarter five-spot model. Figure 6.3 shows the distribution of the base case porosity and permeability. It is important to note that, in this study, the SPE10 model's static properties were used only to ensure realistic heterogeneous porosity and permeability values typical of a North Sea reservoir, and not to evaluate WAG in the Tarbet formation per se.

The average reservoir pressure was maintained at a maximum of 4000 psig throughout the water injection period. This is to ensure that the pressure was slightly above the MMP of the light oil. To ensure a miscible displacement, the average reservoir pressure was always maintained higher than the MMP throughout the WAG injection by injecting 10% more

reservoir barrel than the production. CO_2 injection was continued until the maximum BHP, even when the well operating limits were already reached, to allow for maximum possible CO_2 storage within the duration of the simulation of 25 years.

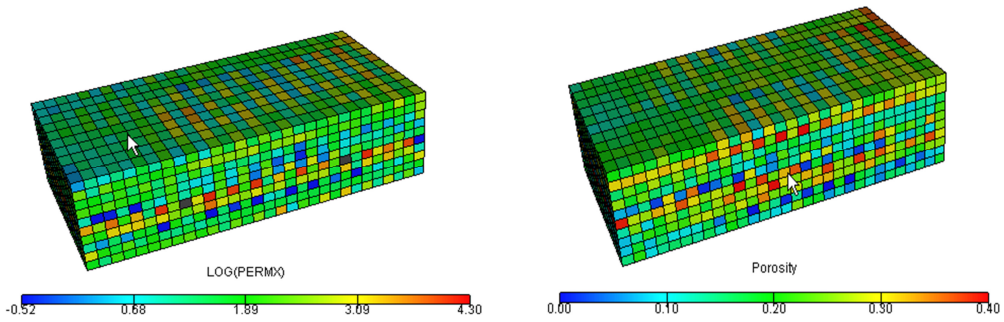

Figure 6.3: (a) Permeability (log scale) and (b) porosity of the heterogeneous model used in the parametric study.

The full list of the 64 simulation cases, as well as the setting of each factor, is given in Tables A6.1 and A6.2 of Appendix A6.1, for the homogeneous and heterogeneous models, respectively.

Analysing the data

A similar approach in analysing the simulation results as described in Section 5.5 was employed and the same economic parameters assumed. The CAPEX involved was the costs for one injection well and the CO_2 recycled plant only. In the cases involving the injection of CO_2, C1 and N_2 gas mixture, the produced lean gas was also recycled with the recycling costs assumed to be half of that of CO_2. A fresh supply of the gas was injected to make up the total amount of gas needed for injection. The sale of the produced gas as well as the CO2 credit was not considered in the economic calculations.

The profit of the oil recovery and CO_2 stored during the tertiary WAG injection period,

expressed as the NPV per barrel of oil, R*, and NPV per Mscf of CO_2 stored, S*, respectively, were used as the response factors (Equation 5.12 and 5.13, repeated here for easy reference).

$$R^* = \frac{NPV}{N_p} \tag{6.3}$$

$$S^* = \frac{NPV}{V^*_{CO2}} \tag{6.4}$$

where NPV is the net present value of the project, V_{CO2}^* is Mscf of CO_2 stored in the reservoir and N_p is the oil produced during the CO_2 injection period. Throughout this chapter, R* and S* will be referred to as the 'oil recovery profit' and 'CO_2 storage profit', respectively. The project with both high R* and S* is targeted.

To facilitate understanding of the discussion in this chapter, it is important to note that these response factors, R* and S*, are different from the objective function of oil recovery, R, and CO_2 storage, S, defined by Equation 5.2 and 5.3, respectively (repeated here for easy reference).

$$R = \frac{N^*_p}{STOOIP} \times 100 \tag{6.5}$$

$$S = \frac{V^R_{CO2}}{PV} \times 100 \tag{6.6}$$

R* and S* are the profit in dollar per barrel of oil recovered ($/stb) and per Mscf of the CO_2 stored ($/Mscf), respectively, while R and S are the oil recovery (%STOOIP) and the amount of CO_2 stored (%PV). Note that the N_p and V_{CO2} are in the inverse position in the respective equations. According to Equation 6.3 and 6.4 above, high profits are obtained when low amount of CO_2 stored and additional oil produced give high NPV. Conversely, according to Equation 6.5 and 6.6, higher R and S are obtained with higher additional oil produced and amount of CO_2 stored. Therefore, it is anticipated that the factors favourable

to high profits of the project, as defined in this study, could be the opposite of those factors resulting in high oil recovery and CO_2 stored.

The response models on the R* and S* were evaluated using ANOVA to identify the factors that have the greatest impact on the responses. ANOVA allows the simultaneous examination of not only multiple independent variables (factors) but also of the interactions between those factors. Interaction occurs when the difference in the response between levels of one factor is not the same at all levels of the other factor (Montgomery, 1991) and is best viewed through interaction plot. When the interaction is large, the corresponding main effects have little practical meaning. Effect is defined as the change in the response as the factor changes from the low to the high level (Montgomery, 1991) and is expressed mathematically as:

$$Effect = \left(\frac{\sum Y_+}{n_+}\right) - \left(\frac{\sum Y_-}{n_-}\right) \tag{6.7}$$

where Y_+ and Y_- represent the response of the high and low levels, respectively, and n is the number of data points collected at each level.

The half-normal probability plot of the effects was then used as a tool to screen for the vital few effects that stand out to the right on the x-axis scale of the absolute response. These few significant effects are included in the model while the rest of the effects are tested using Shapiro-Wilk hypothesis to determine the probability that the sample came from a normally distributed population of observations. The null hypothesis is that the data (the unselected and insignificant terms in the model) come from a normal distribution.

6.2.2. Results and discussion

The summary of the maximum values of the oil recovery and CO_2 storage profits is shown in Table 6.4, while Tables 6.5 and 6.6 show the results for all the simulation cases for the homogeneous and heterogeneous reservoirs, respectively. The maximum oil recovery factor

and CO_2 storage per barrel of oil produced by the end of the CO_2 flood for the homogeneous reservoir, can reach up to about 66 %STOOIP and 29 Mscf/stb, respectively, as compared with only 52 %STOOIP and 8 Mscf/stb for the heterogeneous cases.

Table 6.4: Summary of maximum values for oil recovery and CO_2 storage.

Parameter	MAX. HOM		MAX. HET	
	Run	Value	Run	Value
Incremental oil recovery, %STOOIP	HOM7	65.87	HET2	51.80
CO_2 stored, Mscf/bbl of oil produced	HOM29	29.25	HET57	7.76
R* = Oil recovery profit, $/bbl	HOM18	18.86	HET9	16.73
S* = CO_2 storage profit, $/Mscf	HOM3	30.18	HET46	20.95
f = 0.5(R*+S*)	HOM18	22.25	HET46	18.80

It is evident from the results that the most profitable case is not necessarily given by the project with the highest individual tertiary oil recovery or amount of CO_2 stored but both should be considered. As shown in Table 6.4, the highest tertiary oil recovery for the homogeneous reservoir was given by HOM7 with 65.87 %STOOIP but the best dollar value of the additional oil recovery was attained in HOM18 case, which produced only 28.44 %STOOIP extra oil. Similarly, the highest CO_2 storage of 29.25 Mscf per barrel of oil produced was given by HOM29 but the highest dollar value of CO_2 storage was given by HOM3 with 30.2 $/Mscf of CO_2 stored. The most favourable combination of reservoir and operational factors that lead to the highest value of the f function (i.e., the equally weighted R* and S*), is given by HOM18 and HET46 for the homogeneous and heterogeneous reservoirs, respectively.

Table 6.5: Simulation results for the homogeneous (HOM) reservoir.

Run	Oil recovery during WAG injection	CO_2 injected per barrel of oil produced	CO_2 stored per barrel of oil produced	S*	R*
	%STOOIP	Mscf/stb	Mscf/stb	$/Mscf	$/stb
HOM1	61.75	6.047	3.918	2.228	8.728
HOM2	37.08	0.881	0.862	14.666	12.646

Run	Oil recovery during WAG injection	CO_2 injected per barrel of oil produced	CO_2 stored per barrel of oil produced	S*	R*
	%STOOIP	Mscf/stb	Mscf/stb	$/Mscf	$/stb
HOM3	42.64	1.480	0.462	**30.176**	13.946
HOM4	11.58	6.156	1.949	4.380	8.539
HOM5	44.86	7.299	4.152	1.487	6.173
HOM6	22.47	5.566	3.865	2.032	7.856
HOM7	**65.87**	2.599	2.121	5.896	12.507
HOM8	12.38	3.795	0.759	16.950	12.864
HOM9	40.45	8.305	6.276	0.774	4.860
HOM10	34.30	22.860	6.401	0.544	3.481
HOM11	31.15	6.132	1.001	15.128	15.145
HOM12	56.60	8.266	5.511	1.275	7.027
HOM13	12.27	7.193	2.185	3.056	6.678
HOM14	14.00	6.290	3.363	2.561	8.612
HOM15	17.19	8.880	6.680	0.793	5.298
HOM16	9.33	1.973	0.949	6.820	6.470
HOM17	33.80	4.572	3.174	2.910	9.236
HOM18	**28.44**	**0.917**	**0.736**	**25.637**	**18.863**
HOM19	57.49	7.715	5.334	1.237	6.595
HOM20	50.55	3.510	2.919	1.814	5.295
HOM21	34.85	3.326	2.210	5.765	12.742
HOM22	23.03	2.500	2.467	4.479	11.050
HOM23	10.70	5.864	2.890	0.748	2.163
HOM24	39.55	13.782	8.079	-0.002	-0.017
HOM25	18.77	5.762	4.854	0.657	3.191
HOM26	29.40	3.110	1.437	8.587	12.338
HOM27	45.81	3.234	2.000	3.202	6.403
HOM28	46.88	2.086	1.763	9.330	16.452
HOM29	2.16	29.391	**29.245**	-0.776	-22.681
HOM30	55.40	8.029	6.155	1.415	8.710
HOM31	1.99	14.141	13.838	-1.568	-21.700
HOM32	14.23	7.437	5.826	0.391	2.279
HOM33	25.84	9.324	5.634	1.889	10.642
HOM34	38.46	21.684	6.144	0.438	2.689
HOM35	28.42	3.070	2.878	2.981	8.580
HOM36	53.31	5.166	2.051	6.303	12.925
HOM37	11.34	3.829	1.743	6.503	11.338
HOM38	19.38	8.925	3.780	2.252	8.513
HOM39	7.36	11.735	11.539	0.232	2.675
HOM40	39.98	4.647	3.029	2.677	8.108
HOM41	20.66	3.980	3.683	4.878	17.966
HOM42	17.48	7.549	5.671	0.513	2.911
HOM43	17.94	3.592	2.130	4.143	8.825

Run	Oil recovery during WAG injection	CO_2 injected per barrel of oil produced	CO_2 stored per barrel of oil produced	S*	R*
	%STOOIP	Mscf/stb	Mscf/stb	$/Mscf	$/stb
HOM44	21.11	1.680	1.522	5.086	7.740
HOM45	57.36	11.711	4.614	2.051	9.464
HOM46	30.61	12.891	9.180	-0.026	-0.238
HOM47	13.82	9.979	4.241	1.104	4.683
HOM48	19.68	2.980	2.187	6.574	14.379
HOM49	18.69	10.449	8.137	-0.370	-3.008
HOM50	44.34	4.899	2.345	2.630	6.167
HOM51	49.80	7.010	4.120	1.680	6.920
HOM52	3.04	12.424	12.006	-1.249	-14.993
HOM53	24.30	2.009	1.270	9.199	11.686
HOM54	34.39	4.330	2.985	4.226	12.615
HOM55	52.51	4.094	3.480	3.788	13.182
HOM56	20.59	5.003	3.437	1.602	5.508
HOM57	24.73	8.641	5.138	0.516	2.649
HOM58	7.16	3.744	2.616	1.206	3.155
HOM59	35.11	4.881	3.329	3.555	11.834
HOM60	35.44	3.388	1.299	12.129	15.760
HOM61	28.49	6.562	2.960	2.303	6.818
HOM62	34.37	5.759	4.162	2.592	10.787
HOM63	10.87	11.282	8.166	0.173	1.415
HOM64	28.47	6.276	3.926	2.298	9.023

Table 6.6: Simulation results for the heterogeneous (HET) reservoir.

Run	Oil recovery during WAG injection	CO_2 injected per barrel of oil produced	CO_2 stored per barrel of oil produced	S*	R*
	%STOOIP	Mscf/stb	Mscf/stb	$/Mscf	$/stb
HET1	22.75	6.177	2.516	2.993	7.528
HET2	51.80	3.327	1.906	6.659	12.691
HET3	12.01	3.830	3.077	1.004	3.090
HET4	19.75	9.566	2.626	1.546	4.061
HET5	12.37	1.277	1.124	7.489	8.415
HET6	34.42	4.749	0.939	15.322	14.383
HET7	20.72	2.792	2.169	4.419	9.583
HET8	27.61	10.635	3.596	1.673	6.018
HET9	33.40	2.083	1.439	11.628	16.728
HET10	22.87	6.315	4.088	1.178	4.817
HET11	8.09	1.872	1.033	5.248	5.420
HET12	10.39	1.523	1.067	9.464	10.100
HET13	14.75	5.004	3.371	2.173	7.325

Run	Oil recovery during WAG injection	CO_2 injected per barrel of oil produced	CO_2 stored per barrel of oil produced	S*	R*
	%STOOIP	Mscf/stb	Mscf/stb	$/Mscf	$/stb
HET14	19.01	4.162	2.860	3.863	11.048
HET15	17.59	9.228	4.073	1.436	5.850
HET16	28.13	9.922	5.547	1.769	9.813
HET17	34.71	8.513	3.902	2.162	8.436
HET18	23.99	2.134	1.760	6.557	11.538
HET19	28.87	9.636	4.651	1.522	7.079
HET20	33.99	3.480	1.675	8.696	14.569
HET21	10.21	5.440	4.369	0.559	2.444
HET22	13.29	6.605	3.898	2.035	7.932
HET23	26.29	12.636	4.718	1.800	8.493
HET24	19.08	1.473	1.213	7.126	8.644
HET25	19.70	2.351	1.547	5.843	9.039
HET26	23.06	6.864	4.128	2.241	9.250
HET27	20.42	6.989	3.908	1.913	7.476
HET28	9.11	3.057	2.717	2.819	7.660
HET29	22.31	1.227	0.759	20.802	15.790
HET30	31.89	25.886	6.471	0.106	0.687
HET31	15.67	3.595	3.043	4.068	12.381
HET32	16.29	2.656	1.691	5.727	9.683
HET33	21.96	10.564	7.548	0.543	4.097
HET34	25.65	2.290	1.748	7.305	12.765
HET35	21.97	2.143	1.163	8.585	9.987
HET36	18.79	7.872	5.620	0.577	3.241
HET37	33.22	2.935	2.087	5.182	10.815
HET38	16.70	10.473	4.511	0.757	3.415
HET39	31.16	0.909	0.717	19.740	14.156
HET40	30.48	10.479	4.192	1.803	7.557
HET41	19.64	21.614	6.736	-0.122	-0.825
HET42	43.60	23.162	5.167	0.931	4.812
HET43	35.54	16.746	4.689	1.170	5.484
HET44	24.77	4.686	3.744	3.643	13.642
HET45	29.00	9.860	5.450	1.003	5.465
HET46	**41.47**	**1.405**	**0.794**	**20.954**	**16.644**
HET47	11.80	4.879	3.331	2.928	9.754
HET48	21.05	11.196	7.693	0.603	4.642
HET49	15.57	8.354	6.328	0.724	4.579
HET50	36.86	5.060	3.381	3.717	12.565
HET51	31.02	5.896	4.009	2.437	9.772
HET52	18.69	4.883	2.250	3.021	6.798
HET53	15.92	5.557	2.801	2.585	7.241
HET54	23.78	4.320	2.931	2.839	8.322

Run	Oil recovery during WAG injection	CO_2 injected per barrel of oil produced	CO_2 stored per barrel of oil produced	S*	R*
	%STOOIP	Mscf/stb	Mscf/stb	$/Mscf	$/stb
HET55	21.95	3.129	2.219	3.928	8.716
HET56	41.33	1.410	1.019	12.425	12.655
HET57	6.24	9.474	7.764	0.237	1.836
HET58	8.31	3.333	2.623	2.506	6.574
HET59	16.74	4.861	3.615	2.256	8.154
HET60	10.93	9.022	1.309	6.889	9.016
HET61	40.88	6.521	1.966	5.270	10.359
HET62	36.12	5.055	3.248	2.837	9.215
HET63	37.08	7.923	5.067	2.111	10.696
HET64	16.58	2.991	1.903	4.068	7.741

The results also show that reservoir heterogeneity negatively affects the oil recovery and particularly the CO_2 storage, as demonstrated by a few arbitrary examples in Figures 6.4 and 6.5. The two simulation cases plotted together are different in their porosity, permeability and the corresponding Pc values only. In most cases, CO_2 storage is higher in the homogeneous reservoir and when the waterflooding duration is shorter.

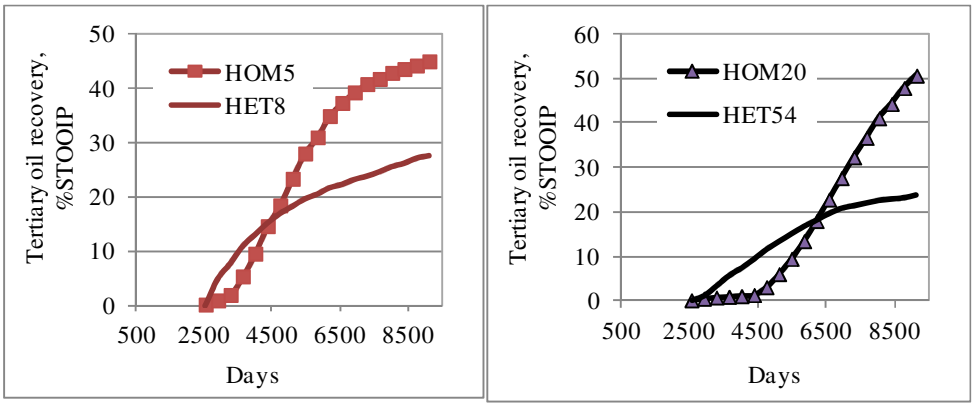

Figure 6.4: Comparison of the oil recovery from the WAG injection between the corresponding homogeneous and heterogeneous reservoirs (differing only in porosity and permeability values).

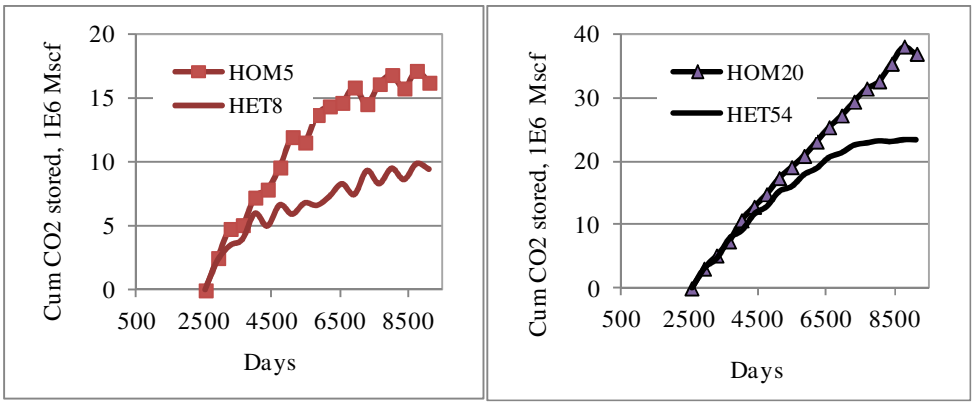

Figure 6.5: Cumulative CO_2 stored for the corresponding simulation cases in Figure 6.4.

The ANOVA results for the R* and S* models as shown in Tables A6.3 and Table A6.5-A6.7 in Appendix A6.4, show that the resultant models were statistically significant with more than 95% confidence level.

Factors influencing the oil recovery profit

As a default, the response data will be analysed in its actual form. The model is statistically significant if the data points on the normal plot of residuals are approximately linear. A residual (or fitting error) of a sample is the difference between the observed and the predicted response (Montgomery, 1991). A non-linear pattern indicates that the equality of variance does not hold for the residuals of the given model, in which case the program automatically identifies the suitable transformation for the data to correct this non-normality in the error term.

Most data transformations can be described by the power function, $\sigma = fn(\mu\alpha)$, where σ is the standard deviation, μ is the mean and alpha (α) is the power. If the standard deviation associated with an observation is proportional to the mean raised to the *a* power, then transforming the observation by the 1 - *a* (or l) power gives a scale satisfying the equal variance requirement of the statistical model (Design-Expert®, 2010).

For the oil recovery profit, R*, of the homogeneous model, a power function provided a

more precise and normal fit for which the model's form is shown in Equation 6.8 below (This is the final equation in terms of coded factors with actual coefficients are disguised by β's, but signed plus or minus true to actual form) where the alphabetical letters are the factors as defined in Table 6.1. No transformation was needed for R* of the heterogeneous reservoir model. The final equations in terms of coded factors and actual factors of R* and S*, for homogeneous and heterogeneous models, are given in Appendix A6.3.

$$(R^* + 29.95)^{2.39}) = \beta_0 + \beta_1 A + \beta_2 B - \beta_3 C - \beta_4 D - \beta_5 E - \beta_6 F - \beta_7 G + \beta_{10} K + \beta_{11} L + \beta_{12} AB + \beta_{15} AE + \beta_{110} AK - \beta_{25} BE + \beta_{27} BG + \beta_{28} BH + \beta_{38} CH - \beta_{510} EK + \beta_{511} EL - \beta_{610} FK \quad (6.8)$$

Figure 6.6 shows the half normal plots of effects for the oil recovery profit, R*, for both reservoirs. These plots are used to evaluate the normality of the distribution of a variable. The standardized effect in the x-axis of the plots is the effect expressed in terms of its difference from the mean, divided by the standard deviation. The significant factors are those which stand out to the right on the x-axis scale. The blue colour in the plots indicates a negative effect, i.e., increasing the factor from its low to high value decreases the response value. For the positive effect, which is shown in orange, increasing the factor from its low to high value increases the response value.

The top ten influential factors to R*, ranked from the highest to the lowest effects, are listed in Table 6.7 (refer to Table 6.1 for the description of the abbreviations and alphabetical letters shown). The duration of the preceding waterflood (G) and the wettability of the reservoir represented in the form of relative permeability (E) top the list for both reservoir types. Many factors are also common share between them, albeit of different ranking.

There are also several interactions of factors influencing the oil recovery profit. These include the combination of permeability with porosity (AB), permeability with relative permeability (AE) and relative permeability with the WAG ratio (EK). Interaction plots can show how the change in one factor affects the way other factor it interacts with influences the response factor. In plotting the interaction plots here, only the interacted factors were varied while the other parameters were kept constant at values shown in Table 6.8.

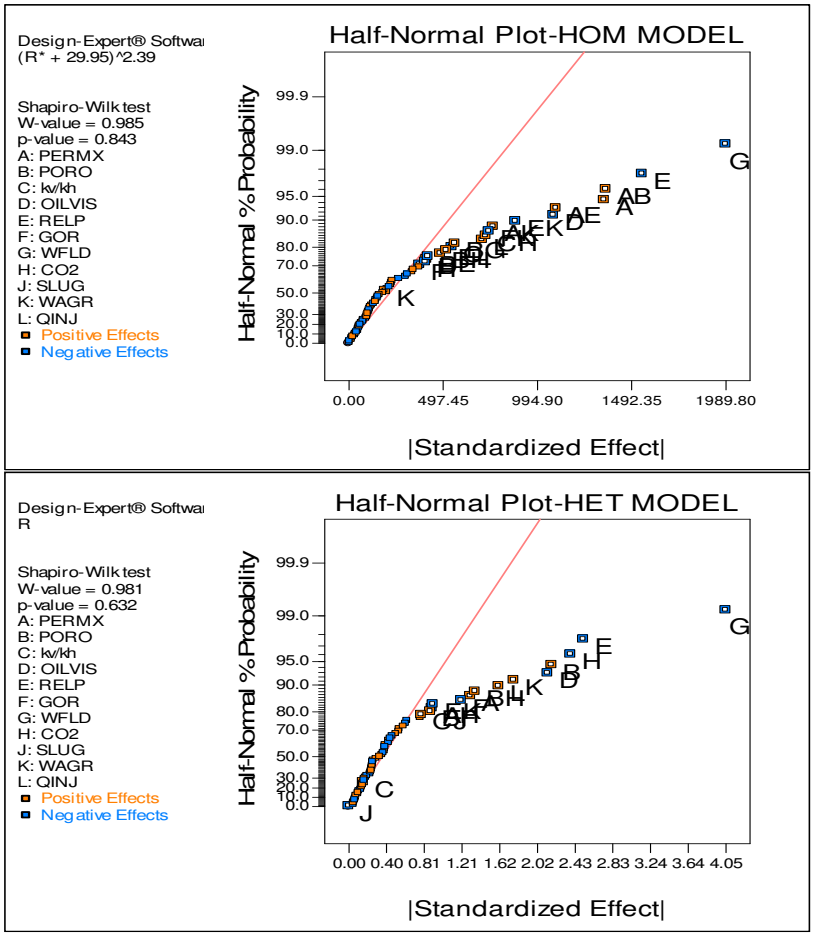

Figure 6.6: Half-normal plots of effects for oil recovery profit, R*, for the homogeneous (top plot) and heterogeneous (bottom plot) reservoirs.

Table 6.7: The top ten effects influencing the oil recovery profit from tertiary WAG injection, ranked from the highest to the lowest.

Rank	HOMOGENEOUS	HETEROGENEOUS
1	(G) WFLD	(G) WFLD
2	(E) RELP	(E) RELP
3	(AB) PERMX*PORO	(H) CO2
4	(A) PERMX	(B) PORO
5	(AE) PERM*RELP	(D) OILVIS
6	(D) OILVIS	(K) WAGR
7	(EK) RELP*WAGR	(L) CO2
8	(AK) PERMX*WAGR	(BH) PORO*CO2
9	(FK) GOR*WAGR	(A) PERMX
10	(CH) KV/KH*CO2	(F) GOR

Table 6.8: The value of the constant factors used in plotting the interactions.

Factor	Value	Factor	Value
Permeability, mD	800	GOR limit	30
Porosity, fraction	0.2	Waterflooding duration, years	5
K_v/K_h ratio	0.1	Injected CO_2, mole fraction	1
Relative permeability table no.	1	Slug size, %HCPV	4
Oil viscosity, cP	4	Gas injection rate, Mscf/day	17445

For the homogeneous reservoir, Figure 6.7a, the effect of WFLD (x-axis) on R* (y-axis) depends on the level of porosity (PORO) represented by the black and red lines, which in turn correspond to the low (-) and high (+) levels of PORO, respectively. The two lines extend from the lowest water flood limit of 3 years on the left to its highest of 7 years on the right. The "I-beam" on the interaction plot is the result of the least significant difference (LSD) calculations (Design-Expert®, 2010). The differences attributed to the factor's effects are significant if the plotted points fall outside the range (i.e., the I-beams of the black and red lines are separated from each other), as can be seen on the 7-years waterflood end and not so if the I-beams overlap as on the left end of Figure 6.7a.

So, from Figure 6.7, we can deduce that a longer preceding waterflood period generally leads to less profitable oil recovery. For the heterogeneous reservoir, extending the waterflood duration from 3 to 7 years reduces the value of the oil recovery from 12 to about 8 $/bbl. For the homogeneous reservoir, the level of reduction in R* due to the increasing WFLD depends on the PORO level (Figure 6.7a). The decline in the profit per barrel of oil with increasing WFLD is steeper if the reservoir porosity is low.

Wettability affects oil recovery by controlling the location, flow and distribution of fluids in the porous medium (Anderson, 1987). Figure 6.8 shows the interaction for the effects of RELP and WAGR on R*. Generally, the oil recovery profit is higher for the water-wet reservoir (black line E-) than for the oil-wet reservoir (red line E+) although the difference is relatively negligible at small WAGR (close or overlapping I-beams). Increasing WAGR results in a higher R* in the water-wet reservoir but the reverse is true for the homogeneous, oil-wet reservoir.

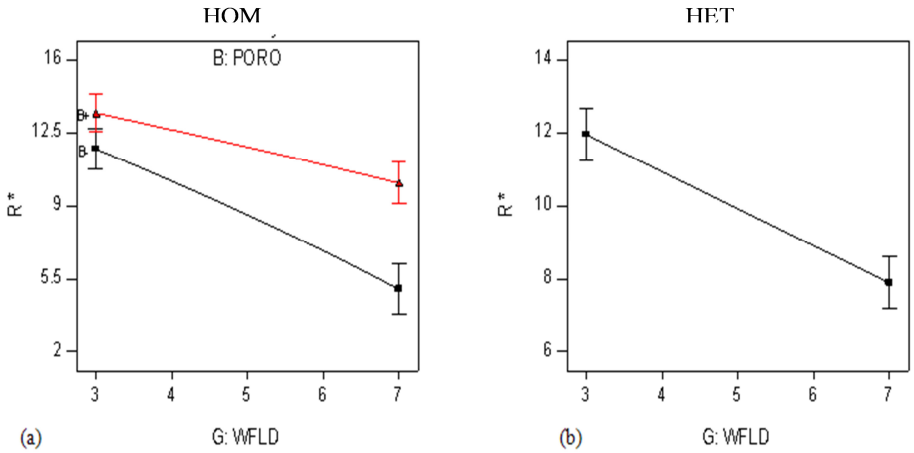

Figure 6.7: (a) Interaction of WFLD and PORO on R*for the homogeneous reservoir and (b) the effect of WFLD on R* for the heterogeneous reservoir.

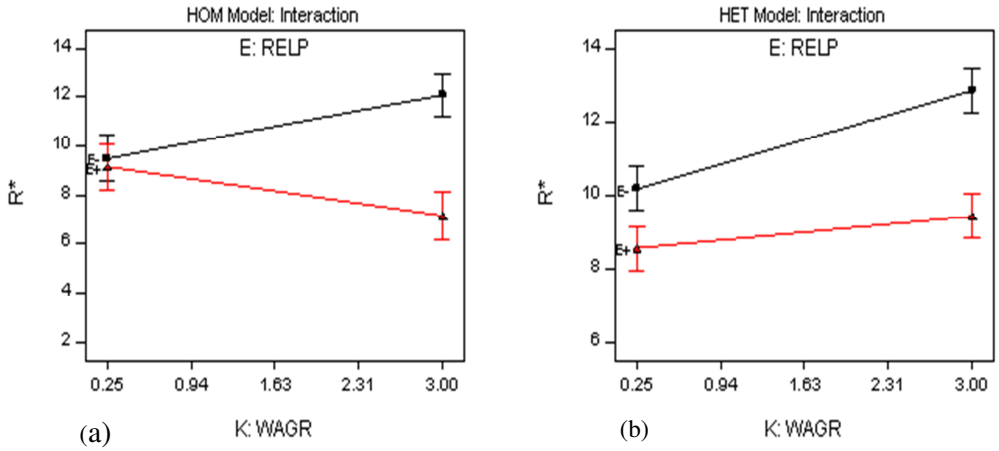

Figure 6.8: Interaction plot for the effect of RELP and WAGR on R* for the (a) homogeneous and (b) heterogeneous reservoirs.

PERMX also influences the effects of REP's and WAGR on R* of the homogeneous reservoir as shown in Figure 6.9a. At high PERMX, RELP has little impact on R* but higher WAGR is beneficial to R*. The profitability of oil recovery in the oil-wet reservoir worsens at low PERMX. Other factors that result in higher oil recovery and lower CO_2 injection costs, such as low viscosity oil that is miscible with the injected CO_2 and injection of the C1, N2 and CO_2 gas mixture rather than pure CO_2, also contribute to higher oil

recovery profit from the WAG injection.

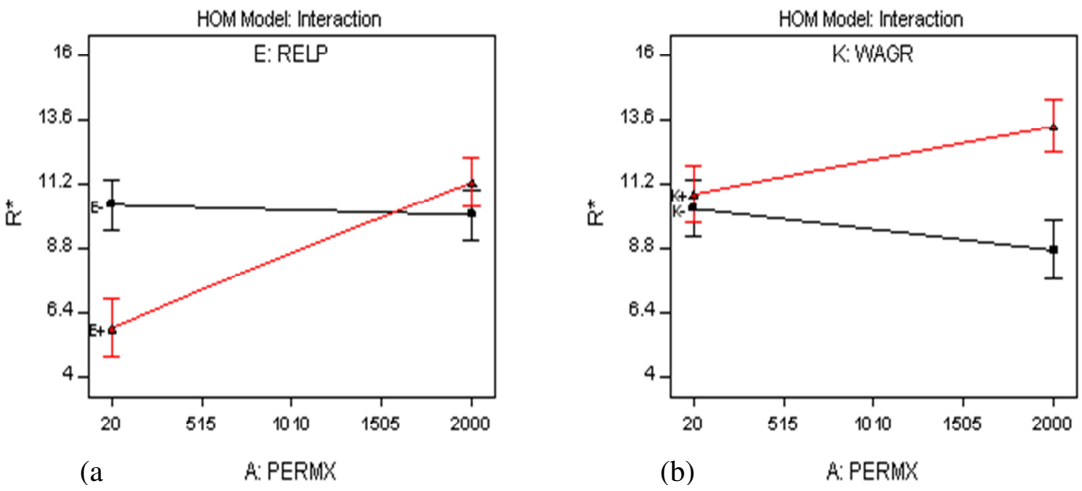

Figure 6.9: Interaction plot for the effect of PERMX versus (a) RELP and (b) WAGR, for the homogeneous reservoir on R*.

Factors influencing the CO_2 storage profit

Table 6.9 shows the top ten effects influencing the CO_2 storage profit, S*, as identified from the half-normal plots of the effects in Figure 6.10. For both reservoir types, the top three important factors are the injected gas composition (CO2), the waterflood duration (WFLD) and reservoir wettability (RELP).

Heterogeneity seems to have lesser roles in determining the influential factors for the S*, as there are more common factors between the two types of reservoir even though the ranking is slightly different. The interaction of factors also has lesser influence, compared with the case of the R*. In the homogeneous reservoir, as shown in Figure 6.11, short WFLD is generally favourable to obtain higher S*, especially for the high permeability (line A+ in Figure 6.11a) and light oil (line D- in Figure 6.11b) reservoir. PERMX and OILVIS, however, cease to have any impact on S* when WFLD is longer.

Table 6.9: The top ten effects influencing the CO_2 storage profit from the WAG injection, ranked from the highest to the lowest.

Rank	HOMOGENEOUS RESERVOIR	HETEROGENEOUS RESERVOIR
1	(G) WFLD	(H) CO2
2	(H) CO2	(E) RELP
3	(E) RELP	(G) WFLD
4	(A) PERMX	(K) WAGR
5	(EK) RELP*WAGR	(D) OILVIS
6	(D) OILVIS	(A) PERMX
7	(AB) PERMX*PORO	(AH) PERMX*CO2
8	(ED) RELP*OILVIS	(CJ) KV/KH*SLUG
9	(CJ) KV/KH*SLUG	(B) PORO
10	B (PORO)	(EK) RELP*WAGR

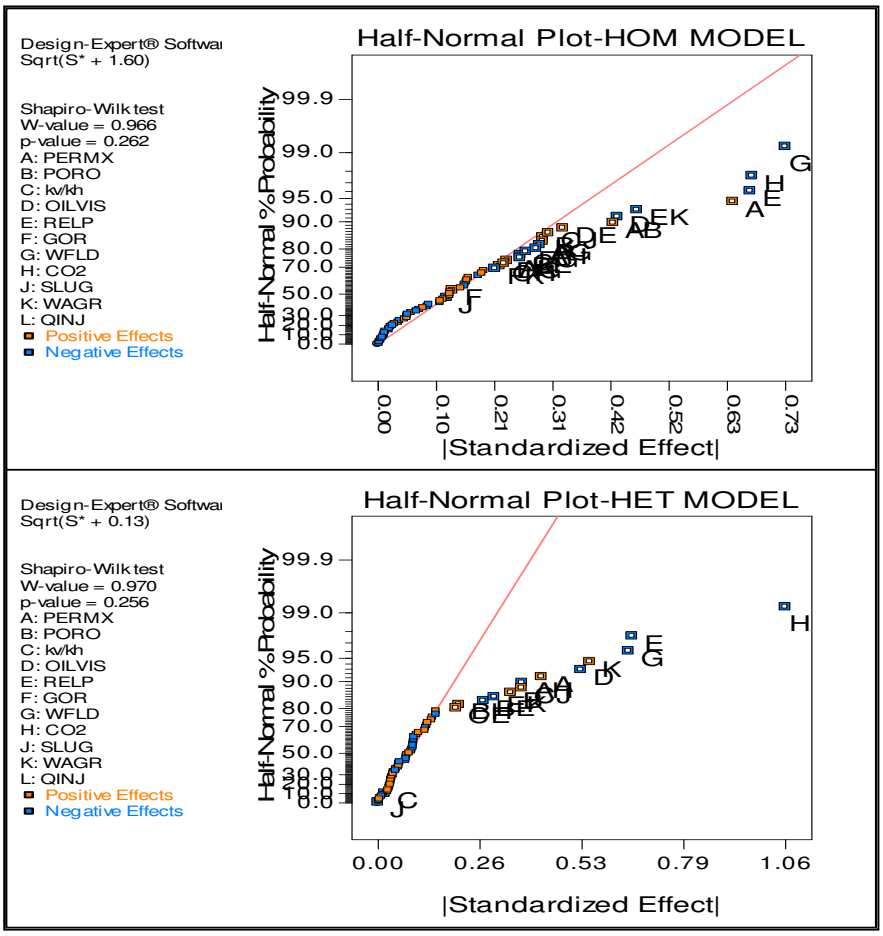

Figure 6.10: Half-normal plots of effects for CO_2 storage profit, S*, for homogeneous (top plot) and heterogeneous (bottom plot) reservoirs.

Whilst the effect of PORO is insignificant if the PERMX is very low, S* increases markedly with PORO if PERMX is high, Figure 6.12. The combination of high PERMX and smaller mole fraction of CO_2 in the injected gas (CO2) is also beneficial to S* for both reservoir types, as demonstrated in Figure 6.13. PERMX nevertheless has no influence on the effect of the injected gas composition on S* when pure CO_2 gas is used. With pure CO_2, the amount of CO_2 stored is higher, since no other injected components are competing for the available pore volume. But the higher cost of pure CO_2 than that of the gas mixture predictably lowers the profit.

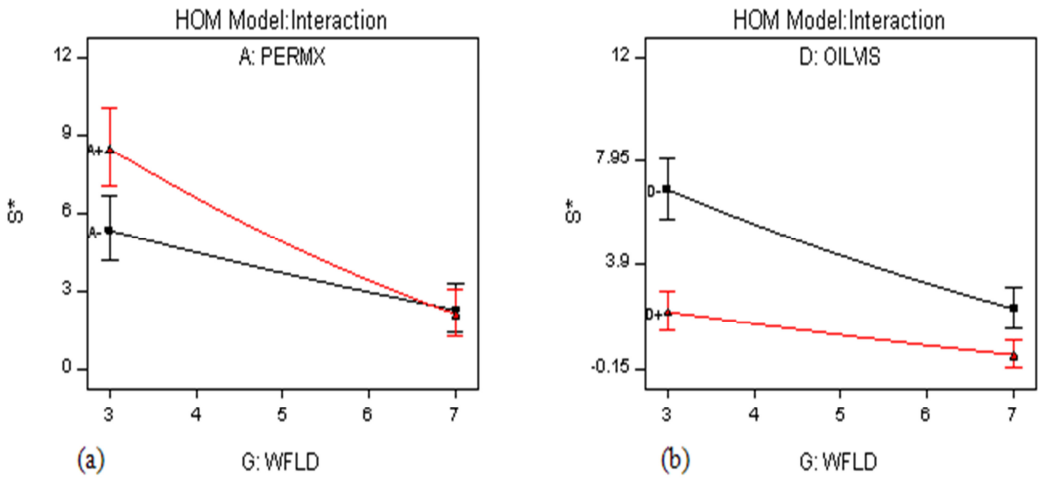

Figure 6.11: Interaction plot for the effect of PERMX and OILVIS versus WFLD on S* for the homogeneous reservoir.

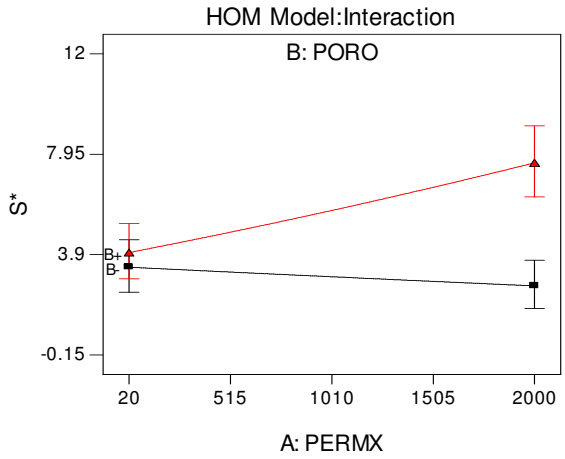

Figure 6.12: The effect of PERMX versus PORO on S* for the homogeneous reservoir.

The reservoir wettability (RELP) is important to the CO_2 storage economics in the same way as it is to the oil recovery profit. S* is much higher for the water-wet reservoir (RELP = 1) than for the oil-wet reservoirs (RELP = 2) but this is highly dependent on the WAGR and PORO as depicted in Figures 6.14a-d. a reservoir with high PORO (B+) and operating at high WAGR (K+) would gain higher S*.

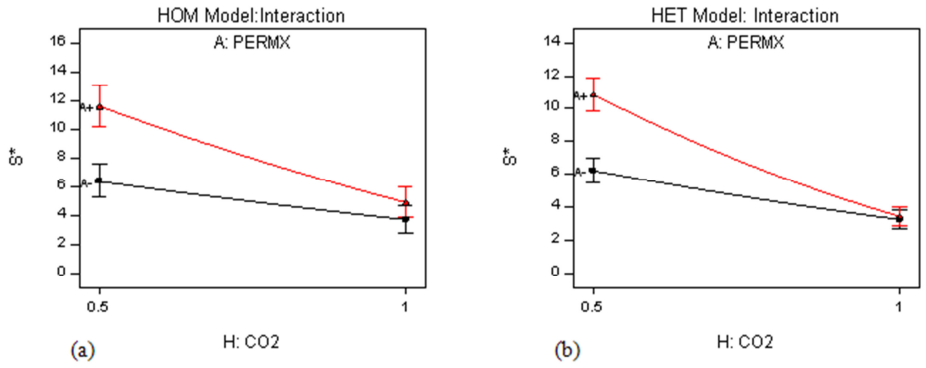

Figure 6.13: Interaction plot for the effect of PERMX versus CO2 on S* for (a) the homogeneous and (b) heterogeneous reservoirs.

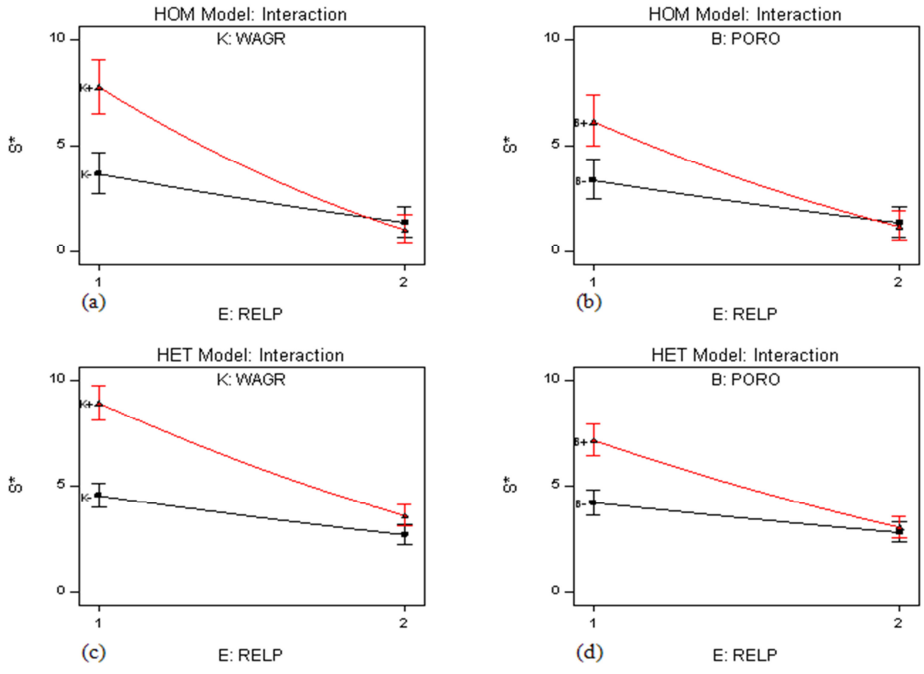

Figure 6.14: Interaction plot for the effect of (a) WAGR and RELP and (b) PORO and RELP on S* for the homogeneous reservoirs; (c) WAGR and RELP and (b) PORO and RELP on S* for the heterogeneous reservoirs.

Factors influencing both oil recovery and CO_2 storage profit

The equally weighted oil recovery and CO_2 storage profit (or *f* function) represents the co-optimized oil recovery and CO_2 storage performance. The higher the *f* value, the more favourable the scheme is to result in profitable oil recovery and CO_2 storage. The Pareto plot of effects for the *f* function, Figure 6.15, identifies waterflood duration prior to WAG injection (G) as the most influential factor for both types of reservoir.

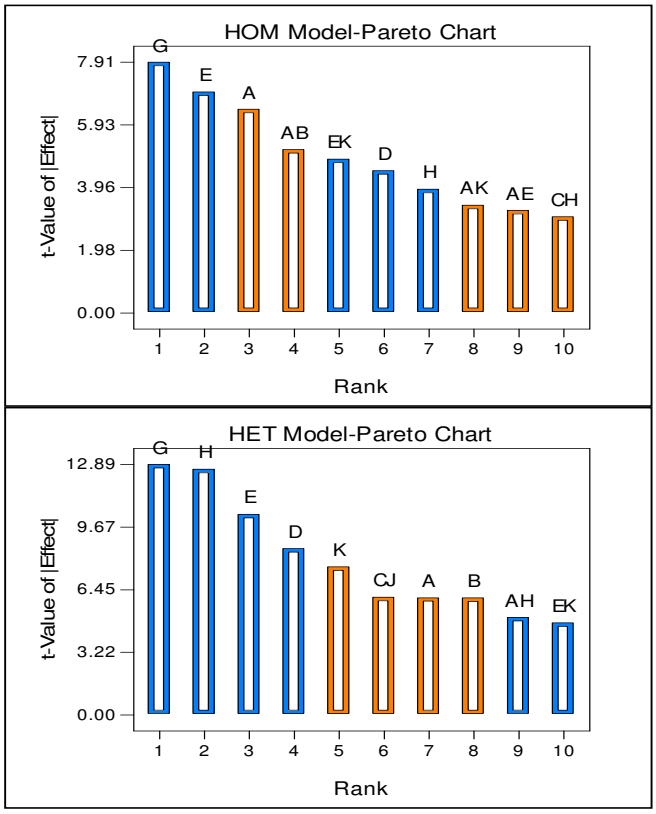

Figure 6.15: Pareto chart of effects for the equally weighted oil recovery and CO_2 storage profit (*f* function) for homogeneous (top plot) and heterogeneous reservoirs (bottom plot).

As listed in Table 6.10, the injected gas composition (CO2), reservoir wettability (RELP) and permeability (PERMX) are also important. For the homogeneous reservoir, there is a lot of interplay between factors, examples of which are shown in Figure 6.16. When the reservoir permeability is high, high porosity (B+) and high WAG ratio (K+) are favourable to achieve an optimized process (i.e., higher *f*) but a large WAG ratio gives lower *f* values to the oil wet reservoir.

Table 6.10: The top ten effects influencing the *f* function ranked from the highest to the lowest.

Rank	HOMOGENEOUS RESERVOIR	HETEROGENEOUS RESERVOIR
1	(G) WFLD	(G) WFLD
2	(E) RELP	(H) CO2
3	(A) PERMX	(E) RELP
4	(AB) PERMX*PORO	(D) OILVIS
5	(EK) RELP*WAGR	(K) WAGR
6	(D) OILVIS	(CJ) KV/KH*SLUG
7	(H) CO2	(A) PERMX
8	(AK) PERMX*WAGR	(B) PORO
9	(AE) PERMX*RELP	(AH) PERMX*CO2
10	(CH) KV/KH*CO2	(EK) RELP*WAGR

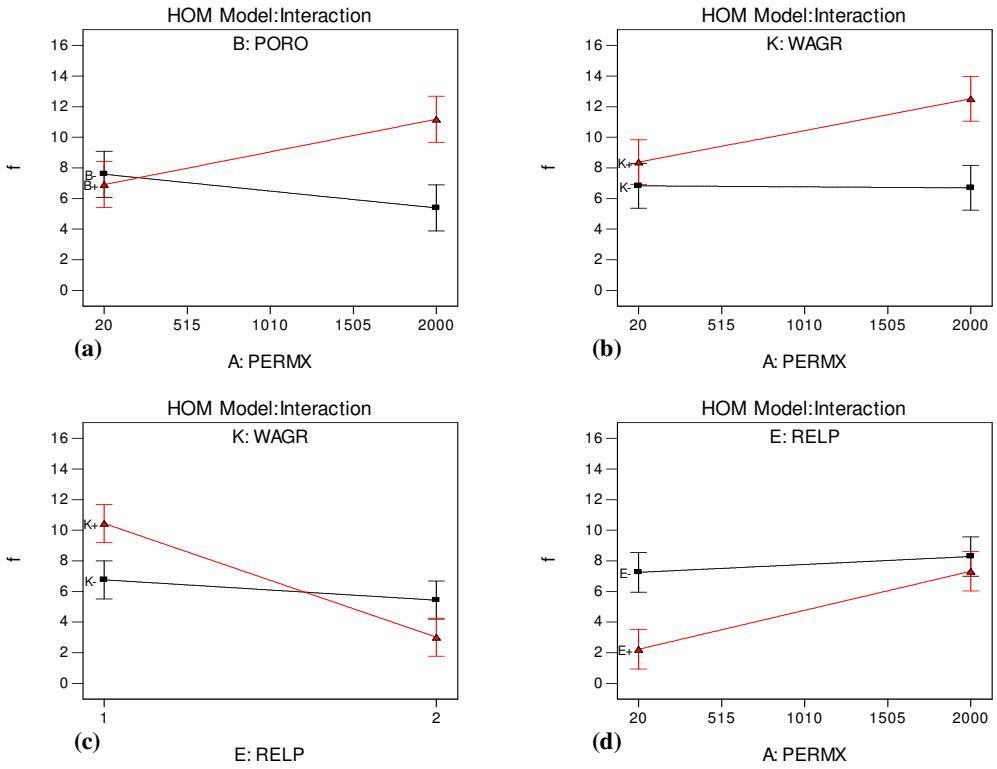

Figure 6.16: Interaction plot for the effect of (a) PERMX and PORO, (b) PERMX and WAGR, (c) RELP and WAGR and (d) PERMX and RELP on the *f* function for the homogeneous reservoir.

For the heterogeneous reservoir, higher *f* was obtained when the reservoir is water-wet with high permeability and porosity, and when leaner gas and high WAG ratio was used (Figure 6.17b and 6.17d). Small slug size results in a high *f* factor for the reservoir with small k_v/k_h ratio, Figure 6.17a.

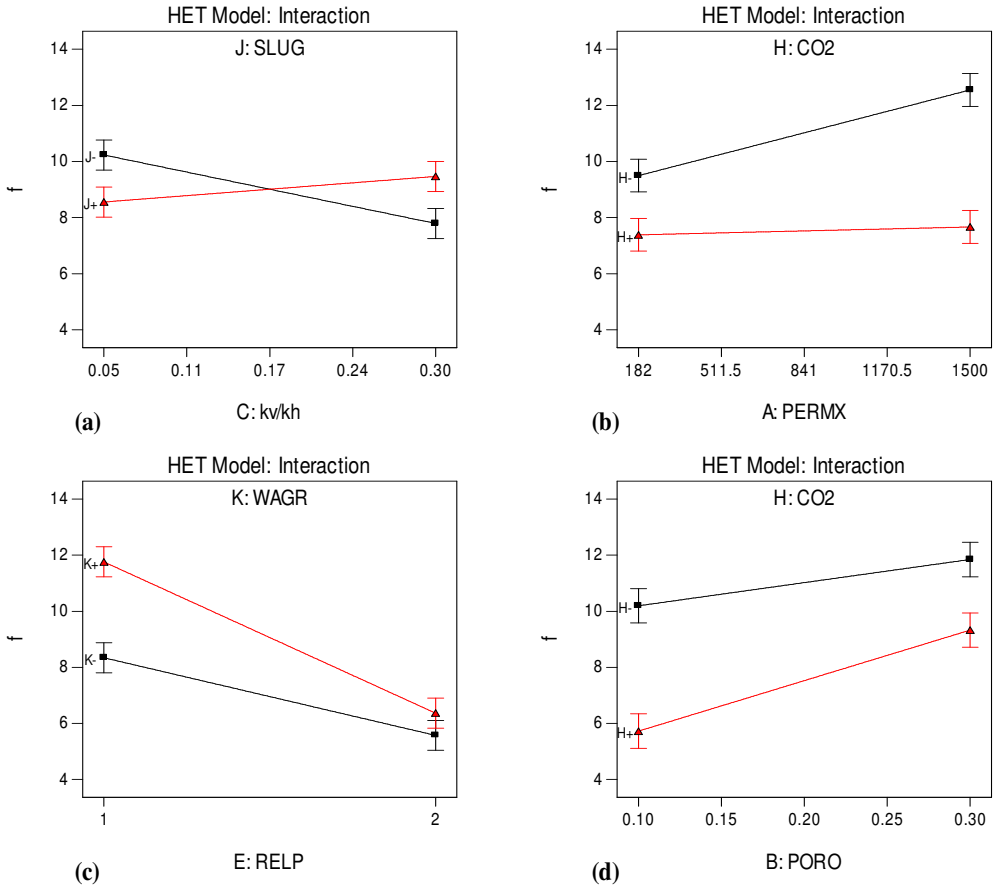

Figure 6.17: Interaction plot for the effect of (a) KVKH and SLUG, (b) PERMX with CO2, (c) RELP and WAGR (d) PORO and CO2, on the *f* function for the heterogeneous reservoir.

While the fractional factorial DOE used is generally effective as a screening method for the significant factors, it should be borne in mind that this design is based on the implicit assumption that higher-order interactions do not matter; but sometimes they do.

6.3. Field scale WAG flood design optimization for EOR and CO_2 storage

The parametric simulation results identify the influential factors to the tertiary miscible WAG injection. The objective of the co-optimization exercise in this study is to search for a combination of operational factor levels that simultaneously satisfy the goals of maximizing profit for oil recovery as well as that for CO_2 storage.

6.3.1. Co-optimization study approach

Model description

The simulations were performed using an E300 compositional simulator on a synthetic PUNQ-S3 reservoir model. The model is a small-scaled but realistic model which was developed based on an actual producing North Sea oilfield. The model was originally constructed for production forecasting with an uncertainty quantification study (Floris et al., 2001) and is electronically available at http://www3.imperial.ac.uk/.

The field is a dome shaped structure, bounded to the east and south by a fault, Figure 6.18. It is linked to the north and west to a fairly strong aquifer. The field is very heterogeneous with connected high permeability streaks observed in all layers. The top views of the porosity and permeability distribution are shown in Figure 6.19. Permeability in the X and Y direction ranges from 0.5 to 999 mD with an average of 269 mD, while the porosity spans 1 to 29.9% averaging at 13.9%. The formation was discretized into 19x28x5 corner-point geometry grid blocks with 1761 active blocks. The average dimension of the gridblock in the X and Y direction is 590 ft. The thickness of the five layers of fluvial sand and shale ranges from 2.5 to 30 ft. The published 'truth case' grid size was used as it is, i.e., no grid sensitivity was carried out. The aquifer was defined analytically in the model.

In the original model, there was a small gas cap in the centre of the dome with six producers located around the gas-oil contact (GOC). However, for this study, the fluid model of the 4 cP Little Knife oil, as described in Chapter 5, was used instead. The GOC was adjusted to a shallower depth so that there was no gas cap in the model at initialization. The reservoir

temperature and initial pressure were set at 150 ^{o}F and 4000 psig, respectively. Different well locations from the original model were also used, where only four producers were specified whilst four injectors were added, locations of which are shown in Figure 6.20. Due to the heterogeneity of the reservoir, the wells were perforated selectively in layers with good permeability and connectivity only. The oil/water and oil/gas relative permeability curves used in the model were the same as those used for the water-wet heterogeneous 5-spot well pattern model described earlier (Figures 6.1 and 6.2). With a pore volume of 217.3 MMrb, the reservoir has 87.2 MMstb STOOIP. The initial oil saturation distribution is shown in Figure 6.20.

The total production was controlled at 22,500 rb/day; a rate equivalent to about 9 %STOOIP/year, with 2000 psig minimum BHP at the producer wells. The well was shut when the oil production fell below 5 bbl/day and upon exceeding 99% water cut, the worst offending connection and all those below it were also shut. Water was injected at 6200 stb/day/well and CO_2 at 14325 Mscf/day/well, respectively, to the maximum BHP of 5860 psig.

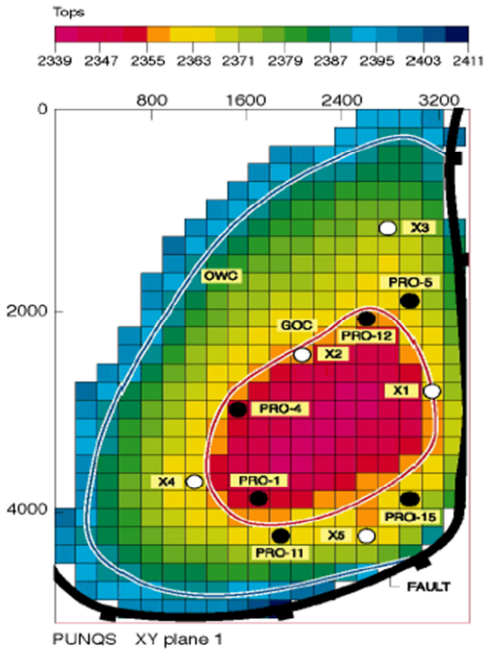

Figure 6.18: The PUNQ-S3 top structure map showing the original GOC and well locations (http://www3.imperial.ac.uk).

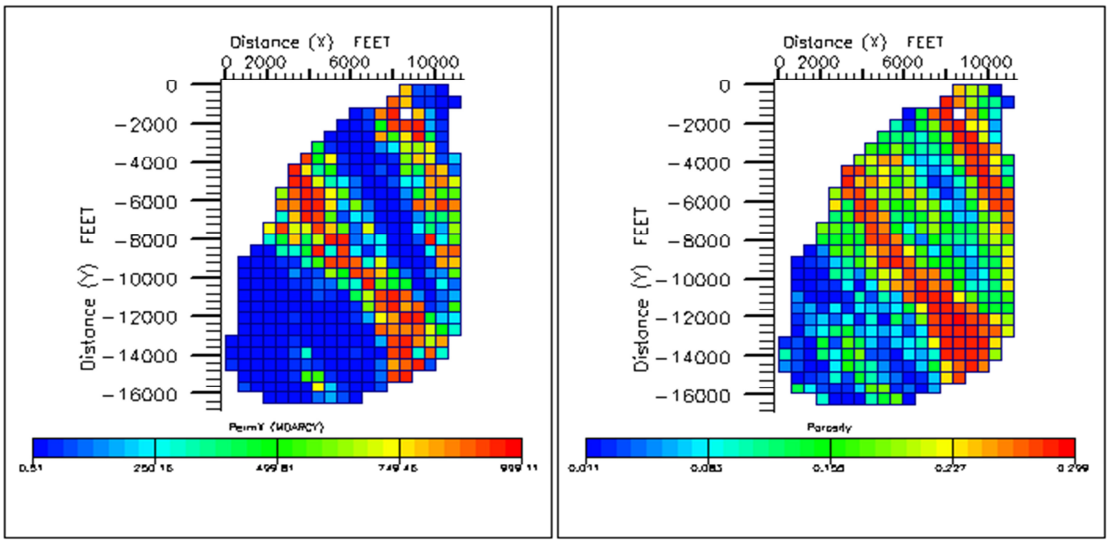

Figure 6.19: Top view of the distribution of permeability (left) and porosity (right).

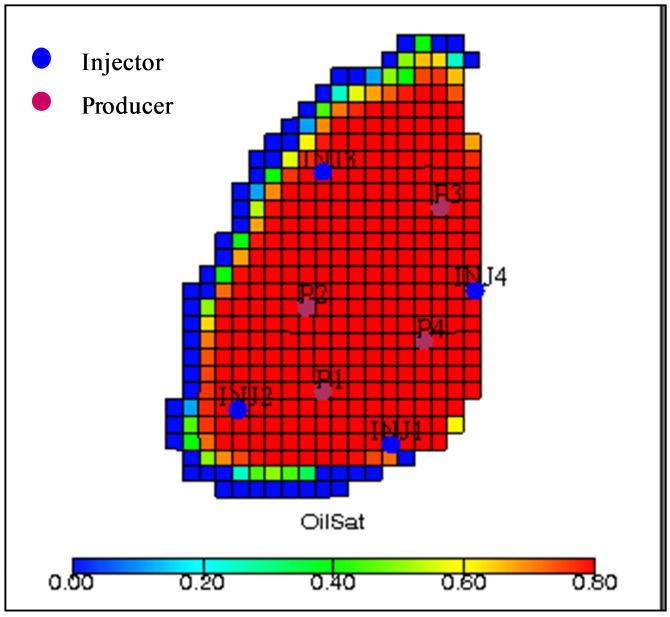

Figure 6.20: The initial oil saturation distribution and well locations used in this study.

The reservoir was first waterflooded prior to the WAG injection. The average reservoir pressure was maintained at around 4000 psig within the waterflooding period. During the WAG injection, the wells were set to operate at 10% more injection than production to ensure the average reservoir pressure was higher than the MMP. The simulation was run for

35 years. CO_2 injection continued until the maximum BHP was reached or until the end of simulation duration, to allow for maximum CO_2 storage possible.

Design of the experiment

The nonlinearity of the partial differential equations governing the fluid flow in the reservoir makes numerical simulation very computationally intensive, particularly when there are a large number of uncertain parameters to be accounted for at once. For this optimization study, DOE was again used, this time via the Response Surface Method (RSM) to develop simulation runs that examine the multiple factor effects simultaneously with relatively fewer runs. RSM creates a multivariate polynomial model that provides an analytical relationship between a response and set of factors, which can be precisely mapped by a mathematical model (Anderson and Whitcomb, 2005).

The D-Optimal design of the Design Expert 8.0.6 program was employed for the co-optimization study. Only the influential design parameters were sensitized for the optimization, while the reservoir properties were fixed. The ranking of the significant factors of the heterogeneous model in the parametric simulation were referred in selecting the influential factors.

Table 6.11 shows the factors and their range incorporated in the co-optimization exercise. The range of the mole fraction of CO_2 in the injected gas has been increased from 0.3 to 1.0, instead of 0.5 to 1 as in the earlier analysis. The injection rate of water and CO_2 gas were fixed, but the injection durations were varied to attain the slug size required. Although the well configuration is believed to be among the important operational parameters, this factor was not included in the optimization study. Reason being, the model has a unique stratification, thus, if the well configuration is included, the results would then become very reservoir-specific. R* and S* were again used as the response parameters.

Based on the number of factors in the design and the number of coefficients in the designed model, a quadratic model that reveals two-component interactions was selected. 44 simulation cases, as listed in Table 6.12, were identified to build the mathematical model.

Table 6.11: Factors evaluated and the range involved in co-optimization of oil recovery and CO_2 stored through tertiary WAG injection.

Factor	Name	Units	Type	Subtype	Minimum (-1)	Maximum (+1)
A	WFLD	years	Numeric	Continuous	3	7
B	WAGR		Numeric	Continuous	0.25	3
C	CO2	mole frac	Numeric	Continuous	0.3	1
D	GOR	Mscf/stb	Numeric	Continuous	10	50
E	SLUG	%HCPV	Numeric	Continuous	0.5	8

Table 6.12: The combination of the design parameters of the WAG injection for all the simulation cases.

Run	A:WFLD, years	B:WAGR	C:CO2, mole fraction	D:GOR, Mscf/stb	E:SLUG, %HCPV
1	7.00	3.00	0.30	50.00	0.50
2	7.00	0.25	0.30	10.00	0.50
3	5.60	0.25	0.30	50.00	5.38
4	7.00	1.21	0.54	50.00	8.00
5	7.00	3.00	1.00	10.00	0.50
6	3.00	2.35	0.30	40.40	0.58
7	3.00	3.00	0.30	10.00	0.50
8	3.00	0.25	1.00	10.00	0.50
9	7.00	0.25	0.30	10.00	0.50
10	4.70	1.83	1.00	50.00	0.50
11	5.02	3.00	0.65	28.71	8.00
12	3.00	0.25	0.30	10.00	8.00
13	3.00	0.25	0.30	50.00	0.50
14	7.00	3.00	1.00	50.00	8.00
15	3.00	3.00	1.00	34.04	0.50
16	3.00	3.00	0.70	50.00	3.65
17	7.00	3.00	0.30	10.00	8.00
18	7.00	3.00	0.30	10.00	8.00
19	4.40	1.76	0.30	23.20	5.00
20	3.00	0.25	1.00	50.00	8.00
21	3.40	0.94	0.68	32.12	0.50
22	3.00	3.00	1.00	10.00	8.00
23	7.00	0.25	1.00	50.00	0.50
24	3.00	0.25	0.30	10.00	8.00
25	7.00	0.25	0.48	19.90	6.88
26	3.00	1.47	1.00	28.60	4.70
27	7.00	0.25	1.00	50.00	0.50

Run	A:WFLD, years	B:WAGR	C:CO2, mole fraction	D:GOR, Mscf/stb	E:SLUG, %HCPV
28	7.00	3.00	1.00	10.00	0.50
29	3.96	2.16	0.74	10.00	2.10
30	3.00	0.25	1.00	50.00	8.00
31	7.00	3.00	0.30	50.00	0.50
32	3.00	3.00	0.30	50.00	8.00
33	7.00	3.00	1.00	50.00	8.00
34	7.00	0.25	1.00	10.00	8.00
35	3.00	3.00	1.00	10.00	8.00
36	3.00	3.00	0.30	10.00	0.50
37	3.00	3.00	0.30	50.00	8.00
38	3.00	0.25	1.00	10.00	0.50
39	7.00	2.90	0.77	36.24	2.90
40	7.00	2.31	0.38	19.60	0.50
41	4.00	1.28	0.74	11.00	8.00
42	7.00	0.68	0.89	19.15	2.38
43	5.98	2.59	1.00	12.00	5.75
44	3.00	0.79	0.53	37.30	8.00

6.3.2. Results and discussion

The simulation results of the 44 runs are summarized in Table 6.13. The incremental oil recovery from the WAG injection ranges from 17% to 59%STOOIP and as much as 36% to 88% of the injected CO_2 could be stored at the end of the WAG injection.

Figure 6.21 shows the perturbation plot for the NPV of the tertiary WAG injection, where we can see that the NPV is very strongly influenced by the duration of the preceding waterflood. Shorter waterflood duration, which means faster oil recovery from the WAG injection, would lead to higher NPV of the project.

Simulation results also reveal that the highest equally weighted R* and S* i.e., the most promising scenario for the co-optimized process, is given by Run 32 (and its duplicate Run 37) which has the highest level of WAG ratio, GOR limit and slug size, and the lowest level of CO_2 content in the injection stream.

Table 6.13: The simulation results for the co-optimization study.

Run	% injected CO_2 stored	Oil recovery during WAG, %STOOIP	NPV for WAG, MM$	S*, $/Mscf	R*, $/stb
1	45.00	26	174.04	2.91	7.77
2	83.44	17	117.79	2.12	7.85
3	45.13	31	204.93	3.15	7.68
4	48.05	30	189.84	2.61	7.33
5	69.75	30	180.46	1.75	6.81
6	60.69	39	574.29	16.00	16.79
7	87.62	36	558.57	13.27	17.57
8	64.60	49	510.30	2.04	12.04
9	83.44	17	117.79	2.12	7.85
10	55.17	42	328.44	2.68	8.95
11	55.15	36	340.54	5.06	10.99
12	81.11	33	467.14	8.20	16.28
13	40.98	43	503.02	8.10	13.52
14	53.14	32	193.19	1.93	6.90
15	63.86	49	580.46	5.59	13.50
16	59.69	47	603.40	8.55	14.57
17	81.53	22	178.86	3.96	9.36
18	81.53	22	178.86	3.96	9.36
19	78.83	31	242.94	4.63	8.96
20	36.43	59	538.78	2.86	10.42
21	45.90	47	535.03	5.17	13.11
22	53.92	51	582.05	5.73	13.11
23	38.83	40	180.46	1.05	5.22
24	81.11	33	467.14	8.20	16.28
25	61.04	28	157.46	1.45	6.48
26	47.03	55	585.37	4.55	12.22
27	38.83	40	180.46	1.05	5.22
28	69.75	30	180.46	1.75	6.81
29	76.71	40	424.38	3.65	12.13
30	36.43	59	538.78	2.86	10.42
31	64.42	22	174.22	6.10	9.22
32	52.80	41	578.67	19.77	16.07
33	53.14	32	193.19	1.93	6.90
34	66.04	34	144.17	0.58	4.87
35	53.64	51	582.08	5.79	13.11
36	87.62	36	559.40	13.29	17.59
37	52.80	41	578.67	19.77	16.07
38	63.55	49	515.05	2.05	11.93
39	70.00	30	198.61	2.19	7.49
40	72.50	22	173.52	3.60	8.85

Run	% injected CO_2 stored	Oil recovery during WAG, %STOOIP	NPV for WAG, MM$	S*, $/Mscf	R*, $/stb
41	73.27	40	431.79	3.07	12.52
42	53.25	37	204.57	1.25	6.33
43	58.55	36	170.09	1.43	5.45
44	49.26	47	571.15	5.81	13.80

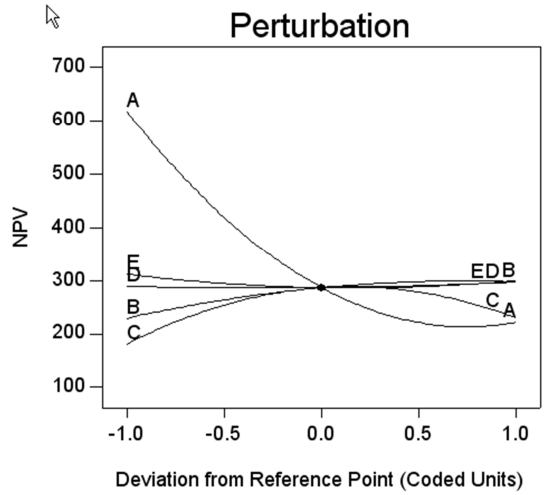

Figure 6.21: Perturbation plot for NPV for the tertiary WAG injection.

Table 6.14 gives the summary of the experimental design. The ANOVA results reveal that a linear and quadratic model provides a good prediction within the design space of R* and S*, respectively.

Table 6.14: Summary of the experimental design.

Name	Units	Analysis	Minimum	Maximum	Transformation	Model
S*	$/Mscf	Polynomial	0.58	19.77	Natural Log	Linear
R*	$/stb	Polynomial	4.87	17.59	None	Quadratic

The normal plot of the residuals was used as diagnostic plot to check if the statistical assumptions underlying the data analysis i.e., that the residuals follow a normal distribution with zero average and a standard deviation equal to that resulting from the analysis of the

data, are met. If so, the normal probability plot will follow a straight line. The residuals versus predicted response values plot will indicate a problem if a pattern exists. More explanation on the residuals and normal plot is given in Appendix A6.2. The normal plot of residuals, for example that of R* in Figure 6.22, has all design points positioned along a line. This verifies that residuals have normal distributions, thus validating the fit of the model. As indicated by R-squared (a measure of the amount of variation around the mean explained by the model) in the summary of the models' statistics shown in Table 6.15, 96% or more variation in the model has been described.

Table 6.15: Summary of the statistics for the model.

	S*	R*		S*	R*
Std. Dev.	0.17	0.35	R-Squared	0.96	1.00
Mean	1.31	10.74	Adj. R-Squared	0.96	0.99
C.V. %	12.93	3.28	Pred. R-Squared	0.95	0.98
PRESS	1.45	14.30	Adeq. Precision	45.60	49.43

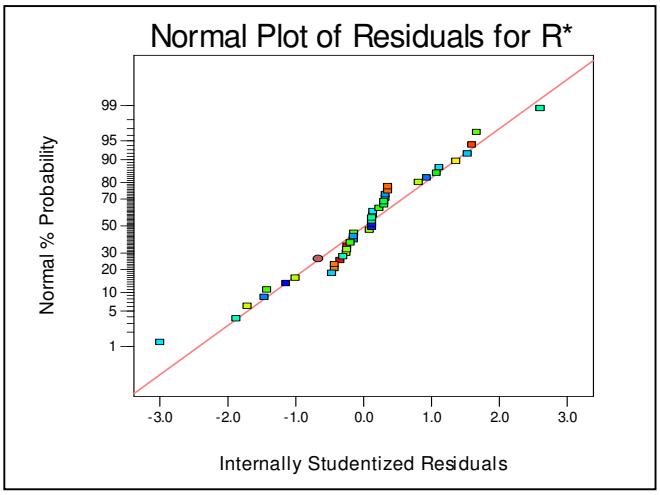

Figure 6.22: Normal probability plot of residuals for R*, tertiary WAG in synthetic reservoir model.

The perturbation plot in Figure 6.23, shows that the R* and S* vary primarily as functions of the waterflood duration (A), WAG ratio (B) and the CO_2 mole fraction in the injected gas

(C). These factors are therefore selected as the axes in plotting the contour and 3D plots.

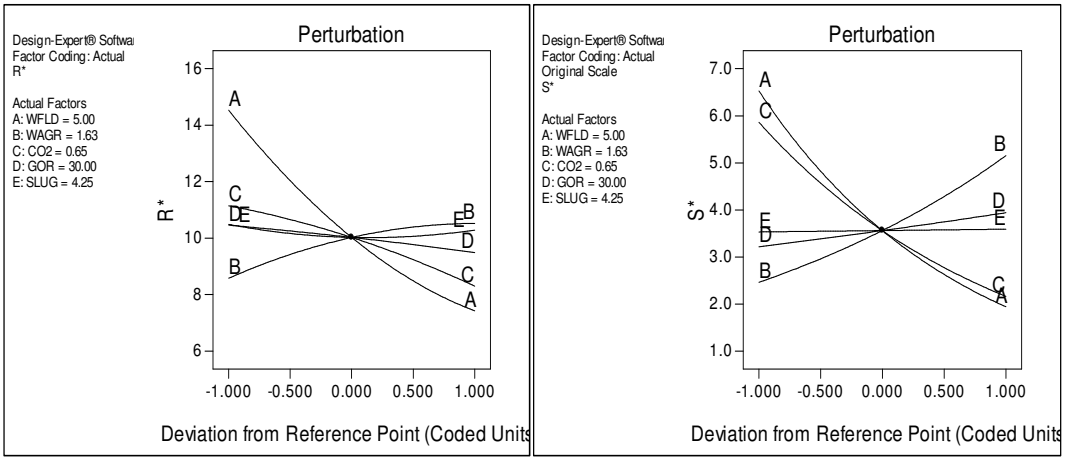

Figure 6.23: Perturbation plot for R* (left) and S* (right).

The 2D response surface contour plots of waterflood duration versus WAG ratio for R* and S* are shown in Figures 6.24 while that of waterflood duration and mole fraction of CO_2 in the injected gas, in Figure 6.25 (other factors set at centre points for this 'slice' of the experimental space). It is evident from these contour plots that within the range included in the model, higher R* and S* could be obtained with high WAG ratio, shorter preceding waterflood duration and a lower amount of CO_2 in the injected gas.

Using numerical optimization, the most desirable factor settings to get maximum R* and S* simultaneously, based on their predictive models, was found. The goal of maximizing R* and S* were combined into an overall desirability function (Equation 6.9 below), which in turn was maximized. The overall desirability, D, is computed by multiplying the individual desirabilities for each response, all of which are scaled from 0 to 1.

$$D = (d_1 \times d_2 \times \ldots d_n)^{\frac{1}{n}} - (\prod_{i-1}^{n} d_i)^{\frac{1}{n}} \quad (6.9)$$

where *n* is the number of responses in the measure. If any of the responses or factors falls outside their desirability range, the overall function becomes zero (Myers and Montgomery, 1995).

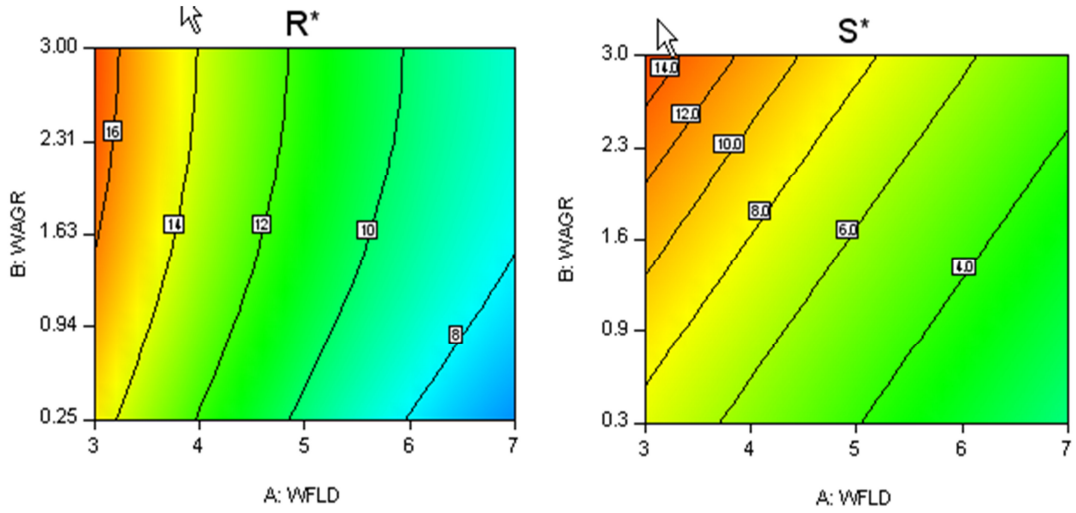

Figure 6.24: Contour plot of waterflood duration (A) and WAG ratio (B) for R*(left) and S* (right) with mole fraction of CO_2 in the injected gas (C) at -1 level.

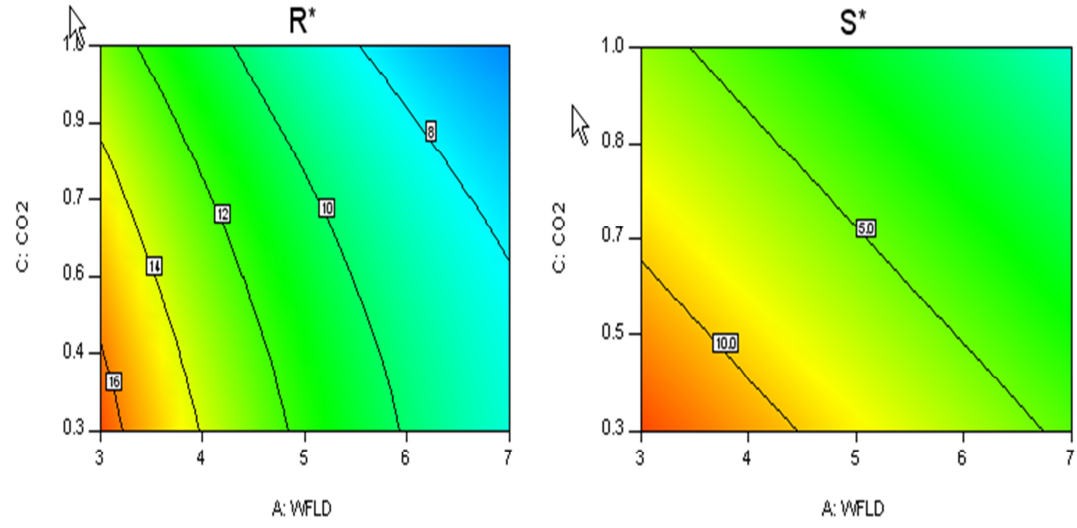

Figure 6.25: Contour plot of waterflood duration (A) and mole fraction of CO_2 in the injected gas (C) for R*(left) and S* (right) with WAG ratio (B) at +1 level.

Figure 6.26 shows the 3D response surface plot of the highest desirability for each response. Figure 6.27 depicts the ramps view of the optimum. A highlighted point shows both the exact value of the factor or response (horizontal movement of the point) and how well that goal was satisfied (how high up the ramp).

For the particular model and injection rates used in this study, to obtain the highest S* ($17.3/Mscf) and R*($16.2/stb), the WAG injection should start after 3 years of waterflood at the WAG ratio of 3:1, using the injected gas mixture of 30 mole % CO_2 and 70 mole% C1+N2. The produced GOR should be limited to about 50 Mscf/stb.

An E300 simulation was run with the same setting of the factors to verify the representativeness of the designed model. The comparison in Table 6.16 confirms that the response surface model obtained adequately represents the relationship between the critical factors and the response. The model can be used as a proxy for the simulation, to quickly explore many different combinations of factors and to identify the best combination to satisfy the study objective. In this case study, the CO_2 EOR and storage project through WAG injection is already economical (positive NPV) even without the CO_2 credit incentive.

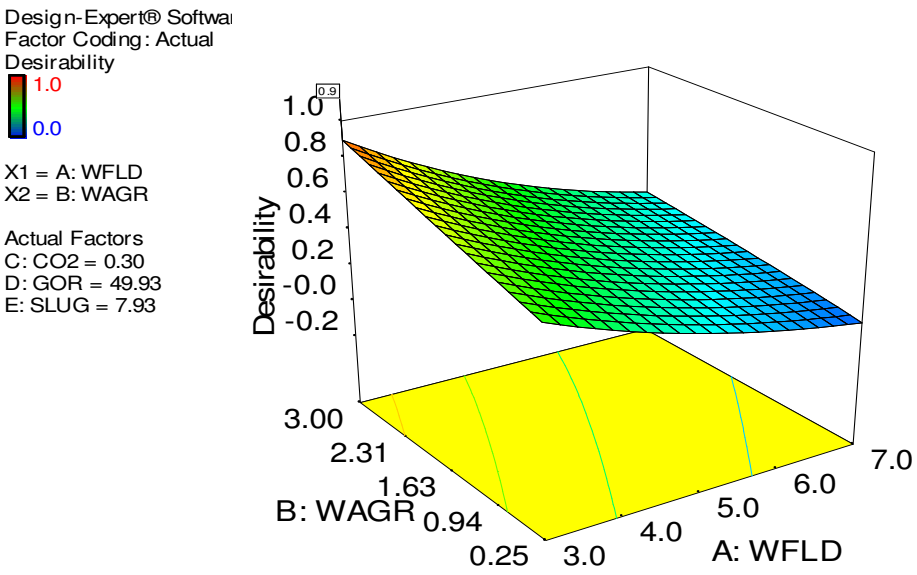

Figure 6.26: Response surface of desirability for maximum R* and S*.

Table 6.16: Comparison of the results predicted by the RSM to the outcome of a confirmation simulation.

Model	A:WFLD	B:WAGR	C:CO2	D:GOR	E:SLUG	S*, $/Mscf	R*, $/stb
E300	3.0	3.0	0.3	49.9	7.9	19.6	16.1
RSM						17.3	16.2

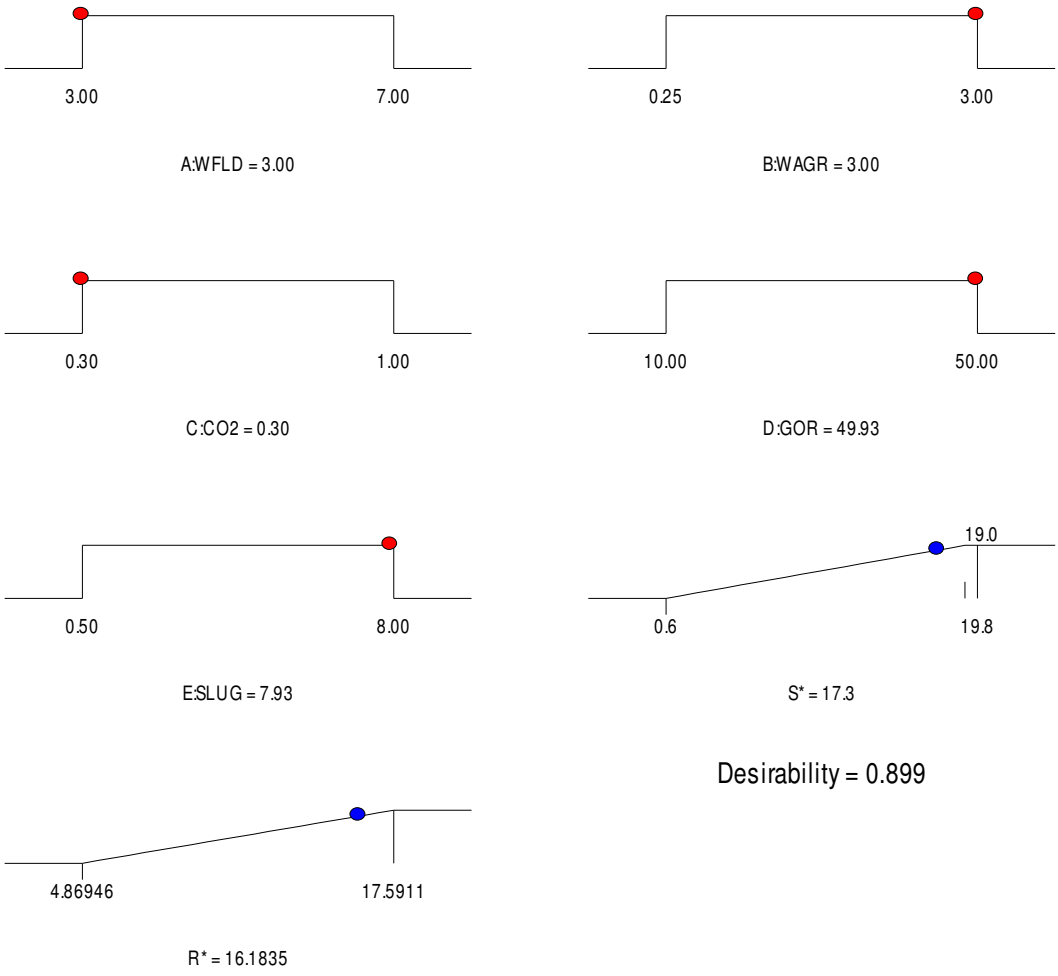

Figure 6.27: Numerical optimization ramps for each factor and each response to achieve the maximum desirability for R* and S*.

Graphical optimization of the response surface is also very useful to find regions where requirements of multiple responses simultaneously meet the critical properties, by

superimposing critical response contours on a contour plot. As an example, let say we want to find the setting whereby the R* and S* is at least $10/stb and $10/Mscf, respectively. Figure 6.28 shows the overlay plot of R* and S* as a function of waterflood duration (A) and WAG ratio (B) with mole fraction of CO_2 in the injected gas (C) at -1 level and the other factors at the centre points. The region that satisfies the constraints is yellow while the area that does not fit the optimization criteria is shaded gray. Similarly, the axis of the contour plot can be changed to find the window of operability of the factor of interest.

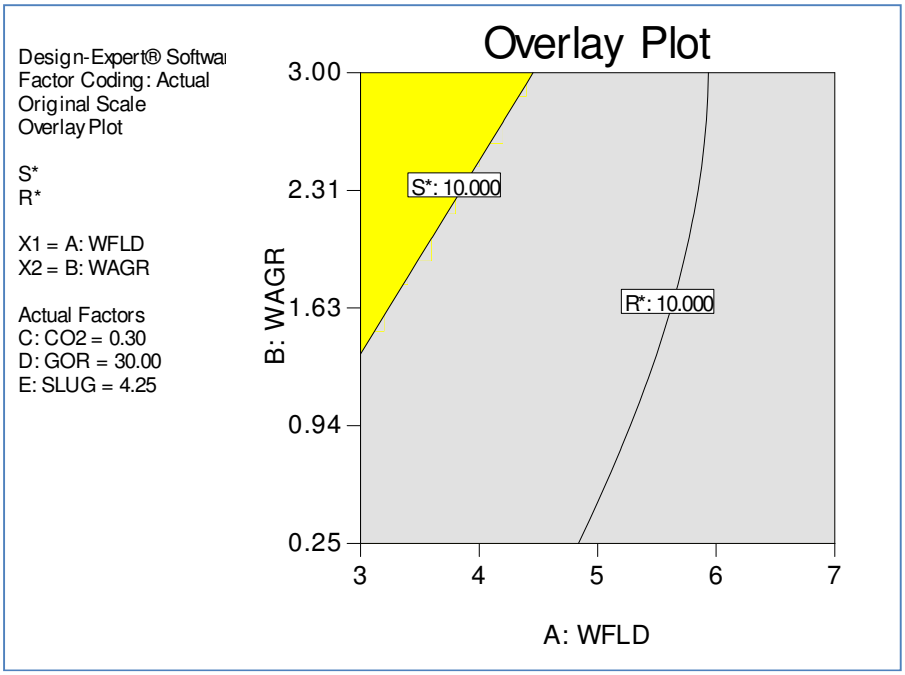

Figure 6.28: Overlay plot reveals window of operability for the specified constraints.

6.4. Summary and conclusions

6.4.1. Parametric simulation study of coupled CO_2 EOR and storage

Parametric simulation on 11 factors was carried out to identify the important operational and reservoir parameters to the oil recovery and the amount of CO_2 stored by tertiary WAG injection. The standard two-level fractional factorial DOE was employed to determine the minimum number of simulation cases that give maximum information on the effects of each

parameter. The oil recovery profit (NPV per barrel of oil produced) and CO_2 storage profit (NPV per Mscf of CO_2 stored) during the tertiary WAG injection were used as the response parameters. The ranked influential factors serve as the quick screening criteria for ranking the candidate reservoirs for CO_2 EOR and storage with WAG injection, as well as identifying the important design variables for optimization. The results of the parametric simulation show that:

- Reservoir heterogeneity has moderate effect on which factors are influential to the oil recovery and CO_2 storage profit. The homogeneous and heterogeneous reservoirs share the three most important factors to the response parameters, albeit with different ranking. There are, nonetheless, differences in the less significant factors, especially those involving interaction, which in turn are more prevalent in the homogeneous reservoir case.
- The tertiary oil recovery profit from the WAG injection is influenced greatly by, in descending order: the duration of the preceding waterflood, relative permeability (wettability) and the injected gas compositions. Short waterflood duration, water-wet reservoir and a mixture of CO_2 and the lean gas injection stream should be preferred for a profitable oil recovery.
- Whilst increasing the WAG ratio reduces the oil recovery profit for the homogeneous, oil-wet reservoir, a higher WAG ratio is favourable for the high permeability, water-wet reservoir.
- While the slug size in the half cycle of the WAG has been reported as one of the influential factors for oil recovery from the WAG injection, it is of the least influence to the profit of the coupled EOR and CO_2 storage process.
- High porosity and WAG ratio are beneficial for the optimized process and the impact is significant when the reservoir permeability is high.
- An oil wet reservoir is not promising for co-optimized oil recovery and CO_2 stored when the WAG ratio is large.
- The provision of CO_2 credit incentive can make certain CO_2 injection schemes, such as immiscible CO2I, economical for EOR and storage purpose.
- The CO_2 credit is strongly influenced by the oil price, CO_2 price and project location whether onshore or offshore.

6.4.2. Field scale WAG flood design optimization for EOR and CO_2 storage

The response surface method with the D-Optimal design has been successfully used to find the combination of factor levels that simultaneously satisfy the goals of maximizing the profit of oil recovery (R*) and CO_2 storage (S*) from the tertiary WAG injection in a full field reservoir. The DOE saves time by reducing the number of simulations required and makes it possible to optimize the design with a higher level of certainty.

From the co-optimization study, it was concluded that:

- Economically viable EOR and CO_2 storage can be achieved simultaneously through tertiary WAG injection.
- Response surface analysis can provide a tool to identify and estimate possible interactions between input parameters, as well as the optimum operating conditions for the tertiary WAG for coupled EOR and CO_2 sequestration.
- Profitability of the integrated process is enhanced by proper control of key operating parameters. Higher profit for both oil recovery and CO_2 storage through WAG injection, in terms of dollar per barrel of incremental oil produced and dollar per Mscf of CO_2 stored can be obtained, if it is implemented at an early stage of waterflooding with the use of a lower amount of CO_2 in the injected gas at high WAG ratio and a higher produced GOR limit imposed at the producer wells.
- While a higher produced GOR limit is good for increasing the oil recovery, the reverse is however true for the amount of CO_2 stored.
- The resulting empirical multivariate model is able to predict the response quickly within an acceptable margin of error. The predictive capabilities of this tool also enable it to be used for screening the economic viability of various oil reservoirs for the sequestration of CO_2, as well as the optimum production through tertiary WAG injection.

6.5. References

[6.1] Anderson, M.J. and Whitcomb, P.W.: DOE Simplified, Practical Tools for

Effective Experimentation, Second Edition, Productivity Press, New York, NY, 2007.

[6.2] Anderson, M.J. and Whitcomb, P.W.: RSM Simplified, Optimizing Processes Using Response Surface Methods for Design of Experiments, Productivity Press, New York, NY, 2005.

[6.3] Awan, A.R., Teigland, R. and Kleppe, J.: A Survey of North Sea Enhanced-Oil-Recovery Projects Initiated During the Years 1975 to 2005, SPE Reservoir Evaluation & Engineering, Vol. 11, 3, 497-512, 2008.

[6.4] Carlson F.M.: Simulation of Relative Permeability Hysteresis to the Non-wetting Phase, SPE 10157, SPE Annual Technical Conference and Exhibition, San Antonio, Texas, 4-7 October 1981.

[6.5] Champion, J.H. and Shelden, J.B.: An Immiscible WAG Injection Project in the Kuparuk River Unit, Journal of Petroleum Technology, Vol. 41, 5, 533-540, 1989.

[6.6] Chen, S. et al.: Optimal Parametric Design for Water-Alternating-Gas (WAG) Process in a CO_2 Miscible Flooding Reservoir, Canadian International Petroleum Conference (CIPC), Calgary, Alberta, Canada, June 2009.

[6.7] Darvishnezhad, M.J., Moradi, B. and Zargar, G: Study of Various Water Alternating Gas Injection Methods in 4- and 5-spot Injection Patterns in an Iranian Fractured Reservoir, SPE 132847, Trinidad and Tobago Energy Resources Conference, Trinidad, 27-30 June 2010.

[6.8] Design Expert version 8.0.6, Stat-Ease Inc, 2010.

[6.9] Floris, F. J. T., Bush, M. D., Cuypers, M., Roggero, F., and Syversveen, A. R.: Comparison of Production Forecast Uncertainty Quantification Methods - An Integrated Study, Petroleum Geoscience, 2001.

[6.10] Forooghi, A., Hamouda, A. and Eilertsen, A.T.: Co-optimization of CO_2 EOR and Sequestration in a North Sea Chalk Reservoir, SPE 125550, SPE/EAGE Reservoir Characterization and Simulation Conference, 19-21 October, Abu

Dhabi, UAE, 2009.

[6.11] Gharbi, R.B.C.: Integrated Reservoir Simulation Studies to Optimize Recovery from a Carbonate Reservoir, SPE 80437, SPE Asia Pacific Oil & Gas Conference and Exhibition, Jakarta, Indonesia, 15-17 April 2003.

[6.12] Ghomian, Y., Pope, G. A. and Sepehmoori, K.: Hysteresis and Field-Scale Optimization of WAG Injection for Coupled CO_2-EOR and Sequestration, SPE/DOE Improved Oil Recovery Symposium, Tulsa, Oklahoma, 2008.

[6.13] Grogan A.T. and Pinczewski W.V.: The Role of Molecular Diffusion Processes in Tertiary CO_2 Flooding, SPE 12706, JPT May 1987.

[6.14] Jarrell, P.M., Fox. C., Stein, M. and Webb, S.: Practical Aspects of CO_2 Flooding, SPE Monograph Series Vol. 22, Society of Petroleum Engineers, 2002.

[6.15] Jessen, K., Kovscek, A. R. and Orr, F. M.: Increasing CO_2 Storage in Oil Recovery, Energy Conversion and Management, 46 (18), 2005.

[6.16] Klins, M.A.: Carbon Dioxide Flooding Basic Mechanisms and Project Design, International Human Resources Development Corp., Boston, 1984.

[6.17] Kovscek, A. R. and Cakici, M. D.: Geological Storage of Carbon Dioxide and Enhanced Oil Recovery II. Co-optimization of Storage and Recovery, Energy Conversion & Management, 46, 15, 2005.

[6.18] Land, C.: Calculation of Imbibition Relative Permeability for Two- and Three-Phase Flow From Rock Properties, SPE Journal, Vol. 8, No. 2, 149 – 156, June 1968.

[6.19] Malik, Q. M. and Islam, M. R.: CO_2 Injection in the Weyburn Field of Canada: Optimization of Enhanced Oil Recovery and Greenhouse Gas Storage with Horizontal Wells, SPE/DOE Improved Oil Recovery Symposium, Tulsa, Oklahoma, 2000.

[6.20] Miller, J.A. and Jones, R.A.: A Laboratory Study to Determine Physical Characteristics of Heavy Oil after CO_2 Saturation, SPE 9789, SPE/DOE Second

Joint Symposium on Enhanced Oil Recovery of SPE, Tulsa, April 1981.

[6.21] Montgomery, D.C.: Design and Analysis of Experiments, John Wiley & Sons, New York, 1991.

[6.22] Myers, R.H and Montgomery, D.C.: Response Surface Methodology: Process and Product Optimization using Designed Experiments, John Wiley & Sons, New York, 1995.

[6.23] Pamukcu, Y.Z. and Gumrah, F.: Simulating Oil Recovery during CO_2 Sequestration into a Mature Oil Reservoir, Journal of Canadian Petroleum Technology, 47 (8), 34-39, 2008.

[6.24] Panda, M.N., Ambrose, J.G., Beuhler, G. and McGuire, P.L.: Optimized EOR Design for the Eileen West End Area, Greater Prudhoe Bay, SPE Reservoir Evaluation & Engineering, Vol. 12, 1, February 2009.

[6.25] PUNQ-S3 Model, http://www3.imperial.ac.uk/earthscienceandengineering/research/ perm/punq-s3model, accessed in March 2010.

[6.26] Qi, R., La Force, T. C. and Blunt, M. J.: Design of Carbon Dioxide Storage in Oilfields, SPE Annual Technical Conference and Exhibition, Denver, Colorado, USA, 2008.

[6.27] Ramirez, W.F., Fathi, Z. and Cagnol, J.L.: SPE Journal, Volume 24, No. 3, 328-332, June 1984.

[6.28] Rivas, O., Embid, S. and Bolivar, F.: Ranking Reservoirs for Carbon Dioxide Flooding Processes, SPE Advanced Technology Series, 2, 95-103, 1994.

[6.29] Rogers, J. D. and Grigg, R. B.: A Literature Analysis of the WAG Injectivity Abnormalities in the CO_2 Process, SPE 59329, SPE/DOE Improved Oil Recovery Symposium, Tulsa, April 3-5, 2000.

[6.30] Sanchez, N. L.: Management of Water Alternating Gas (WAG) Injection Projects, SPE 53714, Latin American and Caribbean Petroleum Engineering Conference, Caracas, Venezuela, 1999.

[6.31] Sifuentes, W., Blunt, M.J. and Giddins, M.A.: Modelling CO_2 Storage in Aquifers: Assessing the Key Contributors to Uncertainty, SPE 123582, SPE Offshore Europe Oil & Gas Conference & Exhibition, Aberdeen, UK, 8-11 September 2009.

[6.32] Stevens, S.H., Kuuskra, V.A. and Taber, J.J.: Sequestration of CO_2 in Depleted Oil and Gas Fields: Barriers to Overcome in Implementation of CO_2 Capture and Storage, Report PH3/22/IEA/CON/98/31, 2000.

[6.33] Naucler, T., Campbell, W. and Rujis, J.: Carbon Capture and Storage: Assessing the Economics, McKinsey Climate Change Initiatives, McKinsey & Co. Inc., September 2008, at http://www.mckinsey.com/Client_Service/Sustainability.

[6.34] White, C.D. and Royer, S.A.: Experimental Design as a Framework for Reservoir Studies, SPE 79676, SPE Reservoir Simulation Symposium, Houston, Texas, 3-5 February 2003.

Chapter 7

Conclusions and Recommendations

In this chapter, the main conclusions of this study will be presented. There are also recommendations, particularly with respect to the CWI studies, for researchers who would like to contribute towards this line of investigation.

7.1. Summary and conclusions

Storing CO_2 in conjunction with EOR in depleting oilfields is one of the most attractive options for sequestering anthropogenic CO_2 into geological formations thanks, mainly, to the wealth of site-characterization data, the infrastructural advantages and the revenue from the incremental oil recovery, which can offset some of the CO_2 storage costs. This study looked into the coupled CO_2 EOR and storage from both a gas-based and water-based injection perspective. CO_2 EOR is more commonly implemented as a gas-based injection process but is well known to suffer from an undesirable gravity override, channelling and viscous fingering due to the high mobility of the CO_2, which lead to a very inefficient sweep and thus a serious reduction in oil production, despite the high displacement efficiency achievable in the miscible cases.

7.1.1. The experimental studies of CWI

In this research, CWI was investigated as an alternative CO_2 injection mode that could minimize the adverse viscosity problem and improve sweep efficiency. CWI is a water-based form of CO_2 injection in which the CO_2 is dissolved in the injected brine prior to injection and transported through the reservoir by the flood water. Despite its potential for EOR and CO_2 storage, this injection mode has not been very much studied. Among the main objectives of this study were, therefore, to further understand the oil recovery mechanisms of CWI and to quantify the increase in oil recovery and the amount of CO_2 stored from the implementation of this process. Through a series of high temperature and high pressure coreflood experiments, this research further adds to the knowledge about the effects of oil viscosity, rock wettability and brine salinity on the performance of CWI.

The coreflood experiments clearly demonstrate that both secondary and tertiary CWI can increase the ultimate oil recovery above that of the plain water injection with higher and earlier incremental oil recovery obtained in the secondary process. It was observed during the secondary CWI experiments that the CO_2 moves ahead of the carbonated water front, indicating good delivery of CO_2 through dispersion and diffusion mechanisms to the oil at the front during the displacement. Amongst the main mechanisms of oil recovery by CWI are oil swelling as a result of CO_2 diffusion into the oil and the subsequent oil viscosity reduction and coalescence of the isolated oil ganglia.

The coreflood test results also reveal that the CWI performance is strongly influenced by core wettability, oil viscosity and brine salinity. This study was the first to report an important observation of the oil recovery profile from CWI in the mixed-wet core, where the additional oil recovery was much higher and faster i.e., occurred at breakthrough (at the displacement front) rather than gradually after the breakthrough as observed for the water-wet system. An additional recovery of 11.8 %PV was measured from the secondary CWI as compared to only 7.6 %PV in the water wet core. These observations are significant for CWI potential, since it is now generally accepted that many oil reservoirs are mixed wet.

In terms of %PV, light oil gives higher oil recovery than the viscous oil, although the oil recovery improvement above that of waterflooding from the secondary CWI is more or less the same in both oils. The oil recovery from the low salinity CWI is also higher than that of the high salinity one.

CWI also has high potential as an injection strategy for combining oil recovery and CO_2

storage. As much as 45 and 51% of the total volume of CO_2 injected (in the carbonated water) was stored at the end of the secondary and tertiary carbonated waterfloods, respectively. If we apply this level of CO_2 storage to all the waterflooded offshore oilfields in the UKCS, North Sea, based on CO_2 solubility of 6.94 lb CO_2/100 lb water, 12.4 Mt of CO_2 could have been injected in those offshore reservoirs in 2010 alone, 6.2 Mt of which would have been stored had carbonated water been injected instead of plain water.

7.1.2. The simulation studies of CWI

This research also assessed three compositional reservoir simulators namely E300, GEM and STARS for their suitability in modelling the CWI process, as no similar simulation study of the process, to the best of the author's knowledge, has ever been reported. Correctly defining the carbonated water as the injection fluid and accounting for the important mechanisms of the process are among the challenges in modelling this injection scheme. Since none of the evaluated simulators has a specific keyword to assign carbonated water composition as a single phase in the injection stream at the surface, in this study, CWI was modelled as a co-injection of CO_2 and water at the same location in proportion corresponding to the CO_2 solubility in water at the test condition. All the three compositional simulators assume instantaneous equilibrium and complete mixing between phases. The difference in correlations to calculate viscosity and solubility of CO_2 in oil and water phases lead to discrepancies in the predicted results by the simulators.

At the core scale investigated, the compositional simulator over-predicted the oil recovery for both secondary and tertiary CWI. One of the main findings in this study is that the local equilibrium was not achieved during the CWI in the core, making the instantaneous equilibrium assumption inappropriate for modelling the process at the core scale. The model predicted a high amount of CO_2 dissolved from the carbonated water into the oil resulting in a large viscosity reduction and thus high incremental oil recovery. Activating CO_2 diffusion within the oil and gas phases in the model does not improve the prediction.

Apart from diffusion within the water phase and also from the carbonated water to the oil phase, which cannot be accounted for by the simulator, dispersion of CO_2 into the oil at the displacement front also plays important role in the CWI core experiments in this study. The

author proposes the addition of the transport coefficient (α-factor) in the compositional model, to account for the dispersive mixing effects and enable a more accurate prediction of the model for the secondary CWI process. This factor was originally introduced for modelling sub-gridblock phenomena to improve the accuracy of compositional simulations performed with coarse homogeneous grid blocks.

This study also found that modelling core-scale CWI without the use of a compositional model by using the relative permeability derived from the CWI displacement tests and the Todd-Longstaff model, may give a first-order approximation of the oil recovery but unreliable predicted gas production.

7.1.3. Numerical simulation of various CO_2 injection strategies for coupled EOR and storage

Storing CO_2 through EOR in an oilfield not only aims to increase the oil recovery but also to maximize the amount of CO_2 left behind at the end of the recovery. These objectives are significantly different from maximizing the oil recovery alone and require optimization. For the gas-based CO_2 EOR, this study focused on the co-optimization of the oil recovery and CO_2 storage.

The most attractive CO_2 injection method to co-optimize EOR and CO_2 storage economically was first identified through compositional reservoir simulations. CO2I, WAG, HYWAG, SSWAG, TAPWAG and a newly conceptualized injection scheme, the intermittent WAG (INTWAG) injection were evaluated. INTWAG injection was examined to gauge the benefit of CO_2 diffusion to the oil recovery by shutting in some wells for certain period of time before switching to the other phase and also the benefit of the drainage-imbibition processes that occur as a result. Simulation results show that under the same conditions, INTWAG performance in terms of oil recovery and CO_2 storage was slightly superior to that of the normal WAG injection.

Two sets of ranking parameters were used in selecting the CO_2 injection method with the highest potential; one was purely based on a technical basis i.e., with equally weighted incremental oil recovery and the pore volume of CO_2 stored, while the other incorporated

economic factors i.e., with equally weighted profit of oil recovery (R* = NPV per incremental barrel of oil produced) and CO_2 storage (S* = NPV per Mscf of CO_2 stored).

The simulation results show that the injection strategy to maximize the oil recovery was different from that to maximize CO_2 storage alone. The injection schemes traditionally designed for minimizing CO_2 utilization per incremental volume of oil produced, such as WAG, SSWAG and TAPWAG, do not technically perform well for CO_2 storage. These results clearly highlight that optimization is essential for achieving a technically and economically viable project integrating EOR and CO_2 storage.

Managing the production/injection strategy to control the reservoir pressure, which in turn determines the miscibility, is extremely important. As expected, miscible CO_2 injections give higher oil recovery than the corresponding immiscible process but the reverse is true for CO_2 storage. For maximum oil recovery and storage, higher reservoir pressure, which reaches the MMP, should be targeted and maintained throughout the flooding.

The study also showed that the most technically promising injection strategy is not necessarily the most profitable. For the reservoir used in this study, miscible WAG was ranked as the injection scheme with highest potential for coupled EOR and CO_2 storage in the tertiary recovery mode, with the economic factors taken into account and miscible continuous CO_2 injection without these factors taken into account. Different priorities in the objectives of the CO_2 injection may, nevertheless, yield different results. As CO_2 EOR projects are usually tied to high investments, the results with the economic consideration were deemed more appropriate.

7.1.4. Parametric study and process design optimization of CO_2 injection for coupled EOR and storage

To identify the influential factors on the simultaneous oil recovery and CO_2 sequestration from the tertiary miscible WAG injection, a detailed parametric study on 11 factors was carried out on both homogeneous and heterogeneous hypothetical reservoir models, using an experimental design approach and numerical simulation. The DOE identifies minimum number of simulation cases that give maximum information on the effects of each parameter.

Results of the simulation show that reservoir heterogeneity has moderate influences on the critical factors to the profit of the oil recovery and CO_2 storage from the miscible tertiary WAG injection process. The three most important factors to the response parameters are common between the homogeneous and heterogeneous reservoirs, namely, the duration of the preceding waterflood, reservoir wettability and the injected gas composition.

For a profitable oil recovery, a short waterflood duration, water-wet reservoir and injection of CO_2-lean gas mixture should be preferred. A higher WAG ratio is favourable for the high permeability, water-wet reservoir but is detrimental to the homogeneous, oil-wet reservoir. High porosity and WAG ratio are beneficial for an optimized process in the water-wet reservoir and their impact is significant when the reservoir permeability is high. This study also found that the slug size injected in the half cycle of the WAG is not influential on the profit of the coupled EOR and CO_2 storage process.

The response surface method with D-Optimal design has been successfully used to find the combination of factor levels that simultaneously satisfy the goals of maximizing the profit of oil recovery and CO_2 storage from the tertiary WAG injection in a full field reservoir. The DOE saves time by reducing the number of simulations required and makes it possible to optimize the design with a higher level of certainty. This study found that economically viable EOR and CO_2 storage may be achieved simultaneously through tertiary WAG injection. Higher profit for both oil recovery and CO_2 storage can be obtained if the WAG injection is implemented at an early stage of waterflooding, with a lower amount of CO_2 in the injected gas at high WAG ratio, and a higher produced GOR limit is imposed at the producer wells.

7.2. Recommendations

The coreflood experiments reported in this study have covered a number of important parameters pertinent to the CWI, for better understanding of the process, but there still remain other equally important factors that also merit further investigation. In particular, the effect of dissolved gas in the reservoir oil on the process performance needs to be taken into account. For this purpose, a study using saturated and under-saturated live crude oil instead of stock tank crude oil would create a more realistic scenario of CWI in an oilfield. The

lighter live oil may be favourable from the displacement and CO_2 miscibility development viewpoint but the effects of the presence of dissolved or free gas on the process performance is yet unknown.

Another important aspect of CWI which needs to be researched is its performance in carbonate reservoirs. These reservoirs make up more than half of the remaining oil in the world, thus presenting a huge possible resource for CWI application. Investigation of the mechanisms of oil recovery and carbonated water flow in fractured core samples, the effects of the change in the rock properties due to contact of carbonate rocks with the carbonic acid and the storage potential in fractured porous media are among the significant studies required.

The reported coreflood results suggested that CWI brings comparable incremental oil recovery for light oil as well as for intermediate viscous oil. However, before this can be made a general conclusion, more coreflood experiments on a wider range of oil viscosities, densities and reservoir temperature and pressure are recommended to be carried out.

More CWI experiments and an appropriate modelling approach are also needed for the mixed-wet cores. The oil/water relative permeability curves from the plain water coreflood were inappropriate for modelling the CWI due to the different oil recovery and ΔP trends of both processes. As highlighted earlier, simulating CWI by incorporating the transport coefficient (α-factor) also does not work adequately for the mixed wet cores. The modelling of the tertiary CWI process with the transport coefficient (α-factor) may also be further improved by incorporating the pseudo-relative permeabilities to correct the oil and gas fluxes.

The INTWAG injection may offer a promising alternative injection scheme for increasing the oil recovery and CO_2 sequestration. Apart from quantification of the performance through laboratory experiments, improvement in predicting the process by properly incorporating the hysteresis and CO_2 diffusion into the water phase should be pursued.

In studying the impact of reservoir heterogeneity on the performance of various CO_2 injection schemes for EOR and storage, heterogeneity modelling should also take into account the variation of kv/kh in addition to different permeability in different grids. The price of emissions permits as well as incentives for EOR and CO_2 storage application

undoubtedly influence the viability of the coupled CO_2 EOR and storage projects. These elements have been only crudely addressed in this study. Upon availability of a more established or regulated system of CO_2 EOR and storage permits and incentives, it is recommended to undertake detailed co-optimization studies considering these economic factors